A NEW PERFORMANCE-BASED APPROACH OF ASR AGGREGATE REACTIVITY PREDICTION AND DEVELOPMENT OF ASR-RESISTANT CONCRETE MIX

A Dissertation

by

KAI-WEI LIU

Submitted to the Office of Graduate and Professional Studies of
Texas A&M University
in partial fulfillment of the requirements for the degree of

DOCTOR OF PHILOSOPHY

Chair of Committee,	Dan G. Zollinger
Co-Chair of Committee,	Anal K. Mukhopadhyay
Committee Members,	Robert L. Lytton
	Youjun Deng
Head of Department,	Robin Autenrieth

May 2015

Major Subject: Civil Engineering

ABSTRACT

The main objective of this study is to develop a rapid, reliable test method to determine the aggregate reactivity due to alkali-silica reaction (ASR) with respect to the overall alkalinity of the concrete. A volumetric change measurement device (VCMD) developed at the Texas A&M Transportation Institute was used in this research. The VCMD simulates the aggregate-pore solution reaction in concrete and measures free solution volume contraction due to ASR over time. The solution volume change over time at multiple temperatures was modeled to determine ASR compound activation energy (CAE) based on the Arrhenius equation. The CAE-based test can reliably predict aggregate alkali silica reactivity in a short period of time (5 days) in terms of measuring CAE. A representative CAE can be determined by testing as-received aggregates (i.e., field aggregates) with 0.5N NaOH (NH) + $Ca(OH)_2$ (CH) solution (similar to concrete pore solution) and with permissible repeatability. A CAE-based aggregate classification system is developed, which can serve as a potential screening parameter in an aggregate quality control program. A relationship between CAE and alkalinity is also developed, which became the basis to determine threshold alkalinity (TH_A). The proposed method has the potential to be considered as an alternative method to the current ASR test methods (e.g., accelerated mortar bar test (AMBT)).

An effective way of tailoring ASR mix design depending on the level of protection needed is developed based on CAE, TH_A, pore solution alkalinity (PSA),

and concrete validation testing. An accelerated concrete cylinder test (ACCT) using VCMD at 60°C is developed with no involvement of errors due to operation and temperature change along with arresting alkali leaching to test concrete mixes in a short time. Composite spherical and finite element modeling where relevant gel properties and free strain of ASR are the main inputs were developed for prediction of the measured linear ACCT expansion in a pure phase system as a proof of concept. An expansion limit of 0.04% using 0.82% Na_2O equivalent (Na_2O_e) cement without alkali boosting after a testing period of 28 days is proposed for the ACCT to diagnose ASR aggregate reactivity. The ACCT method has the ability to emerge as a potential method to test job mix and to validate the ASR-resistant mix design.

DEDICATION

To my parents who dedicated their lives for the education of their two children

And to my beloved sister

For their endless love, encouragement and support

ACKNOWLEDGEMENTS

I would like to thank my committee chairs, Drs. Dan G. Zollinger and Anal K. Mukhopadhyay, for their guidance, advice and support throughout this research, as well as Drs. Robbert L. Lytton and Youjun Deng of the dissertation committee members for many valuable comments and effort in evaluating my dissertation. I would also like to thank Dr. Zachary Grasley for the invaluable suggestions conducting the experimental program. My gratitude also goes to the crew of McNew lab, Civil Engineering lab, and my office mates, who have provided valuable insights and suggestions for this research, and friends and relatives for their moral support and encouragement throughout my time spent at Texas A&M University.

This study was funded by the Texas Department of Transportation (TxDOT Project 0-6656). Their support is greatly appreciated.

TABLE OF CONTENTS

Page

LIST OF FIGURES

Page

LIST OF TABLES

Page

CHAPTER I

INTRODUCTION

Background and Research Significance

Alkali-silica reaction (ASR) in Portland cement concrete is a deleterious chemical reaction which induces expansive stress in presence of sufficient moisture and is recognized as a major concern in Texas. New cases of ASR are continuously being reported despite the advancement of the last decades. Prior to the early 1990s, ASR was not considered an issue in Texas, although cases of ASR in prestressed and cast-in-place concrete were at least visually observed. In 1999, a rigorous ASTM C 1260 testing of virtually every concrete aggregate source was initiated, which resulted in the preparation of special provision of ASR in 2004 (TxDOT Item 421-024). The special provision recommended using one of the mix-design options (e.g., the use of Class F Fly ash (20-35%), Class C Fly ash, ground granulated blast-furnace slag (GGBS) (35-50%), silica fume (10%), ultrafine Fly ash (UFFA), metakaolin, less than 2.4 kg/m^3 (4.0 lb/$yard^3$) of the total alkali contribution from cement in the concrete, etc.) if the cementitious material content exceeds 308.5 kg/m^3 (520 lb/$yard^3$). These measures in the special provision were thought to be adequate in order to avoid ASR distress.

However, in early 2008, the prestressed girders in Central Texas (cast in 2004) showed ASR cracking, although one mix had 20% Class F Fly ash and another mix had less than the required total alkali limit (2.4 kg/m^3 (4.0 lb/$yard^3$)). It was found that some

aggregate sources in Texas would not be sufficiently limited by 2.4 kg/m^3 (4.0 lb/yard^3) of alkali and could fool ASTM C 1567 (ASTM 2008). As a result, an exclusion list of aggregate sources was created in Texas Department of Transportation (TxDOT) (TxDOT Item 421-031). Subsequently, a new special provision was developed, where the total alkali contribution from cement changed from 2.4 to 2.1 kg/m^3 (4.0 to 3.5 lb/yard^3) of concrete, and the 14-day ASTM C 1567 expansion limit went from 0.10% to 0.08% (TxDOT Item 421-034). In May 2008, another special provision was issued to disallow some options (e.g., the use of lithium nitrate admixture, ASTM C 1567 expansion limit) for major prestressed members and raise the minimum Class F Fly ash content to 25% (TxDOT Item 424-001). In July 2008, additional aggregates in Texas were added to the exclusion list of aggregate sources. In early 2009, girders (fabricated mostly in 2007 with a few in 2005-2006 using total alkali limit, 2.1 kg/m^3 (3.5 lb/yard^3)) in a prestressed plant in Texas began showing signs of distress. The fine aggregates were tested by petrography, x-ray diffraction (XRD), ASTM C 1260 (ASTM 2008), and the acid insoluble percentage; identified as reactive; and added to the exclusion list of aggregate sources in TxDOT.

It is clear that some options in special provision mentioned above did not provide enough protection, and some aggregates have been found to produce expansive gel even at low alkali loadings. The possible options that were suggested to minimize the occurrence of ASR are:

- Create a stratified aggregate classification system using a new testing approach that will address reactivity and source variability in an efficient manner.

- Define the testing frequency for pits/stockpiles (an important item to address source variability).
- Change the alkali loading equation to account for Na_2O and K_2O effects separately.
- Investigate alkali levels in pore solution.
- Encourage plants to acquire soils for Fly ash if they do not currently have one. Using Fly ash (25-35%) should be considered as a required item.

It would be beneficial to accurately, fairly, and rapidly assess the ASR potential of each aggregate at various alkali loadings. An effective way of tailoring mix design depending on the level of protection needed is warranted. This will ensure valuable resource conservation and avoid paying for premium ASR protection when only minor protection is needed.

Since the ASR-related problems were identified in the early 1940s, extensive work has been carried out on ASR over the decades. One of the main areas of research was to develop a rapid and reliable test method to access ASR potential of aggregates and concrete through a simulative type of approach. The main purpose of an ASR test method is to measure aggregate reactivity prior to their use in concrete structures and develop ASR-resistant mixes. The current approach of ASR testing and mitigating damaging ASR heavily depends on accelerated mortar-bar tests (AMBT) and concrete prism tests (CPT). Although these approaches have resulted in significant advances in the avoidance of ASR damage in concrete structures, there were limitations and drawbacks. The test conditions of AMBT are severe and the test results are unrelated to field performance. CPT has been considered as the best index for field performance, but

the test duration and alkali leaching impose major limitations. Therefore, there is a strong need for developing a rapid and reliable ASR test method.

A device called volumetric change measurement device (VCMD) has been developed at Texas A&M Transportation Institute (TTI) where as-received aggregates were immersed in alkaline solution of varying concentrations and allowed to react at different temperatures. The device measures solution volume contraction over time (till 4 days) as the reaction between aggregate and solution proceeds. A model has been developed to characterize the measured volume change over time and calculate reaction rate. The reaction rates at multiple temperatures allowed to calculate ASR compound activation energy (CAE) based on Arrhenius equation. CAE is used as a measure of alkali silica reactivity of aggregate.

A procedure for ASR mix design adjustment, verification, and validation is developed by applying both mix design controls and special protection measures (as needed) based on CAE-based reactivity prediction, threshold alkalinity (TH_A), pore solution alkalinity (PSA), and concrete validation testing. An accelerated concrete cylinder test (ACCT) using VCMD at 60°C is developed with no involvement of errors due to operation and temperature change along with arresting alkali leaching to test concrete mixes in a short time (28 days). The ACCT method has the ability to emerge as a potential method to test job mix and to validate the ASR-resistant mix design.

Objectives

The main objective of this study was to develop a rapid, reliable test method to determine aggregate alkali-silica reactivity based on the time-dependent nature of the

onset and speed of reaction. The test method should also determine the aggregate sensitivity to the overall alkalinity of the concrete. The VCMD was identified as a potential method to fulfill these requirements. The specific objectives of the research were:

- Both coarse and fine aggregates were selected from both the TxDOT exclusion list (poor performance) and approved list (satisfactory performance) covering different types of aggregates with a wide range of reactivity
- Testing the selected aggregates by VCMD-based aggregate-solution test and measure CAE. CAE is considered as a single fundamental material property to represent aggregate alkali-silica reactivity.
- Monitoring soak solution chemistry changes and microstructural studies on the reaction products were proposed as supporting tools for the VCMD test.
- Developing an ASR aggregate classification system based on CAE.
- Highlighting the benefits of the proposed method by establishing a comparative assessment among ASTM C 1260, ASTM C 1293 (ASTM 2008), and the proposed test method. The expected benefit was consistent identification of the aggregate belonging to false positives and negatives categories in a short period of time.
- Development of a procedure to determine alkali threshold of aggregate based on aggregate-solution test at multiple levels of alkalinity.
- Development of a chemical method based on CAE, TH_A, and PSA to formulate/adjust/verify mix design with the expectation that the verified mixes will

either not show any ASR or little ASR with no visible or measurable distress during the expected service life.

- Mix-design validation through direct concrete testing. It was proposed that an attempt will be made to develop an accelerated concrete cylinder test (ACCT) that can be used to (i) test a mix at varying levels of alkalinity and determine aggregate reactivity to the overall alkalinity of concrete and (ii) test a job mix with or without alkali boosting.

In the past 5.5 years, TxDOT has already paid approximately $2 million for recasting precast concrete products. Hundreds of other precast elements with the same mix designs were placed in the past, and future maintenance costs are expected to increase for these structures. It is expected that the proposed fast, reliable test method will eventually replace ASTM C 1260/C 1567 and improve the special protection (TxDOT Item 421-034). This option is more commonly used as Class F Fly ash becomes increasingly unavailable. A CAE-based classification system in conjunction with ASTM C 1260 and ASTM C 1293 data will be used to create stratified lists of aggregate reactivity, allowing for progressive mitigation options to be used. Recommendations for specification changes will be provided. An effective way of tailoring mix design depending on the level of protection needed will be developed, which will ensure valuable resource conservation and help to avoid paying for premium ASR protection when only minor protection is needed. The locally available aggregate and supplementary cementitious materials (SCMs) can be judiciously used with the proposed approach, thus minimizing the number of aggregates in the exclusion list.

Organization of the Dissertation

This dissertation consists of seven chapters, which are briefly summarized below.

Chapter I is an introduction addressing the research background and objectives, followed by a description of dissertation organization.

Chapter II provides the background information based on a literature review relevant to the proposed study. The current test methods and their limitations are highlighted.

Chapter III presents the basis of aggregate material selection and characterization (petrographic examination).

Chapter IV describes the test equipment and methodology.

Chapter V presents all material testing results (CAE, soak solution chemistry, and microstructures, etc.) and a new ASR aggregate classification system based on CAE. A comparative assessment between CAE-based classification system and ASTM C 1260/C 1293 is also presented and discussed in this chapter.

Chapter VI presents a step-by-step approach to develop an ASR-resistant mix, i.e., (i) formulation/adjustment/verification of a mix based on CAE, TH_A, and PSA, and (ii) validation through concrete testing. An ACCT was developed in this study and used for concrete validation testing. This chapter also presents a detailed description of this rapid concrete testing along with numerical models for prediction of concrete expansion in a pure phase system due to ASR.

Finally, Chapter VII provides summaries and conclusions based on the research findings from this study and potential recommendations for future research.

CHAPTER II

LITERATURE REVIEW

This chapter provides a comprehensive literature review on ASR relevant to this study in four sections. The first section describes the factors that initiate and sustain ASR. The second section deals with the current reaction and expansion mechanisms of ASR. The third section provides a brief background on the current test methods for predicting the ASR potential of aggregates along with some discussions on the usefulness and limitations of these methods. The current kinetic approaches for determining ASR aggregate reactivity are summarized in the last section.

Introduction

ASR in Portland cement concrete is a deleterious chemical reaction that induces expansive stress in the presence of sufficient moisture. Since the identification of ASR-related problems in the early 1940s, extensive research has been carried out on ASR over the decades. The development of ASR test methods to assess ASR potential of aggregates and concrete through a simulative type of approach was one of the main portions of that research. The other areas of research include:

- A better understanding of both reaction and expansion mechanisms
- Development of specifications for preventing ASR in new concrete
- Management guidelines for existing ASR-induced damaged concrete structures

The main purpose of an ASR test method is to measure aggregate reactivity prior to their use in concrete structures. The most commonly used ASR testing heavily

depends on the AMBT (e.g., ASTM C 1260) and CPT (e.g., ASTM C 1293). The AMBT is rapid (i.e., 14 days) but the test conditions (i.e., 1N NaOH and 80°C) are severe and the test results are sometimes unrelated to field performance. Marks (1996) used AMBT to evaluate ASR reactivity of 30 sands and concluded that more research was needed due to mismatch of AMBT and field performance. Swamy (1992) stated that AMBT is problematic due to aggregate crushing and higher amount of cement than those used in concrete construction. The results obtained from AMBT cannot be applied to concrete. Mukhopadhyay et al. (2009) stated that when aggregates are tested according to AMBT, a good ASR field performance can sometimes be classified as reactive due to aggregate crushing. Aggregates are heterogeneous materials containing a random distribution of reactive constituents (e.g., reactive siliceous impurity in limestone or reactive cementing materials in sandstone). Either losing or exposing the reactive phases during aggregate crushing will result aggregates being passed/rejected by AMBT but rejected/passing by field performance. The CPT has been considered as the best index for field performance (Foarnier and Malhorta 1999; Lane 1999; Thomas and Innis 1998, 1999) but the long testing time (i.e., 1 year minimum) and alkali leaching are some of the limitations (Bauer et al. 2006; Liu and Mukhopadhyay 2014; Mukhopadhyay et al. 2009).

ASR is a kinetic type of chemical reaction. It is known that some threshold values of alkalinity and moisture need to be satisfied in order to initiate ASR and make ASR expansive. CAE of ASR can serve as a single chemical material parameter to represent the combined effects of alkalinity, temperature, and moisture and can be used

as a measure of alkali silica reactivity of aggregate. Many researchers in the past have applied kinematic type models to characterize mortar bar expansion over time and determine a constant that was used to differentiate between reactive and non-reactive aggregates effectively (Johnston et al. 2000; Uomoto et al. 1992). The main purpose was to provide a better interpretation of the AMBT data through kinematic approach but not intended to improve the test procedure. There is a growing demand for a rapid and reliable ASR test procedure.

It is important to understand the basics of ASR, responsible factors, expansion mechanisms, some limitations of the current test methods, and effectiveness of the remedial measures in order to identify the more effective test method. A brief discussion on these topics is given below.

Factors Influence Alkali-Silica Reaction (ASR)

ASR is a chemical reaction between alkali hydroxides in a pore solution and the reactive form of silica in aggregates. It is widely accepted that three essential conditions (Figure 2.1) are necessary in order to create ASR-induced damage in concrete structures (Chatterji et al. 1989; Mukhopadhyay et al. 2006; Ponce and Batic 2006):

a) Sufficient availability of OH^- ions and alkalis (Na^+ and/or K^+) - a highly alkaline concrete pore solution (pH > 13.2) ensures enough supply of alkali hydroxides
b) Presence of a reactive siliceous component(s) in aggregates (both coarse and fine aggregates) at optimum level (i.e., pessimum proportion)
c) Sufficient moisture (> 80% relative humidity (RH))

The optimum combination of conditions a) and b) is essential to initiate ASR, whereas condition c) is essential to make ASR expansive (i.e., deleterious). If any one of the three factors is not present in the concrete, then the reaction will either not proceed or not become deleterious. The higher the temperature the higher the rate of ASR is. Increasing temperature causes higher expansion at early age but lower ultimate expansion (Diamond et al. 1981). The product of this reaction is a gel known as ASR gel. In the presence of sufficient moisture (> 80% RH), the gel absorbs moisture due to its hygroscopic nature and swells. Swelling leads to tensile stresses in concrete. When these stresses exceed the tensile strength of concrete, cracks develop. Typical visual manifestation of ASR includes map cracking, misalignment of structural elements, and expansive features such as joint closure and heaving/blow-ups, etc. ASR cracks act as open passages for moisture and other chemicals (chloride ions, sulfate ions, etc.), leading to more damage. In addition to the three requirements listed above, the presence of calcium hydroxide ($Ca(OH)_2$) in concrete pore solution also found to be an important factor. Chatterji et al. (1989) believed that sufficient Ca^{2+} concentration in the pore solution (vicinity of the aggregate) is needed for ASR gel to be expansive inside aggregate.

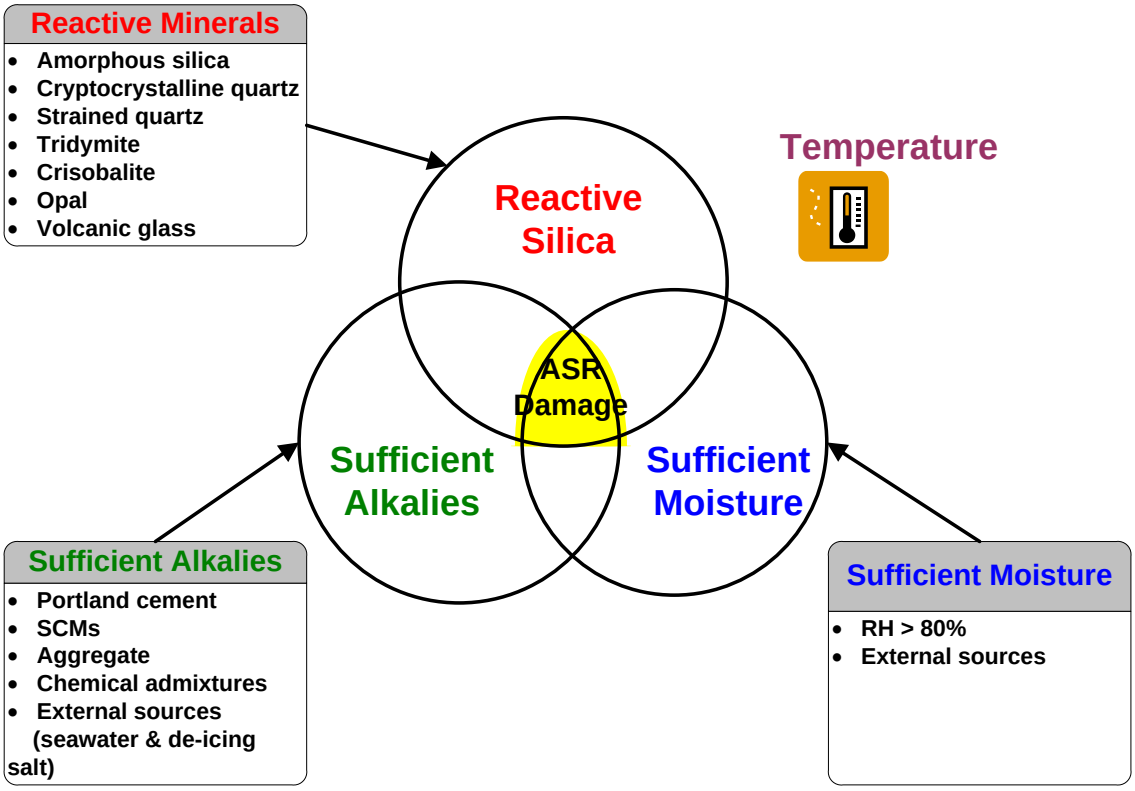

Figure 2.1 Three Essential Factors that Initiate ASR and Make ASR Expansive in Concrete (Mukhopadhyay and Liu 2014).

Reactive Siliceous Components in Aggregates

The occurrence of silica or silicate minerals in aggregates (both coarse and fine) is a common feature. Aggregate alkali-silica reactivity is a function of the form/degree of crystallinity, grain size, texture, and proportion of the reactive silica within the reactive aggregate (Mindess 2003; Stanton 1940). Not all forms of silica are ASR reactive. The more disordered the structure of the silica phase, the greater the reactivity. The basic structure of silicates involves a framework of silicon-oxygen tetrahedron. Each oxygen atom is shared between two silicon atoms, where each silicon atom is

bonded to four oxygen atoms (called Siloxane Bridge). A regular (ordered) arrangement of the basic Si-O tetrahedron creates a crystalline structure (Figure 2.2a, e.g., quartz) whereas an irregular (disordered) arrangement of the tetrahedron creates poorly crystalline (e.g., chalcedony) to amorphous structure (Figure 2.2b, e.g., opal,), depending on the degree of irregularity. Diamond (1976), Mehta and Monteiro (1992), and Tatematsu and Sasaki (1989) have designated the degree of reactivity of these reactive forms of silica, with decreasing order as follows: Opal, Crystobalite, Tridymite, Microcrystalline quartz, Cryptocrystalline quartz, Chalcedony, Chert, Volcanic glass, Strained quartz. The crystalline quartz (e.g., present in igneous rocks) is not considered susceptible to ASR, whereas strained quartz (e.g., present in metamorphic rocks) is reactive.

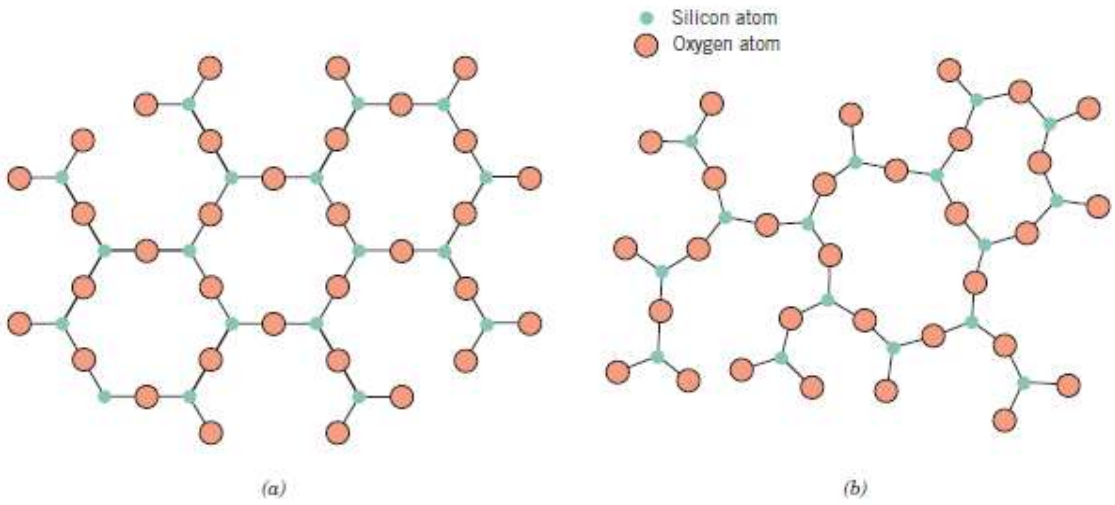

Figure 2.2 Two-Dimensional Schemes for the (a) Crystalline and (b) Non-Crystalline SiO_2 (Callister 2007).

Mindess et al. (2003) summarize the forms of reactive silica in aggregates that can participate in ASR (Table 2.1). In general, the metastable types of silica (e.g., opal, chalcedony, tridymite, crisobalite, and some disordered forms of quartz (cryptocrystalline and strained quartz)) and alumina-silicate glasses (e.g., acid volcanic glass) are known to be highly reactive with the alkalis in concrete (Broekmans 2002; Fernandes and Noronha 2004; Gillott et al. 1973; John et al. 1998).

Table 2.1 Forms of Reactive Silica in Aggregates Susceptible to ASR (Mindess et al. 2003).

Reactive Component	Physical Form	Rock Type in which It is Found	Occurrence
Opal	Amorphous	Opaline limestone (e.g., Spratt limestone), chert, shale, flint	Common as a minor constituent in sedimentary rocks
Silicate glass		Volcanic glasses (rhyolite, andesite, dacite) and tuffs; synthetic glasses	Regions of volcanic origin; river gravels originating in volcanic areas; container glass
Chalcedony	Microcrystalline quartz	Siliceous limestones and sandstones, cherts, and flints	Widespread
Cristobalite (Tridymite)	Crystalline but metastable	Opaline rocks, fired ceramics	Uncommon
Strained Quartz	Disordered due to strain effects	Metaquartzite, sands, gravel, sandstones, many metamorphic rocks (e.g., granite gneiss and schists)	Common

The degree of crystallinity and amount of defects in the lattice affect the potential alkali reactivity and solubility of siliceous aggregates (Grattan-Bellew 2001). However, the form of silica is not the only parameter that determines alkali reactivity of an aggregate. The other important factors that determine aggregate reactivity are as follows:

- Amount and nature of distribution of the reactive constituents inside aggregates.
    - Homogeneous or inhomogeneous distribution
    - Whether the whole aggregate particle is reactive (e.g., acid volcanic rock) or certain reactive constituent(s) inside an aggregate is reactive
    - In certain sandstones, the fine cementing material is reactive, but the coarser grains are nonreactive
- Role of aggregate porosity, pore connectivity and other internal structures (e.g., layering, schistose/foliated structures, etc.) on ingress of OH^-, Na^+, K^+ ions into the aggregates
    - High porosity/pore connectivity can enhance the ingress of ionic species and increase the chance for ASR to occur with a much faster rate, provided enough reactive constituents are present (Broekmans 2002; Gogte 1973; John 1998; Wenk et al. 2008)

Petrographic studies play an important role in understanding the above additional factors related to aggregate reactivity. It is unlikely that mineralogy and percentage of reactive constituent will remain the same for a particular quarry/pit (especially for an aggregate with high source variability) over time, and therefore users may not be able to confidently use aggregates from sources that have performed satisfactorily in the past without re-testing. The frequency of aggregate testing as a function of source variability is an important item that needs to be addressed.

Pessimum Effect Related to the Quantity of Reactive Constituent(s)

A pessimum effect is defined as increasing expansion with increasing reactive silica content in aggregate up to a certain level (i.e., the pessimum proportion) followed by decreasing expansion with increasing reactive silica content (Hobbs 1988, Figure 2.3). Concrete prism tests with different types of aggregates have shown that a maximum expansion occurs at a particular amount of the reactive siliceous constituent in aggregates (Gillott 1975; Grattan-Bellew 2001; Hobbs 1988; RILEMTC AAR-1 2003). However, the pessimum proportion effect differs for various reactive constituents. For example, for aggregates containing opal, the maximum expansion occurs for the reactive silica content below 10% (Bektas et al. 2004; Shayan 1992; Vivian 1947). Slowly reactive aggregates don't even show a pessimum effect. It was reported that as little as 2% of reactive silica is enough to observe distress in concrete structures (Swamy 1992).

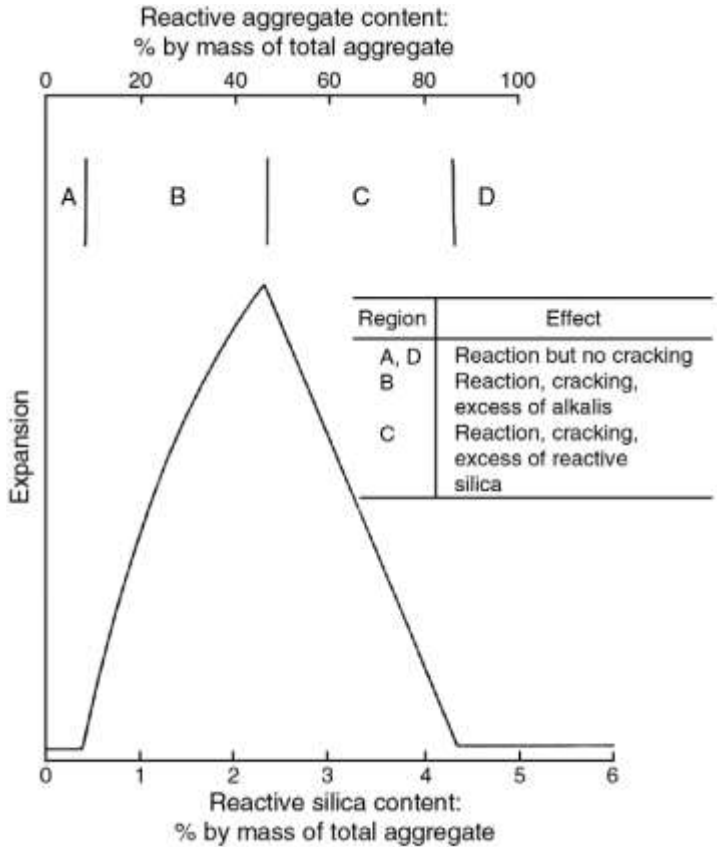

Figure 2.3 Pessimum Curve of Pure Siliceous Aggregate (Hobbs 1988).

Garcia-Diaz et al. (2010) investigated the ASR pessimum behavior of the siliceous limestone aggregates. The results show that high alkali content in concretes containing reactive siliceous limestone aggregates (both fine and coarse aggregates) have less expansion than concretes containing fine reactive siliceous limestone aggregates and non-reactive coarse aggregates.

The pessimum effect is based on the assumption of limited amount of alkali hydroxide in the system so that it will not be expected to occur if the concrete is immersed in a continuously alkali hydroxide-supplied system (Ichikawa 2009).

However, Bleszynski and Thomas (1998) observed that expansion of concrete containing reactive flint sand and inert limestone reached maximum at the proportion of 25% flint when the concrete was stored in an alkaline solution for two to three years.

Pessimum Effect Related to Aggregate Size

In general, expansion increases as particle size decreases (i.e., surface area increases) if the reaction occurs at the surface of the reactive particles. Researchers have investigated the effects of aggregate size to achieve maximum/insignificant mortar bar or concrete prism ASR expansion (Table 2.2).

Table 2.2 Mortar Bar/Concrete Prism ASR Expansion as a Function of Aggregate Size.

Researchers	Max. ASR Expansion with the Size Ranges	Insignificant ASR Expansion with the Size Ranges	Type of Materials / Test
Stanton (1940)	0.17–0.6mm		Siliceous magnesium limestone containing opal and chalcedony (Mortar bar / concrete prism)
Woods (1968)	0.07–0.85mm		Opaline aggregate particles in mortar bar
Zhang (1999)	0.15mm		Mortar bars made of siliceous aggregates
Kuroda et al. (2000, 2004)	0.48mm		Mortar bars made of only reactive aggregates
	0.15–0.30 mm		Using both reactive and nonreactive aggregates in mortar bars
Han and Tang (1984) Hobbs and Gutteridge (1979)		Less than 0.02 mm	Mortar bar expansion
Kawamura et al. (1983) Multon et al. (2008) Shayan (2002) Zhang et al. (1990)		Less than 0.05-0.15mm	
Moisson et al. (2004) Shayan (2002) Shao et al. (2000)		Up to 0.1 mm (Counteract the effect of ASR)	Mortar bar

Table 2.2 indicates that different results pertaining to the aggregate size that yields maximum ASR expansion are reported by different researchers. Some of the explanations for these differences in results are:

- ASR expansion not only depends on the aggregate size but also depends on the nature and composition of the aggregate.
- If the ASR occurs within the particle, the expansion is independent of the aggregate size (Hobbs and Gutteridge 1979).
- Ramyar et.al. (2005) has reported that aggregate with intermediate angular size fractions gives higher mortar bar expansion than that made of rounded aggregates of

the same size based on their work on the effect of angularity and size of crushed aggregates on mortar-bar expansion.

- Crushing certain types of aggregates (especially for reactive aggregates) for laboratory tests changes their reactivity characteristics (Lindgard et al. 2012).

Gao et al. (2013) also found the pessimum effect of ASR expansion with specimen to aggregate size ratio. The expansion rate is slower in all sizes of specimens containing the largest aggregates due to a delay in the diffusion of the hydroxyl ions into the reactive silica in aggregates. This pessimum effect is not an intrinsic phenomenon but depends on specimen-to-aggregate size ratio.

Role of Concrete Moisture

Moisture is an essential ingredient for ASR to occur and become expansive. Water is the main carrier of hydroxyl and cations in a form of pore solution to the reaction site, thus facilitating ASR to occur. Subsequently, the reaction product (i.e., ASR gel) absorbs moisture, causing swelling. The swelling causes high stress inside aggregates, resulting in aggregate cracking and subsequent concrete deterioration. Although concrete looks dry during its service years, it can still maintains RH in the range of 80% to 90% in the inner portions (Mukhopadhyay et al. 2009). Pedneault (1996) found that concrete displayed very small expansion at a RH less than 80%, and expansion increases exponentially when RH increases above 80%.

The moisture level might be reduced below 80% in concrete by limiting the exposure of concrete structures to moisture or the use of low permeability (concrete with low water to cement ratio (w/c)) concrete. In addition, improving drainage conditions

can also be applied as an effective way to reduce the availability of external moisture. A higher w/c can cause both increasing and decreasing of expansion due to ASR. The following phenomena can cause increase of expansion:

- Higher porosity/permeability causing higher ionic mobility and more reaction.
- Greater availability of free (capillary) water to make the gel more expansive.

The possible mechanisms that may cause reduction in expansion are: (i) higher available space (high capillary porosity due to high w/c) for gel accommodation, and (ii) relatively lower pore solution concentration (dilution effects due to high w/c) may cause slower expansion rate and lower level of expansion.

It seems that higher ionic mobility and greater availability of free water are the dominant factors for ASR and hence the net expansion should be higher with high w/c than the concrete with low w/c.

Alkalinity

Concrete consists of innumerable pores that are filled with solution containing OH^- and alkali ions (i.e., Na^+ and K^+), which play an important role in developing ASR. The primary source of alkali in concrete is cement. The alkalis primarily present in cement clinker as alkali sulfates with minor bounded alkalis in the crystal structure of the silicate phases. Alkalis are immediately released from alkali sulfates in pore solution when portland cement is mixed with water. Other sources, such as SCMs (Buck and Mather 1987; Diamond 1981), certain aggregates (e.g. mica, clay minerals, alkali feldspars, etc.) (Berube et al. 2002; Constantiner and Diamond 2003; Grattan-Bellew 1994), chemical admixtures (e.g., superplasticizers) (Mukhopadhyay et al. 2009),

seawater-contaminated aggregates or concrete, and de-icing chemicals can also contribute additional alkalis other than cement alkalis and enhance the pH of the pore solution.

The concentration of OH^-, Na^+, and K^+ in a mature cement paste (w/c = 0.5, Type I cement with 0.91% Na_2O equivalent (Na_2O_e)) was reported as 0.8N, 0.2N, and 0.4N, respectively, with a negligible concentration of Ca^{2+} (Diamond 1983). Diamond (1983) suggested that a threshold concentration required to initiate and sustain ASR is 0.25M (pH = 13.4). Kolleck et al. (1986) found that the threshold concentration to initiate ASR is 0.2M (pH = 13.3). Several other authors (Kagimoto et al. 2004; Kollek et al. 1986; Rivard et al. 2003; Shehata and Thomas 2006; Thomas et al. 2006;) have also reported the threshold concentration of hydroxyl ions in the pore solution in the range between 0.2 (pH = 13.3) to 0.3 M (pH = 13.5). Kawamura and Iwahori (2004) observed that the expansive pressure is approximately proportional to the amount of ASR gel formed, provided the alkali content of the ASR gel is less than a critical value. Different aggregates have different threshold values to initiate the reaction, which largely depends on the aggregate reactivity (Sibbick and Page 1992). If the whole aggregate is reactive and the aggregate is homogeneous, the threshold may be lower. On the other hand, if the aggregate is heterogeneous and reactive constituents occur as isolated pockets within the non-reactive phases, the threshold level may be high as the non-reactive phases (i.e., physical adsorption) may consume some alkalis. The porous aggregate may have lower threshold than less porous and low defects aggregates. A reactive aggregate may not react or have low potential to react when the alkali level in the system is below the

threshold concentration. Therefore, assigning a common total concrete bulk alkali (e.g., 4 lb/yard^3 as in special provision (TxDOT Item 421-024) irrespective of aggregate reactivity may not provide enough protection.

Cement having a Na_2O_e of less than 0.6% is generally considered as low-alkali cement. However, this kind of low alkali level in cement found to be sufficient to cause ASR in highly reactive aggregate. The bulk Na_2O_e of cement (0.6% requirement) may not always accurately define the potential of cement alkali to cause ASR and might be misleading in certain cases. Cements with similar Na_2O_e can have different K^+/Na^+ ratios and are found to be the reason for the observed differences in concrete expansion (Leeman and Lothenbach 2008). The amount of alkalis that are soluble in the concrete pore solution and hence available for the reaction is more important than the total bulk alkali content of the concrete materials. The approach of using low-alkali cement alone does not necessarily prevent ASR-induced damage because the contribution of alkalis from other sources is not considered. Alkalis may also become concentrated in a portion of the concrete through migration with moisture. Therefore, many agencies and countries specified total permissible alkali between 2.5 and 4.5 kg/m^3 (4.21 and 7.58 lb/yard^3), and stated that the boundary of total permissible alkali is not rigid but depends on the aggregate reactivity (Nixon and Sims 1992). Sibbick and Page (1992) advocated that the alkali threshold based on CPT test is between 3 to 5 kg/m^3 (5.05 and 8.43 lb/yard^3) for reactive aggregates but is lower for highly reactive aggregates. A value of 3.0 kg/m^3 (5.05 lb/yard^3) was reported as threshold concrete alkali based on the relationship between 2 years CPT expansion and concrete alkali content (Figure 2.4). However, the

occurrence of ASR expansion has also been reported even with the total concrete alkali content less than 3 kg/m^3 (Folliard et.al. 2007).

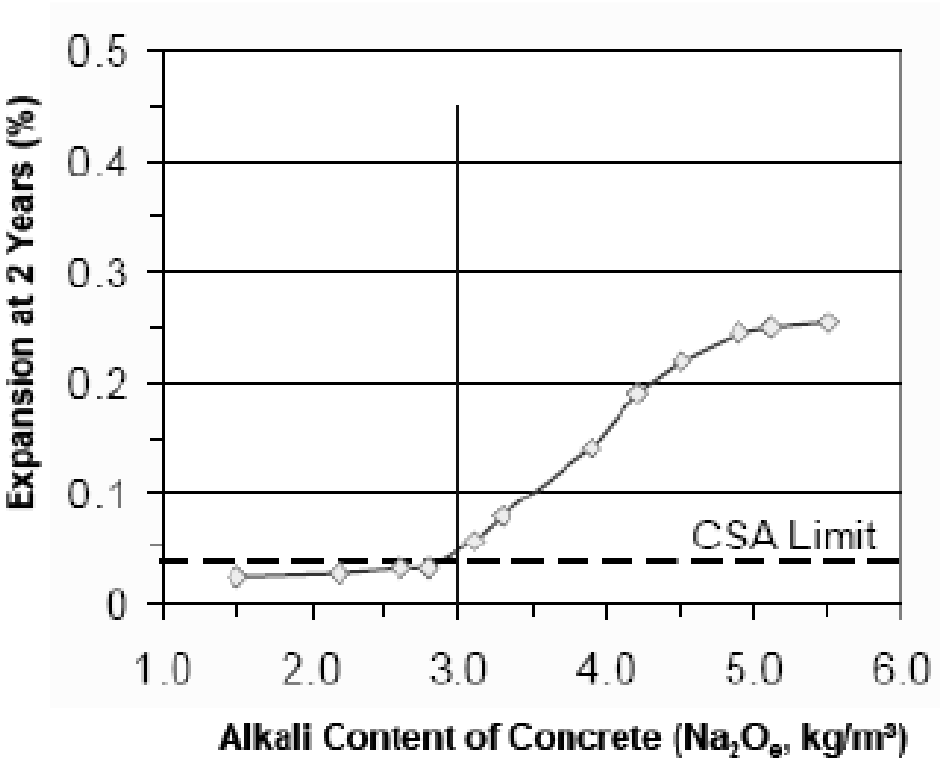

Figure 2.4 Effects of Alkali Content on Expansion of Prisms Stored over Water at 38^{o}C (Folliard et al. 2007).

Environmental Effects/External Factors

The two main environmental factors that affect ASR are:

- Variation of moisture content and temperature and associated alkali redistribution inside concrete due to seasonal climatic variations (e.g., temperature and wetting/drying cycles).

- Penetration of alkalis from external sources (e.g., seawater and deicers).

It has been reported that wetting and drying cycles enhance ASR (Mukhopadhyay et al. 2009). The concentration of alkalis in pore solution increases during drying and can concentrates locally in certain portion of the concrete elements. ASR can occur in those alkali-enriched portions, although total concrete alkali loading may be reasonably low. During the next wetting cycle, rewetting causes dilution of alkali-rich portions (making ASR slow in those areas), but it creates favorable situation for swelling of the gels that already formed during the drying cycle.

During laboratory performance testing, researchers have found that higher temperature accelerates ASR. Hobbs (1992) found that the reaction occurred for specimens stored at 38°C was seven times faster than those stored at a temperature of 9°C, and was four times faster than those stored at 20°C. Nilsson (2006) reported that an increase in temperature raises internal RH for small concrete prisms (w/c = 0.4) stored over water in a sealed container. The internal RH increases approximately 0.25%/°C, but the effect decreases when w/c increases. Therefore, when the concrete temperature increases from 25°C to 45°C, the internal RH might be increased by approximately 5%.

RH values higher than 80% are able to sustain expansive ASR in most of the pavement below the top surface layer, even in the summer in a hot desert climate (Stark et al. 1993). The data also show that humidity conditions are sufficiently moist to support expansive ASR in much of the concrete in pavements and structures for at least part of each year in most of the continental United States.

One reactive aggregate with conventional mix design mitigation measures may perform well in one geographic locations with mild environmental effects (e.g., low rainfall, low temperature, and low RH and temperature variation) but may show ASR distress in another geographic location with severe environmental factors (e.g., high rainfall, high temperature, and high temperature and RH variation, etc.). Therefore, lowering concrete total alkali loading alone might not provide enough protection for a concrete under severe ambient conditions. Applying additional protection measures depending on the severity of environmental factors is highly recommended

Role of Supplementary Cementitious Materials (SCMs)

In general, SCMs such as Fly ash, GGBS, and condensed silica fume are all used to reduce ASR expansion in concrete. The mechanisms are not well understood, but it is agreed that the reactive silica in SCMs combines with the cement alkalis (i.e., Na^+ and K^+) more readily through pozzolanic reaction than the siliceous phase(s) in aggregate. Therefore, alkalis are rapidly consumed, and the level of hydroxyl ions is reduced to a level at which aggregates react very slowly or not at all (Carrasquillo and Farbiaz 1988; Diamond and Penko 1992). Furthermore, the pozzolanic reaction results in the formation of alkali-calcium-silicate-hydrates, which is non-expansive, unlike the water-absorbing expansive ASR gels. However, not all SCMs increase ASR resistance. Some SCMs can be a source of additional alkalis. Diamond (1981) reported that Class F Fly ash is more effective in controlling ASR than Class C Fly ash. Shehata and Thomas (2000) and Shon et al. (2003, 2004) supported that Class C Fly ashes are less effective than Class F Fly

ashes in controlling ASR because some Class C Fly ashes (those with Na_2O_e greater than the cement) actually enhance alkali ions (e.g., Na^+ and K^+) and OH^- in pore solution.

Current Mechanisms of ASR

Reaction Mechanisms

ASR is the reaction between the hydroxyl (OH^-) ions present in pore solution and reactive siliceous component(s) in aggregates. The alkali cations (i.e., Na^+, K^+, Ca^{2+}, etc.) are important because their presence in high concentration leads to an equally high concentration of hydroxyl to maintain equilibrium in the pore solution. When they are incorporated into the ASR gel, the role of alkali becomes relevant.

In general, there are 4 steps in the chemical reaction mechanism of ASR (Garcia-Diaz et al. 2010; Glasser et al. 1981; Poole 1992; Wang et al. 1991).

Step 1: Neutralization of surface silanols of the reactive silica by the alkali base:

$$SiO_{5/2}H + Na^+/K^+ + OH^- \rightarrow SiO_{5/2}(K, Na) + H_2O$$

Step 2: Breaking up of siloxane bonds (Q_4) by hydroxyl ions to form Q_3 tetrahedrons:

$$SiO_2 + Na^+/K^+ + OH^- \rightarrow SiO_{5/2}(K, Na) + ½\ H_2O$$

In this step, the OH^- reacts with Si-O-Si bonds to form silanol bonds:

$$Si\text{-}O\text{-}Si + H_2O \text{ –> } Si\text{-}OH\ldots.OH\text{-}Si$$

Step 3: Dissolution of silica due to continued hydroxyl ions attack on the Q_3 tetrahedron to form silica ions and small polymers:

$$SiO_{5/2}(K, Na) + Na^+/K^+ + OH^- + ½\ H_2O \rightarrow H_2SiO_4^{2-} + 2(Na^+/K^+)$$

Step 4: "Gelation" of expansive ASR silica gels from the silica saturated pore solution.

The products of the above acid base reaction (Step 2) are a molecule of water and the negatively charged Si-O^-. These negative charges attract positive alkali cations such as sodium, potassium, and calcium and form ASR gel (Steps 3 and 4). The number of positive cations should be sufficient enough to maintain charge balance in the system. Dent-Glasser and Kataoka (1981) summarized the entire ASR chemical reaction as:

$$H_{0.38}SiO_{2.19} + 0.38Na_2O \rightarrow Na_{0.38}SiO_{2.19} + 0.38H_2O$$

As shown in the above equation, sodium was involved to achieve charge balance, but in reality other cations (e.g., K^+, Ca^{2+}) also participate in charge balancing. The product of the above reaction is called ASR gel and composed of SiO_2, Na_2O, K_2O, CaO, and water. According to many researchers, ASR may take the form of either a gel or poorly crystalline material (Stewart 2005). The ASR product by itself is not deleterious; however, the problem occurs when this gel absorbs water, resulting in greater volume than the one that it replaces, and creating high swelling pressure and expansion. Studies have shown that these gels maintained quasi-state equilibrium with water. During drying cycles, the alkali concentration increases and therefore the ionic content of the gel increases. On the other side, during wet cycles, the reverse reaction happens. Since these gels have different chemical composition and different densities at different periodic cycles, the amount of swelling is extremely difficult to predict (Swamy 1992).

Expansion Mechanisms

Although the chemical reaction mechanisms that govern ASR are well understood, the expansion mechanisms still remain unclear and are a point of controversy. The most common and circulated theories in the literature regarding ASR expansion mechanism are briefly described below:

Formation of Osmotic Pressure Cell

Hansen (1944) proposed that the cracking that occurred in the concrete was due to the formation of an osmotic pressure cell surrounding the aggregate. In the theory, hardened cement paste act as a semi-permeable membrane on silicate ions passage. The membrane allows water molecules and alkali hydroxides to diffuse in, but prevents silicate ions to diffuse out. The alkali silicate that formed on the surface on an aggregate surface would draw solution from the cement paste to form a liquid-filled pocket. The liquid that was drawn in would then exert an osmotic pressure against the confining cement paste, leading to cracking.

Swelling Theory

McGowan and Vivian (1952) postulated that cracking in concrete should relieve the osmotic pressure and prevent any further expansion. Instead, they proposed the "Swelling theory" in which alkali silica gel (a product of reacted aggregates) absorbs water, leading to swelling in the gel, which causes expansive pressure and eventually causes concrete cracking. Other researchers (Tang 1981) also agreed with this theory.

Swelling Theory Controlled by Lime

Powers and Steinour (1955) believed that the theories that both Hansen (1944) and McGowan and Vivian (1952) proposed were fundamentally similar. They thought that the primary damage mechanism was swelling of the solid reaction product as controlled by the amount of lime it contained, but the osmotic pressure might also develop. When a silica particle is exposed to a strong base, the hydroxyl ions attack the surface and gradually penetrate the particle. If the attack occurs in the presence of excess lime, then a non-swelling lime-alkali-silica complex is formed when chemical equilibrium with the lime is reached. However, if the alkali-silica complex is not in equilibrium with the lime, then swelling will occur. When the alkali-silica complex imbibes water, the researchers believe that the swelling is due to the displacement of colloidal units with respect to one another.

One cause of insufficient lime is that alkalis in the solution depressed the lime, so not enough lime may be available at the reaction site to form the non-expansive gel. Another cause is that the lime-alkali-silica complex can hinder the diffusion of the calcium ion to the reaction site while allowing the other ions to diffuse to form additional gel that can swell. For the osmotic pressure to buildup, the researchers explained that water within concrete would tend to move to regions where it has the lowest free energy. The water that the alkali-silica complex held has lower free energy than water external to the complex. As the strength of the solution within the alkali-silica complex increases, greater osmotic pressure is required to prevent the entry of additional water into the complex. If the alkali-silica complex is fluid and confined, then osmotic

pressure may be generated. If the alkali-silica complex is solid, the swelling of the reaction rim may still generate pressure.

Diffusion Theory Controlled by Calcium

Chatterji et al. (1986, 1989) proposed that when hydroxyl ions are placed in a solution with a pH of 7 or greater, these ions penetrate reactive siliceous particles, in amounts increasing with solution pH and ionic strength. At a constant solution pH and ionic strength, the absorption of OH^- decreases with the increasing size of the associated hydrated cation (OH^- absorption decreases in the series K^+, Na^+, Li^+, Ca^{2+}). In a pore solution with mixed ionic species (e.g., $Ca(OH)_2$ and NaCl), the cations will penetrate into the reactive silica grain following the penetrating OH- ions; however, more of the smaller hydrated cations will do so than the larger ones (in this example, hydrated Na+). After that, penetrating OH^- ions attack siloxane bonds, and this reaction further opens up the reactive silica grain to attack. Silica ions are liberated from their original sites, enabling them to diffuse out of the reactive grains. Ca^{2+} controls the rate of silica diffusing out of reacting grains in the immediate vicinity. A higher Ca^{2+} ion concentration lowers or impedes silica diffusion away from the reactive grains. Finally, when the net amount of materials (Na^+, K^+, Ca^{2+}, OH^-, and H_2O) entering a reactive silica grain exceeds the amount of materials leaving (Si^{4+}), expansion occurs.

Diffuse Double Layer Theory

A theory was proposed citing electrostatic repulsion between diffuse double layers (DDLs) as responsible for generating expansive forces (Prezzi 1997; Rodrigues

et al. 1999). Very high negative charges are observed at the surface of the silica grains (Bolt 1957; Rodrigues et al. 1999). To counterbalance the negative silica charges, an electric double layer of positive charges (cations) develop and adsorb around the silica surface. Two layers defined as the Gouy-Chapman layer or the Stern layer has a collective thickness of a few nanometers that can be calculated from the ionic strength of the pore solution electrolyte. The double layers are composed of calcium, potassium and sodium, and some other anions, but the net charge of the whole system is equal to zero. This system will form a colloidal suspension and then conglomerate into a gel (Prezzi 1997). The chemistry of this gel depends on the chemistry of the pore solution, the pore structure in the concrete, and the environmental condition. The amount of repulsive forces and the thickness of the electric double layer depend on the valence of the cations in the gel and their concentration in the double layer (Prezzi 1997; Rodrigues et al. 2001). Consequently, bivalent ions (Ca^{2+}) will generate more repulsive forces and a larger electric double layer thickness than monovalent ions (Na^{+}). Therefore, gels with a high concentration of calcium will produce lower expansive forces than those containing a high amount of sodium and vice versa (Rodrigues et al. 1999). Diamond (1989) indicated that the expansive pressures because of gel swelling are in the range 6 to 7 MPa, but expansive pressure of 10.3 MPa was calculated using conventional double layer equations (Rodrigues et al. 1999).

Expansive Pressure Theory due to the Formation of Reaction Rim

In 2007, Ichikawa and Miura conducted research on the effect of ASR-generated hydrated alkali silicate on the development of expansive pressure inside aggregates. The

results show that the alkali silicate does not develop expansive pressure unless an insoluble, dense reaction rim surrounds the aggregate. ASR consumes alkali hydroxide and then induces the dissolution of Ca^{2+} ions into pore solution. The Ca^{2+} ions react with alkali silicate to form an insoluble reaction rim. The reaction rim acts like a barrier, which allows the penetration of alkaline solution but prevents the leakage of alkali silicate. This accumulates the formation of viscous alkali silicate by ASR in the aggregate to develop an expansive pressure enough to crack the aggregate and the surrounding cement paste.

Aggregate Swelling Associated with Siloxane Bond Breaking (Q4 to Q3 Transformation)

Garcia-Diaz et.al. (2006) proposed a novel mechanism for the ASR damage. Two reaction steps are taken into account in the mechanism: the Q_3 tetrahedrons formation by breaking up siloxane bonds (Q_4) and the dissolution of these Q_3 tetrahedrons. They demonstrated that the Q_3 tetrahedrons formation in the aggregate prevails over dissolution during the swelling step and contributes to an internal silica gel generation (may not be similar to conventional ASR gel). The Q_4 to Q_3 transition is expansive and is responsible for the swelling and cracking of the aggregate. They observed significant increase of the aggregate pore volume associated with this transition. They observed a linear relationship between the mortar bar swelling and the aggregate swelling due to this transition.

Current Test Methods for Predicting ASR Potential

The section provides an overview of the main laboratory test methods that are currently used to evaluate alkali silica reactivity of aggregates. Figure 2.5 shows several of the current test methods to assess ASR prior to their use in concrete structures. The current test methods are classified into two categories: aggregate testing and cement-aggregate combination testing.

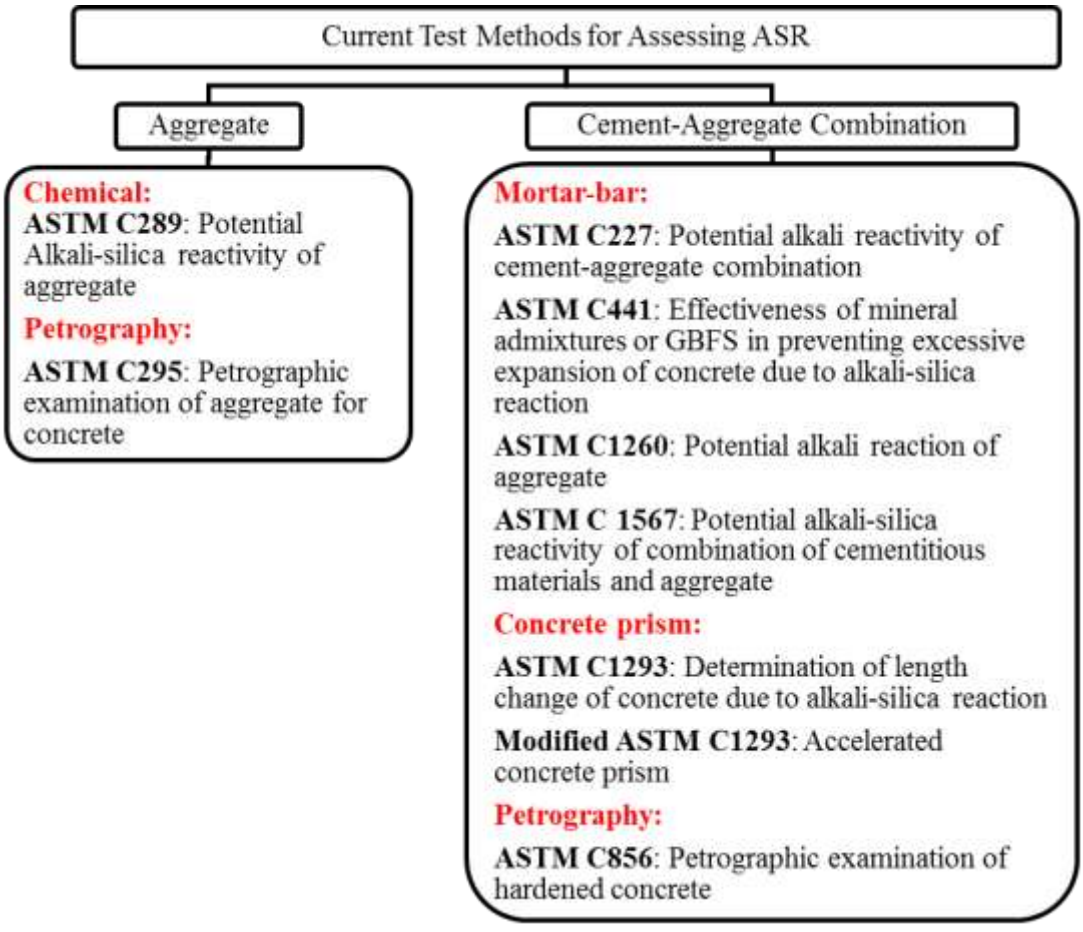

Figure 2.5 Current Test Methods for Assessing ASR.

The most commonly used tests for assessing aggregate ASR potential are ASTM C 1260/ASTM C 1567 (AMBT) and ASTM C 1293 (CPT). A brief description of the procedure along with its usefulness and limitations of AMBT and CPT are summarized below.

ASTM C 1260: Standard Test Method for Potential Alkali Reactivity of Aggregates (Mortar-Bar Method) is a modification of ASTM C 227 (ASTM 2008) for assessing the potential reactivity of aggregates. Aggregates are crushed to meet specific grading requirements. Prepared mortar bars are soaked in 1N NaOH solution at 80°C for 14 days. The purpose of using severe test conditions such as high level of alkalinity and temperature along with crushing aggregate is to accelerate ASR in mortar bars. As a result, expansions of mortar bars are obtained within as little as 16 days. The test method was developed because of the shortcomings of ASTM C 227 and ASTM C 289 (ASTM 2008). Several researchers and agencies have also referred to the ASTM C 1260 method as the accelerated mortar bar test method.

Earlier research indicates that the AMBT method should be used with caution when rejecting aggregates. The test conditions (i.e., 1N NaOH and 80°C) are severe and the test results are unrelated to field performance. Aggregates with a good field track record in terms of ASR can sometimes be classified as reactive when tested according to this method. This is supported by the observation that some aggregates failed by the AMBT method actually passed by the CPT method (i.e., false negatives). A heterogeneous distribution of reactive constituents within the aggregate is common for certain aggregates (e.g., reactive cementing materials in sandstone, reactive siliceous

impurity in limestone, etc.). Losing the reactive phases during crushing and sieving of these aggregates (part of sample preparation in C 1260) sometimes causes aggregates passed by the AMBT but failed by the CPT (i.e., false positives).

ASTM C 1293: Standard Test Method for Concrete Aggregates by Determination of Length Change of Concrete due to Alkali Silica Reaction involves measuring length change of concrete prisms made with the coarse or fine aggregates under investigation. A non-reactive fine aggregate is used when the coarse aggregate is reactive and vice-versa. Additional alkali (NaOH) is added to the concrete mixture in order to elevate the alkali level (1.25% Na_2O_e by mass of cement) of the concrete. De-molded prisms are stored above water at 38°C in a sealed container.

Test method ASTM C 1293 is considered the best index for field performance, but the duration of the test (a year or more) represents a major drawback. Experience has shown that a higher level of alkali is required to initiate expansion in the CPT than in field concrete produced with the same aggregate. Quick reduction in pH of the pore solution as a result of significant alkali leaching is reported in the CPT than it does in actual field concrete. Moreover, no wetting or drying takes place in this test method. As a result, this test tends to underestimate the extent of the reaction that would take place in a field concrete made with the same mix as the test. Berube et al. (2000) suggested that the test conditions are too severe as the concrete prism test may identify some aggregates with generally good field performance as being potentially reactive. Moreover, both the CPT and the AMBT tests are conducted at a single alkali level, which is quite high compared to the field concrete. As a result, these methods cannot

study the effects of cement alkali and threshold alkalinity cannot be determined. The CPT method is not capable of evaluating field mixes (i.e., job mixes) as the CPT prescribes a standard mix design. Similarly, there are no provisions to test differently, or to use different limits for different exposure or service conditions. And thus for many situations, the level of prevention that will satisfy the test may be overly conservative. It can be generalized that the AMBT is harsher than field service, while the CPT is milder than field service.

The primary requirements for any accelerated ASR test method are: (i) it should be able to predict correctly the potential reactivity of aggregate in over 95% of the cases (Grattan-Bellew 1989, 1997), and (ii) inter-laboratory coefficient of variation should be low, preferably less than 12%.

Owing to the complexity and variability in composition and grain size of aggregates, it is unlikely that a single test method can correctly evaluate all types of aggregates. Researchers and agencies worldwide have proposed some of the new methods or modifications of existing methods to overcome some of the limitations associated with aggregate crushing, alkali content, storage conditions (alkalinity of test solution and temperature), and leaching. However, current test procedures are largely empirical and yield test results that are applicable to a narrow band of conditions. It is clear that there is a lack of a unified approach to address how different combinations of concrete materials may interact to affect ASR behavior and warrant a different approach for ASR testing. A fast and reliable testing protocol that can measure aggregate reactivity matching with field levels of alkalinity and temperature is warranted.

Kinetic Approach for the Determination of ASR Aggregate Reactivity

ASR is a chemical reaction where some initial conditions related to alkalinity, aggregate reactivity, moisture, and temperature conditions must be met to initiate ASR. ASR is a kinetic type of chemical reaction that integrates the combined effects of temperature, alkalinity, moisture, and time relative to the kinetics of ASR expansion.

Kawamura and Iwahori (2004) found that the expansive pressure is approximately proportional to the amount of ASR gel formed provided the alkali content of ASR gel is less than a critical value. The authors also found that even when AMBT greatly expanded in tests without restraint, mortar bars containing ASR gel with higher alkali content (similar to ASTM C 1260) than the critical value showed extremely low expansive pressure. The authors, therefore, concluded that in existing ASR-affected concrete structures containing gels with higher alkali content than a critical value, damages due to the secondary stresses caused by restraint might not be so significant, even if reactive aggregates used in the concrete have showed greater expansions in mortar bar tests in the laboratory. This knowledge allows for greater understanding of the kinetics involved with the formation of gel and its subsequent expansion. Therefore, kinetic-type models can be used to derive characteristic material properties and assess ASR fundamentally. In the past, researchers have investigated the use of a kinetic-type ASR model for either the prediction of mortar bar expansion (Uomoto et al. 1992) or for better interpretation of the existing test methods (Johnston et al. 2000). A brief discussion on previous kinetic type approaches and applications are shown as follows.

Sorrentino et. al. (1992) introduced the French kinetic chemical test similar to the ASTM C 289 chemical method. The method consists of measuring the amount of silica dissolved into 1N NaOH solution at 80°C for 96 hours, which includes the time parameter. After conducting many tests, the authors suggested a chart (Figure 2.6) displaying different degree of ASR reactivity with zones representing deleterious and innocuous aggregates. They also mentioned that based on the test results, their new test procedure was able to detect aggregates that displayed a pessimum effect.

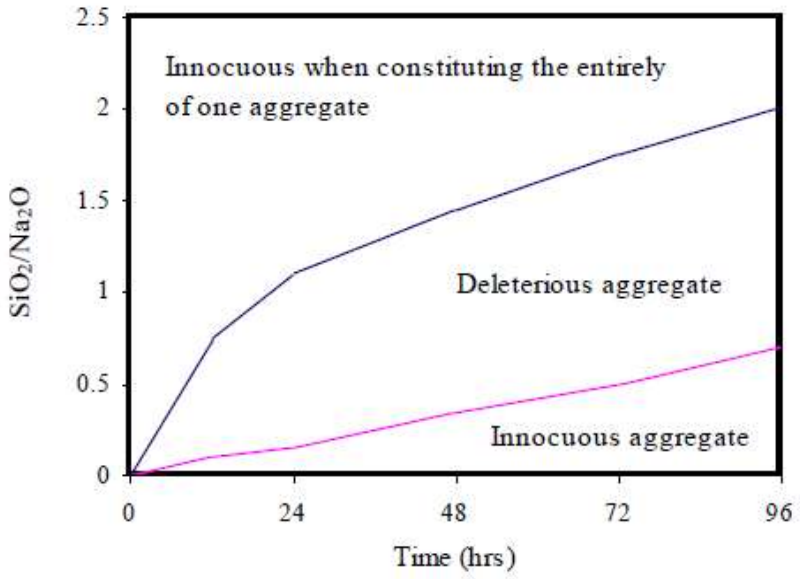

Figure 2.6 Chart of the Kinetic Test (Sorrentino et al. 1992).

Uomoto et.al. (1992) introduced a kinetic model to predict the expansion behaviors of mortar bars. The expansion behaviors were calculated by alkali diffusion coefficients in aggregates and alkali-silica ratio (RS) of reaction products. The alkali

diffusion coefficients and RS were determined by the leaching test in accordance with ASTM C 289. However, the model is based on many assumptions without experimental verification. Thus, experiments are needed in order to improve the model.

Using the Kolmogorov-Avrami-Mehl-Johnson model, Johnston et al. (2000) proposed a kinetic-based approach to overcome some of the deficiencies in specifying the percentage of expansion to distinguish between reactive and non-reactive aggregates in ASTM C 1260. This procedure is based on growth and nucleation where the power of time and the percent expansion are related to each other exponentially as follows:

$$\alpha = \alpha_0 + (1-\alpha_0)(1-\exp(-k(t-t_0)^M))$$

where

α_0 is the degree of reaction at time t_0

k is the rate constant

t_o is the time when growth and nucleation are dominant

M is exponential factor.

By applying a least square fit to the logarithmic form of the kinetic model, two parameters, ln(k) and M, were generated. Figure 2.7 shows two distinctive areas by plotting M against ln(k). The test results show that reactive aggregates are associated with ln(k) > -6 and non-reactive aggregates are associated with ln(k) < -6. This method was effective in determining the amount of mineral admixtures necessary to mitigate ASR. The main disadvantage of this procedure is that the analysis was done using AMBT, which only takes 16-day testing periods. However, the aggregates needed to be

crushed and therefore the surface area and the reactivity of the aggregate were altered and no longer represented real concrete.

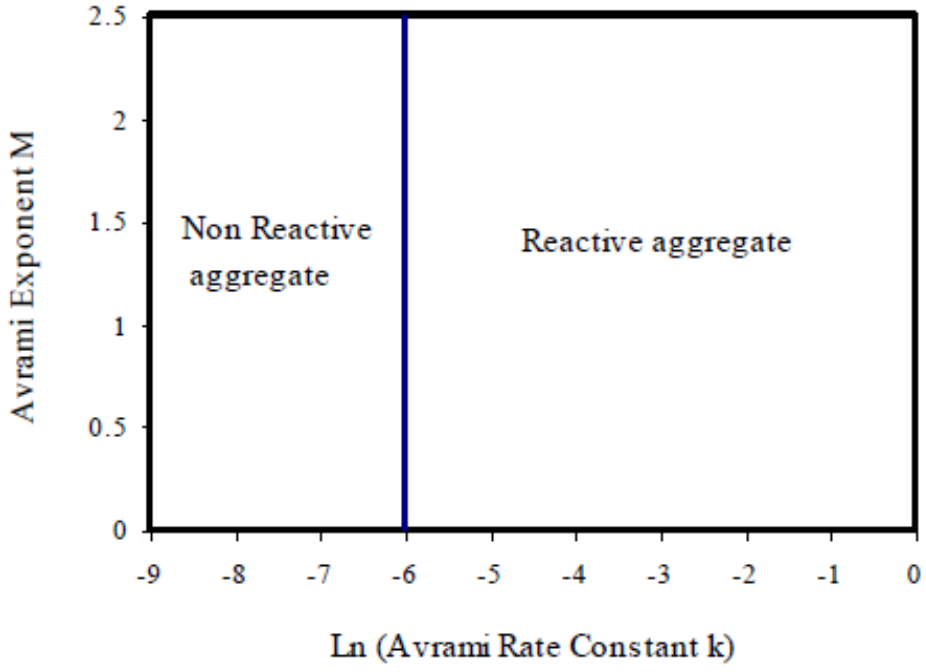

Figure 2.7 Avrami Exponent vs. Rate Constant (Johnston et al. 2000).

CHAPTER III

MATERIAL CHARACTERIZATION

This chapter presents aggregate selection, collection and characterization. The selected aggregates were critically evaluated by the record of alkali silica reactivity based on the current methods (e.g., ASTM C 1260 and C 1293) and field performance (as much as available from beams/blocks, precast girders, field structures, etc.) data to cover a wide range of reactivity, mineralogy and geographic locations. More emphasis on selection of aggregates from the exclusion list as well as aggregates belong to false positives/negatives categories was also performed. The selected and collected aggregates were evaluated in terms of overall mineralogical composition, type, and distribution of the reactive components through petrographic examination of thin sections (ASTM C 295).

Material Selection

Pure phase material (borosilicate glass balls) and aggregates (both coarse and fine aggregates) were selected in this study. The pure phase material was tested first to validate the proposed approach before any aggregate testing. One aggregate (i.e., New Mexico Rhyolite (NMR)) from the previous study (Ghanem et al. 2010) was collected and tested in this study for verification purpose. Table 3.1 provides detailed information on the selected aggregates.

Table 3.1 List of Selected Aggregates.

Aggregate	ASTM C 1260 (14-day Expansion, %)	ASTM C 1293 (1-year Expansion, %)	Block 0.95% / 1.25% Na_2O_e
NMR	1.3	-	- / -
FA1	0.554	0.590	- / -
FA2	0.334	0.171	0.5492 / 0.9064
FA3	0.317	0.058	- / -
FA4	0.242	0.043	- / -
FA5	0.079	0.035	0.0026 / -
CA1	0.417	0.078	- / 0.2609
CA2	0.250	0.047	- / -
CA3	0.227	0.071	- / -
CA4	0.179	0.149	0.004 / 0.1864
CA5	0.140	0.020	0.165 / 0.0697
CA6	0.100	0.097	- / -
CA7	0.040	0.129	- / -
CA8	0.012	0.027	0.0026 / -
FA6	0.381	0.391	- / -
FA7	0.019	-	- / -

FA: fine aggregate; CA: coarse aggregate, NMR-New Mexico Rhyolite

For comparison purposes, the gradations for coarse and fine aggregates were kept as a fixed parameter and met ASTM C 33 (ASTM 2008) specification (Figure 3.1). Grading requirements for coarse aggregates are based on nominal size from 1 inch to No. 4. Additionally, all aggregate-related properties (i.e., dry unit weight (DRUW), specific gravity (SG), and absorption capacity (AC)), were also measured using ASTM C 127, C 128, and C 138, and summarized in Table 3.2

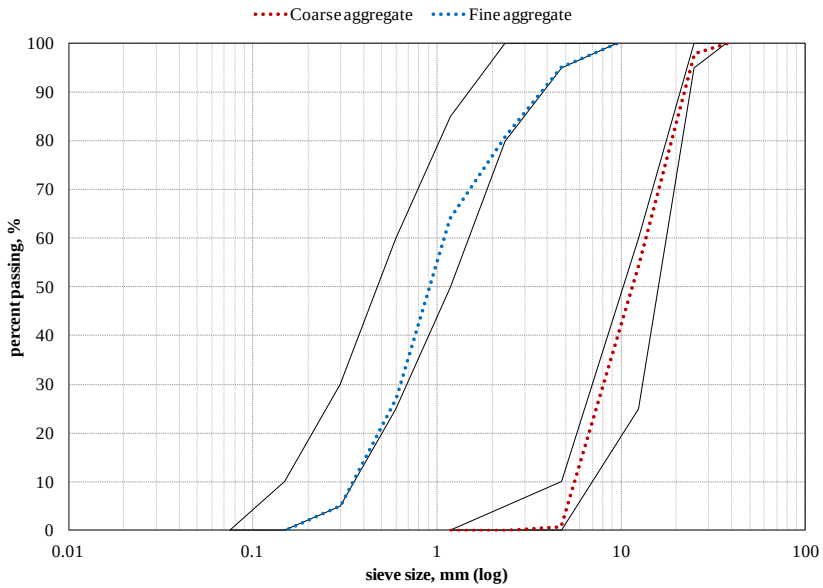

Figure 3.1 Gradation Curves of Aggregates.

Table 3.2 Properties of Aggregates.

Aggregate	DRUW, lb/ft^3	AC, %	SG_{od}	SG_{ssd}
NMR	100.037	1.41	2.56	2.59
FA1	108.627	1.98	2.56	2.61
FA2	109.148	2.22	2.52	2.58
FA3	108.515	1.32	2.59	2.62
FA4	103.855	1.08	3.08	3.11
FA5	102.542	6.18	2.34	2.48
CA1	102.447	0.86	2.58	2.60
CA2	109.751	1.45	2.58	2.62
CA3	96.134	1.43	2.57	2.61
CA4	100.209	0.87	2.57	2.59
CA5	97.103	1.30	2.57	2.61
CA6	95.119	0.98	2.71	2.73
CA7	102.575	0.60	2.56	2.58
CA8	95.317	2.47	2.50	2.56
FA6	110.777	2.69	2.52	2.59
FA7	109.685	2.33	2.52	2.58

DRUW: dry unit weight; AC: absorption capacity; SG: specific gravity

Aggregate Characterization

The aggregates that were collected (Table 3.1) were evaluated in terms of overall mineralogical composition, type, and distribution of the reactive components through petrographic examination of thin sections (ASTM C 295). The type (mineralogy), nature of distribution, and content of the reactive constituent(s) determine the reactivity of an aggregate. Aggregate alkali-silica reactivity is a function of the form/degree of crystallinity, grain size, texture, and proportion of the reactive silica within the reactive aggregate. Not all forms of silica are ASR reactive. The more disordered the structure of the silica phase, the greater the reactivity. In general, the metastable types of silica (e.g., opal, chalcedony, tridymite, crisobalite, and some disordered forms of quartz (e.g., cryptocrystalline and strained quartz)) and alumina-silicate glasses (e.g., acid volcanic glass) are known to be reactive with the alkalis in concrete. The crystalline quartz (e.g., present in igneous rocks) is not considered susceptible to ASR, whereas strained quartz (e.g., present in metamorphic or sedimentary rocks) is reactive.

The petrographic characterization of an aggregate in terms of determining (i) mineralogy, (ii) type, and (iii) distribution of reactive constituent(s) by optical microscope is the first step in assessing aggregate reactivity (ASTM C 295). An effective use or better interpretation of any ASR testing can only be possible if the above aggregate characterization parameters are known. For example, petrographic observations can provide very useful information to explain why an aggregate passes by ASTM C 1260 but fails by ASTM C 1293 (e.g., sandstone aggregate). Aggregate porosity can have considerable influence on the ultimate expansion of concrete. Studies

done on Demark flint aggregates have shown this effect (Broekmans 2002). Migration of reactive ions (Na^+, K^+, Ca^{2+}, and OH^-) can be facilitated by interconnected pores as well as layered structures and other weak planes in aggregates. Certain aggregates, such as granite, glassy volcanic rocks, and clay minerals in siliceous limestone can contribute additional alkalis in pore solution, which can be considered one of the factors for ASR, even with low-alkali cement.

Representative particles of different sizes were selected for each aggregate to prepare thin section. The thin sections (50 by 75 mm or 2 by 3 inch) for all the aggregates were prepared with blue dye impregnation to highlight the pores and microcracks. A Nikon Labophot 2-POL transmitted light microscope with magnification range 4-40X was used to observe the thin sections. A Lumenera Infinity 1-3C digital camera at 3 megapixel resolutions was used to acquire digital micrographs. A scanning electron microscope with field-emission gun (SEM-FEG) attached with a FEI Quanta 600 EDS was used to perform higher magnification observation of some selective aggregates. Aggregates were coated with 8nm Pt / Pd before being examined in secondary electron mode (SE). The operating conditions were set at 10 kV with beam current greater than 100 nA.

Based on the thin section observations, the reactive constituents for each aggregate were identified (Table 3.3). The representative photomicrographs of the reactive constituent(s) for each aggregate are presented in Figures 3.2 to 3.16. Figure 3.17 is the Scanning Electron Microscope (SEM) images of borosilicate glass and an acid volcanic particle from a fine aggregate (FA1) before testing.

Table 3.3 Reactive Component (s), Mineralogy, and Other Relevant Material Data.

Aggregate	Rock type	Reactive Constitute
NMR	Volcanic rock	Acid volcanic
FA1	RG (Volcanics, Cherty)	Acid volcanic, chert, strained QTZ (Figure 3.2)
FA2	RG	Mainly chalcedony, chert, strained QTZ (Figure 3.3)
FA3	RG	Strained QTZ, chert, chalcedony (Figure 3.4)
FA4	LS	Chert, strained QTZ, siliceous inclusions (Figure 3.5)
FA5	LS	NR w/ few siliceous inclusions (Figure 3.6)
CA1	RG (Volcanics, Cherty)	Acid volcanic, chert, QTZ (Figure 3.7)
CA2	LS	Chert, strained QTZ, siliceous inclusions (Figure 3.8)
CA3	LS	Chalcedony (Figure 3.9)
CA4	RG	Chalcedony, chert, QTZ (Figure 3.10)
CA5	LS	Separate chert particle (Figure 3.11)
CA6	LS	Strained QTZ, siliceous inclusions (Figure 3.12)
CA7	RG	Chalcedony, chert, QTZ (Figure 3.13)
CA8	LS	NR w/ few siliceous inclusions (Figure 3.14)
FA6	RG	Acid volcanic, chert, QTZ (Figure 3.15)
FA7	LS	NR w/ few siliceous inclusions (Figure 3.16)

LS: limestone; RG: river gravel; QTZ: quartz; NR: non-reactive.

Acid volcanic Microcrystalline quartz/Chert Strained quartz

Figure 3.2 Petrographic Observations of FA1.

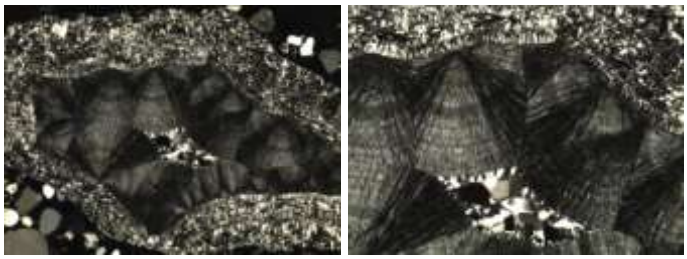

Mainly chalcedony

Chert Chert Strained quartz

Figure 3.3 Petrographic Observations of FA2.

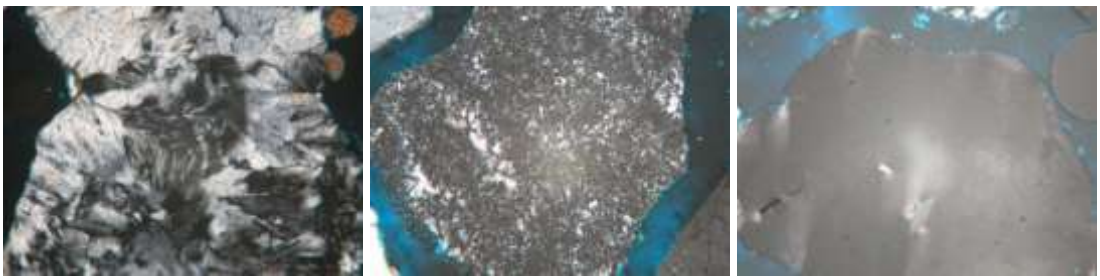

Chalcedony/chert Micro-crystalline quartz/chert Strained quartz

Figure 3.4 Petrographic Observations of FA3.

Figure 3.5 Petrographic Observations of FA4.

Mainly Limestone (nonreactive) with few siliceous inclusions

Figure 3.6 Petrographic Observations of FA5.

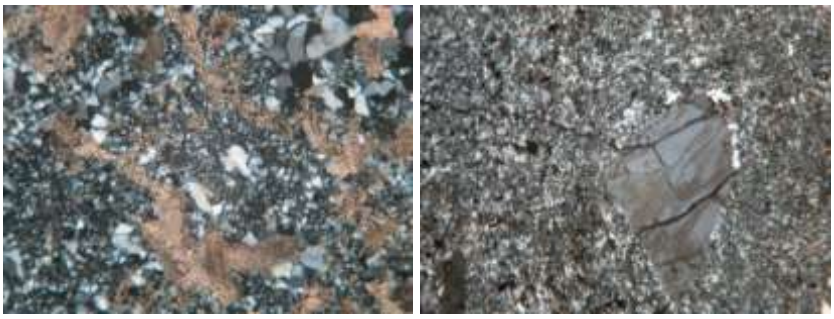

Cherty particles in limestone matrix Acid volcanic

Figure 3.7 Petrographic Observations of CA1.

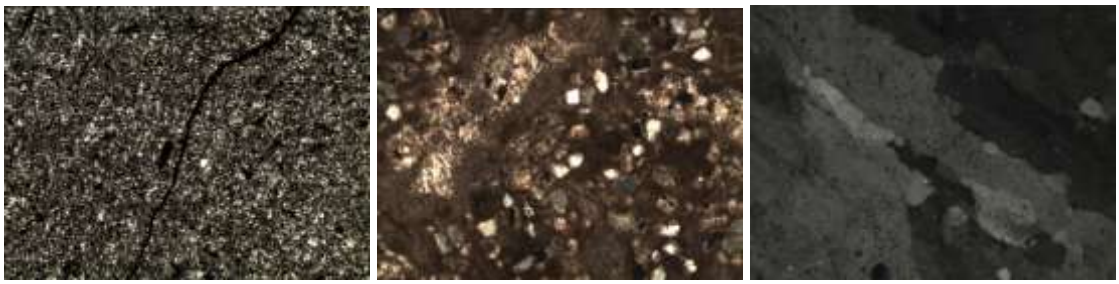

Chert Siliceous inclusions in Lst Strained quartz

Figure 3.8 Petrographic Observations of CA2.

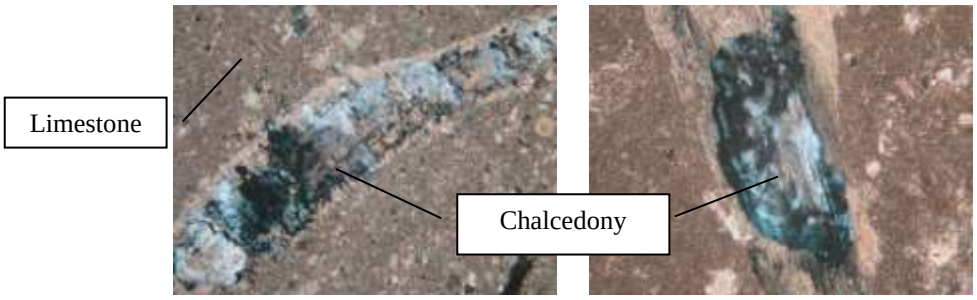

Chalcedony within limestone

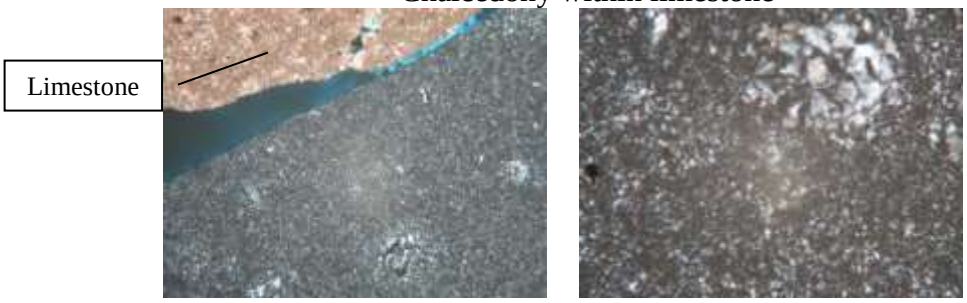

Separate Chert particles

Figure 3.9 Petrographic Observations of CA3.

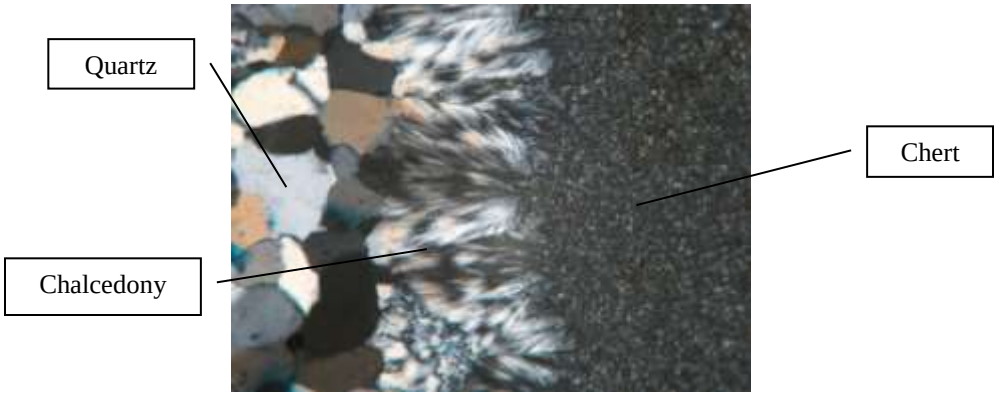

Quartz/Chalcedony/Chert

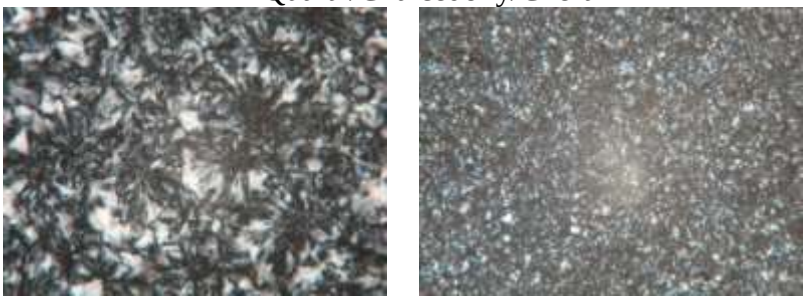

Chalcedony/chert Micro-crystalline quartz/chert

Figure 3.10 Petrographic Observations of CA4.

Separate chert particles

Figure 3.11 Petrographic Observations of CA5.

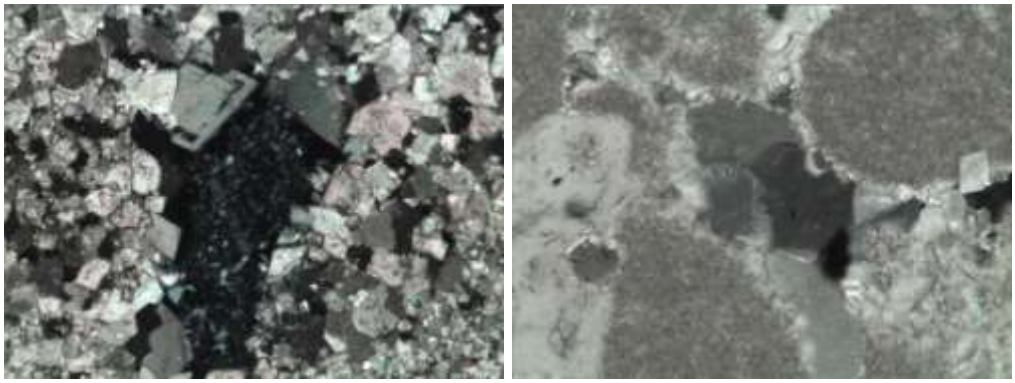

Siliceous inclusions Strained quartz

Figure 3.12 Petrographic Observations of CA6.

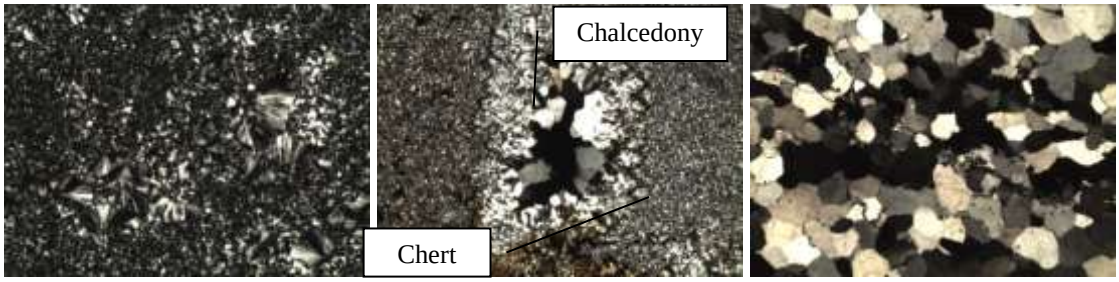

Chert Chalcedony/Chert Multigrain quartz

Figure 3.13 Petrographic Observations of CA7.

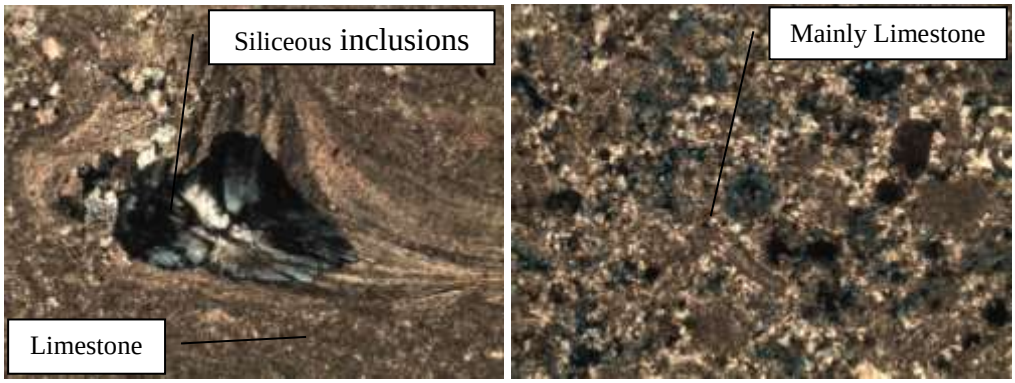

Mainly Limestone (nonreactive) with few siliceous inclusions

Figure 3.14 Petrographic Observations of CA8.

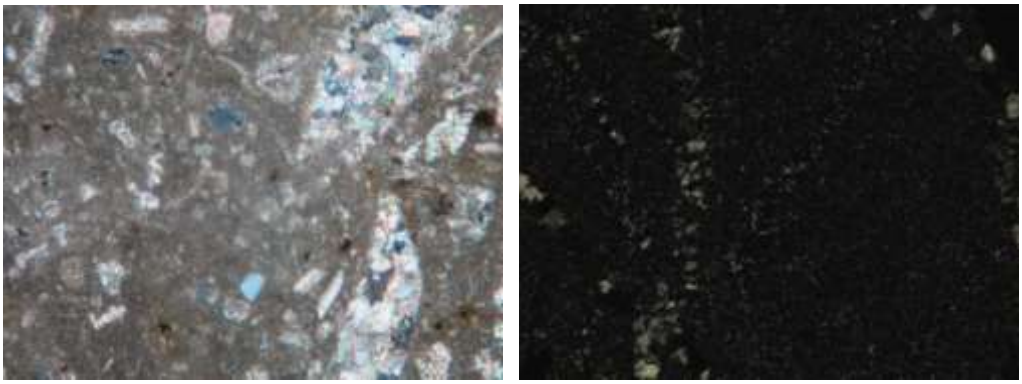

Acid volcanic Quartz/Chert

Figure 3.15 Petrographic Observations of FA6.

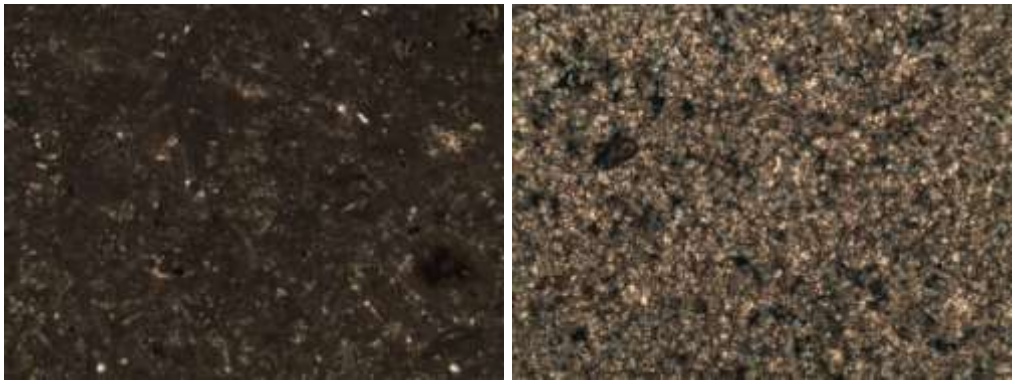

Mainly Limestone (nonreactive) with few siliceous inclusions

Figure 3.16 Petrographic Observations of FA7.

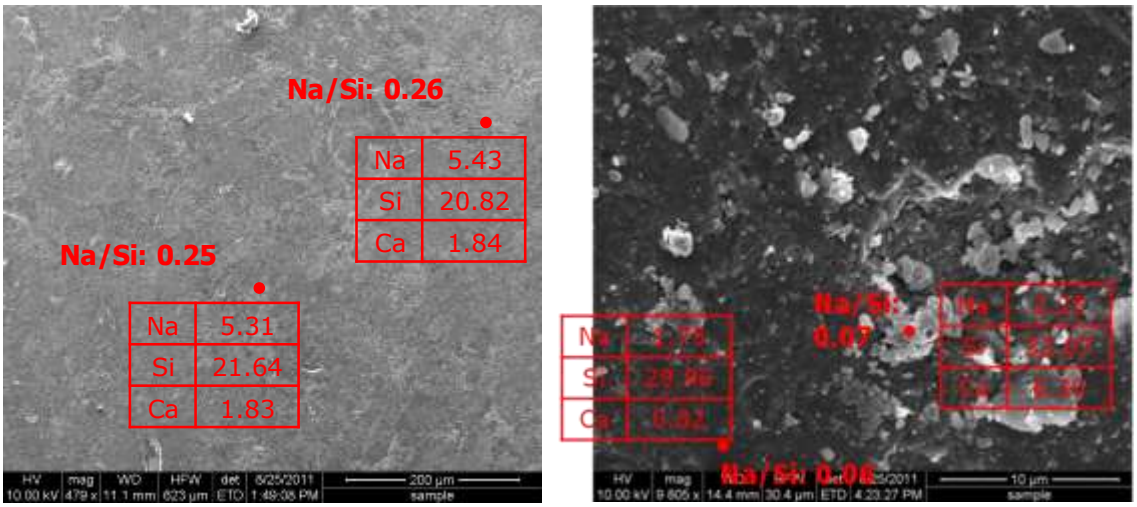

Figure 3.17 Secondary Electron Images and EDS of (Left) A Borosilicate Glass Ball, (Right) A Reactive Particle in Fine Aggregate (FA1). *Note: Even at high magnification, the presence of micro-crystalline structure is not observed in Figure 3.17 (Right). This kind of particle will be highly reactive in alkaline solution.*

Aggregates containing acid volcanic glass are considered highly reactive (Barringer 2000), and strained quartz and chalcedony are susceptible to alkali attack due to its poor crystal structure (Roger 1999). If the aggregates contain microcrystalline quartz/chert inclusions, they are considered slow / late reactive aggregates (Gillott et al. 1973). Based on the Petrographic observations, an attempt has been made to predict the reactivity of each aggregate (Table 3.4). In general, aggregates that have high expansion from ASTM C 1260 14-days AMBT testing contain more than one reactive constituent, e.g., (i) silica minerals with poorly crystalline structure (e.g. chert with predominantly chalcedony [cryptocrystalline silica with fibrous structure]), (ii) strained quartz, and (iii) acid volcanic rocks. For the aggregate passes by ASTM C 1260 but fails by ASTM C 1293 (e.g. CA7), quartzite particles along with chalcedony and cherty materials were identified. Some of the reactive constitutes (e.g., cementing materials in quartzite) might have been

lost during crushing, which explains why this aggregate was passed by ASTM C 1260. Aggregates with high porosity enhance the ASR reactivity due to increased permeability and easier access to concrete pore solution (Broekmans 2002; John et al. 1998). For the aggregate passes by ASTM C 1293 but fails by ASTM C 1260 (e.g., CA5), chert particles mostly occur as inclusions within limestone, which is considered to be slowly reactive constitute. The low porosity of the aggregate along with slowly reactive siliceous inclusion might be the reason why ASTM C 1293 gave a passing mark.

Table 3.4 ASR Aggregate Reactivity Based on Petrography Observations.

Aggregate	ASTM C 1260 (14 days)	ASTM C 1293 (1 year)	ASTM C 295 (Dominated Reactive Constitute)	ASR Reactivity
NMR	1.3	-	Acid volcanic (HR)	HR
FA1	0.554	0.590	Acid volcanic (HR) + high strain QTZ (HMR) + Chert (SR)	
CA1	0.417	0.078	Acid volcanic (HR) + Chert (SR)	
FA6	0.381	0.391	Acid volcanic (HR) + Chert (SR)	
FA2	0.334	0.171	High strained QTZ (HMR) + Chalcedony (HMR) + chert (SR)	
FA3	0.317	0.058	Low strained QTZ (MR) + Chalcedony (HMR) + Chert (SR)	
CA2	0.250	0.047	High strained QTZ (HMR) + Chert (SR)	MR
FA4	0.242	0.043	High strained QTZ (HMR) + Chert (SR)	
CA3	0.227	0.071	Chalcedony (HMR) + Chert (SR)	
CA4	0.179	0.149	Chalcedony (HMR) + Chert (SR)	
FA5	0.079	0.035	Few siliceous (e.g., Chert) inclusions	NR, but depending on the concentration of the siliceous inclusions, some batches of sample may be identified as SR
CA8	0.012	0.027	Few siliceous (e.g., Chert) inclusions	
FA7	0.019	-	Few siliceous (e.g., Chert) inclusions	
CA7*	0.040	0.129	chalcedony (HMR) + chert (SR)	MR
CA6*	0.100	0.097	Low strained QTZ (MR) + siliceous inclusions	MR
CA5**	0.140	0.020	limestone (NR) + limited separate Chert (SR)	NR or SR

*: Passed by 1260 but failed by 1293; **: Failed by 1260 but passed by 1293; QTZ: quartz; HR: highly reactive; MR: medium reactivity; SR: slowly reactive; NR: non-reactive; HMR: high to medium reactivity.

Summary

The degree of ASR and associated distress in the field not only depends on the type of siliceous component but also other field-related parameters (TH_A and extra alkali sources, moisture, temperature, load capacity, etc.). The field performance of aggregates containing strained quartz shows the occurrence of ASR after decades, and some of the laboratory tests are ineffective (Fernandes et al. 2004; Shayan et al. 2008) to identify these aggregates as reactive. Therefore, the petrographic techniques should be considered as a good supporting tool at best. A correlation between petrographic observations (Table 3.4) and the reactivity prediction based on volumetric change measuring device (VCMD) (Chapter V) will be established.

CHAPTER IV

TEST EQUIPMENT AND METHODOLOGY*

The previous chapter explained that ASR is a kinetic type of chemical reaction that integrates the combined effects of temperature, alkalinity, moisture, and time relative to the kinetics of ASR expansion. CAE can serve as a single chemical material parameter to represent this kinetic type of combined effect and can be used to evaluate the ASR susceptibility of aggregates. A simple chemical test by simulating the aggregate–pore solution reaction that exists in concrete will be appropriate to determine ASR CAE. Previously, a test method based on VCMD at the Texas A&M Transportation Institute was developed (Mukhopadhyay et al. 2009). The VCMD simulates the aggregate-pore solution reaction that exists in concrete and measures net solution volume change due to ASR over time. This test is performed with as-received aggregates (the error due to crushing is eliminated) and within a short period of time (approximately 5 days including sample preparation). By fitting a kinetic type of performance model to measured volume change data over time, rate constant (β) is calculated. βs at multiple temperatures (a minimum of three temperatures, e.g., 60°C, 70°C, and 80°C) are then determined, and the CAE is calculated by plotting ln(β) versus (1/T). Based on the Arrhenius equation (Callister 2007), the slope of the linear regression is equal to (−CAE/R) where R is the universal gas constant and CAE is the compound activation

* Part of this chapter is reprinted with permission from "A Kinetic-based ASR Aggregate Classification System" by Kai-Wei Liu and Anal K. Mukhopadhyay, 2014. *Construction and Building Materials*, 68, 525-534. Copyright 2014 Elsevier

energy. The VCMD has been used to measure the alkali-silica reactivity of selective minerals and aggregates in terms of their CAE (Mukhopadhyay et al. 2006; Shon et al. 2007). The same VCMD-based procedure was used in this study to measure CAE of the collected aggregate materials (presented in Chapter III)

This chapter describes the upgradation of the previously developed VCMD test equipment and protocol development through:

- Identification of areas of reconditioning and upgradation of the devices.
- Fine-tuning the calibration and test procedure.
- Testing a pure phase material (e.g., non-porous borosilicate glass balls) as a proof of concept to verify that VCMD actually measures net solution volume contraction over time (solution curve) due to ASR.
- Verification of deducting water curve (water volume change over time from a parallel aggregate-water test) from the solution curve as a procedure to determine expansion (solid volume increase) indirectly. Earlier, it was observed that deducting the water curve from the solution curve for the same aggregate material (mainly coarse aggregate) provides a way to measure expansion (i.e., solid volume increase) indirectly.
- Further reduction of testing period.

Test Equipment

A detailed description of the VCMD and the test procedure to measure net solution volume change from aggregate-solution test is presented in Appendix A. A brief description of the equipment and the test procedure is given below.

The VCMD (Figure 4.1) consists of a container, a Teflon-coated brass lid, a hollow tower, and a steel float. The container and tower are made of stainless steel whereas the lid is made of naval brass. At the top of the tower, a casing is installed to ensure proper alignment of the linear variable differential transducer (LVDT) and the float. The LVDT used is the Schaevitz Model HCA-1000 HCA, which has a maximum range of 2 inches with a sensitivity of 0.84 mV/V/0.001 inch. The LVDT is placed with an O-ring located at the bottom of the casing and secured with six set screws though the side of the cylinder. In Appendix A, Figures A1 and A2 show detailed drawings of the separate and assembled parts of the VCMD. As the chemical reaction between aggregate and the test solution (i.e., NaOH + saturated $Ca(OH)_2$) progresses, the volume of test solution in the container changes and the float sitting in the solution also moves. As the float moves, the stainless steel rod moves inside the LVDT and generates electrical signals. Therefore, the physical phenomenon (i.e., movement of the rod) is converted into a measurable signal. All LVDT signals are amplified through the use of signal conditioners and then transferred though a USB cable to a workstation where a program in LabVIEW was developed to display, analyze, and store the generated data.

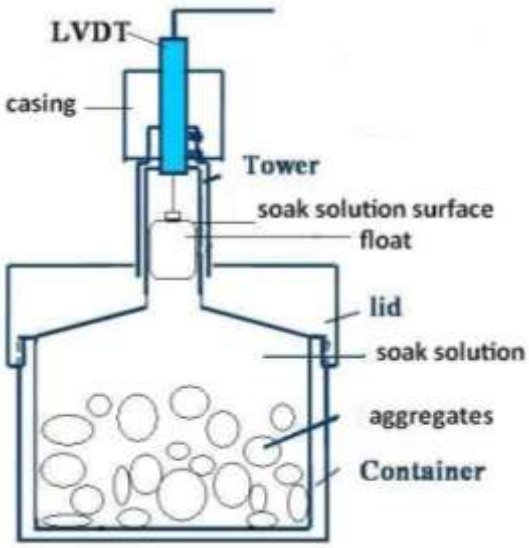

Figure 4.1 VCMD Test Setup.

The towers of the three devices out of the total eight VCMDs had the old design, so efforts have been made to make all the devices identical. To achieve this, the towers of the three old VCMDs were modified. In the earlier version of the VCMD, LVDT casing on the top of the tower was not introduced. Application of glue at the junction between the LVDT and the tower was the common practice to seal the junction. However, this practice sometimes causes evaporation of the solution after several tests. Therefore, the old towers in these three old VCMDs were replaced by the new towers with LVDT casing. The inside of the tower and lid were reconditioned to make them smooth, which eliminates/reduces the chances of float sticking issues and achieves identical inside diameter for all the VCMDs.

To check smooth float movement and ensure that the devices are leak-proof, water testing at 80°C with the same testing duration for all the VCMDs were conducted.

Each VCMD was filled up with water, vacuumed with vibration (to remove air bubbles), and then placed inside the oven where it experienced a temperature change from the starting temperature (50-55°C) to 80 °C. The water in the container experiences thermal expansion due to the temperature increase, which makes the float move upward. The float displacements (in inches) and solution temperatures data for all the eight VCMDs were recorded over four days and are presented in Figure 4.2. The figure shows that when the temperature reaches 80^{o}C, the float also reaches a stable displacement level in all the VCMDs. The float movement doesn't change thereafter. This verifies that the devices are leak-proof and no measurable evaporation loss situation during the 4-day test duration.

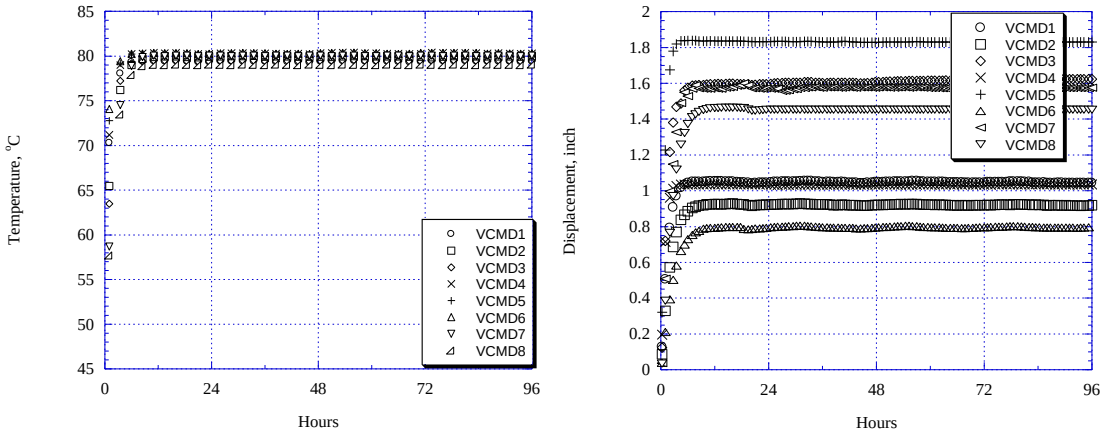

Figure 4.2 Temperatures (Left) and Float Displacements (Right) over Time in all the VCMDs from Water Tests (Liu and Mukhopadhyay 2014).

To verify smooth float movement, each VCMD was filled up with water, followed by vacuuming with vibration and placed inside the oven where it experienced a

temperature increase from 40°C to 60°C. The temperature of water inside the VCMD and the LVDT displacement due to volume expansion (thermal) of water were continuously recorded through the data acquisition system. The initial and final positions of LVDT are taken from the average of 2-hour displacement data at a stable initial temperature (i.e., 40^{o}C) and final temperature (i.e., 60^{o}C) respectively. The difference between average final and initial LDVT readings represent the total LVDT displacement (ΔH) due to thermal expansion (ΔT, i.e., 20°C). The coefficient of variation (COV) of ΔH for each VCMD (3 tests for each VCMD) is under 2%, whereas the COV of ΔH between VCMDs is around 6%. The relatively higher COV between VCMDs is possibly due to the combined effects of slight differences in float weight, initial water weight, volume of the container, and temperature change (ΔT) for each VCMD. Based on these results, it can be concluded that the smooth float movement was achieved in all the VCMDs. A one-time calibration testing should be sufficient. However, it is recommend to perform the above calibration testing whenever there is: (i) a change in float, (ii) a repair in the device, and/or (iii) an abnormal LVDT reading during data collection.

Test Solution

The 1 N, 0.5N and 0.25N NaOH (NH) solutions are prepared by diluting 40, 20 and 10 grams of NH crystals into 0.9 liter of distilled water. Water is added to raise the total volume of solution to 1 liter. $Ca(OH)_2$ (CH) crystals are then added (1 gram per liter solution) to the above respective NaOH solutions slightly above saturation in order to prepare an alkaline solution saturated with CH. Adding CH crystals slightly above the saturation point ensures presence of undissolved CH crystals, which represents a

situation similar to concrete pore solution. Thorough mixing ensures homogeneity of all the prepared solutions.

Test Procedure to Measure Solution Volume Change due to ASR

The VCMDs are filled up with as-received aggregate (approximately 8-9 lb) and alkaline solution of different concentrations (e.g., 1N, 0.5N, and 0.25N NH + CH) and tested at different temperatures (e.g., 60, 70, and 80°C) inside an oven according to the experimental design (details in next section). The weight of the oven-dried material corresponded to the 80% volume of the VCMD container. A constant aggregate/solution volume ratio and gradation were used for all the aggregate.

The VCMD test procedure is summarized below (details in Appendix A):

- Keep the device filled up with clean and dried aggregate and alkaline solution overnight at room temperature to allow maximum saturation of voids in the alkaline solution.
- Place the device on a vibrating table and conduct vacuuming under vibration for 2 hours to mainly remove entrapped air bubbles in the solution. This also helps to saturate the unfilled voids (likely to be present) in aggregates after overnight saturation.
- Place the device inside an oven and heat it to the selected target temperature (~ 6 hours).
- Apply a second stage vacuuming under vibration of 45 minutes to facilitate further removal of air bubbles (may be generated during heating at target temperature) from solution.

- The device was placed inside an oven, whose temperature was then raised to the selected target temperature. It takes around 5-6 hours to reach the target temperature.
- Solution volume changes as the chemical reaction between aggregate and alkaline solution progresses; this makes the float move. As the float moves inside the tower, the stainless steel rod attached with the float also moves inside the LVDT. Through the data acquisition system, the computer records LVDT readings over time.

LVDT displacement readings at the stable target temperature represents the reference (initial) LVDT reading for calculating displacement due to ASR. This ensures separation of thermal solution volume expansion from solution volume change due to ASR. All subsequent LVDT readings (i.e., after reference reading) minus the reference LVDT reading represent displacement due to ASR over time. The percent volume change of solution due to ASR is calculated by using Eq. 4.1.

$$V(\%) = \frac{\Delta V_{ASR}}{V_{Aggregate}} \times 100 \tag{4.1}$$

where V(%) is percent volume change of solution due to ASR, ΔV_{ASR} is solution volume change due to ASR, and $V_{Aggregate}$ is initial volume of aggregate.

Pure Phase Materials and Aggregate Testing

Pure phase material (e.g., borosilicate glass balls) and aggregates (both fine and coarse) (Table 3.1 in Chapter III) were tested using the above updated devices and procedures. The design of experiments and the test results are presented below:

Design of Experiment

Table 4.1 presents the design of experiments, i.e., the effective factors and their levels. 15 aggregates with different types of reactive silica and varying ranges of reactivity were selected (Table 3.1). For each aggregate, researchers conducted a total of 18 test runs (3 levels of temperatures and a minimum of 2 levels of alkalinities with 3 replicas).

Table 4.1 Factors and Levels in the Design of Experiments.

Factors	No. of Levels	Level Description
Material type	16	Borosilicate glass + 15 aggregates in Table 3.1
Temperature	3	(1) 60°C, (2) 70°C, and (3) 80°C
Alkali level	2-3	0.5N NH + CH, 1N NH + CH, and 0.25N NH + CH for some selected aggregates

Pure Phase Material

The use of borosilicate glass as a highly alkali silica reactive material has been reported both in conducting ASR research and ASR test developments (ASTM C 441 2008; Ostertag et. al. 2007,). The composition of the borosilicate glass balls is composed of SiO_2: 81%, Na_2O: 4%, Al_2O_3: 2%, B_2O_3: 13%. This is a non-porous material. Borosilicate glass balls were tested at three levels of temperatures and at 0.5N NH + CH, 1N NH + CH, and 1N NH + KOH (KH) + CH alkalinities. Three tests (corresponding to three different temperatures) at each alkalinity with total 3 alkalinities gives total 9 test runs. Figure 4.3 shows the net solution volume changes in a form of contraction over time at three levels of temperatures and at all alkalinities for borosilicate glass balls-

solution. A net solution volume contraction over time due to ASR between glass balls and alkaline solution was invariably observed for all the tests at different levels of temperatures and alkalinities. Note that glass balls are non-porous and there was no effect of absorption on the measured net solution volume contraction over time. This observation suggests that the VCMD in closed system set up measures net solution volume contraction over time due to ASR. The glass ball solid volume increases but the net solution volume decreases.

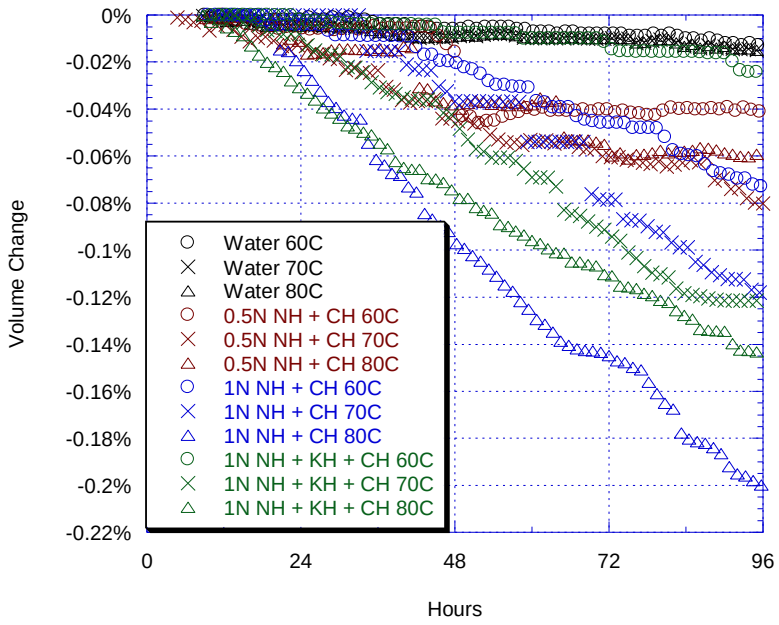

Figure 4.3 Net Solution Volume Change from Borosilicate Glass Balls at 1N NH + CH Solution at Three Temperatures (Liu and Mukhopadhyay 2014).

Aggregates

For each aggregate, researchers conducted 18 test runs (3 temperatures, 2 levels of alkalinities, and 3 replicas). Eight VCMDs were simultaneously run inside an oven for 5 days. The approximate total time to complete all 18 test runs is 15 days without any interruption. All aggregates were tested using the VCMD according to the experimental design in Table 4.1 and net solution volume change over time was measured. Figure 4.4 shows the average of measured volume change over time at three levels of alkalinity and temperatures (60, 70, and 80°C) for FA1 as an example. The data for all the aggregates at different levels of alkalinities and temperatures are presented in Appendix B. Note that net solution volume contraction over time was also invariably measured for all the tested aggregates (irrespective of coarse or fine aggregates). This is in agreement with earlier findings in the previous project (Mukhopadhyay et al. 2009).

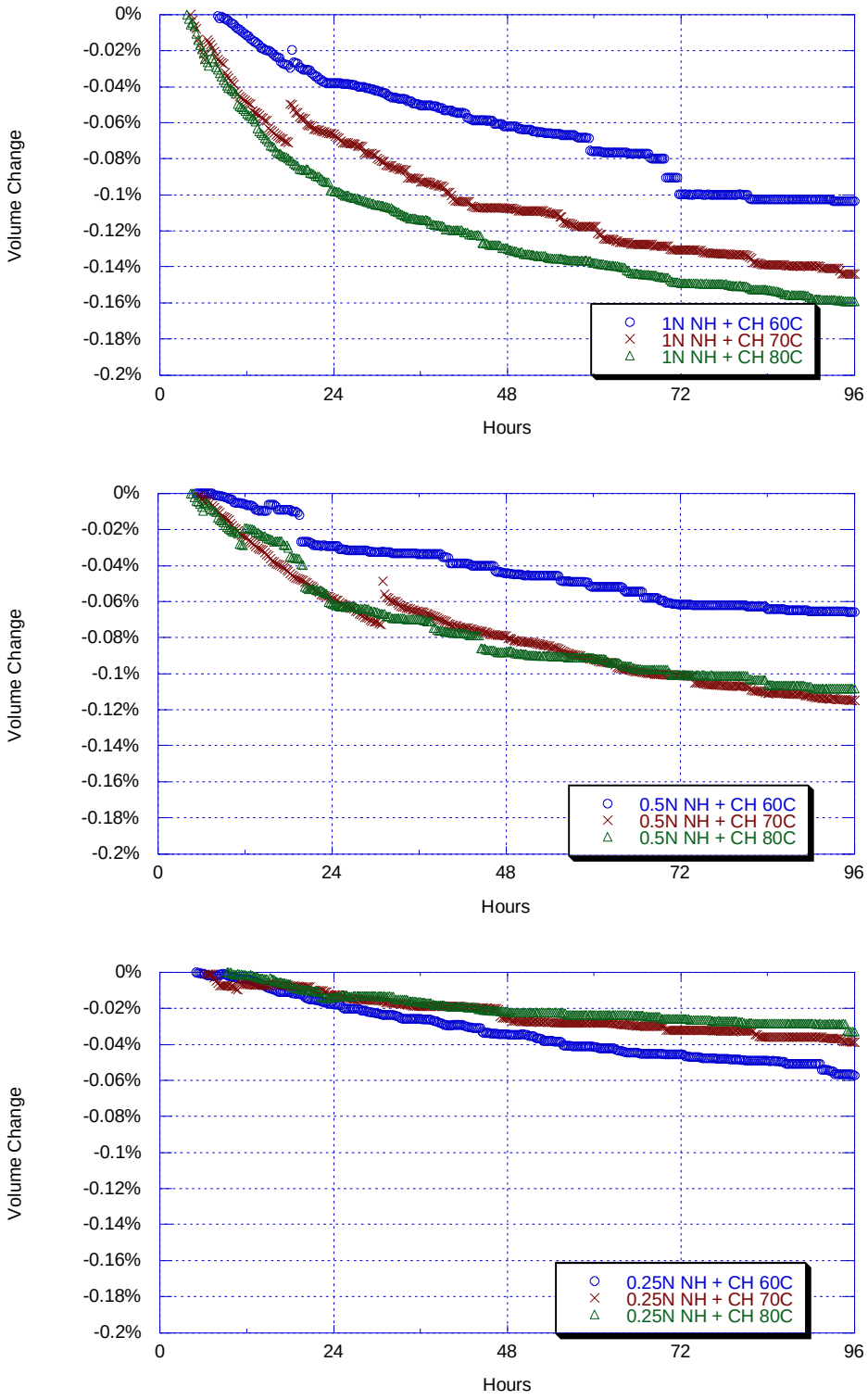

Figure 4.4 Solution Volume Change with Different Levels of Alkaline Solutions (1N, 0.5N, and 0.25N NH + CH) at Three Temperatures (60, 70, and 80ºC) for FA1.

Aggregate absorption capacity (AC) is affected by its porosity/permeability which can be divided into two categories: porosity and crack porosity. The change of crack porosity is associated with the aggregate thermal decompaction and mineral composition. The crack porosity increases with an increase of temperature due to different thermal expansion of the minerals in aggregates (Zharikov et al. 2000). However, during the preheat step of the sample preparation procedure, the effect of crack porosity is eliminated. For the porosity, it has been reported that the permeability of tight rocks decreases with an increase in temperature from 20 to 200^{o}C, and the relative change of porosity has no change with an increase of temperature (Deng 2012). Amro and Benzagouta (2009) also found that the permeability of carbonate reservoir rocks reduced significantly when temperature raised from 25 to 50^{o}C and the reduction is in a continuous trend up to 100^{o}C. Therefore, the effect of aggregate absorption/permeability in measuring net solution volume change in this test would be very negligible.

Concrete aggregates that have high AC reach 85% of their total AC in less than 30 minutes of soaking in water, and reach 95% of their AC within 24 hours of soaking in water (Adams et al. 2012). The total submerged time of aggregate in alkaline solution before achieving the stable target temperature in the test is around 26±1 hours. Moreover, the two-stage vacuum saturation is a part of the sample preparation procedure, which enhances absorption (should be more than 95%). It is extremely difficult to fully saturate (i.e., achieving 100% AC) an aggregate by prolonging soaking time. Therefore, it is unlikely that the saturation (pore filling by solution) will continue

during testing (i.e., 4 days). Even if this continues, it would be very negligible. The dominant phenomenon is net solution volume contraction due to ASR.

Measuring chemical shrinkage in fine aggregate-alkaline solution system over time has been reported earlier by Kundsen (1986). In Kundsen's procedure, sand samples were boiled for 3 hours to eliminate the effect of absorption capacity. A flask is filled up with sand samples and 10N NaOH solution, and then stored in a thermostatic bath at 50°C. The researchers used the data solution volume change over time (recorded manually) to calculate chemical shrinkage due to ASR over time. The chemical shrinkage was used as a measure of aggregate reactivity. The authors stated that the measured chemical shrinkage in their test procedure is very similar to the cement hydration. The total volume (cement and water) decrease and the volume of calcium silicate hydrate (C-S-H) increase during cement hydration. Similarly, when ASR occurs in concrete, water coming from outside the system allows the ASR gel to expand and to occupy a volume greater than the amount of water in the reaction. This test was widely used in Demark.

In earlier work (Mukhopadhyay et al. 2009), the subtraction of net water volume change over time (water curve) in aggregate-water test from the net solution volume change over time (solution curve) in aggregate-solution test was adopted as an indirect way to measure solid volume change due to ASR. A net upward displacement was observed based on four coarse aggregates testing and interpreted as a measure of solid volume increase, i.e., expansion. In this study, aggregate-water tests at the three selected temperatures were conducted for all the aggregates in Table 3.1. Deductions of water

curves from solution curves are performed and the net displacements after water curve deduction are summarized in Table 4.2.

Table 4.2 Net Displacement after Water Deduction for All Aggregates.

	CA			**FA**			**All Aggregates**		
Net displacement	U	D	LC	U	D	LC	U	D	LC
Occurrence, %	60	34	6	14	75	11	41	51	8

U: Upward, D: Downward; LC: Little Change.

Table 4.2 shows that the consistent trend of upward movement after deducting the water curves from solution curves is not obtained. The coarse aggregates shows higher percentage of net upward displacements (sometimes with very less upward movement) than the fine aggregates. Based on these findings (inconsistent trends), it is concluded that simply deducting water curves from solution curves does not necessarily provide direct measurement of solid volume change (i.e., expansion). The water curve can be considered a perfect reference curve if the aggregate-water system remains totally inert (i.e., no reaction between tested aggregates and water at high tested temperatures). However, the following discussion indicates that this assumption may not be correct.

Researchers found that the solubility of amorphous silica depends on both temperature and pH value. Alexander et al. (1954) and Morey et al. (1964) observed that the solubility of amorphous silica in water increases with an increase of temperature shown in Figure 4.5a). Alexander et al. (1954) also concluded that the solubility was

about 0.012% to 0.014% in the pH range 5 to 8 at 25°C and increased at high pH (pH > 8) (shown in Figure 4.5b) because of the formation of silicate ion in addition to $Si(OH)_4$ in solution. This phenomenon is also observed from borosilicate glass tested with distilled water in this study (Figure 4.3).

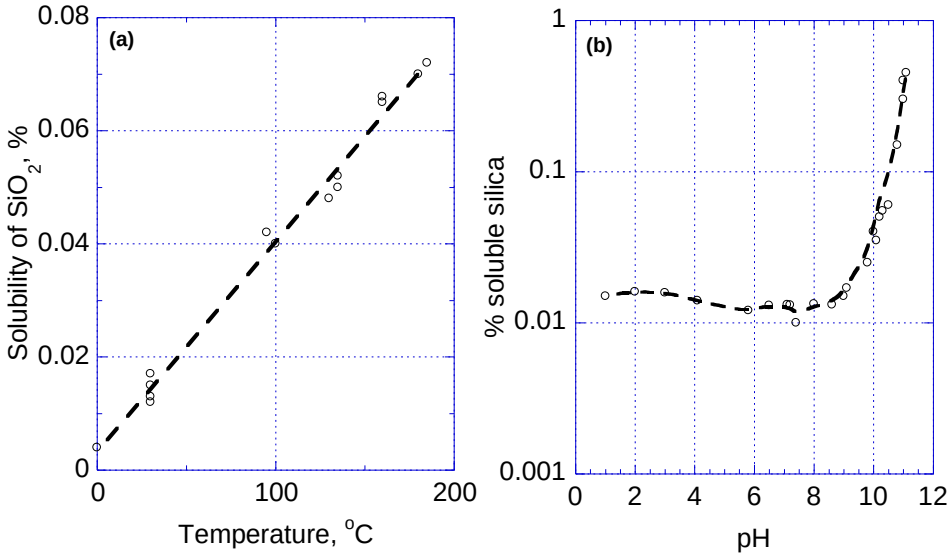

Figure 4.5 Solubility of Amorphous Silica in (a) Water and (b) Different pH Solution at 25oC (Alexander et al. 1954).

In addition, it has been found that solubility of limestone depends on inclusion, temperature and pH value. The solubility of limestone in water increases with an increase in calcite and decreases with an increase in dolomite in limestone (Hazim and Kawaz 2010). Paler (1991) also showed that the solubility of calcite decreased with an increase of temperature when the limestone was in alkaline solution. Regardless of the temperature change, the solubility of calcite increases with a raise of pH in solution.

Therefore, it is unlikely that aggregate-water system remains inert at high temperatures and water curves obtained from aggregate-water tests do not serve as a good reference curves. This explains the inconsistency of the results in Table 4.2.

ASR Mechanism in terms of Chemical Shrinkage

ASR is the reaction between the hydroxyl (OH^-) ions present in pore solution and reactive siliceous component(s) in aggregates. The alkali cations (i.e., Na^+, K^+, Ca^{2+}, etc.) are important because their presence in high concentration leads to an equally high concentration of hydroxyl to maintain equilibrium in the pore solution. When they are incorporated into the ASR gel, the role of alkali becomes relevant. In general, there are four steps in the chemical reaction mechanism of ASR (Garcia-Diaz et al. 2010; Glasser and Kataoka 1981; Poole 1992; Wang and Gillott 1991). Although the reaction mechanisms that govern ASR are well understood, the mechanism in terms of chemical shrinkage due to ASR has not been clearly explained. Based on the results in this study, a mechanism between aggregate and solution due to ASR in a closed system is proposed. A decrease of net solution volume is due to the combined effects of: (i) Si-O-Si bond breaking and silica dissolution which cause solution volume decrease, (ii) consumption of reactants such as water and ionic species which causes solution volume decrease, (iii) ASR product formation and expansion which cause solution volume increase, (iv) solution going into micropores (pores that developed due to the formation of high-volume less dense ASR products) and microcracks related to the degree of ASR which cause solution volume decrease, and (v) incomplete absorption (negligible but

may be responsible for slight solution volume decrease) in a closed system condition of the VCMD.

Summary

The main observations based on the results and discussions in this chapter are summarized below:

- The experiments with pure glass material support measuring net solution volume contraction over time in VCMD.
- A decrease of net solution volume is due to the combined effects of:
    - Si-O-Si bond breaking and dissolution (solution volume decreases).
    - Consumption of reactants such as water and ionic species (solution volume decreases).
    - Product formation and expansion (solution volume increases).
    - Solution goes into micropores (pores that developed due to the formation of high-volume less dense ASR products) and microcracks. The degree of micropore and microcrack formation is related to the degree of ASR (solution volume decreases).
    - Incomplete absorption (negligible but may be responsible for slight solution volume decrease) in a closed system condition of the VCMD.
- Deduction of water curves from solution curves does not provide an effective way to directly measure solid volume change (i.e., expansion). Therefore, the requirement of conducting parallel aggregate-water tests is no longer needed and facilitates reduction of total testing time.

- It is recommended to characterize the net solution volume contraction over time to determine β constants at different temperatures followed by CAE calculation, which is presented in the next chapter.

CHAPTER V

DEVELOPMENT OF A KINETIC-BASED ASR AGGREGATE CLASSIFICATION SYSTEM*

This chapter presents:

- Determination of CAE from net solution volume contraction measurements over time (presented in Chapter IV) at different temperatures and alkalinity for both borosilicate glass and all the tested aggregates.
- Developing a CAE-based ASR aggregate classification system to categorize aggregates based on their reactivity.
- Establishing a characteristic trend between CAE and alkalinity and determine a TH_A for each aggregate.
- The use of monitoring test solution chemistry change and microstructural studies on the reacted aggregate particles by SEM-EDS as supporting tools for the VCMD test results.

Measurement of ASR Compound Activation Energy (CAE)

A kinetic-type model (Eq. 5.1) was developed to model measured non-linear type solution volume change data over time (Hassan et al. 2010). By fitting the model

* Part of this chapter is reprinted with permission from "A Kinetic-based ASR Aggregate Classification System" by Kai-Wei Liu and Anal K. Mukhopadhyay, 2014. *Construction and Building Materials*, 68, 525-534. Copyright 2014 Elsevier

(Equation 5.1) to the measured data over time, the characteristics parameters (i.e., ε_0, β, t_0, ρ) are calculated.

$$\frac{1}{\varepsilon} = \frac{1}{\varepsilon_0} . e^{(\frac{\rho}{t-t_0})^{\beta}} \tag{5.1}$$

ε_0 is volume change due to ASR, β is rate constant, t_0 is initial time of ASR occurrence (hour), and ρ is time corresponding to a volume change ($\varepsilon_0/\varepsilon$).

The β values at multiple temperatures (minimum 3 temperatures) are then determined and activation energy (E_a) is calculated by plotting ln(β) versus (1/T). Based on the Arrhenius equation (Callister 2007) shown in Equation 5.2, the slope of the linear regression is equal to ($-E_a/R$) where R is the universal gas constant and E_a is the activation energy.

$$\ln \beta = -\frac{E_a}{R}\frac{1}{T} + A \tag{5.2}$$

where A is a constant.

Since the initial time of ASR occurrence (t_0) is affected by various factors such as temperature (T), degree of reactive constituents in aggregates, etc., the Eq. 5.2 is modified into Eq. 5.3 for E_a calculation in this study (Figure 5.1).

$$\ln \beta = -\frac{E_a}{R}\frac{1}{T} + A - Bt_0 \tag{5.3}$$

$$t_0 = C - DT$$

where B is the slope of the linear regression of ln β versus t_0 plot, C is a constant, and D is the slope of the linear regression of t_0 versus T plot. By applying Gauss elimination to solve 3 linear regressions respected to 3 temperatures, the modified β and E_a can be determined.

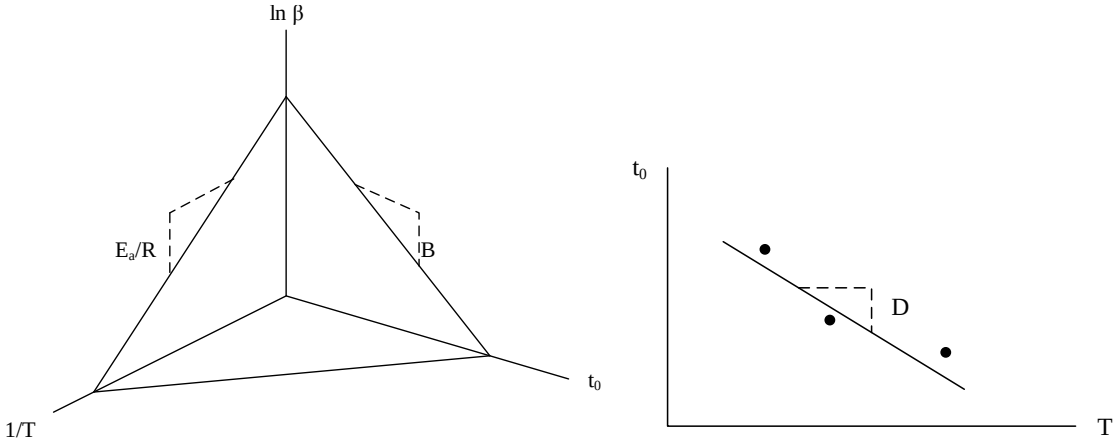

Figure 5.1 Modification of E_a Calculation.

For ASR, E_a is considered as the minimum energy required initiating ASR taking into account the combined effect of alkalinity, temperature and time. In analytical chemistry, E_a is defined as the minimum energy required for a chemical reaction to proceed (Ebbing et al. 2005). Consequently, it can be considered as an energy barrier. For ASR, E_a is considered as the minimum energy required to initiate ASR, taking into account the combined effect of alkalinity, temperature, and time. It is important here to mention that the ASR E_a should be considered as a CAE as aggregate is a heterogeneous material that is often composed of different mineral phases, i.e., reactive phases (one or more phases) and non-reactive phases (crystalline minerals). The concept of ASR CAE was introduced as a representative single parameter of alkali silica reactivity of minerals and aggregates earlier (Liu and Mukhopadhyay 2014; Mukhopadhyay et al. 2006, 2012).

Pure Phase Material

For nonporous borosilicate glass balls, the solution volume changes over time are measured at three temperatures and at 0.5N NH + CH, 1N NH + CH, and 1 N NH + KH + CH alkalinities (Chapter IV). The alkalinity of the test solution was selected in such a way so that the behavior of Na and K can be investigated separately. A numerical approach was developed based on the model in Eq. 5.1 to calculate solution volume change over time (Ghanes et al. 2010). Figure 5.2 shows the measured and calculated volume changes over time at three different temperatures (60, 70, and 80°C). At the best fit between the predicted and measured data over time (Figure 5.2), the CAE is determined.

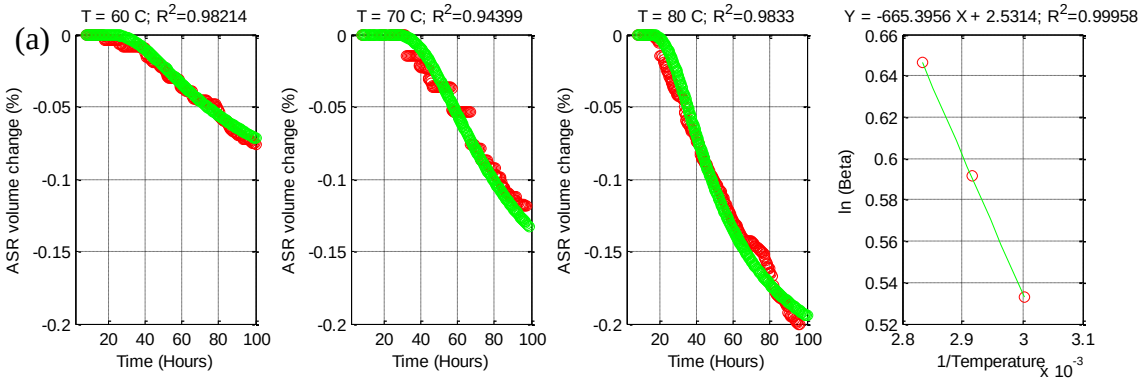

Figure 5.2 Measured (Red) and Modeled (Green) Solution Volume Change over Time for Borosilicate Glass with (a) 0.5N NH + CH, (b) 1N NH + CH, and (c) 1N NH + KH + CH Solutions at Three Temperatures.

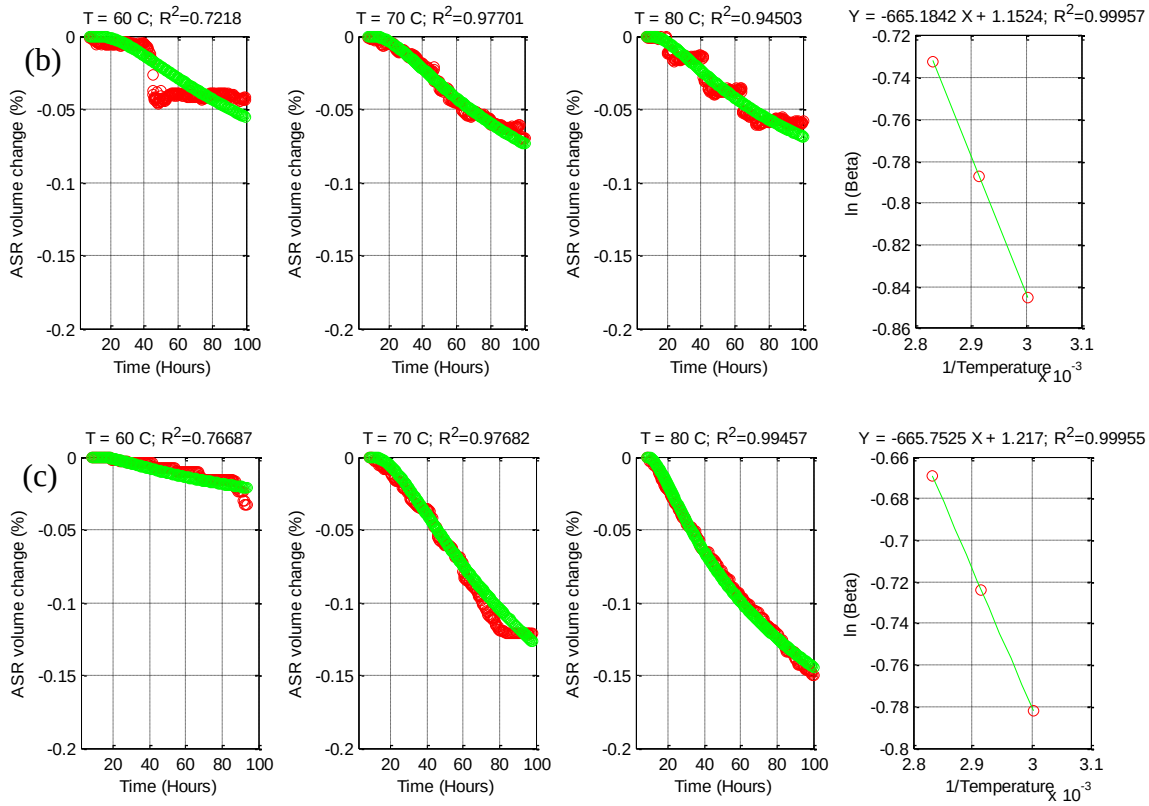

Figure 5.2 Continued.

The calculated CAEs for highly-reactive borosilicate glass (Figure 5.2) at 1N NH + CH, 0.5N NH + CH, and 1N NH + KH + CH are 5.53, 5.53, and 5.54 KJ/mole respectively which do not show much difference. In a pure phase system, Na and K show similar behavior in terms of ASR. It has been found that borosilicate glass alters differently from neutral to alkaline solutions (Liu and Mukhopadhyay 2014). The formation of surface layers on glass is caused by constituent elements of the glass passing into solution, with the elements initially in solution diffusing into or being adsorbed onto the glass. This surface layer (usually called ASR gel) consists of: (i) an

innermost diffusion layer (partially hydrated and depleted of soluble elements, i.e., B and Na), (ii) an outermost precipitated layer (amorphous and crystalline phases), and (iii) a gel layer (amorphous and crystalline phases) between them. The structure and/or composition of the surface layer differ from the original glass and are formed by more than one reaction process (i.e., ion exchange, water diffusion, network hydrolysis and condensation, and precipitation described in Chapter II) occurring simultaneously. Therefore, the measured CAE in this study represents a combined effect of all the above processes. It is logical to say that the CAE of borosilicate glass measured represents a combined effect of multi-steps ASR reaction mechanisms with dissolution–precipitation possibly the dominating factor.

Aggregate

All aggregates were tested according to the experimental design in Table 4.1 and free solution volume change over time due to ASR was measured. Each test run at a particular temperature and at a particular alkalinity was repeated three times to verify the repeatability (within the lab) of the test results. The solution volume changes over time for all these replicas at different levels of temperatures and alkalinities are presented in Appendix B. The same modeling approach (Eq. 5.1) was applied to the measured solution volume changes over time at a particular temperature and at a particular alkalinity to determine β. Three β corresponding to the three replicas were used to calculate the coefficient of variation (COV). Figures 5.3 to 5.5 show repetition of the same test run three times for FA1 as an example, and the calculated β and COV are

presented in Table 5.1. Figure 5.6 represents the COV based on β from the repeated tests for all the tested aggregates.

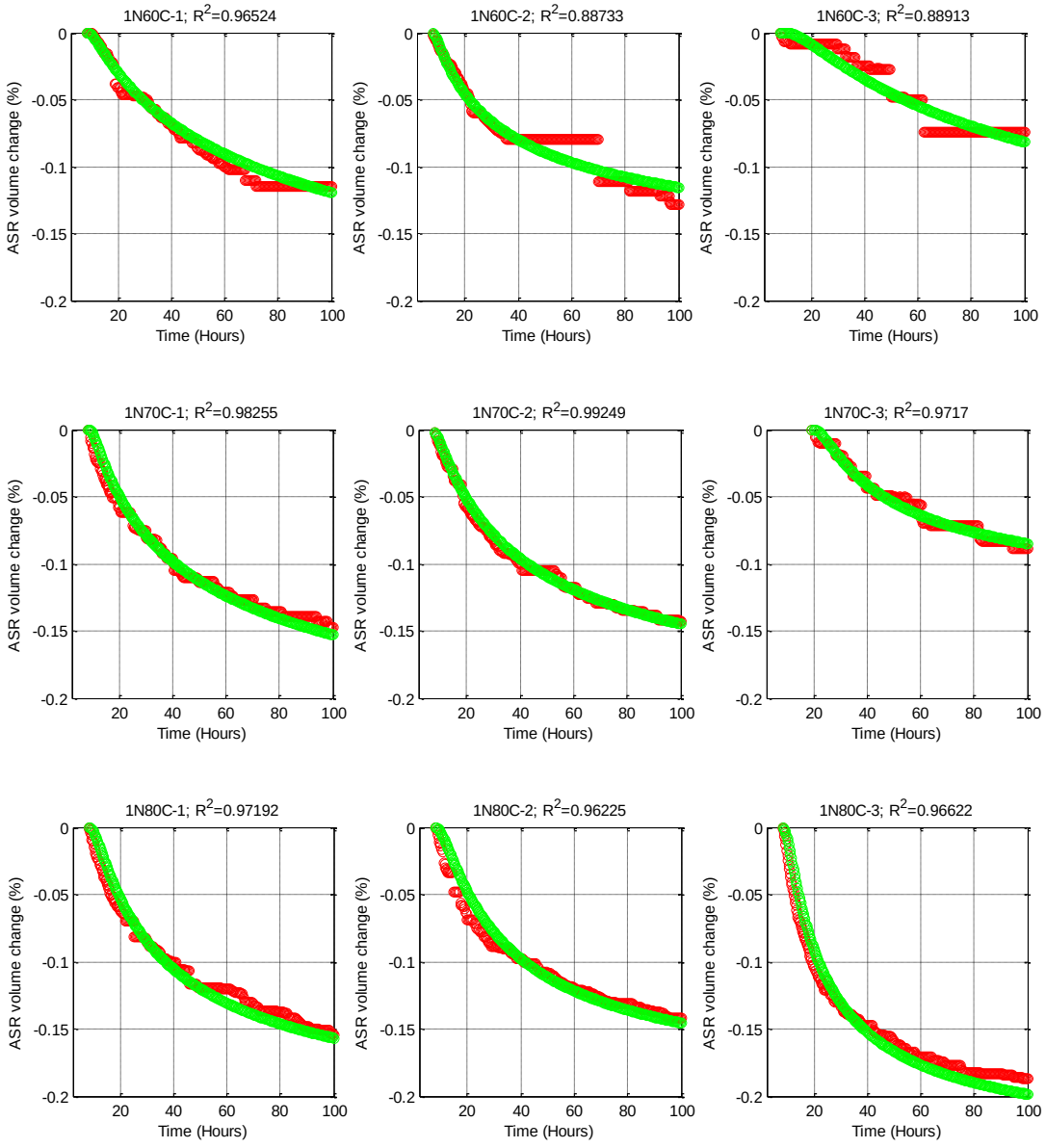

Figure 5.3 Repetition of Measured (Red) and Modeled (Green) Solution Volume Change over Time for FA1 with 1N NH + CH at Each Temperature (60, 70, and 80°C).

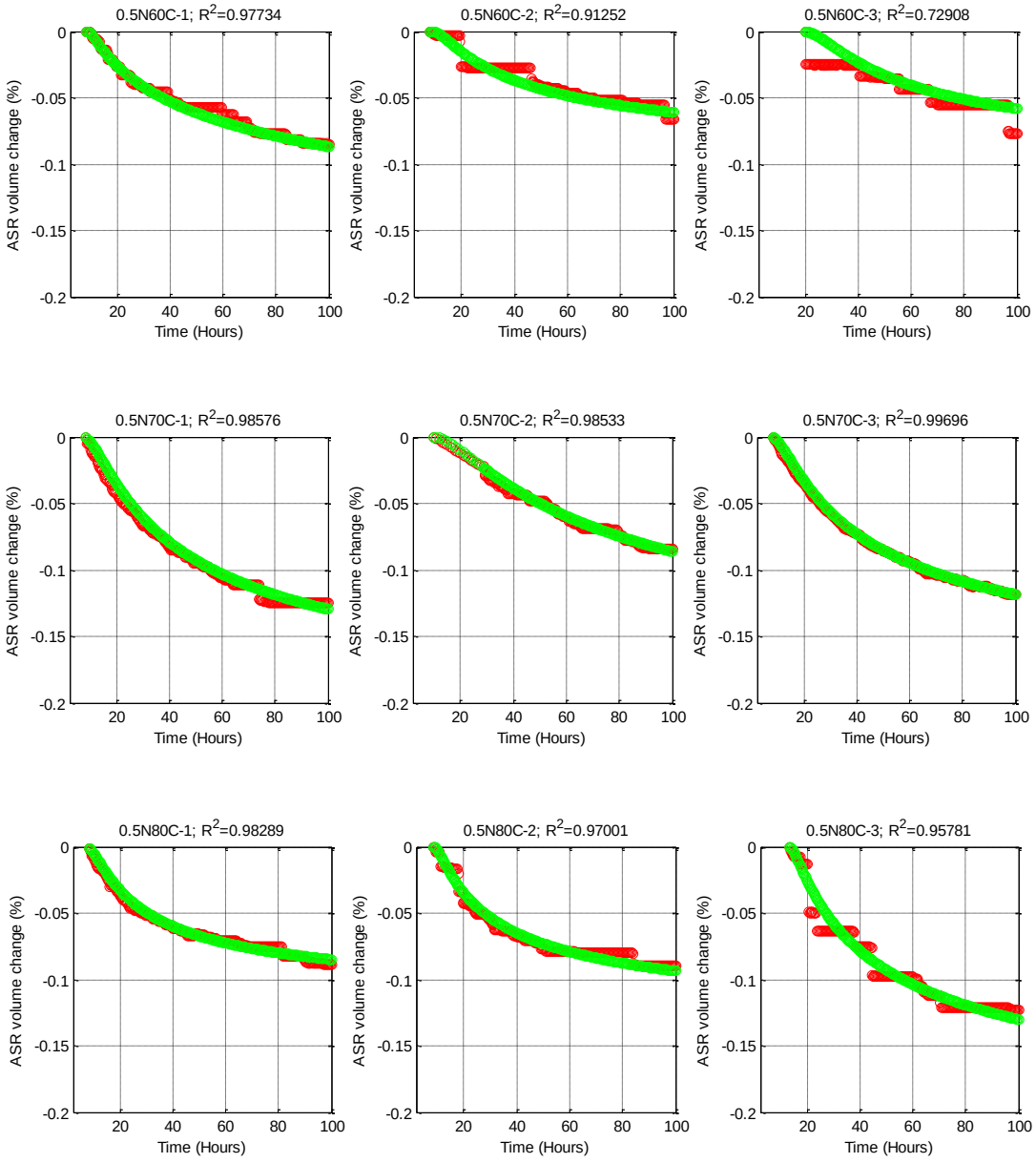

Figure 5.4 Repetition of Measured (Red) and Modeled (Green) Solution Volume Change over Time for FA1 with 0.5N NH + CH at Each Temperature (60, 70, and 80°C).

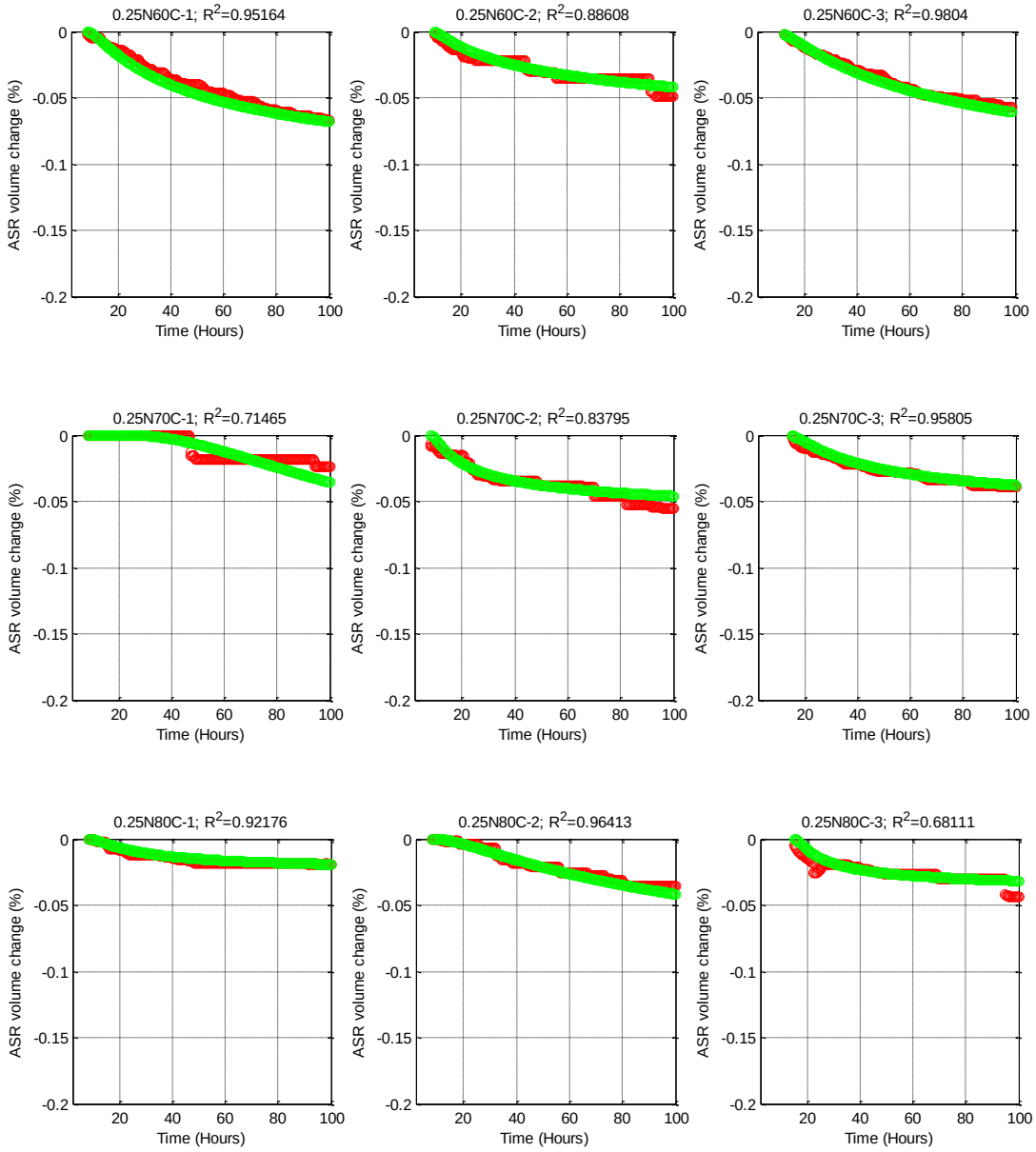

Figure 5.5 Repetition of Measured (Red) and Modeled (Green) Solution Volume Change over Time for FA1 with 0.25N NH + CH at Each Temperature (60, 70, and 80°C).

Table 5.1 Calculated Rate Constant Based on the Modeled Curve (Green) in Figures 5.3 to 5.5 for FA1.

Normality	Temperature °C	β			Average	COV %
		Test 1	Test 2	Test 3		
1	60	0.3968	0.4237	0.4468	0.4224	5.92
	70	0.4954	0.5069	0.5345	0.5123	3.92
	80	0.5842	0.6195	0.6134	0.6057	3.12
0.5	60	0.3776	0.3645	0.3872	0.3764	3.03
	70	0.4842	0.4835	0.5107	0.4928	3.15
	80	0.5964	0.6062	0.6014	0.6013	0.81
0.25	60	0.3143	0.3322	0.3253	0.3239	2.79
	70	0.4108	0.4309	0.4067	0.4161	3.11
	80	0.5792	0.6009	0.6038	0.5946	2.26

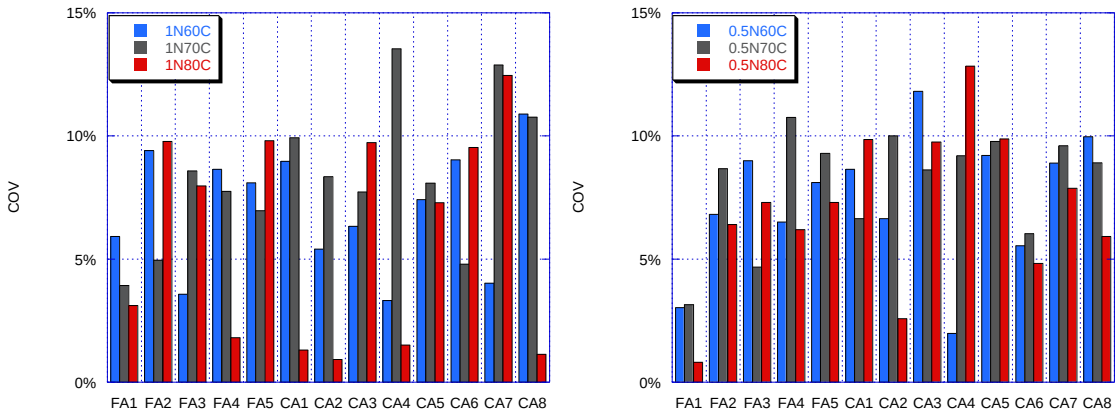

Figure 5.6 COV Based on β from the Repeated Tests for All the Tested Aggregates.

The net solution volume change over time for the tested aggregates at three levels of temperatures and alkalinities are presented in Appendix C. Any curve at a particular temperature and alkalinity in Appendix C represents an average of three replicas (i.e., repetition of the same test run three times). The same modeling approach (Eq. 5.1) was

applied to the average measured solution volume changes over time and representative CAE values at the studied levels of alkalinity were calculated. Figure 5.7 shows the measured (red) and calculated (green) volume change over time at three different temperatures (60, 70, and 80°C) with different alkali levels for FA1 as an example. The data representing measured vs. predicted volume changes over time along with CAE calculation for the remaining aggregates are presented in Appendix C. The CAE for all the tested aggregates along with ASTM C 1260 14-day expansion (%) and ASTM C 1293 1-year expansion (%) are listed in Table 5.2.

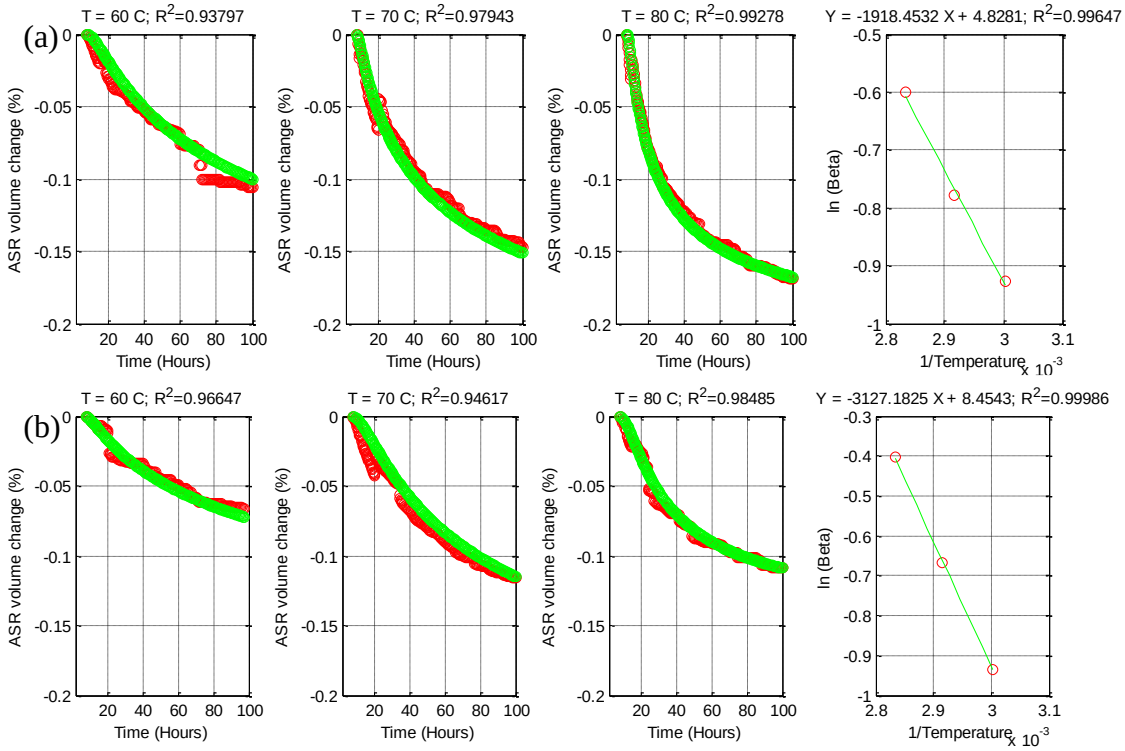

Figure 5.7 Measured (Red) and Modeled (Green) Solution Volume Change over Time for FA1 with (a) 1N NH + CH, (b) 0.5N NH + CH, and (c) 0.25N NH + CH Solutions at Three Temperatures.

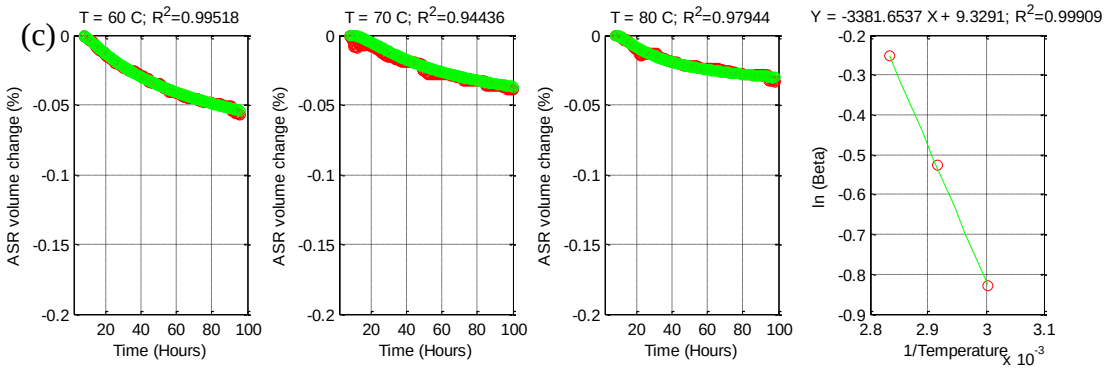

Figure 5.7 Continued.

Table 5.2 Measured ASR CAE as a Function of Alkalinity and Temperature.

Aggregate	CAE, KJ/mole			ASTM C1293 1YR Exp.%	ASTM C1260 14D Exp. %
	1N NH + CH	0.5N NH + CH	0.25N NH + CH		
Borosilicate Glass	5.53 5.54#	5.53	-	-	-
NMR, CA	-	17.56	-	-	1.3
FA1	15.98	26.00	28.11	0.590	0.554
CA1	22.15	29.73	-	0.078	0.417
FA3	22.55	32.64	-	0.058	0.317
CA3	21.29	41.78	-	0.071	0.227
CA4	30.33	39.18	42.81	0.149	0.179
FA5	52.78	60.36	-	0.035	0.079
CA8	46.77	61.70	-	0.027	0.012
CA7*	27.24	35.72	-	0.129	0.040
CA5**	45.35	57.03	-	0.020	0.140
FA4	26.82	36.39	-	0.043	0.242
CA2	29.68	35.95	-	0.047	0.250
FA2	28.70	29.41	-	0.171	0.334
CA6*	29.65	36.74	-	0.097	0.100
FA6	19.95	26.98	-	0.391	0.381
FA7	-	Not measurable	-	-	0.019

*#: 1N NH + KH + CH; *: Passed by ASTM C 1260 but Failed by ASTM C 1293; **: Failed by ASTM C 1260 but Passed by ASTM C 1293*

Here are some observations on Figures 5.3 to 5.7 and Table 5.2:

- The COV of β in Figure 5.6 are mostly within 10% for the tested aggregates at all levels of alkalinity, which indicates that the results are highly repeatable.
- The ASR E_a (i.e., 18.1 KJ/mole) for NMR at 0.5N NH + CH in the literature (Ghanem et al. 2010) is very close to the CAE (i.e., 17.56 KJ/mole) that has determined in this study. This indicates that the proposed CAE-based approach is promising.
- The lower the energy, the higher the reactivity becomes. In general, a high 14-day expansion of ASTM C 1260 and 1-year expansion of ASTM C 1293 match well with lower CAE value. This indicates that a CAE-based test procedure can reliably measure aggregate reactivity within a short period of time (i.e., 5 days). CAE is a measure of aggregate reactivity, and reactivity prediction based on a fundamental kinetic parameter (i.e., CAE) is more scientific and reliable.
- A representative CAE can be determined by testing aggregate with a test solution of 0.5N NH + CH alkalinity based on the followings:
    - In general, solution volume change plots (Appendix C) at 0.5N NH + CH alkalinity are smoother than those with 1N NH + CH. The repeatability (Figure 5.6) is better with 0.5N NH + CH than that with 1N NH + CH.
    - CAE values at 0.5N NH + CH are well separated in comparison with CAE values at 1N NH + CH. This facilitates assigning effective CAE ranges to categorize aggregates based on their reactivity.

- As 0.5N NH + CH is close to concrete pore solution alkalinity (Berube et al. 2004; Brouwers and Eijk 2003; Lorenzo et al. 1996; Lothenbach and Winnefeld 2006), testing aggregate with solution chemistry (0.5N NH + CH) is close to simulation of aggregate-pore solution reaction in concrete.

- Consistently identified the aggregates (e.g., CA5, CA6 and CA7) that the ASTM C 1260 method has passed/failed, but which the ASTM C 1293 has failed/passed in a short period of time.

Test-Solution Chemistry

Filtrates of test solution from VCMD tests are analyzed using the pH meter and atomic absorption spectrometer (AAS) to determine pH and Na^+ concentration respectively in the test solution both before and after the test. The changes of OH^- and Na^+ concentrations (% reduction) in the test solution due to ASR in tested aggregates were calculated for all the test runs and the results are presented in Figures 5.8 and 5.9.

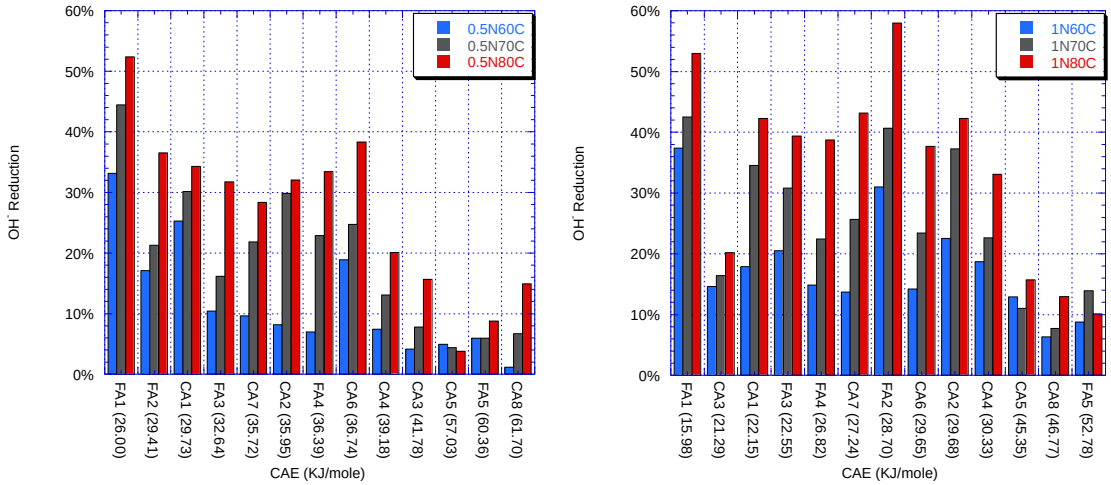

Figure 5.8 Percentage Reduction of OH^- at 0.5N NH and 1N NH + CH versus CAE.

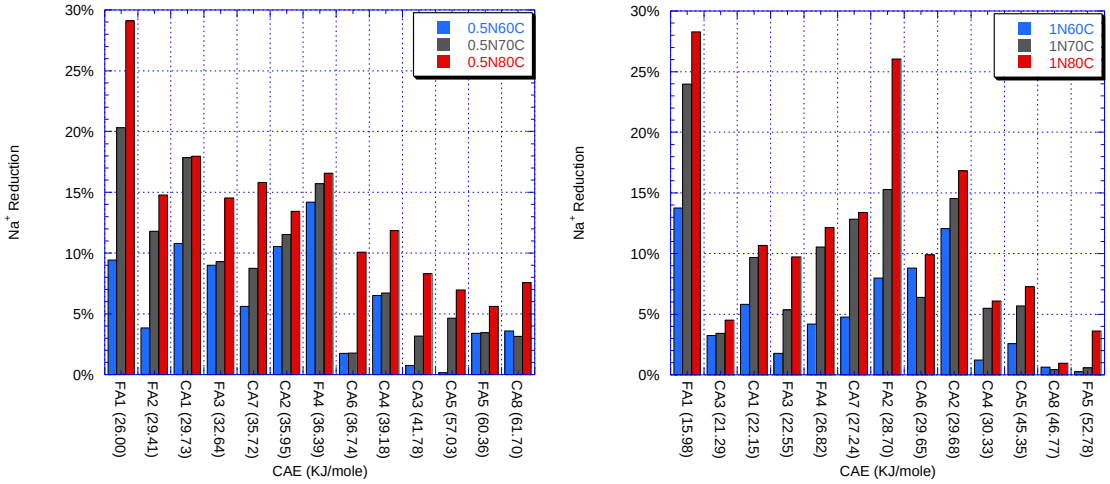

Figure 5.9 Percentage Reduction of Na^+ at 0.5N NH and 1N NH + CH versus CAE.

Here are some observations regarding Figures 5.8 and 5.9:

- In majority, the lower the CAE, the higher the consumption of Na^+ and OH^- ions is. The consumption of OH^- and Na^+ is more for highly reactive aggregates than that for slowly reactive aggregates.
- For non-reactive or slowly reactive aggregates (higher ranges of CAE), the consumption of Na^+ and OH^- ions are negligible (some consumption due to possibly physical adsorption without any measurable ASR).

Therefore, monitoring change of test-solution chemistry was served as a supporting tool for the VCMD test results. The samples of 3 different soak solutions from 3 different test runs (after each test run is terminated) were collected and analyzed to verify the repeatability of the soak solution chemistry determination. The COV was calculated using OH^- and Na^+ concentrations data from the 3 replicas corresponding to each test combination and the results are presented in Figures 5.10 and 5.11. The majority of COV is within 10% for the tested solution at all levels of alkalinity, which indicates that the procedure to collect solution sample and measure soak solution chemistry generate repeatable results.

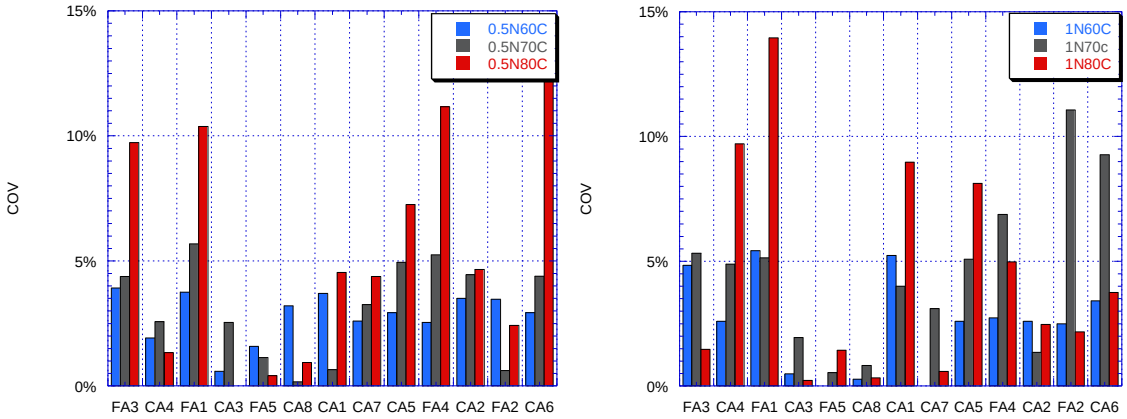

Figure 5.10 Coefficient of Variation (COV) Based on OH^- Concentrations at 0.5N and 1N NH + CH.

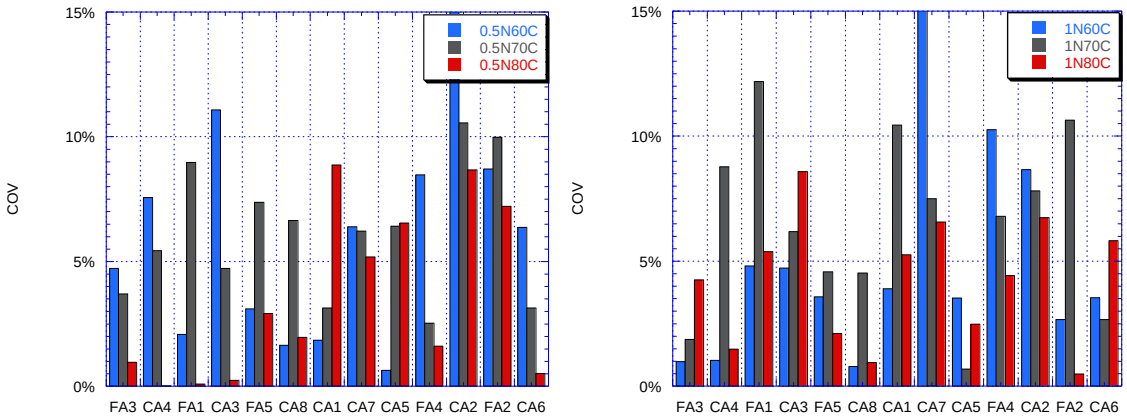

Figure 5.11 Coefficient of Variation (COV) Based on Na^+ Concentrations at 0.5N and 1N NH + CH.

Microstructure of Reacted Materials

Figure 5.12 shows the present of reaction product due to ASR on a borosilicate glass ball surface. The presence of mainly “Si” with some amount of “Na” was evident from SEM-EDS analysis. These observations suggest that ASR products (similar to ASR

gel) formed on the aggregate surfaces due to ASR and the measurement of solution volume change in a form of chemical shrinkage in VCMD is due to the same ASR. The obvious presence of reaction products indicate occurrence of all the 4 steps of reaction mechanisms (i.e., Si-O-Si bond breaking, dissolution, and product formation through precipitation described in Chapter II). It is expected that all the 4 steps will occur simultaneously at a much faster rate for a highly reactive aggregate and reaction products will be visible under SEM.

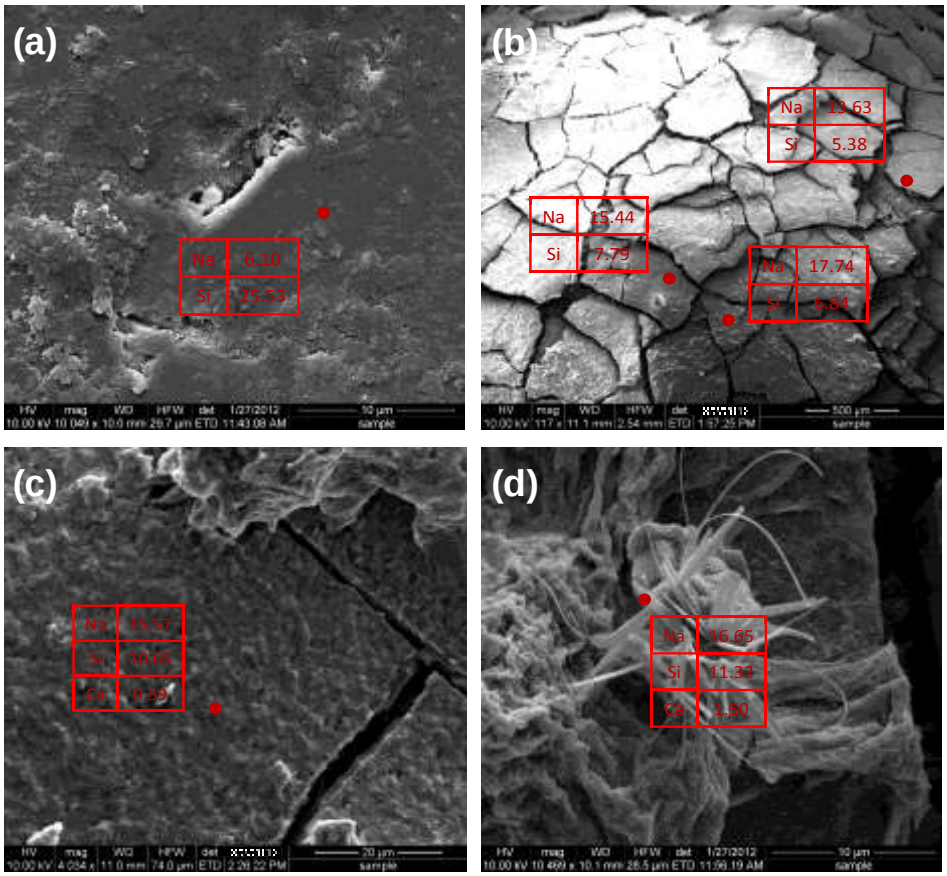

Figure 5.12 Secondary Electron Images of Reaction Products on a Borosilicate Glass Ball with Different Magnification: (a) Original, Na/Si: ~ 0.25, (b)(c)(d) 1N NH + CH at 96 hours, Na/Si: 1.46 to 2.59.

For highly reactive aggregates (e.g., FA1 and CA1) the presence of in-situ type reaction products were observed (Figures 5.13 and 5.14). For a slowly reactive aggregate, the presence of surface etching and cracking was observed with no obvious presence of gel within 4-5 days of the testing period. Note that Q_4 to Q_3 transformation (Garcia-Diaz et al. 2006) can be responsible for aggregate volume expansion without forming any typical ASR gel. Therefore, it may be possible to measure some volume change due to ASR in VCMD with no obvious presence of ASR products in case of slowly reactive aggregates. From the above discussion, it is logical to claim that microstructural studies on the reacted aggregate particles by SEM-EDS support the CAE-based reactivity prediction.

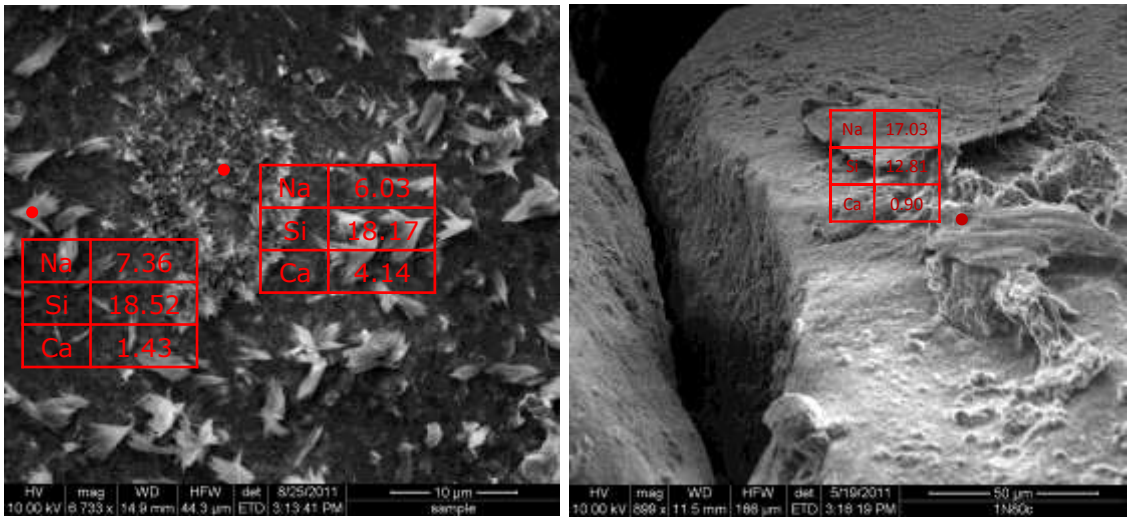

Figure 5.13 Secondary Electron Images of Reaction Products on Aggregate Particles at 1N NH + CH (80^oC), FA1.

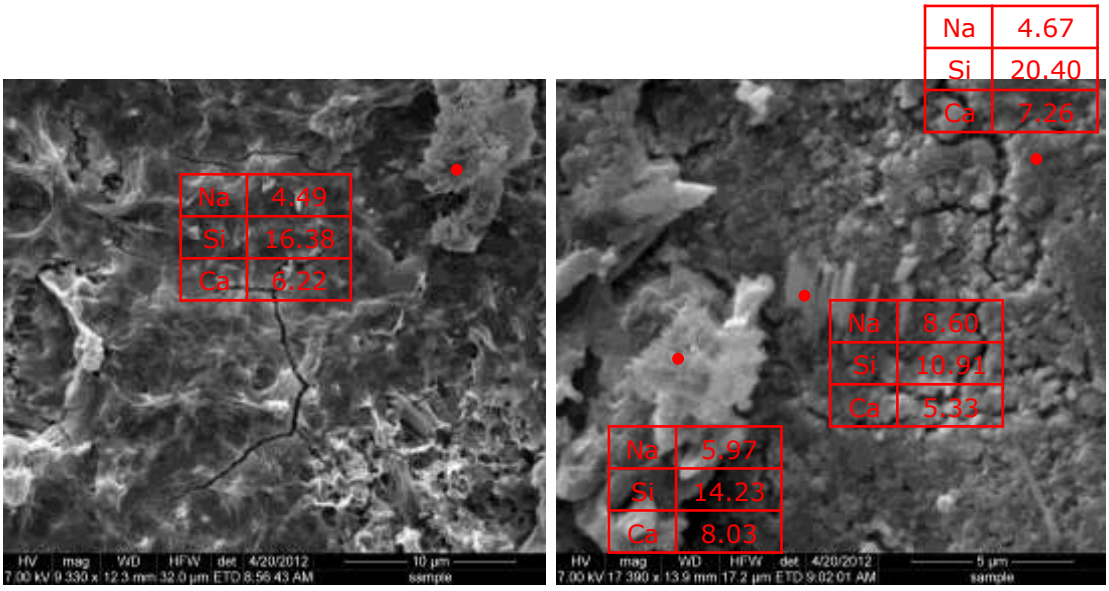

Figure 5.14 Secondary Electron Images of Reaction Products in Aggregate Particles at 1N NaOH + $Ca(OH)_2$ (80°C), CA1.

Prediction of Threshold Alkali Level

An apparent relationship between CAE and alkalinity is evident from the results of the studied aggregates (Table 5.2). The higher the alkalinity, the lower the CAE is. An attempt was made to establish a mathematical relationship between CAE and alkalinity. The following model (Eq. 5.3) was used to establish a relationship between CAE and alkalinity:

$$E = E_0 + \frac{C_0}{C^m} \tag{5.3}$$

where E is CAE (KJ/mole), E_o is CAE-theoretical threshold (KJ/mole), C_0 is CAE curvature coefficient (KJ/(mole)$^{1-m}$, m is CAE curvature exponent, and C is alkalinity (mole).

The existence of a characteristic TH_A for each aggregate can be manifested from the plots. By fitting the model (Eq. 5.3) to the measured CAE and solution alkalinity, the characteristic trend is obtained (Figure 5.15). Based on the trend, a TH_A for each aggregate can be assigned through the intersection of two tangent lines. When the distance between the intersection and the trend is the shortest, the intersection (e.g., Intersection 3 in Figure 5.15) is predicted as a TH_A.

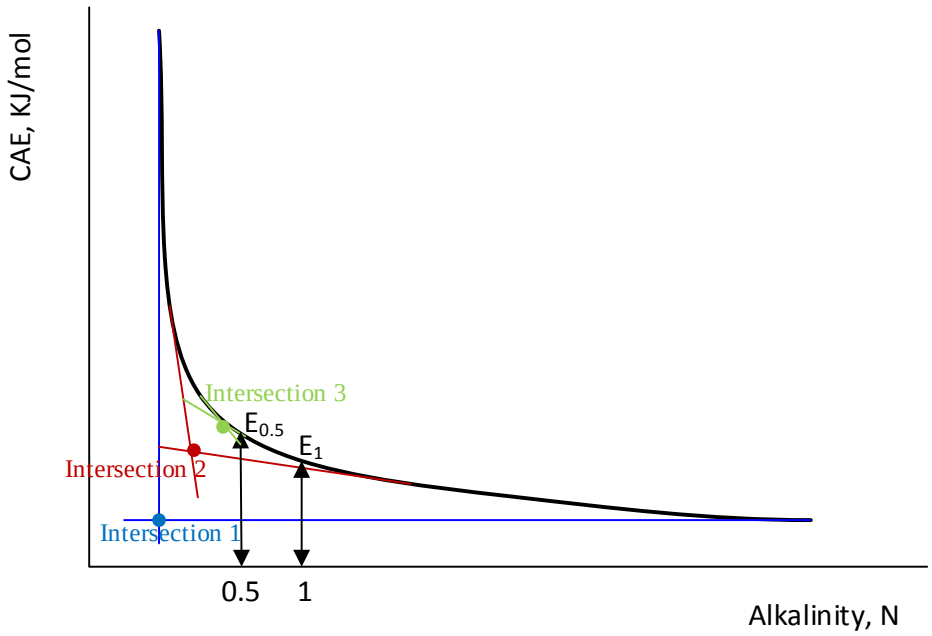

Figure 5.15 Determination of TH_A through CAE vs. alkalinity.

The results are presented in Figures 5.16 to 5.18 for the tested aggregates. The plots show that as alkalinity increases, the CAE decreases for all the aggregates. A good

fit between the measured and predicted CAE values is manifested, and this demonstrates the applicability of the proposed model.

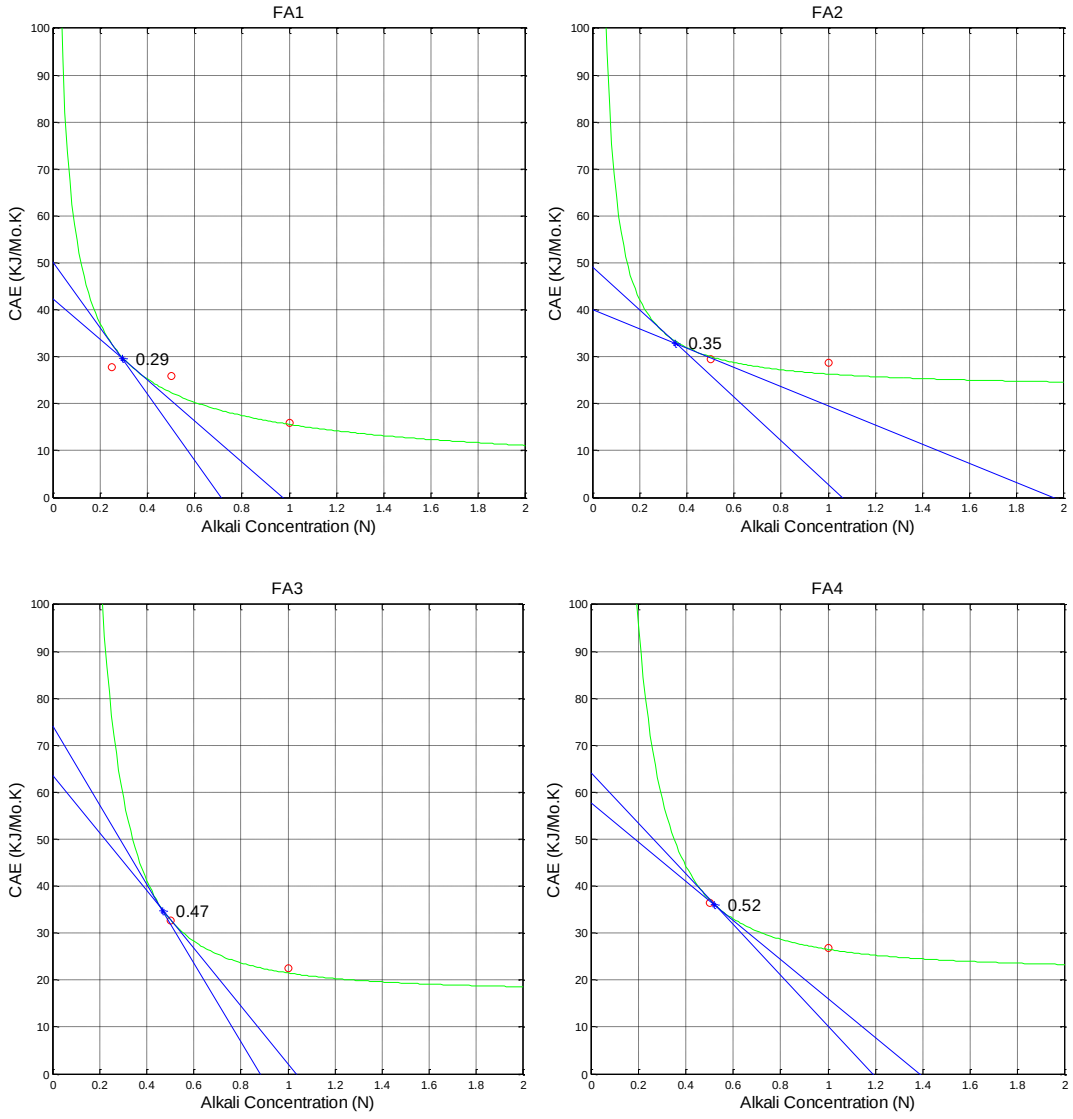

Figure 5.16 Prediction of TH_A for Tested Fine Aggregates.

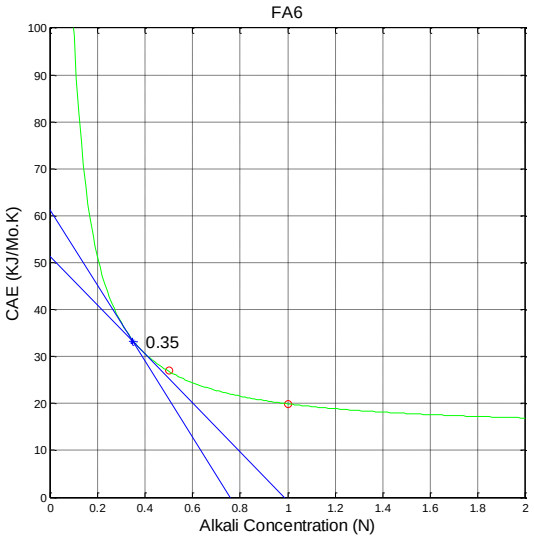

Figure 5.16 Continued.

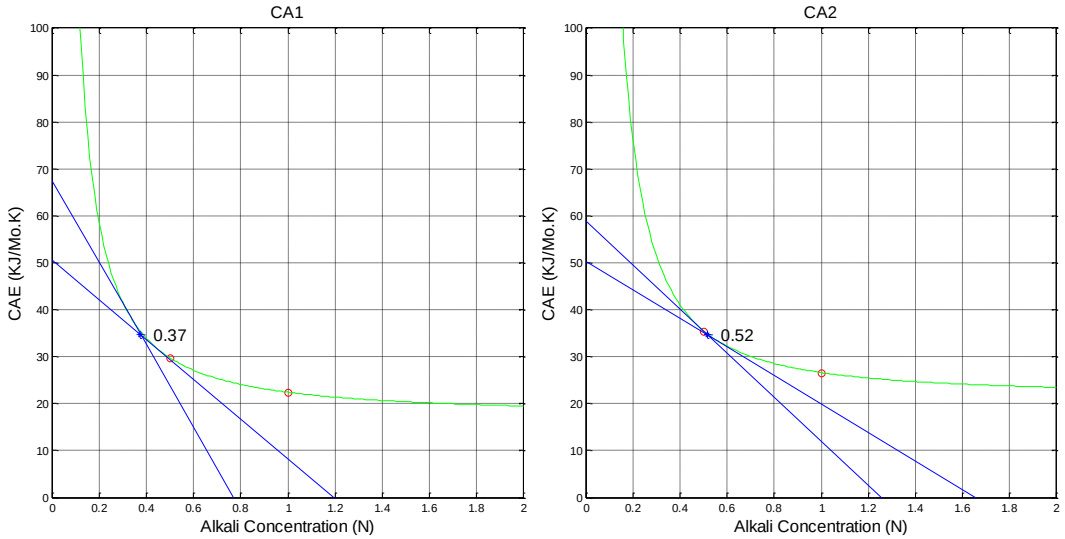

Figure 5.17 Prediction of TH_A for Tested Coarse Aggregates.

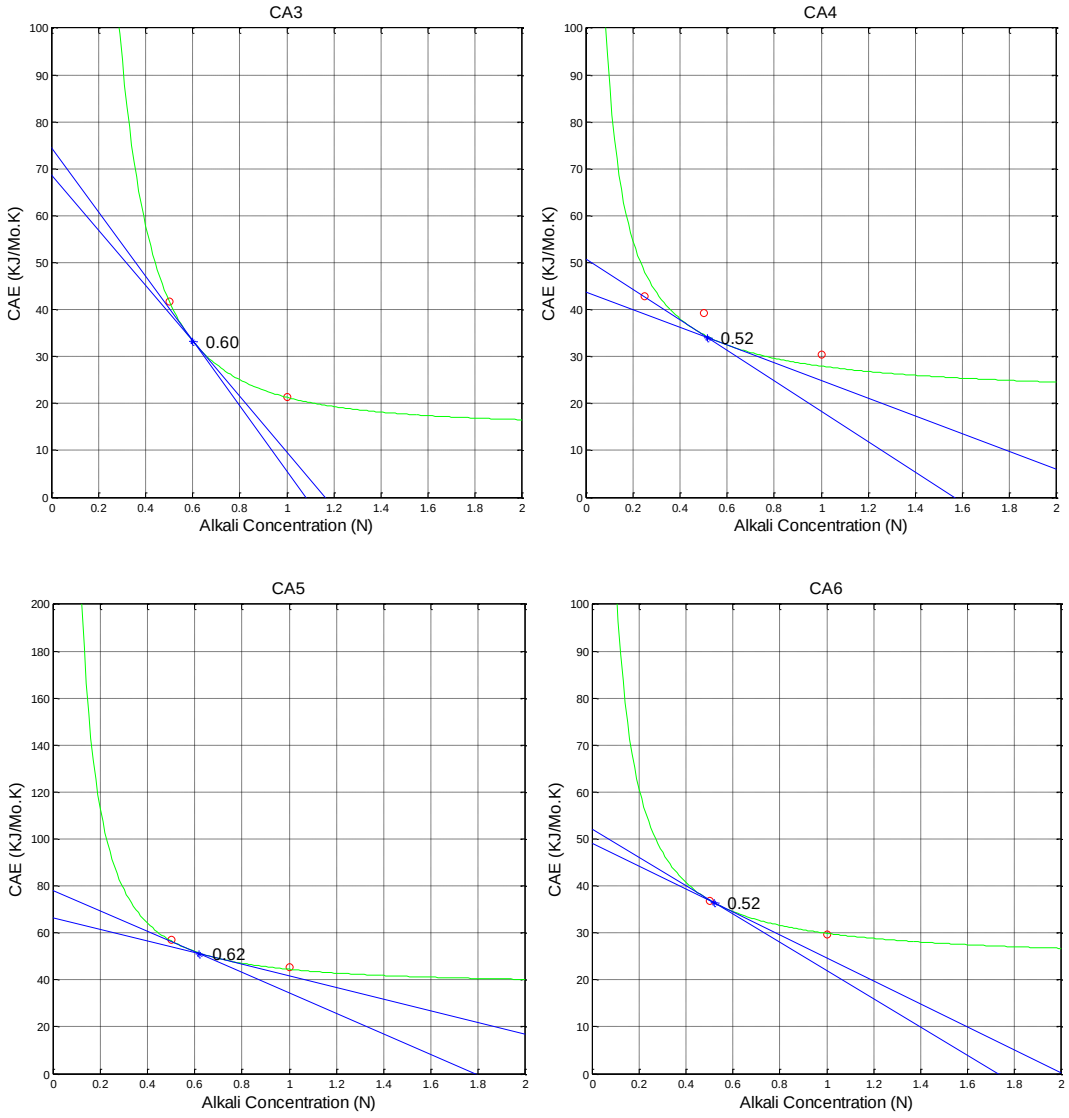

Figure 5.17 Continued.

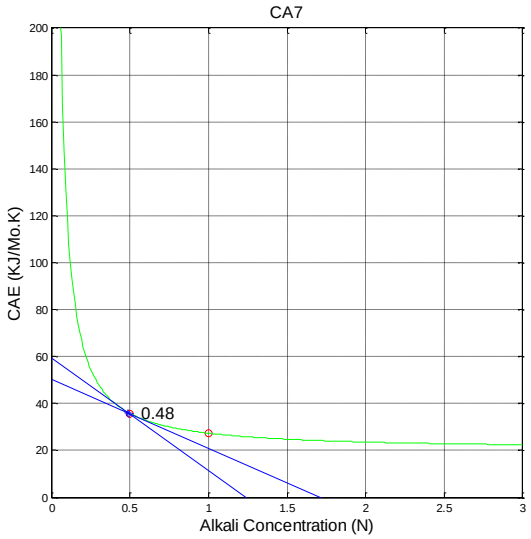

Figure 5.17 Continued.

A TH_A for each aggregate is mathematically calculated from the CAE vs. alkalinity plot (Figures 5.16 and 5.17) and is summarized in Table 5.3. In general, the higher the reactivity, the lower the TH_A.

Table 5.3 Summary of Threshold Level of Alkalinity (TH_A).

Aggregate	CAE (1N NH + CH, KJ/mole)	CAE (0.5N NH + CH, KJ/mole)	TH_A (N)
FA1	15.98	26.00	0.29
CA1	22.15	29.73	0.37
FA3	22.55	32.64	0.47
CA3	21.29	41.78	0.60
CA4	30.33	39.18	0.52
CA7	27.24	35.72	0.48
CA5	45.35	57.03	0.62
FA4	26.82	36.39	0.52
CA2	29.68	35.95	0.52
FA2	28.70	29.41	0.35
CA6	29.65	36.74	0.52
FA6	19.95	26.96	0.35

A reactive aggregate can practically behave as non-reactive or very slow reactive if concrete pore solution alkalinity (PSA) can be maintained below the TH_A. The common approaches to achieve a low level of PSA are (i) use of low alkali cement, (ii) use of good quality Fly ash with low alkali contents (lower than cement alkali contents), (iii) use of ternary blends instead of Fly ash alone, and (iv) ensuring minimum contribution of additional alkalis from external source(s). Chapter VI discusses these aspects in greater detail.

Development of a CAE-based ASR Classification System

A CAE-based ASR aggregate classification system is developed based on the number of aggregates that are tested in this study and presented in Table 5.4. The CAE for all the tested aggregates along with ASTM C 1260 14-day expansion (%) and ASTM

C 1293 1-year expansion (%) are graphically presented in Figures 5.18 and 5.19. It is recommend to use the classification system based on CAE at 0.5N NH + CH (close to concrete pore solution alkalinity, i.e., field levels of alkalinity) in all practical purposes.

Table 5.4 CAE-based ASR Aggregate Classification System.

CAE Range, KJ/mole		Reactivity
1N NH + CH	0.5N NH + CH	
< 20	< 30	4 (highly reactive)
20-35	30-45	3 (reactive)
35-46	45-60	2 (potentially/slowly reactive)
> 46	> 60	1 (nonreactive)

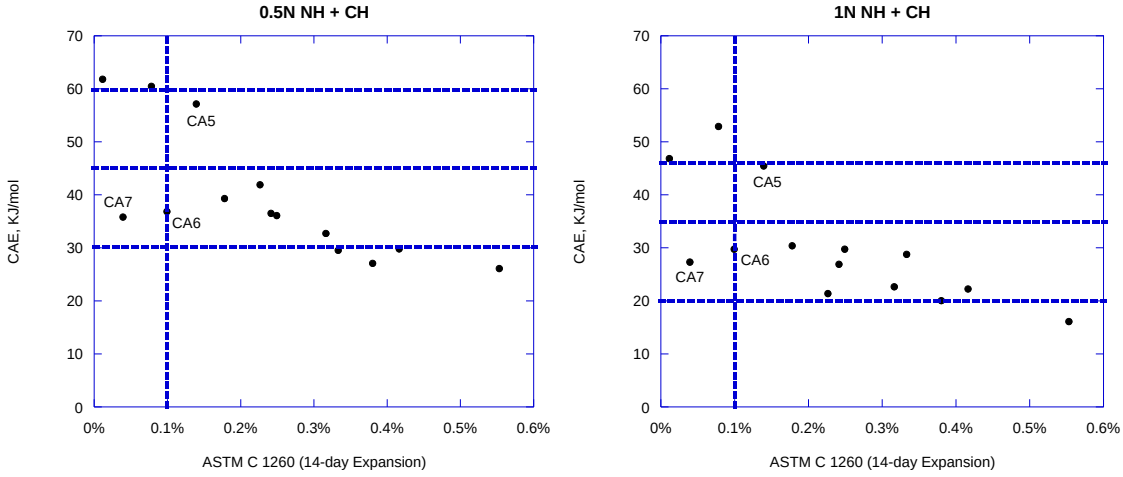

Figure 5.18 Correlation between ASR CAE of Aggregate and ASTM C 1260 14-day Expansion.

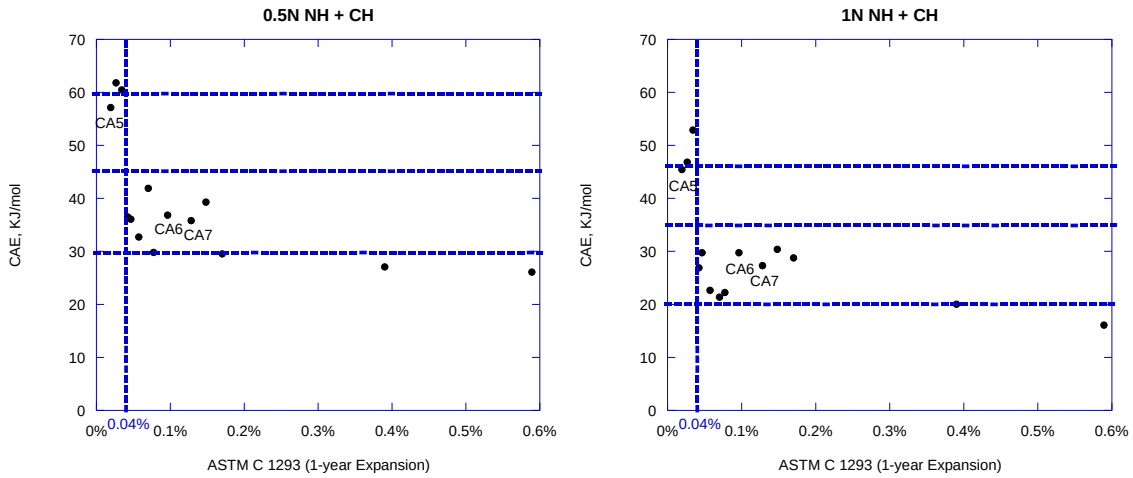

Figure 5.19 Correlation between ASR CAE of Aggregate and ASTM C 1293 1-year Expansion.

The benefits of the CAE-based aggregate classification system are presented in Table 5.5. Case 1 and 2 are the examples where CAE and standard AMBT tests shows a very good match, which suggests that a CAE-based method is a good choice as it takes less time and produces data with higher repeatability than AMBT test. Case 3 and 4 indicate the CAE-based test method has the potential to overcome the limitations of the current test methods (especially AMBT) and has the ability to identify the aggregates that belong to false positive and negative categories (i.e., passed by ASTM C 1260 but failed by ASTM C 1293 and vice versa) reliably in a short period of time. In case 4, if ASTM C 1293 underestimates the reactivity (incidents of underestimation by ASTM C 1293 due to significant alkali leaching is reported) and that aggregate shows reaction in exposure blocks, the CAE-based classification system will identify that aggregate as a slowly/potentially reactive (i.e., Reactivity 2 in Table 5.4) and will not pass that

aggregate. Moreover, the CAE-based test has the ability to test as-received aggregates (i.e., field aggregates) and determine reactivity matching with the field level of alkalinity (measuring CAE at 0.5N NH + CH).

Table 5.5 Comparison between CAE-Based Aggregate Classification System, Current Methods, and Field Performance.

Case #	ASTM C 1260	ASTM C 1293	Performance in Field or Exposure Blocks	CAE-Based Aggregate Reactivity (Table 5.4)
1	Passed	Passed	No ASR	1
2	Failed	Failed	Severe ASR	4
3	Passed	Failed	Considerable ASR	3, 4
4	Failed	Passed	No ASR or little ASR with no ASR distress	1, 2

Summary

- The experiments with pure glass balls support solution volume contraction over time and used to validate the VCMD procedure.
- The VCMD-based test can reliably predict aggregate alkali silica reactivity in a short period of time in terms of measuring CAE. This test has the ability to test as-received aggregates (i.e., field aggregates) and determine CAE (reactivity) matching with the field level of alkalinity (recommended to test aggregate with 0.5N NH + CH solution). This reduces the gap between lab and field.
- The majority of COV based on β is within 10%, which indicates the results are highly repeatable (Figure 5.6).

- Measuring low CAE (high reactivity) of an aggregate using the VCMD is supported by higher consumption of OH^- (Figure 5.8) and/or greater reduction of Na^+ (Figure 5.9) in the test solution, which supports the VCMD test results.
- The formation of ASR product is observed by SEM-EDS on the reacted aggregate surfaces for the pure phase borosilicate glass and reactive aggregates (Figures 5.12 to 5.14). It is evident that microstructural studies on the reacted aggregate particles by SEM-EDS support the CAE-based reactivity prediction.
- The results in Figures 5.18 and 5.19 show that the aggregate that is failed by ASTM C 1260 but passed by ASTM C 1293 (i.e., CA5) has a relatively high CAE (slowly reactive or almost non-reactive). On the other hand, the aggregates that are passed by ASTM C 1260 but failed by ASTM C 1293 (i.e., CA6 and CA7) have a relatively low CAE (reactive). Therefore, the VCMD based test method has correctly identified the aggregates belong to false positives/negatives categories in a short period of time. This is the main benefit of the CAE-based method.
- The ASR CAE can serve as a single chemical material parameter to represent alkali silica reactivity of aggregate. The CAE-based ASR aggregate classification can be used as an alternative to the current test method (e.g., ASTM C 1260) and can serve as a potential screening parameter in aggregate quality control program.

CHAPTER VI

DEVELOPMENT OF A PROCEDURE FOR ASR-RESISTANT MIX DESIGN*

Determination of CAE and TH_A of the studied aggregates and development of a CAE-based ASR aggregate classification system are presented in the previous chapter. This chapter presents a procedure for developing ASR resistant concrete mixes as well as verification of poorly performing mixes. The procedure involves:

- Formulation, adjustment, and verification of ASR resistant mix through a chemical method based on CAE and TH_A determined in the previous chapter and concrete PSA (presented in this chapter).
- Mix-design validation by using an accelerated concrete cylinder test (ACCT)-a concrete cylinder test using VCMD has been proposed, which will also be presented in this chapter.

An attempt has been made to develop an effective way of tailoring mix design depending on the level of protection needed. This will ensure valuable resource conservation and avoid paying for premium ASR protection when only minor protection is needed.

* Part of this chapter is reprinted with permission from "A Kinetic-based ASR Aggregate Classification System" by Kai-Wei Liu and Anal K. Mukhopadhyay, 2014. *Construction and Building Materials*, 68, 525-534. Copyright 2014 Elsevier.

Guidelines to Formulate an ASR-Resistant Concrete Mix

An ASR-resistant mix is formulated by applying both mix design controls and special protection measures (as needed) depending on CAE based reactivity, TH_A and some consideration on the severity of ambient conditions (Table 6.1). Table 6.1 only shows two extreme combination of CAE, TH_A and ambient conditions as examples. Based on the two extreme combination guidelines in Table 6.1, mix design controls and special protection measures (as needed) can be selected for all other possible case specific combinations.

Table 6.1 Guidelines through Examples for Formulation of ASR-Resistant Mixes.

CAE-Based Aggregate Reactivity	TH_A	Severity of Ambient Conditions	Mix-Design Controls	Special Protection Measures (SPM)
High	Low (i.e., low alkali tolerance)	High Example: High rainfall (high RH) ± high T ± seawater-contaminated aggregates ± use of deicers	• Low alkali cement • Relatively low CF • Higher amount (25–35%) of good quality Fly ash (soluble alkalis should be below the cement alkali) replacement • Low w/c– ○ Create low permeability which reduces the ingress of external alkalis and moisture ○ Less free water available for gel swelling ○ Increase of PSA due to low w/c should be counteracted by high amount of good quality Fly ash or ternary blends (SPM)	Use of: • Ternary / quaternary blends instead of Fly ash alone (e.g., Fly ash + GGBS, Fly ash + silica fume (SF), Fly ash + metakaolin, Fly ash + SF + GGBS etc.) • 100% or higher dosage of $LiNO_3$ • Porous light weight aggregate (LWA) and/or aggregate blend
High	Low	Low Example: Low rainfall (low RH) ± low temperature ± no source of external alkalis	• Low alkali cement • Relatively low CF • Higher amount (25-35%) of good quality Fly ash replacement	Use of: • LWA and/or aggregate blend • Lower dosage of $LiNO_3$ depending on TH_A
Low	High (i.e., high alkali tolerance)	High	• Cement with low-intermediate alkali content can be allowed as high alkali tolerance is indicated by TH_A. • Medium quality Fly ash (e.g. alkali content ≤ cement soluble alkali, Fly ashes with relatively high CaO contents) can be used. • Conventional CF and Fly ash replacement	Use of: • Low w/c concrete (low permeability) • Ternary blends depending on the severity of ambient conditions
Low	High	Low	Same as above	No need

Procedures for Mix Design Adjustment and Verification

The procedure for adjustment and verification of ASR resistant mixes based on CAE, TH_A, and PSA are presented in Table 6.2 and brieFly described below:

Step I: Determination of CAE and TH_A from aggregate-solution test (Chapter V)

Step II: Development of an ASR-resistant mix by applying both mix design controls and special protection measures (as needed in Table 6.1)

Step III: Mix design adjustment/verification based on TH_A-PSA relationship

The developed ASR-resistant mix (Step II) is adjusted/verified based on PSA and TH_A.

a) If the PSA is lower than TH_A, the mix should perform well in the field without any ASR.
b) If the PSA is higher than TH_A, the mix needs adjustment by both mix design controls (help to reduce the PSA) as well as special protection measures (help to make gel less expansive and/or increasing the space for gel accommodation) (Table 6.1).
c) If the PSA is equal to TH_A, the mix may not need any further adjustment under mild ambient conditions. However, special protection measures (Table 6.1) may be needed under severe ambient conditions.

Table 6.2 Procedures to Adjust and Verify ASR-resistant Concrete Mixes

	Test	Test Conditions	Duration	Measured Parameters	Adjustment/Verification
Development of ASR-Resistant Concrete Mix	CAE-Based Aggregate-Solution Test	Temperatures: 60°, 70°, and 80°C. Soak solution alkalinity: 1N and 0.5N NH + CH	15–20 days	Aggregate reactivity based on CAE TH_A based on CAE @ multiple levels of alkalinity	If PSA < TH_A: mix should perform satisfactorily in the field with no symptoms of ASR If PSA = TH_A: mix should perform well without any measurable ASR under mild ambient conditions (Table 6.1) If PSA > TH_A: stringent mix design controls as well as special protection measures are highly needed before concrete placement (Table 6.1)
	Pore Solution Extraction		10 days	PSA based on both Na^+ and K^+	

The adjusted mix (step III) should perform well in the field without any ASR or with no measurable ASR distress. In order to verify the efficacy of the above chemical method to formulate ASR resistant mix, it is necessary to perform mix design validation through concrete testing. Validating the adjusted concrete mix (step III) through an accelerated concrete testing will be the ideal in order to recommend an ASR-resistant mix with high reliability. The ASTM C 1293 takes a year and doesn't serve the purpose if one can't wait that long. Efforts have been made by different researchers to develop a modified (accelerated) version of ASTM C 1293, which can be used provided the reliability of the modified version is established. Therefore, the demand of a rapid and reliable concrete test is still very high. An ACCT which is presented in next section has

been developed and used as a mix design validation method in this study along with ASTM C 1293 data.

If the pore solution extraction method is not available, the dependency on concrete validation testing will be high in order to develop safe ASR-resistant mix with high reliability. As CAE based reactivity prediction is reliable and dependable, an expert can design ASR resistant mix based on CAE-based reactivity, TH_A, knowledge gained based on concrete validation testing, and the recommended guidelines on mitigation practices (Table 6.1) without pore solution data and concrete validation testing. This practice may be acceptable but some amount of risk might be involved.

An Accelerated Concrete Cylinder Test (ACCT) for Mix-Design Validation

The CPT (e.g., ASTM C 1293) has been considered as the best index for field performance, but alkali leaching and test duration are still of concern. Ranc and Debray (1992) first introduced the accelerated concrete prism Test (ACPT) in the early 1990s. The concrete prisms were stored over water at 60^{o}C instead of 38^{o}C. The results show a good correlation between the 38^{o}C and 60^{o}C tests after 56 days of testing period. Other researchers (Grosbois 2000; Touma et al. 2001) also show a reasonably good correlation between 1 year concrete prism expansions at 38^{o}C and 2 to 4 months prism expansion at 60^{o}C. Although the test duration is shortened by simply increasing the test temperature, a significant reduction in expansion associated with high alkali leaching was noticed in the ACPT compared to the CPT (Folliard et al. 2004; Ideker et al. 2006). When alkali leaches out of the specimens, the sulfate ions replace the leached alkali hydroxides and decrease the pH of pore solution. This eventually causes the reduction of expansion.

An ACCT has been proposed in this study to overcome some of the above limitations (e.g., alkali leaching, test duration) and come up with an alternative ASR concrete test method. The unique steps that are taken for the proposed test to be considered as a rapid and reliable concrete ASR test method are: (i) introduction of an automatic LVDT based length change measurement system with no involvement of errors due to operation and temperature change, (ii) measurements to avoid alkali leaching at relatively high temperature (60^{o}C), (iii) testing cylinders made with borosilicate glass balls and measuring its volume change (through the change of solution level) and length change as a proof of concept, (iv) tests at varying levels of alkali (alkali-boosted concrete to reduce testing period as well as alkali levels similar to job mix), and (v) proposition of a concrete validation testing. The different steps that were involved to develop the ACCT method are presented below:

Materials

Concrete cylinders made with pure phase material (i.e., borosilicate glass balls) and aggregates were tested in ACCT. Aggregates with different types of reactive silica and varying ranges of reactivity (e.g., ASTM C 1260, ASTM C 1293) were selected. Table 6.3 summarizes the reactivity data that the ASTM C 1260, ASTM C 1293, and CAE for these aggregates had determined (Chapters III and V). The 4 levels of alkali (i.e., 1.8, 2.4/2.7, 4.0, and 5.3 kg/m^3 (3, 4/4.5, 6.7, and 8.9 lb/yard^3)) were selected. A low-alkali (CM1 0.57% Na_2O equivalent (Na_2O_e)) and a high-alkali (CM2 0.82% Na_2O_e) Portland cement were chosen in order to reach the desired alkali levels over the range from (1.8 kg/m^3 (3.0 lb/yard^3, 0.57% Na_2O_e without alkali boosting) to 5.3 kg/m^3

(8.9 lb/yard^3, 1.25% Na_2O_e with alkali boosting) with varying levels of cement factor (CF). Table 6.4 presents the chemical analyses for the 2 cements used in this study.

Table 6.3 List of Aggregate with Relevant Material Data.

Aggregate	ASTM C 1260 (14-day Expansion, %)	ASTM C 1293 (1-year Expansion, %)	CAE-based Reactivity (Table 5.4)
Borosilicate glass	-	-	HR (4)
CA8	0.012	0.027	NR (1)
CA1	0.417	0.078	HR (4)
FA3	0.317	0.058	R (3)
FA6	0.381	0.391	HR (4)
FA5	0.079	0.035	NR (1)
FA4	0.242	0.043	R (3)

NR-nonreactive, HR-highly reactive, R-reactive.

Table 6.4 Chemical Analysis of the Cements Used.

Composition, wt.%	Na_2O	K_2O	SiO_2	Al_2O_3	Fe_2O_3	CaO	MgO	SO_3	Na_2O_e
Cement 1 (CM1)	0.07	0.76	20.7	5.3	2.9	64.4	0.9	2.9	0.57
Cement 2 (CM2)	0.12	1.06	19.29	5.47	2.71	65.14	1.1	3.13	0.82

Test Equipment

The device used in this study to measure length change of cylindrical concrete specimen over time is the same VCMD that is described in Chapter IV. Use of the same device to measure solution volume change (Figure 6.1a) and length change (Figure 6.1b) of cylinders made with borosilicate glass were conducted as a proof of concept.

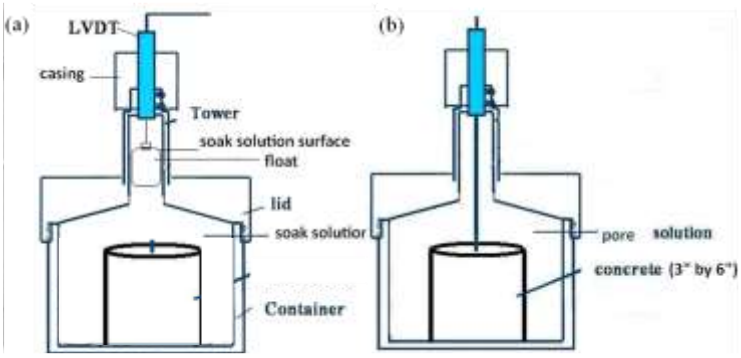

Figure 6.1 VCMD Test Setup for (a) Solution Volume Change (b) Length Change.

A 7.2 cm by 15.2 cm (3 inch by 6 inch) concrete cylinder with cast-in place threaded rod (Figure 6.1b) is placed inside the container. The 7-day curing specimen is then immersed with soak solution of specific alkalinity (equal to PSA of the specimen). The LVDT rod is connected to the threaded rod attached to the specimen, which moves inside the LVDT during ASR expansion of the specimen and creates electrical signals. These signals are converted to LVDT displacements (inch) through the data acquisition system and recorded by the attached computer through the LabVIEW program. The detailed test procedure is described later.

Mix Design and Specimen Preparation

All the ACCT mixes are ASTM C 1293 type mix with or without alkali boosting. Table 6.5 presents a detailed description of the mix designs. Concretes were mixed by hand following ASTM C 192 procedures. The cement and fine aggregates were thoroughly dry blended in a clean stainless steel bowl. The coarse aggregates were then added into the bowl and dry mixing continued until a homogeneous mix of cement,

coarse aggregate, and a fine aggregate is achieved. Deionized water was then added and mixing continues for an additional 5 minutes until a homogeneous concrete mix is achieved. Concrete cylinders using each mix (Table 6.5) were cast for ACCT.

Table 6.5 Concrete Mix Design for Conducting ACCT

Mix	Alkali (kg/m^3)	CA	FA	w/c	CAF	Cement type	CF (kg/m^3)	Additional alkali (NaOH, kg/m^3)	Na_2O_e (%)
1a	2.4	CA8	FA4	0.45	0.76	CM1	420	-	0.57
1b	4.0					CM1	420	1.6	0.95
1c	5.3					CM1	420	2.9	1.25
2a	2.4	CA1	FA5			CM1	420	-	0.57
2b	4.0					CM1	420	1.6	0.95
2c	5.3					CM1	420	2.9	1.25
3a	1.8	CA8	FA3			CM1	312	-	0.57
3b	2.7					CM2	325	-	0.82
3c	5.3					CM2	420	1.8	1.25
4a	1.8	CA8	FA6			CM1	312	-	0.57
4b	2.7					CM2	325	-	0.82
4c	5.3					CM2	420	1.8	1.25
5	2.7	CA1	FA6			CM2	325	-	0.82
6	2.7	CA8	FA5			CM2	325	-	0.82
7	2.7	CA1	FA5			CM2	325	-	0.82

w/c-water to cement ratio, CAF-coarse aggregate factor.

Pore Solution Extraction

The cement paste cylinders (5.1 cm by 10.2 cm) corresponding to each mix in Table 6.5 were cast and covered with plastic foil, and then stored under 100% relative humidity (RH) at 25±2˚C for 7 days. After the 7-day curing, the specimens were de-molded and pore solutions were extracted from each paste specimen. The pore solution

extraction from cement paste specimens was conducted by using a high-pressure squeezing method (Barneyback and Sidney 1981). Figure 6.2 shows the pore-solution extraction apparatus, which consists of a removable base equipped with a drain, a hollow cylinder, and a piston that can be inserted into the cylinder. The specimen is placed within the cylinder, and the piston applies pressure, which gradually increases by means of a hydraulic loading to a maximum of 181.4 kg (400 lb). The loading was applied and released twice for all specimens in order to get a sufficient quantity (i.e., 2-5 ml (Ideker et al. 2010)) of the pore fluid. The extracted pore solution for Na^+ and K^+ ion concentration was analyzed by AAS. Table 6.6 presents the composition (Na^+ and K^+) of pore solution extracted from the studied cement pastes. A minimum of 3 cement paste specimens for each mix in Table 6.5 was squeezed to extract pore solution followed by mixing the extracted solutions to get a representative pore solution. The Na equivalent (Na^+_e) (French 1980) represents the total alkali levels for each mix in this study. Note that the same alkali level using two different types of cement with varying Na_2O_e percentages and different amounts of extra alkali addition does not ensure the same PSA. For example, the PSA with 5.3 kg/m^3 using CM1 is 0.88 N but the PSA with 5.3 kg/m^3 using CM2 is 1.04N. Therefore, cement composition (especially the type of alkali-bearing phases in cement) plays an important role in controlling the PSA and the same alkali level using different cements do not necessarily provide the same PSA.

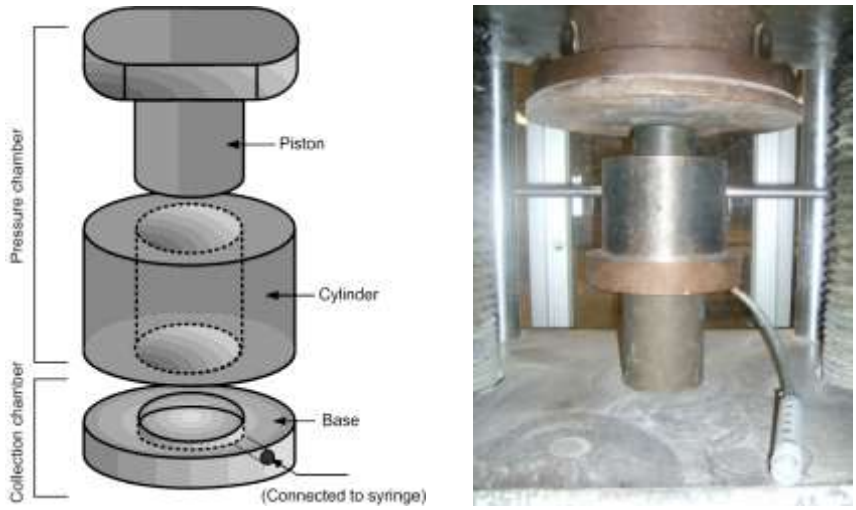

Figure 6.2 Pore-Solution Extraction Apparatus.

Table 6.6 Concentration of the Extracted Pore Solution from Cement Paste.

Alkali (kg/m^3)	CF (kg/m^3)	Na_2O_e (%)	Mix (Table 6.5)	Na^+ (ppm)	K^+ (ppm)	Na^+ (N)	K^+ (N)	Na^+_e (N)
2.4 (CM1)	420	0.57	1a, 2a	1800	19000	0.08	0.49	0.37
4.0 (CM1)	420	0.95	1b, 2b	4898	16100	0.21	0.41	0.46
5.3 (CM1)	420	1.25	1c, 2c	14132	17300	0.61	0.44	0.88
1.8 (CM1)	312	0.57	3a, 4a	1539	21031	0.07	0.54	0.38
2.7 (CM2)	325	0.82	3b, 4b, 5, 6, 7	4153	31562	0.18	0.81	0.66
5.3 (CM2)	420	1.25	3c, 4c	12755	31865	0.55	0.81	1.04

Pore solution chemistry data in the published literature (Berube et al. 2004; Brouwers and Eijk 2003; Lorenzo et al. 1996; Lothenbach and Winnefeld 2006) are very similar to the alkali concentrations in Table 6.6 that the pore-solution extraction method has determined in this study. Therefore, these pore solution concentrations were used to generate the soak solutions for the concrete cylinder test that correspond to each mix in Table 6.5. The quantities of NaOH and KOH pellets needed to generate an artificial

solution of the same composition for each mix in Table 6.6 were first calculated and then dissolved in deionized water to prepare the soak solutions. Calcium hydroxide crystals were then added (1 gram per liter solution) to the above respective solutions slightly above saturation in order to prepare an alkaline solution saturated with calcium hydroxide. Adding calcium hydroxide crystals slightly above the saturation point ensures presence of undissolved calcium hydroxide crystals, which represents a situation similar to concrete pore solution.

Test Procedure

The ACCT procedure is briefly described below:

- A 27.9-cm (11-inch) stainless steel threated rod was embedded (2.54 cm depth) on top of each concrete cylinder (7.6 cm by 15.2 cm) during specimen casting. After casting, the molds were covered with plastic foil and kept inside a 100% RH chamber at 25±2°C for 7 days.
- After 7 days, the concrete cylinders were de-molded and placed inside the VCMDs, which were filled up by soak solution with chemistry that is equal to the pore solution chemistry of each mix (each mix has a specific level of alkalis according to Table 6.5). The purpose of creating soak solution chemistry equals to pore solution chemistry is to prevent alkali leaching from the specimen.
- Each VCMD was tightly closed and placed inside an oven at 60°C.
- Expansion measurements were recorded every 15 minutes automatically through data acquisition-computer system over time.

Initially the concrete specimen expands due to temperature increase from the starting temperature to the target temperature (60°C). The subsequent LVDT readings after temperature stabilization (the reference/initial LVDT reading) represent displacement due to ASR. The displacement due to ASR over time divided by the original length at the reference point multiplied by 100 represents the percent expansion of the concrete cylinder due to ASR over time

Mix-Design Verification

Based on Table 6.2, if the PSA (Table 6.6) is higher than the TH_A determined from aggregate-solution test (Table 5.2), the aggregate will react (degree depends on aggregate reactivity and PSA). On the other hand, if the PSA is lower than the TH_A, the aggregate will not react or react very slowly. Table 6.7 compares the PSAs of the selective mixes and TH_A of the reactive aggregates in those mixes. For example, the TH_A of the reactive fine aggregate (FA3) in mix 3 is 0.47N and the PSAs for 3a, 3b, and 3c mixes are 0.38, 0.66, and 1.04N respectively (Table 6.7). Only the concrete cylinder with alkaline level 1.8 kg/m^3 (0.38N) is lower than the TH_A (0.47 N). Therefore, it can be expected that the reactive fine aggregate (FA3) in mix 3a will not show any ASR, but the same aggregate in mixes 3b and 3c, where PSA > TH_A will react and give ASR expansion in cylinder test. The higher the PSA the higher the expansion will be. For other mixes, the corresponding reactive aggregates can also be expected to react when the PSA is higher than TH_A and gives expansion as a function of alkalinity. The concrete validation testing (next section) using these mixes will verify the expected expansion behavior based on PSA-TH_A relationship (Table 6.7).

Table 6.7 TH_A of the Reactive Aggregates and Pore Solution Alkalinity (PSA) Comparison.

Alkali (kg/m^3)	Mixes (Table 6.5)	TH_A (N)	PSA (N)	Expected Concrete Cylinder Expansion Behavior
1.8 (CM1)	3a	0.47	0.38	No expansion
	4a	0.35	0.38	Will expand
2.4 (CM1)	1a	0.52	0.37	No expansion
	2a	0.37	0.37	May or may not expand
2.7 (CM2)	3b	0.47	0.66	Will expand
	4b	0.35	0.66	Will expand
	5	0.35/0.37	0.66	Will expand
	7	0.37	0.66	Will expand
4.0 (CM1)	1b	0.52	0.46	No expansion
	2b	0.37	0.46	Will expand
5.3 (CM1)	1c	0.52	0.88	Will expand
	2c	0.37	0.88	Will expand
5.3 (CM2)	3c	0.47	1.04	Will expand
	4c	0.35	1.04	Will expand

Mix-Design Validation by ACCT

This section presents the concrete validation testing results for the selected mixes from Table 6.5. Mortar cylinders made of highly reactive borosilicate glass balls were tested first to validate the proposed concrete cylinder test before testing actual concrete mixes.

Pure Phase Materials

Measurement of Volume Change and Linear Expansion

Mortar cylinders with highly reactive borosilicate glass balls were tested first to verify its applicability to measure ASR expansion before any concrete testing. The glass-mortar cylinders were cast, and measurements of net solution volume change and the length change were conducted as a proof of concept. The mortar mix used alkali level

2.7 kg/m^3 (4.5 lb/$yard^3$, equivalent to 0.82% Na_2O_e) with 40% glass. The curing conditions (i.e., 7 day fog-room curing before de-molding) and testing conditions (i.e., 60°C, immersing in PSA) were the same for both cylinder tests. For the cylinder of solution volume change measurement, the device is firstly filled up with PSA overnight at room temperature to allow maximum saturation of voids in the PSA. On next day, the device is placed on a vibrating table and conducts vacuuming under vibration for 2 hours to mainly remove entrapped air bubbles in the solution and also help to saturate the unfilled voids in the cylinder after overnight saturation. The device is then placed inside an oven and heated to 60^{o}C to eliminate the effect of porosity due to temperature change. When the solution reaches 60^{o}C, the device is removed from the oven and applied a second stage vacuuming under vibration of 45 minutes to facilitate further removal of air bubbles (may be generated during preheating at 60^{o}C) from solution. The device is placed back inside the oven whose temperature is then raised to 60^{o}C. The float movements due to solution volume changes as initial thermal expansion and the chemical reaction between cylinder and alkaline solution progresses are then recorded through a data acquisition system. Figure 6.3 shows the solution volume change and length change of glass-mortar cylinders at 60^{o}C over time. The macro-crack pattern of the cylinder and nature of micro-crack under microscope are presented in Figure 6.4.

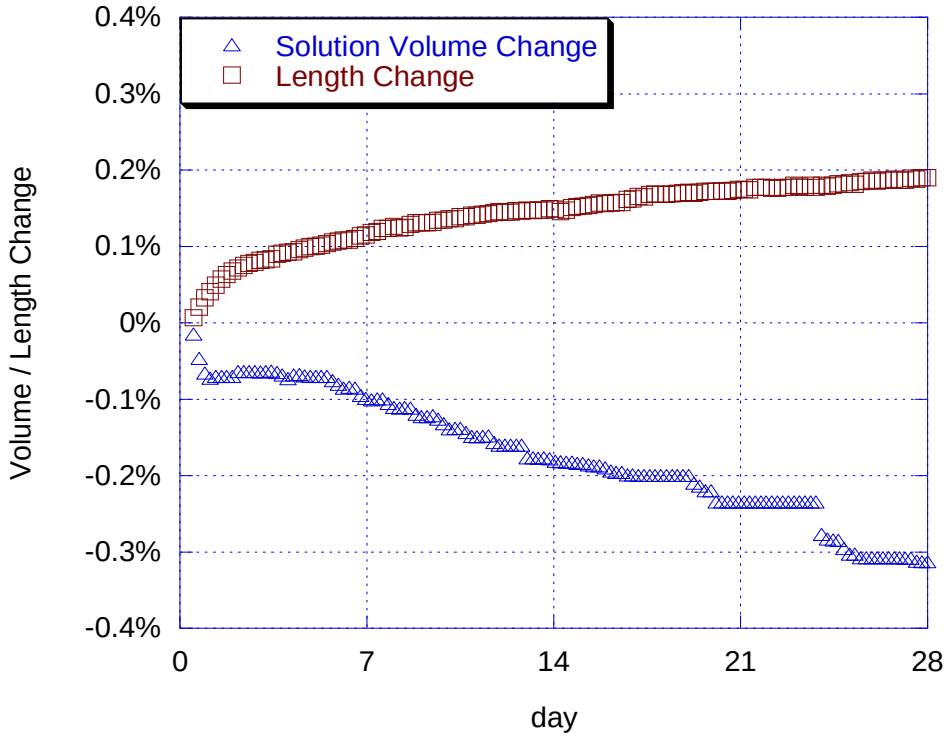

Figure 6.3 Solution Volume Change and Length Change of Glass-Mortar Cylinder.

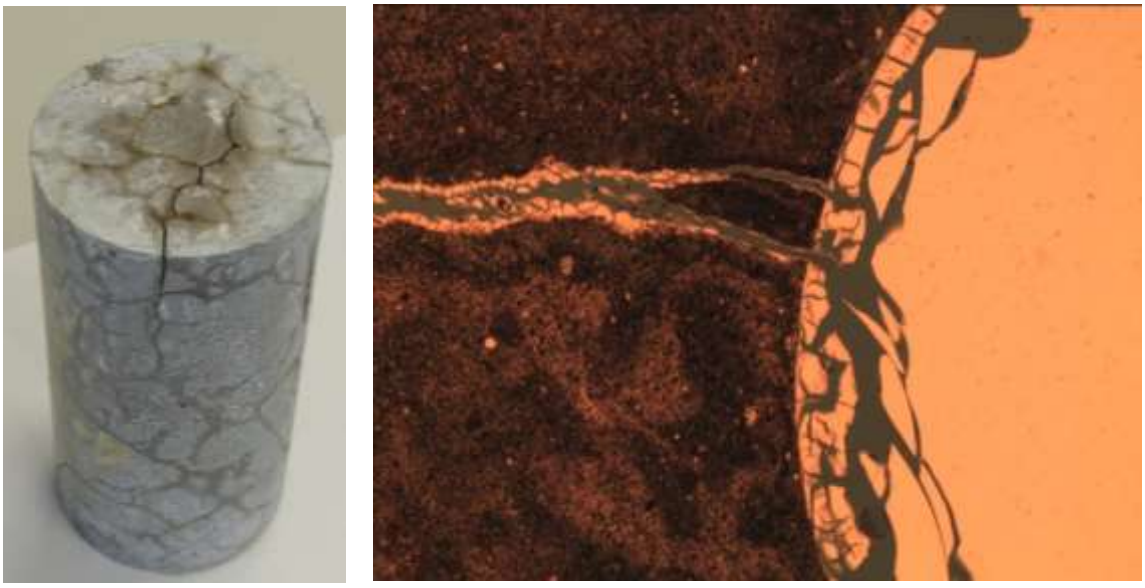

Figure 6.4 Macrocrack Pattern and Thin Section of Glass-Mortar Cylinders.

The measurement of the length change of the glass-mortar cylinder shows expansion but the measurement of the solution volume change shows reduction (Figure 6.3) which might be due to the consumption of reactants (e.g., water, ionic species) and the formation of micro-/macro- cracks. These cracks create fresh surfaces and act as open passages for alkali solution to flow into the matrix of the cylinder leading more solution level reductions. Therefore, the reduction of solution volume in Figure 6.3 might be caused by new open passages due to new cracks formations, and measurement of the change of solution level cannot guarantee to measure the expansion of specimen due to ASR.

Base on Figure 6.4, the followings confirm the presence of a high degree of ASR: (i) presence of macrocracks in the cylinder, (ii) presence of microcracks in a reacted glass ball, (iii) microcracks passing through both the reacted glass ball and cement paste, and (iv) presence of ASR gel at the periphery of the reacted glass ball. The ASR features (both macro- and micro-scale) supports the high linear expansion measurement (Figure 6.3) in the cylinder test. Therefore, the proposed cylinder test is capable of measuring ASR expansion in a short period of time.

Prediction of ASR Expansion using Composite Spherical Model and Finite Element Model

Both composite spherical and finite element modeling where relevant gel properties and free strain of ASR are the main inputs are developed in this section. The purpose of the models is to predict the physical behavior (i.e., linear expansion) of the glass-mortar cylinder due to ASR as supporting tools.

Composite Sphere Model

Concrete is considered as a composite material and modeled in different aspects. A two-phase composite model consisting aggregate particles and a cement paste matrix is usually used to describe overall properties of concrete (Mura 1987). Christensen (1979) developed a two-phase composite sphere model to predict the composite free strain. Taking the inclusion as aggregate and the matrix as cement paste, and adding an ITZ layer in between the inclusion and matrix layer, Christensen's model can be extended to a three-phase sphere model (Zheng and Zhou 2008). The porous ITZs in concrete provide a sufficient region for inhabitation of ASR gel. Therefore, three-phase model is used in this study to represent ASR gel in concrete, as shown in Figure 6.5. In the composite sphere model, all phase are assumed to be isotropic and water diffusivity is independent for expansion for simplicity in this study.

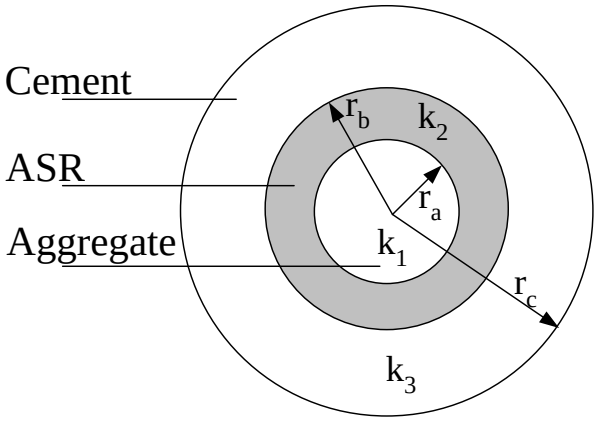

Figure 6.5 Three-phase Sphere Model.

In Figure 6.5, r_a is the radius of aggregate, r_b-r_a is the thickness of ASR layer, and r_c-r_b is the thickness of cement layer. The area outside of cement layer is the equivalent medium. Other physical-mechanical parameters are k1, k2, k3, and k, which represent the bulk modulus of aggregate, bulk modulus of ASR gel, bulk modulus of cement, and effective bulk modulus of the system (e.g., concrete), respectively.

Equation 6.1 shows the overall free strain (ε^f) for the composite sphere model (Figure 6.5) proved by Christensen (1979):

$$\varepsilon^f = \frac{1}{\overline{1/k} - 1/k}\{\frac{\overline{k\varepsilon}}{\overline{k}}\left[\frac{\overline{1}}{k} - \frac{1}{k}\right] + \varepsilon\left(\frac{1}{k} - \frac{1}{\overline{k}}\right) + \sqrt{\left(\frac{\overline{1}}{k} - \frac{1}{k}\right)\left(\overline{k\varepsilon^2} - \frac{\overline{k\varepsilon}^2}{\overline{k}}\right) - (\varepsilon^2 - 2\frac{\overline{k\varepsilon^2}}{\overline{k}} + \frac{\overline{k\varepsilon}^2}{\overline{k}^2})}\sqrt{\frac{\overline{1}}{k} - \frac{1}{k}}\sqrt{\frac{1}{k} - \frac{1}{\overline{k}}} \quad (6.1)$$

where

$$\overline{k\varepsilon} = \sum k_i c_i \varepsilon_i \; ; \varepsilon = \sum c_i \varepsilon_i \; ; \frac{\overline{1}}{k} = \sum \frac{c_i}{k_i}; \; \overline{k} = \sum c_i k_i \; ; i = 1, 2, 3$$

c is the volume fraction of the inclusion phase

By applying both the stress and displacement to the same boundary conditions between each phase, the effective bulk modulus k is shown in Eq. 6.2 (Li et al. 1999)

$$k = k_3 + \frac{(k - k_3)(b^3/c^3)}{1 + [(1 - b^3/c^3)(k_2 + \frac{(k_1 - k_2)(a^3/b^3)}{1 + [(1 - a^3/b^3)(k_1 - k_2)/(k_2 + \frac{4}{3}G_2)]} - k_3)/(k_3 + \frac{4}{3}G_3)]} \quad (6.2)$$

where G_2 and G_3 are the shear modulus of ASR and cement layer respectively.

It can be seen from Eqs. 6.1 and 6.2 that the free strain of the concrete depends on the volume fraction, free strain, and elastic properties (E) of each phase. From the glass-mortar cylinder, the volume fraction of each phase can be calculated. The elastic properties of glass (E_1) and cement (E_3) can be obtained from existing publications. This means the only unknown parameters are elastic properties and free strain of ASR gel. In order to determine those two parameters, two measurements are conducted and described below.

Determination of Elastic Modulus of ASR Gel

The elastic modulus of ASR gel (E_2) in this study is measured using Triboindenter Nanoindenter with a Berkovich indenter tip. There has been considerable interest in the last two decades in the mechanical characterization of materials using depth-sensing indentation tests. Usually, the principal goal of such testing is to obtain values for elastic modulus and hardness of the specimen material from experimental readings of indenter load and depth of penetration. But other properties such as residual stress, fracture toughness, and visco-elastic behavior may also be measured. The indentation technique can be used on both brittle and ductile materials where conventional testing may result in premature specimen fracture. The forces involved are usually in the millinewton range and measured with a resolution of a few nanonewtons while the depths of penetration are in the order of nanometres, hence the term "Nanoindentation" (Fischer-Cripps 2002).

In a traditional indentation test, a hard tip with its mechanical properties are known (frequently made of a very hard material, e.g., diamond) is pressed into a sample

whose properties are unknown. The load placed on the indenter tip is increased as the tip penetrates further into the specimen and soon reaches a user-defined value. At this point, the load may be held constant for a period or removed. The contact area in the sample is measured and the hardness (H), is defined as the maximum load, P_{max}, divided by the contact area, A_c. A record of the depth of penetration and load can be plotted on a graph to create a load-displacement curve (Figure 6.6). These curves can be used to extract mechanical properties of the material (Oliver and Pharr 1992; Velez et al. 2000).

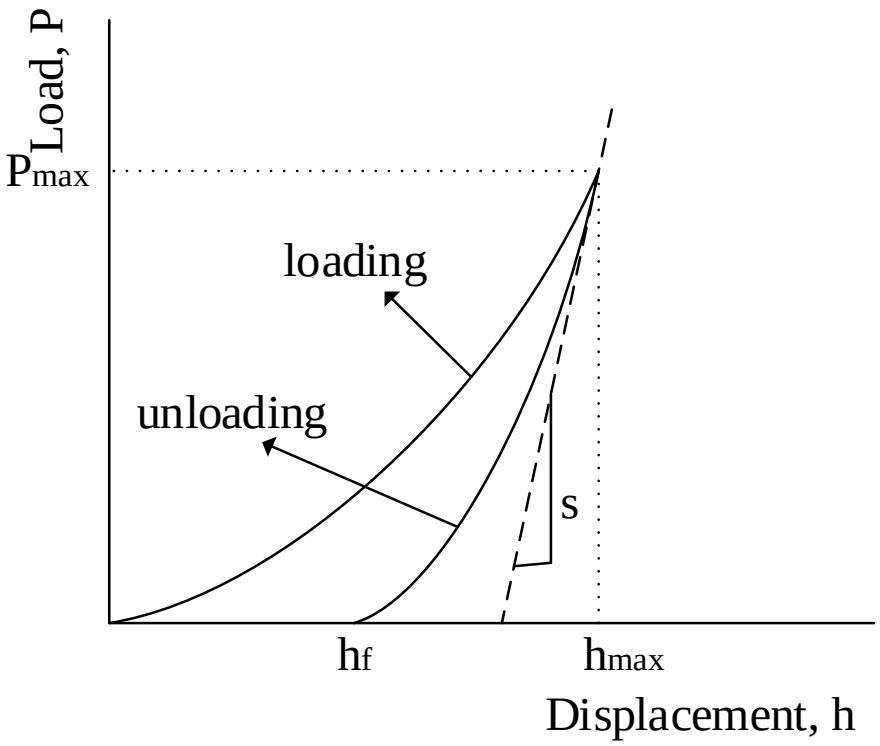

Figure 6.6 Schematic Representation of Load-Displacement Curve for Nanoindentation Test. S (Stiffness) is the Slope of the Unloading Curve, P_{max} Represents the Maximum Load Applied, h_{max} is the Corresponding Displacement, and h_f is the Final Displacement.

The slope of the curve, dP/dh, upon unloading is indicative of the stiffness S of the contact. This value generally includes a contribution from both the material being tested and the response of the test device itself. The stiffness of the contact can be used to calculate the reduced elastic modulus, E_r:

$$E_r = \frac{1}{\beta}\frac{\sqrt{\pi}}{2}\frac{S}{\sqrt{A_p(h_c)}} \tag{6.3}$$

where $A_p(h_c)$ is the projected area of the indentation at the contact depth h_c, and β is a geometrical constant (approximately equal to 1.034 for the Berkovich indenter) (Velez et al. 2000). $A_p(h_c)$ is often approximated by a fitting polynomial as shown below for a Berkovich tip:

$$A_p(h_c) = C_0 h_c^2 + C_1 h_c^1 + C_2 h_c^{1/2} + ... + C_8 h_c^{1/128} \tag{6.4}$$

where C_0 for a Berkovich tip is 24.5 while for a cube corner (90°) tip is 2.598. The E_r is related to elastic modulus of the sample (E_s) through the following relationship from contact mechanics:

$$\frac{1}{E_r} = \frac{1-\upsilon_i^2}{E_i} + \frac{1-\upsilon_s^2}{E_s} \tag{6.5}$$

Here υ is the Poisson's ratio and the subscript i refers to the indenter and s refers to the sample. For a diamond indenter tip, E_i is 1140 GPa and Poisson's ratio is 0.07. The υ_s is generally between 0 and 0.5 for most materials and the appropriate selection of this is a crucial decision.

ASR gel was simulated in the laboratory by adding borosilicate glass slides (with same composition used in previous chapters) into beakers containing PSA solutions. The

sample (glass slide) was placed in alkali level 2.7 kg/m^3 (4.5 lb/yard^3) solution. A temperature of 60^{o}C was maintained to enhance the reaction. A white gel formation occurs on the glass slides in 4 days and the gel was dried at 40^{o}C for 24 hours before the nanoindentation testing. A load of 500 μN was applied to the sample and the load-displacement graph was plotted which is used for determining the reduced elastic modulus of the gel. Eq. 6.5 is then used to find the actual elastic modulus of the gel. The selection of Poisson's ratio for the gel is critical in determining its elastic modulus. To be sure of the Poisson's ratio of the ASR gel more experiment needs be carried out and this is outside of the scope of this paper. According to Li et al (1999), the Poisson's ratio of ASR gel can be taken as 0.3. Thus, a Poisson's ratio of 0.3 was assumed throughout the experiment for simplicity.

ASR gels are generally considered to be isotropic and homogenous, with material properties independent of direction (Gaboriaud et al. 2000). The elastic modulus of the gel is measured by nanoindentation at penetration depths of about 400 and 600 nm. Figure 6.7 depicts the load-displacement curve for an applied force of 500 μN on the sample. Table 6.8 shows an average (7 readings) of reduced elastic modulus of the gel along with the calculated actual elastic modulus when a Poisson's ratio of 0.3 was assumed.

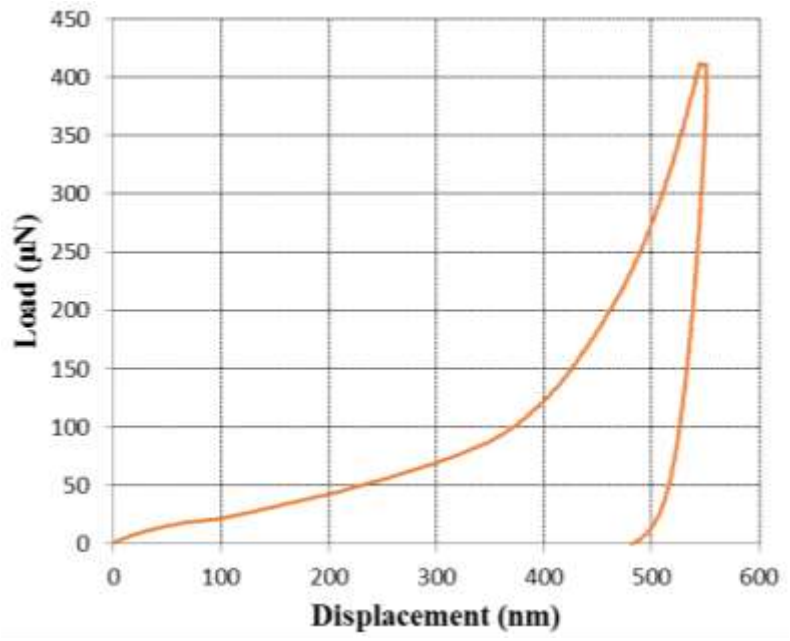

Figure 6.7 Load-Displacement Curve for ASR Gel.

Table 6.8 Elastic Modulus of the ASR Gel.

Solution	Load (μN)	E_r (GPa)	ν	E_s (GPa)	COV	Hardness (GPa)
2.7 kg/m^3	500	5.39	0.3	4.905	17.8%	0.0398

The measured elastic modulus of gel, formed by reacting borosilicate glass slides in alkali level 2.7 kg/m^3 solution was found to have a mean value of 4.91 GPa. Phair et al. (2005) used Brillouin scattering to measure bulk elastic modulus of ASR gel. The bulk moduli were found to be 4 to 8 GPa for the gel formed from 0.08M CH solution and 10 to 25 GPa for the gel formed from 0.8M CH solution. Converting these value to elastic modulus using the Poisson's ratio of 0.3, the elastic modulus were found to be 4.8

to 9.6 GPa for 0.08 M CH and 12 to 30 GPa for 0.8 M CH. Leemann and Lura (2013) determine elastic modulus on undried, polished concrete samples taken from a structure damaged by ASR using micro-indentation. The results indicate that the elastic modulus of ASR product is between 7 and 9 GPa in different aggregates and is relatively homogenous. These results are different from the one obtained using Nanoindenter. However, studies have shown that the chemical composition of ASR gels have a molar ratio of $(Na_2O + K_2O)/SiO_2$ = 0.2 to 0.5 with CaO content ranging up to 20%, and it has been found that varying this composition affects the swelling behavior of the gels (Kundsen and Thaulow 1975; Struble and Diamond 1981). Therefore, it is expected that the elastic modulus of the gel will vary with composition.

Determination of Free Strain of ASR Gel

Free strain due to ASR is measured by applying Archimedes' principle and is shown in Figure 6.8.

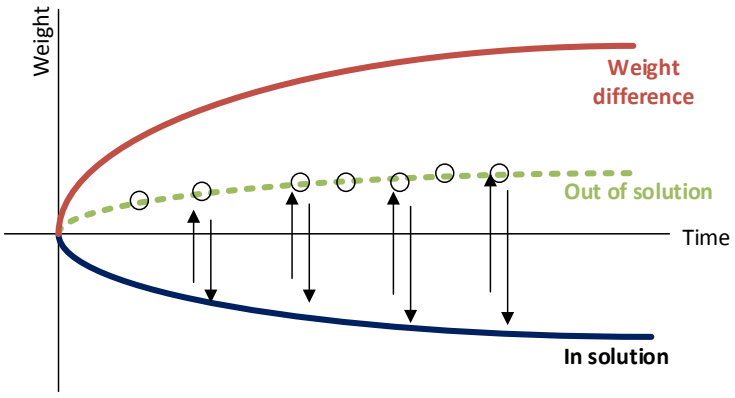

Figure 6.8 Representation of Archimedes' Principle.

The difference between the sample weight in solution and out of solution divided by the density of solution is equal to the volume change of sample. By dividing the volume change of sample to the original sample volume, the free strain of the reaction product can be obtained. Figure 6.9 presents the experiment for measuring ASR free strain.

Figure 6.9 Measurement of Free Strain due to ASR.

A bucket made with a stainless steel mesh is filled up with borosilicate glass balls (same amount used in glass-mortar test) and then submerging in alkaline solution of 2.7 kg/m^3 in VCMD container and tested at 60^{o}C inside a water tank. The in-solution sample weight is measured by holding the bucket with a fishing line and connecting to a scale shown in Figure 6.9. After the in-solution weight is recorded, the bucket is taken out of VCMD container and placed on the scale for the measurement of out-solution weight. Weight measurements were recorded every 24 hours over 28 days and the results

are presented in Figure 6.10. By dividing the volume change to the original volume of glass balls, the free strain of glass balls due to ASR is obtained (Figure 6.11).

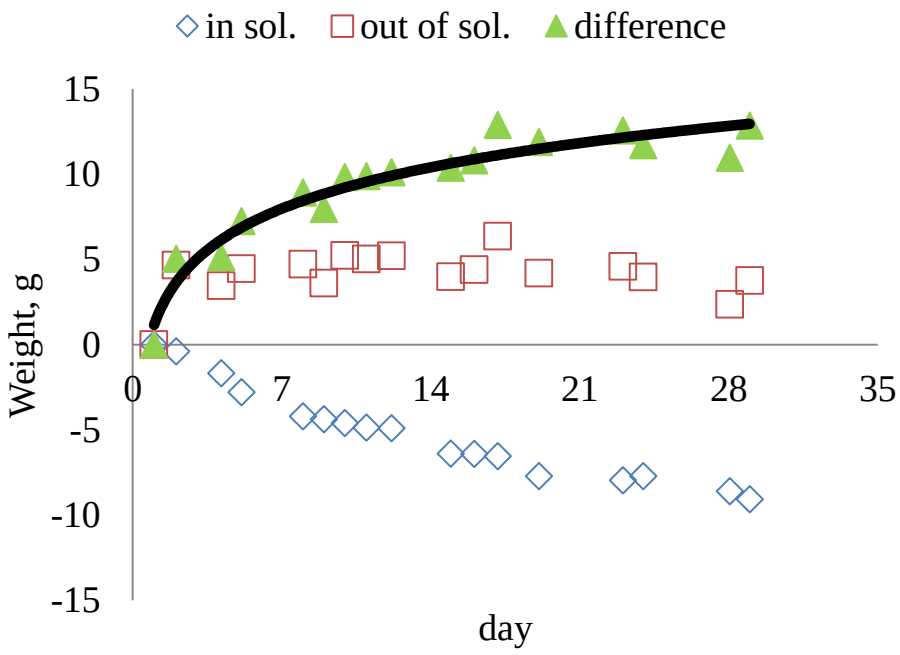

Figure 6.10 Free ASR Volume Change.

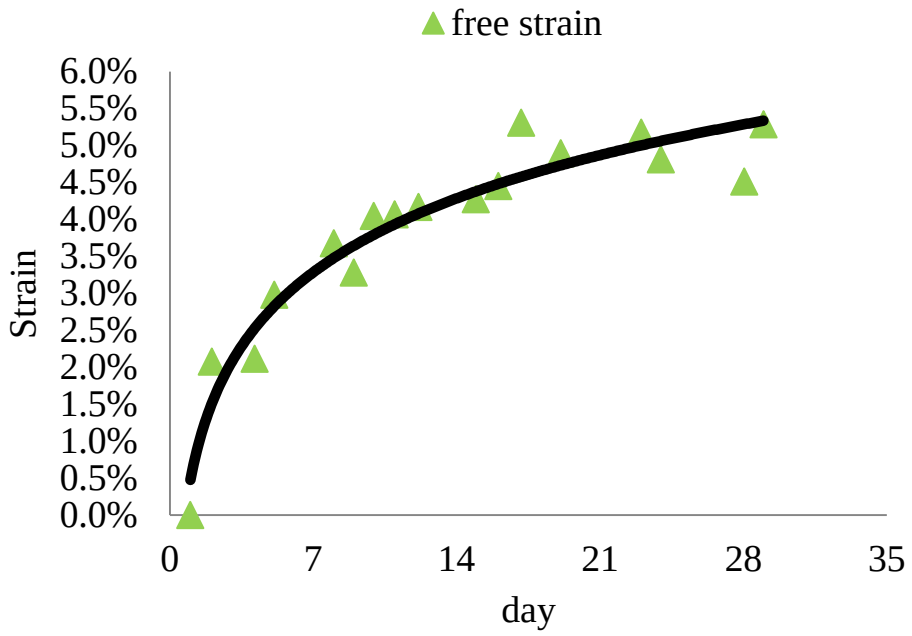

Figure 6.11 Free Strain due to ASR.

Finite Element Model (FEM)

The well-known finite element code Abaqus is used for the meso-scale analysis and a 4-mode bilinear plane stress quadrilateral element is used for all models. The representative volume element of size 7.62 cm by 15.24 cm with the statistical distribution of glass balls, which has the same size as glass-mortar cylinder is shown in Figure 6.12.

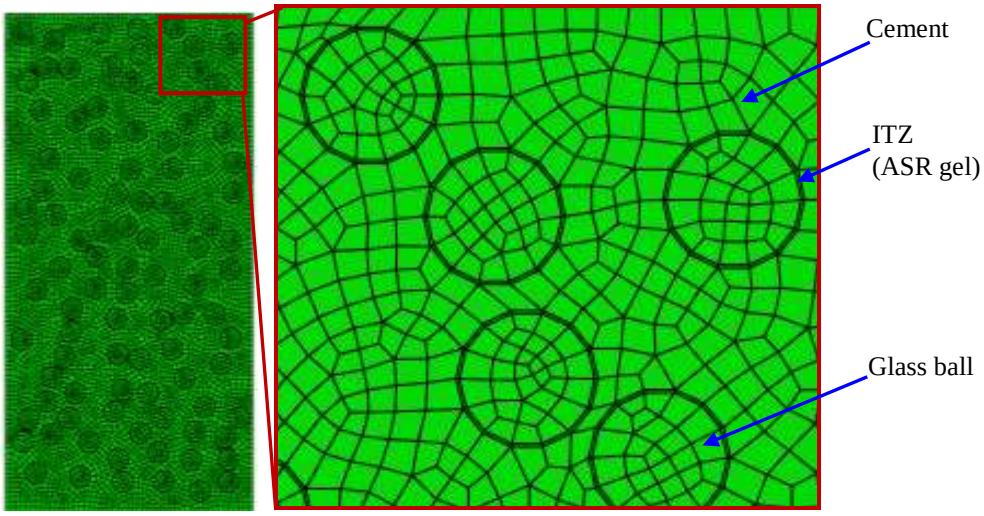

Figure 6.12 2-D Meso-Scale Analysis Model of the Glass-Mortar Cylinder.

The radius of the glass balls is 0.3175 cm (0.125 inch) with uniform gradation. When conducting simulation in Abaqus, the parameters used are as follow: the thickness of interfacial transition zone (ITZ) = 0.015 cm, E_1 = 63 GPa, E_2 = 4.905 GPa, E_3 = 15 GPa, $\nu_1 = 0.2$, $\nu_2 = 0.3$, and $\nu_3 = 0.25$.

Comparison of Expansion Prediction

Composite sphere and finite element model are adopted for predicting the expansion behavior of the glass-mortar cylinder in VCMD. Figure 6.13 shows the expansion comparison of glass-mortar cylinder between model prediction (composite sphere model and FEM) and ACCT measurement.

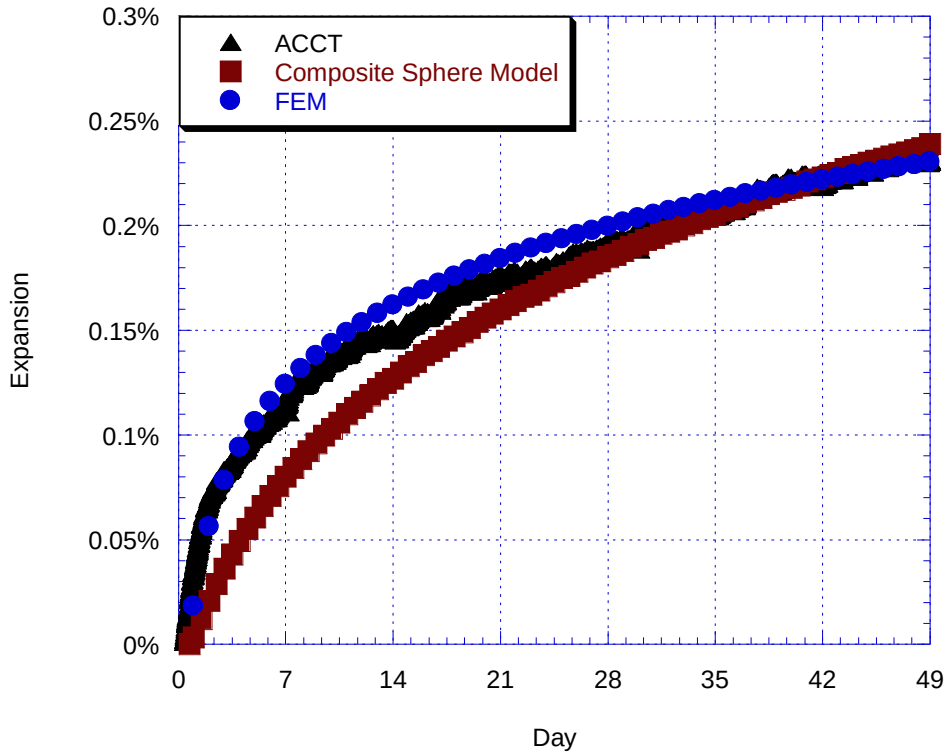

Figure 6.13 Expansion Comparison among Composite Sphere Model, FEM, and ACCT Measurement.

In general, the expansions of model prediction are matched well with the measured expansion in ACCT. Some errors may be due to the facts: (i) the composite sphere model was proposed based on the assumption of elastic material. However, cement and ASR gel are viscoelastic material which might cause creep of cylinder and (ii) the composite sphere model contains specific gradation of size particles, so it would be expected to only provide approximate results for systems containing single size particles.

Aggregate

The selected mixes in Table 6.5 were tested using ACCT at 60°C and varying levels of alkalinity. For each test corresponding to each mix (Table 6.5), the soak solution chemistry was equal to PSA (Table 6.6).

Mix 4 was used to cast two cylinders for each alkali level (i.e., 1.8, 2.7, and 5.3 kg/m^3) to verify the variability (within the lab) of ACCT test results. The expansion corresponding to two replicas were used to check the variations and the expansion results are presented in Figure 6.14. The majority of expansion-based coefficient of variation is within 10% after the 28-day expansion for the tested mixes at all alkali levels, which indicates that the variations of measured expansion of ACCT are low. Figure 6.15 shows the expansion curves of all mixes at each alkali level. For each mix, the higher the alkali level, the higher the level of expansion is.

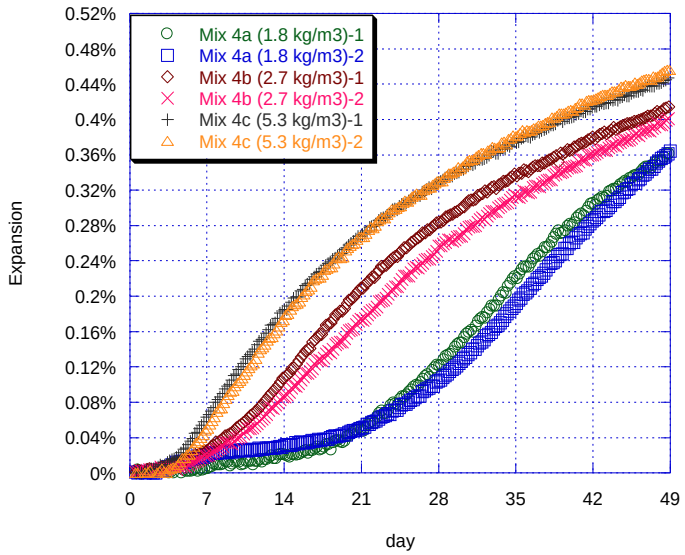

Figure 6.14 Expansion Curve of Mix 4 with Different Alkali Levels.

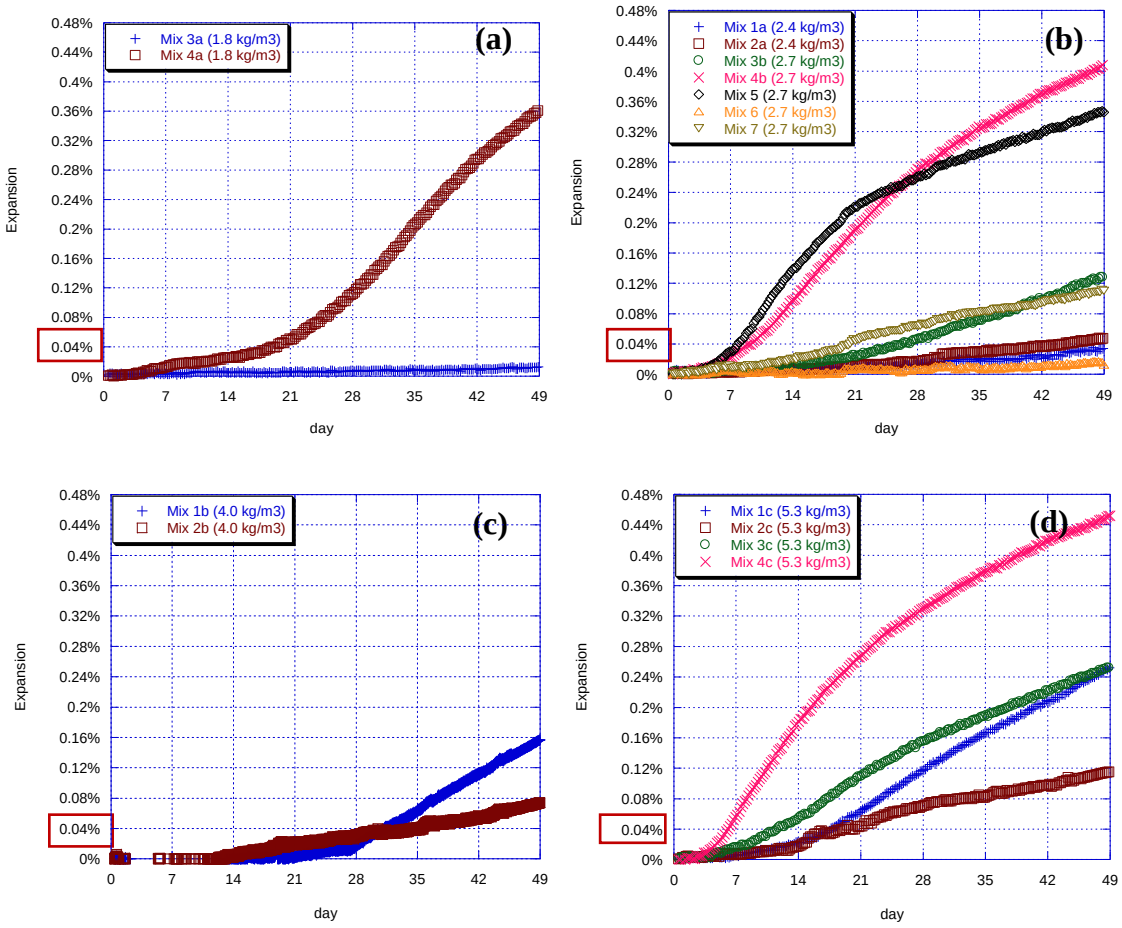

Figure 6.15 Expansion curve of ACCT at each alkali level (a) 1.8 kg/m^3, (b) 2.4/2.7 kg/m^3, (c) 4.0 kg/m^3, and (d) 5.3 kg/m^3.

Proposed expansion limits of ACPT at 60ºC were found from a range of 0.02% to 0.08% at 8 weeks (Bolotte 1992; De Grosbois 2000; Ranc and Debray 1992) and 0.03% to 0.04% at 13 weeks (Bolotte 1992; Touma et al. 2001). In this study, same exposure block/CPT expansion limit of 0.04% (Ideker et al. 2012) is chosen and shown in Figure 6.15. Table 6.9 summarizes the aggregate reactivity based on the ACCT expansions in Figure 6.15 and compares with ASTM C 1293 1-year expansion data. For

the mixes 1 to 4 with high alkali levels (2.7, 4.0, 5.3 kg/m^3 with Na_2O_e > 0.6%), the expansion limit of 0.04% can be reached within 49 days (Figures 6.15b to 6.15d). The alkali level 5.3 kg/m^3 (1.25% Na_2O_e) in Figure 6.15d is same as conventional concrete prism (e.g., ASTM C 1293). If the same expansion limit of 0.04% and the same alkali level 1.25% Na_2O_e in ASTM C 1293 are applied in this study, the ACCT have identified these aggregates as reactive aggregates within 4 weeks (mixes 1c, 2c, 3c, and 4c in Table 6.9), which matches with the ASR reactivity diagnostic of ASTM C 1293 1-year values. This suggests that ACCT in VCMD can be used as an alternative approach of concrete test for ASR.

Table 6.9 Aggregate Reactivity Based on the ACCT Expansion.

Mix	Alkali (kg/m^3)	Na_2O_e (%)	PSA (N)	Time to reach 0.04% expansion (day)	ASTM C 1293 1-year Exp. (%)	CAE Classification (Table 5.4)
1a	2.4	0.57	0.37	NIR till 49	0.043	Reactive
1b	4.0	0.95	0.46	32		
1c	5.3	1.25	0.88	18		
2a	2.4	0.57	0.37	46	0.078	Highly reactive
2b	4.0	0.95	0.46	36		
2c	5.3	1.25	0.88	20		
3a	1.8	0.57	0.38	NIR till 49	0.058	Reactive
3b	2.7	0.82	0.66	27		
3c	5.3	1.25	1.04	12		
4a	1.8	0.57	0.38	19	0.391	Highly reactive
4b	2.7	0.82	0.66	10		
4c	5.3	1.25	1.04	7		
5	2.7	0.82	0.66	8	-	Highly reactive
6	2.7	0.82	0.66	NIR till 49	0.027/0.035	Nonreactive
7	2.7	0.82	0.66	20	0.078	Highly reactive

NIR-Not identified as reactive.

The outdoor exposure blocks are generally cast with a high-alkali cement (0.9 +/- 0.1% Na_2O_e) with a CF of 420 kg/m^3 (Fournier et al. 2004). Fournier et al. (2004) found that the exposure blocks using high alkali cement without alkali boosting (nominally 0.95% Na_2O_e) correlate best with boosted (1.25% Na_2O_e) concrete prisms. Based on the results in Table 4, it seems that ACCT with alkali level 2.7 kg/m^3 (4.5 lb/yard^3, 0.82% Na_2O_e without alkali boosting) with a CF of 325 kg/m^3 might be a good choice to pass/fail a concrete mix with the same exposure block/CPT expansion limits (i.e., 0.04%). A concrete mix with a conventional CF (e.g., 325-390 kg/m^3) will be sufficient to achieve 2.7 kg/m^3 alkali levels if the Na_2O_e of the cement is relatively high (e.g., 0.6% < $Na_2O_e \leq$ 0.82%). However, if the Na_2O_e of the cement is low (e.g., < 0.6%), a high CF may be needed in order to achieve 2.7 kg/m^3 alkali levels.

Based on the above discussions (i.e., the variations of measured ACCT expansion are low after the 28-day expansion (Figure 6.15), the alkali level 5.3 kg/m^3 (1.25% Na_2O_e) is same as conventional CPT, the alkali level 2.7 kg/m^3 (0.82% Na_2O_e without alkali boosting) might be a good choice to pass/fail a concrete mix in this study), Figure 6.16 only shows plots of 1-year expansions in ASTM C 1293 versus the 28-, 35-, 42-, and 49-day ACCT expansions at alkali levels of 2.7 (0.82% Na_2O_e) and 5.3 kg/m^3 (1.25% Na_2O_e). The linear regression line is shown how expansions at 1 year of ASTM C 1293 correlate well with ACCT expansion at each testing time. A better correlation factor (R^2) is found at 28 days than other days for both alkali levels. At 28 days expansion, the correlation is also better at alkali level 2.7 kg/m^3, compared to 5.3 kg/m^3 with respective R^2 of 0.99 and 0.87. Therefore, ACCT with cement without alkali

boosting (2.7 kg/m^3, 0.82 % Na_2O_e) is a good candidate to pass/fail a concrete mix in this study.

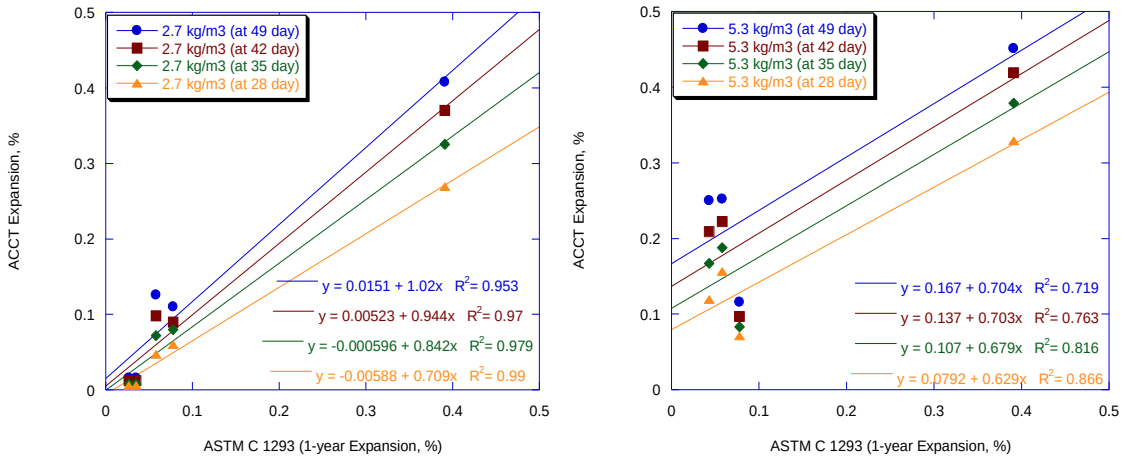

Figure 6.16 Comparison of expansion at 1 year in ASTM C 1293 test versus expansion at 28, 35, 42, and 49 days in the ACCT test with alkali levels of 2.7 and 5.3 kg/m^3.

The measured ACCT expansion with alkali levels of 2.7 and 5.3 kg/m^3 at 28 days along with ASTM C 1293 1-year expansion are graphically presented in Figure 6.17. The line of equity (Ideker et al. 2010) is shown where expansions at alkali level 2.7 kg/m^3 match better than alkali level 5.3 kg/m^3 to 1 year ASTM C 1293 expansions. Based on the above discussions, it is recommend to use cement without alkali boosting (2.7 kg/m^3, 0.82% Na_2O_e) to evaluate the ASR reactivity in ACCT.

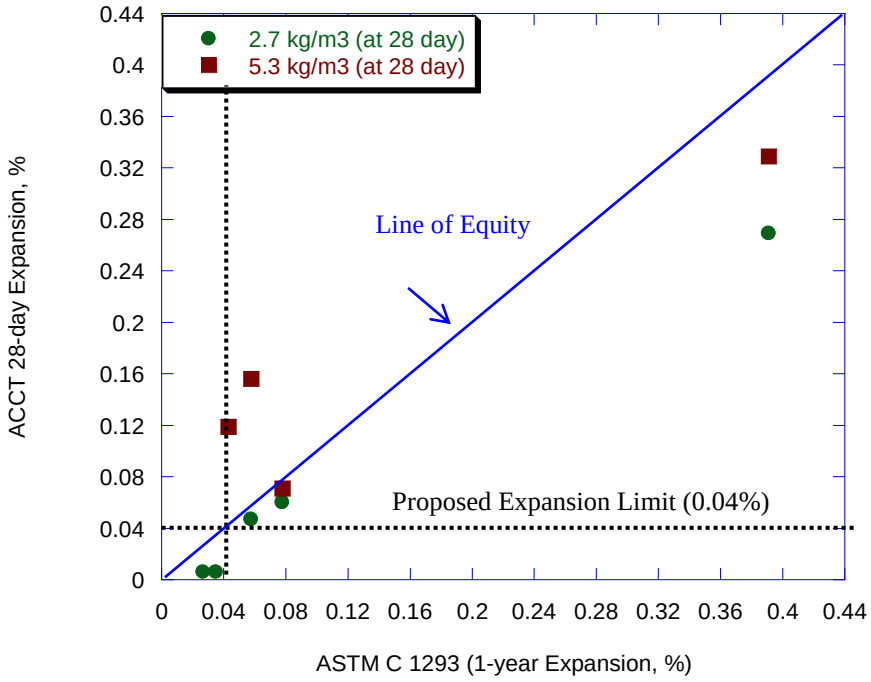

Figure 6.17 Comparison of expansion at 1 year in ASTM C 1293 versus expansion at 28 days in the ACCT with alkali levels of 2.7 and 5.3 kg/m^3.

Figure 6.18 shows the expansion curve of mixes 3 to 7 using alkali level 2.7 kg/m^3 (0.82% Na_2O_e). The 28-day ACCT expansions (%) are 0.047, 0.269, 0.006, and 0.064 for mixes 3, 4, 6, and 7 respectively, which match well with the reactivity diagnostic of 1-year ASTM C 1293 (%) (i.e., 0.058, 0.391, 0.027/0.035, 0.078) and CAE classification in Table 5.4 (i.e., the lower the ASR CAE, the higher the reactivity is). It indicates that a straight cement concrete mix with alkali level 2.7 kg/m^3 (0.82% Na_2O_e) is sufficient to delineate ASR reactivity at 28 days. Therefore, ACCT with relatively low alkali levels (as opposed to high alkali levels, i.e., 4.0-5.3 kg/m^3 in the current CPT

test/exposure block) can be effective to identify the ASR reactivity in a relatively short period of time. It may be close to testing a job mix if a job mix is a straight cement mix.

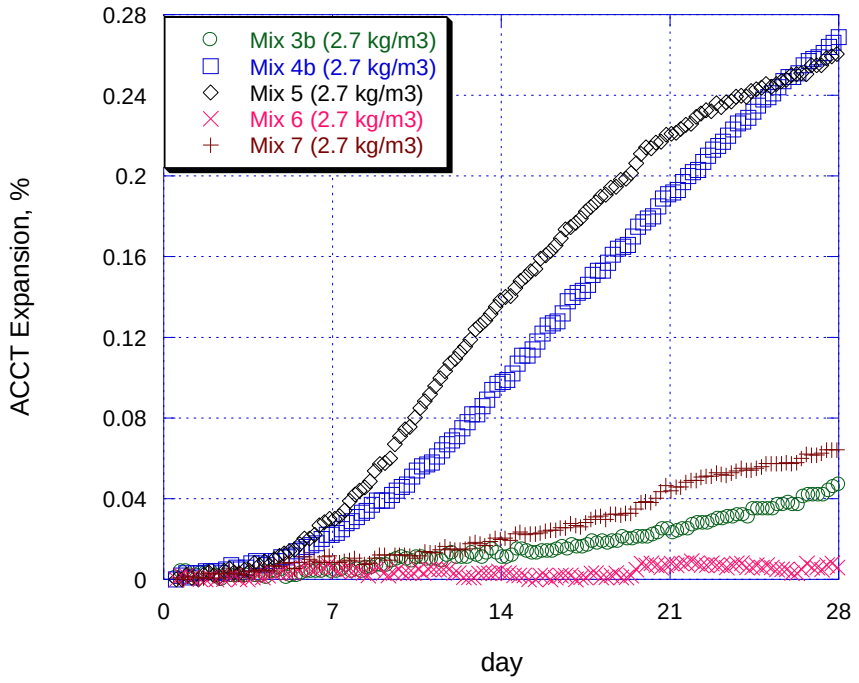

Figure 6.18 Expansion curves of ACCT (mixes 3 to 7 with alkali level 2.7 kg/m^3) over time.

Verification of Alkali Leach Proof

The changes of soak solution chemistry were monitored to verify the leach-proof situation as well as the possibility of ions migration from soak solution to the specimen. An increase of OH^-, Na^+, and K^+ ions concentrations in soak solution represents leaching of these ions from the specimen. On the other hand, a reduction in concentration of these ions in soak solution indicates ion migration from the soak solution to the specimen

while ASR is in progress in the specimen. The results are shown in Figure 6.19 for the change of OH^-, Na^+, and K^+ concentrations of soak solution of mixes 3 and 4 with alkali levels 1.8, 2.7 and 5.3 kg/m^3 due to ASR after the testing period of 49 days.

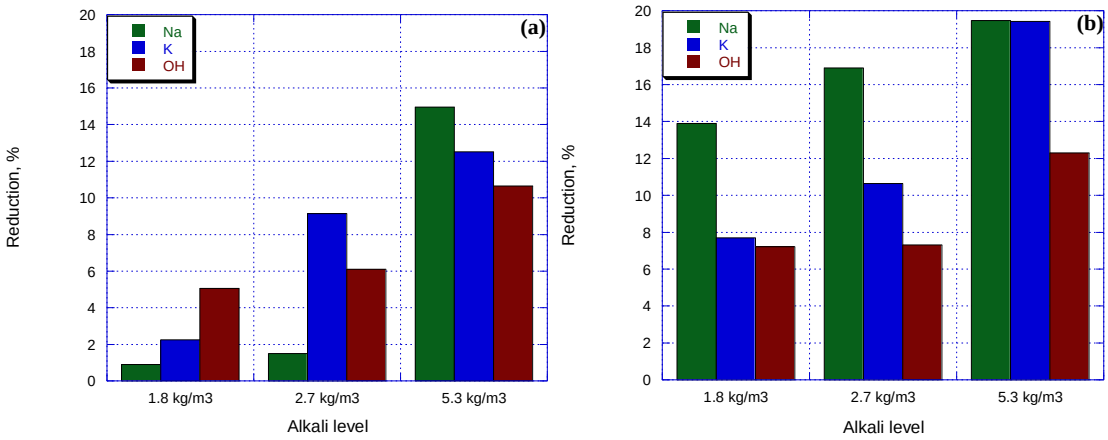

Figure 6.19 The change of Na^+, K^+, and OH^- of soak solution of (a) reactive mix 3 and (b) highly reactive mix 4 with alkali levels 1.8, 2.7, and 5.3 kg/m^3 after testing period of 49 days.

Initially, the ionic concentrations in pore solution and soak solution are equal, which does not allow ion migration between pore solution and soak solution. As ASR progresses, Na^+, K^+, and OH^- concentrations reduce in the pore solution of the specimen, which triggers ion migration from the soak solution to the pore solution. The decrease in Na^+, K^+, OH^- concentrations in soak solution after the test (Figure 6.19) suggests ion migration from soak solution to the specimen. However, the degree of reduction of the ions in soak solution is not that high. It seems the effect of leach-proof situation on the measured expansion is more pronounced than the effect due to ions migration from the

soak solution into the specimens. However, a continuous increase of expansion instead of gradually approaching an asymptotic shape may be supported by ingress of ions from soak solution. Note that this effect is very pronounced in the case of ASTM C 1260 where the soak solution is 1N NH, which is way higher than the mortar bar pore solution and might lead to false positive. The use of soak solution that is equal to pore solution may cause a little accelerating effect on the test result itself. However, it can be used as a method of simulating a field situation where an external source of alkalis (e.g., sea water ingress, deicing chemicals) and alkali redistribution (i.e., concentration of alkalis in certain zones within the main concrete body due to intense ambient temperature and RH variations) are significant factors.

Validation of Fly Ash Contents

Mix 4b (2.7 kg/m^3, 0.82% Na_2O_e) with and without Fly ash F replacement was conducted to validate the adjusted mix in ACCT. Fly ash F replaced 25% and 35% of cement in the mix, and pore solution was extracted to generate the soak solution. The pore solution (Na^+_e) is reduced from 0.66 N to 0.43 N with 25 % Fly ash replacement and from 0.66 N to 0.33 N with 35% Fly ash replacement. It can be expected that the expansion can be reduced due to a reduction of alkali concentration in pore solution. Figure 6.20 shows the expansion curves of mix 4b with and without Fly ash replacement. The expansion at 28 days is reduced from 0.269% to 0.067% with 25% Fly ash replacement and reduced to 0.004% with 35% Fly ash replacement. This indicates that 25% Fly ash replacement does not provide sufficient protection measure (i.e., ACCT expansion > 0.04%) for the highly reactive ASR aggregate in mix 4b; instead, 35% Fly

ash replacement will ensure a safe mix (i.e., ACCT expansion < 0.04%). This is also an indication that the proposed concrete cylinder test might be effectively used to determine Fly ash contents, cement contents, and contents of ternary blends in order to develop safe ASR-resistant mixes.

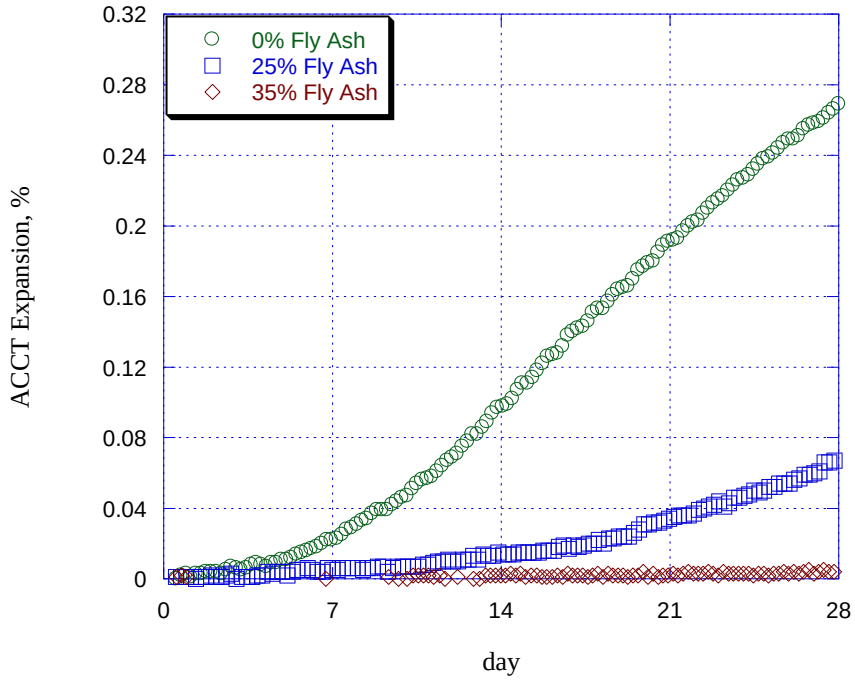

Figure 6.20 Expansion of mix 4b (2.7 kg/m^3) with and without Fly ash replacement.

Summary

The observations based on the results and discussion of this chapter are summarized below:

- Because the data collection in ACCT is automatic through LVDT (no error due to operation) under constant temperature (no error due to temperature difference), the

reliability of the proposed cylinder test is expected to be high. Creating a leach-proof situation in the proposed cylinder test is another advantage that enhances the reliability of the proposed cylinder test.

- The ACCT method was developed to determine the length change of concrete cylinder (7.6 cm by 15.2 cm) due to ASR at a temperature of 60°C. ACCT with relatively low alkali levels (2.7 kg/m^3, 0.82% Na_2O_e as opposed to high alkali levels, i.e., 4.0/5.3 kg/m^3, 0.95%/1.25% Na_2O_e in the current exposure block/CPT test) at 60°C can effectively be used to pass/fail a concrete mix in a relatively short time (i.e., 28 days) with an expansion limit of 0.04%.
- An attempt has been made to predict free expansion of cylinder due to ASR in a pure phase system by using both composite sphere and finite element modeling where relevant gel properties and free strain of ASR are the main inputs. A preliminary study using highly reactive borosilicate glass balls has been undertaken in order to verify the proposed approach in a pure phase system. The work that have been done to develop the proposed approach are (i) designing an experimental program where borosilicate glass balls (highly reactive in alkaline solution) allowed to react with solutions of PSA and measure the physical properties of the reaction products (e.g., elastic modulus, hardness, chemical composition etc.) by nanoindentation, (ii) developing a procedure based on Archimedes' principle to measure free strain due to ASR, (iii) developing both composite sphere and finite element modeling to predict ASR free expansion by incorporating physical properties of gel and free strain as the main inputs, (iv) casting mortar specimens using the studied glass balls and

measuring free expansion in ACCT, and (v) comparing predicted vs. measured free expansion and verify the model.

- The proposed ACCT has the ability to emerge as a potential method to test job mix (e.g., a mix with typical ASR mitigation measures) in the laboratory and serve as an alternative method to validate an ASR-resistant mix. It also provides an effective measure to determine Fly ash contents, cement contents, and contents of ternary blends in order to develop safe ASR-resistant mixes.
- A procedure to design an ASR-resistant concrete mix based on CAE, TH_A, PSA, and concrete validation testing is developed. The guidelines to select mix-design controls and special protection measures depending on CAE, TH_A and severity of ambient conditions are developed.
- Since measuring CAE is established as a reliable method to predict aggregate alkali silica reactivity, all four steps are recommended for aggregates belonging to false positive and negative categories. The four steps are (i) determination of CAE and TH_A from aggregate-solution test, (ii) determination of PSA, (iii) mix design adjustment based on TH_A-PSA relationship (i.e., PSA needs to be below TH_A in order to prevent/minimize ASR), and (iv) mix design validation through concrete testing.
    - Determination of CAE and TH_A based on the proposed VCMD concrete cylinder test without conducting aggregate-solution test is also possible. Measurement of expansion of concrete specimens at a minimum three levels of alkalinity (e.g., 1.8, 2.7, and 5.3 kg/m^3) and three temperatures (e.g. 60, 70, and 80^oC) is needed

in order to determine both CAE and TH_A. After determining CAE and TH_A, the same procedures for mix-design adjustment and verification as used in Table 6.2 can be applied. As generating concrete expansion data at multiple levels of temperatures and alkalinity involves in determining CAE and TH_A in this option, separate concrete mix-design validation testing may not be needed. If one feels more comfortable with the mix design development based on concrete testing alone, this is a good choice. Although, this approach provides reliable data but longer testing time may be a drawback.

- For the aggregates where the reactivity prediction based on the current test methods is satisfactory, CAE measurement through aggregate-solution test may not be needed. In that situation, mix design verification/validation through direct ACCT is recommended. The mix design based on the current test methods and mitigation practices can be tested with or without added alkalis and verify if the expansion stays below the assigned limits at the specified testing period. Addition of alkali (NH pellets) in the mix can accelerate the reaction but applicability/reliability needs to be verified. If the expansion is above the assigned limit, the mix needs further adjustment before placement.

- For the aggregates where the reactivity prediction based on the current test methods are satisfactory, CAE measurement through aggregate-solution test may not be needed. However, mix design verification/validation through direct ACCT is highly recommended.

- Although there are no data on field performance (i.e., exposure block) of the same mixes at this time, further research is needed to verify the applicability of the proposed expansion limit (i.e., 0.04% at 28 days) by testing more number of aggregates in ACCT and exposure block. This can be accomplished by generating more concrete data using different mixes, followed by a comparative assessment between the proposed cylinder test and field performance.

CHAPTER VII

CONCLUSIONS AND RECOMMENDATIONS

This section summarizes the main findings of this study and offers recommendations for further investigation of ASR aggregate and concrete testing.

Conclusions

- From the borosilicate glass balls-solution tests (closed system), it was observed that the VCMD measures net solution volume contraction due to ASR over time. This same solution volume contraction over time was invariably observed in all aggregate-solution tests. The pure phase experiments using glass balls were used to validate the VCMD test method as a proof of concept.
- The net solution volume contraction in a closed system condition of the VCMD is due to the combined effects of (i) Si-O-Si bond breaking and dissolution (solution volume decreases), (ii) consumption of reactants such as water and ionic species (solution volume decreases), (iii) product formation and expansion (solution volume increases), (iv) solution goes into micropores (pore developed due to the formation of high-volume, less dense ASR products) and microcracks - the degree of micropore and microcrack formation is related to the degree of ASR (solution volume decreases), and (v) incomplete absorption - negligible but may cause slight solution volume decrease.
- It was explained in Chapter 4 that aggregate absorption should achieve more than 95% AC during sample preparation time and before starting the VCMD test for

ASR. It is unlikely that the absorption (filling the remaining most inaccessible pores by solution) will continue during the VCMD testing period (i.e., 4 days). Even if it continues, it would be very negligible. Therefore, the effect of aggregate absorption in measuring net solution volume contraction over time in the VCMD test is very negligible. The main phenomenon in creating net solution volume contraction is ASR.

- A modified kinetic-type model was developed to model the measured non-linear type solution volume change over time. By fitting the model volume change data to the measured volume data over time, the β are calculated. The β (rate constant) values at multiple temperatures (minimum 3 temperatures) are then determined and CAE is calculated. As the device measures the net combined effects of the different steps of ASR (i.e., breaking Si-O-Si bond, dissolution, product formation, swelling, etc.) in the form of chemical shrinkage over time, it is better to use the term "CAE." Moreover, aggregates are multi-phase and sometimes very heterogeneous materials. The distribution of the reactive constituents inside the aggregate is in general inhomogeneous in nature. The CAE that the proposed method will measure should not be confused with the activation energy of a single (one step) chemical reaction of a pure phase in chemistry.
- The CAE-based test can reliably predict aggregate alkali silica reactivity in a short period of time in terms of measuring CAE. A representative CAE can be determined by testing as-received aggregates (i.e., field aggregates) with 0.5N NH + CH solution

(similar to concrete pore solution) and with permissible repeatability. This helps further reduction of testing time and reduces the gap between lab and field.

- The majority of COV based on β is within 10%, which indicates the results are highly repeatable.
- The CAE-based method has correctly identified the aggregates that the AMBT method has passed/failed but that the CPT had failed/passed in a short period of time. This is the main benefit of the CAE-based test method.
- A good correlation among CAE-based aggregate reactivity, ASTM C 1260 (14 days expansion), and ASTM C 1293 (1-year concrete prism expansion) indicates that the proposed method has the merits to be considered as a rapid and reliable ASR test method on one hand, and have the potential to be considered as an alternative method to the current ASR test method on the other hand.
- ASR CAE can serve as a single chemical material parameter to represent alkali silica reactivity of aggregate. The CAE-based aggregate classification can serve as a potential screening parameter in an aggregate quality control program.
- Measuring low CAE (high reactivity) of an aggregate using the VCMD is supported by the higher consumption of Na^+ and/or greater reduction of OH^- in the test solution. Therefore, the test solution monitoring method has supported the VCMD test results as a supporting tool. Similarly, the microstructural studies on the reacted aggregate particles by SEM-EDS have also supported the CAE-based reactivity prediction.

- An apparent relationship between CAE and alkalinity was observed, i.e., the higher the alkalinity, the lower the CAE is. An attempt was made to model this relationship between CAE and alkalinity, and determine TH_A for each aggregate. In general, the higher the reactivity (i.e., the lower the CAE) the lower the TH_A. A reactive aggregate can practically behave as non-reactive or very slow reactive if concrete PSA can be maintained below the TH_A
- A procedure to design an ASR-resistant concrete mix based on CAE, TH_A, PSA, and concrete validation testing is developed. The stages that are involved in developing an ASR resistant mix are listed below:
  - Determination of CAE and TH_A from aggregate-solution test.
  - Development of an ASR-resistant mix by applying both mix design controls and special protection measures (as needed) depending on CAE-based reactivity prediction, TH_A, and some consideration on the severity of ambient conditions.
  - Determination of PSA using the pore solution extraction method or any other suitable method.
  - Mix design adjustment/verification based on TH_A-PSA relationship: PSA needs to be below TH_A in order to prevent/minimize ASR.
  - Mix design validation through concrete testing–An ACCT using VCMD was proposed to test concrete mixes in a short time.
- All the stages described above are recommended (until enough data are generated and better understanding is achieved) for aggregates that belong to false positive and negative categories. If the pore solution extraction method is not available, the

dependency on concrete validation testing will be high in order to develop a safe ASR-resistant mix with high reliability. As CAE-based reactivity prediction is reliable and dependable, an expert can design ASR-resistant mix based on CAE-based reactivity, TH_A, and knowledge gained based on concrete validation testing without pore solution data and concrete validation testing. This practice may be acceptable, but some amount of risk will be involved.

- For the aggregates where the reactivity prediction based on the current test methods is satisfactory, CAE measurement through aggregate-solution test may not be needed. However, mix design verification / validation through direct ACCT is highly recommended.
- Because the data collection in the VCMD cylinder test is automatic through LVDT (no human error) under constant temperature (no error due to temperature difference), the reliability of the ACCT is expected to be high. Creating a leach-proof situation in the ACCT is another advantage that enhances the reliability of the ACCT.
- The proposed ACCT method was developed to determine the length change of concrete cylinder (7.62 cm by 15.24 cm) due to ASR at a temperature of 60°C. Making soak solution chemistry equal to pore solution chemistry ensures no leaching test condition. ACCT with relatively low alkali levels (2.7 kg/m^3, 0.82% Na_2O_e as opposed to high alkali levels, i.e., 4.0/5.3 kg/m^3, 0.95%/1.25% Na_2O_e in the current exposure block/CPT test) at 60°C can effectively be used to pass/fail a concrete mix in a relatively short time (i.e., 28 days) with an expansion limit of 0.04%.

- The proposed ACCT has the ability to emerge as a potential method to test job mix (e.g., a mix with typical ASR mitigation measures) in the laboratory and serve as an alternative method to validate an ASR-resistant mix. It also provides an effective measure to determine Fly ash contents, cement contents, and contents of ternary blends in order to develop safe ASR-resistant mixes.
- An attempt has been made to predict free expansion of cylinder in ACCT due to ASR in a pure phase system by using both composite sphere and finite element modeling where relevant gel properties and free strain of ASR are the main inputs.
    - An experimental program where borosilicate glass balls (highly reactive in alkaline solution) allowed to react with solutions of PSA and measure the physical properties of the reaction products (e.g., elastic modulus, hardness, chemical composition etc.) by nanoindentation have been developed.
    - A procedure based on Archimedes' principle to measure free strain due to ASR was developed.
    - Both composite sphere and finite element modeling to predict ASR free expansion by incorporating physical properties of gel and free strain as the main inputs were developed.
    - Models have been verified by casting mortar specimens using the studied glass balls and measuring free expansion in ACCT, and comparing predicted vs. measured free expansion.

Recommendations for Future Research

- The CAE-based aggregate classification system is developed based on testing 16 aggregates in this study. More aggregates that the AMBT method has passed / failed but that the CPT has failed/passed are needed in order to verify the benefit (i.e., consistent identification of aggregates that belong to false positive and negative categories) of the CAE-based procedure. Identification of the critical aggregates (those belonging to false positive and negative categories) followed by the VCMD aggregate-solution test to determine CAE and TH_A is highly warranted in order to correctly identify the reactivity of these aggregates.
- It may be necessary to generate CAE at one or two additional levels of alkalinity (e.g., 0.25 to 0.3N NH + CH and/or 0.7N NH + CH) and improve the TH_A calculation procedure in order to increase the reliability of the proposed approach of TH_A determination.
- Develop a procedure to determine optimum dosages of Li-compounds - one approach could be the dosage needed to make CAE falls in the non-reactive or slowly reactive ranges. The other approach could be through concrete testing using the proposed ACCT method (described below).
- More concrete testing and verification of the proposed testing period that can be used to test concrete mixes of varying reactivity (i.e., from slowly reactive to highly reactive).

- It is proposed that the ACCT with relatively low alkali loadings, i.e., 2.7 kg/m^3 (0.82% Na_2O_e) and 60 °C can effectively be used to pass/fail a concrete mix in a relatively short time. It is necessary to do more testing to verify its efficacy.
- The results indicated that the situation of pore solution = soak solution causes a little accelerating effect for the ASR, which could be used to make a test rapid. Further research on modification of soak solution (e.g., soak solution ½, ¼ of PSA, lime-saturated water, etc.) and its effect on concrete expansion is needed to decide whether a reduced testing time with pore solution = soak solution is acceptable, or a relatively high testing period with soak solution << pore solution is way to go.
- The possibility of testing a job mix (e.g., a typical ASR-mitigated mix) by the proposed ACCT is high. Further research is needed to test several job mixes that cover concrete mixes with wide range of reactivity. The results indicated that adding a little alkali to the job mix could be allowed to reduce the testing time. Generating supporting evidence through more concrete testing with and without alkali boosting would justify this step.
- Verification of different options in Chapter VI that are proposed to develop ASR-resistant concrete mixes using the proposed ACCT method.
- Assigning optimum dosage of Li-compounds to control ASR using the proposed VCMD concrete cylinder test.
- Further research is needed to verify the applicability of the proposed expansion limit (i.e., 0.04% at 28 days) by testing more number of aggregates in ACCT and exposure block. This can be accomplished by generating more concrete data using different

mixes, followed by a comparative assessment between the proposed cylinder test and field performance

- Measurement of ASR expansion using concrete specimens of different dimensions (e.g., prism of 7.62 cm by 7.62 cm by 11.94 cm and prism of 10.16 cm by 10.16 cm by 28.58 cm) in VCMD at different temperatures (i.e., 38ºC and 60ºC) and under alkali leach-proof condition should be helpful in understanding the effects of specimen sizes and temperatures on the concrete expansion behavior. It will allow establishing a comparison between conventional ASTM C 1293 data and the VCMD cylinder test using the same specimen size and under the same temperature conditions, but with no leaching and automatic data collection with the VCMD cylinder test.
- It is reported that testing concrete at 60°C is associated with increased sulfate concentration and reduction of OH^- ions in the pore solution, which causes reduction in expansion.
- Further research is need to (i) verify application of the same approach (composite spherical model and FEM) for prediction of ASR expansion of concrete cylinders made with aggregates, (ii) measure and predict of ASR gel properties (e.g., viscoelastic properties) under different conditions (e.g., RH) by nonoindentation and composite sphere model.
- Prediction of ASR expansive stress in concrete by linking lab measured physical/chemical properties of ASR products and relevant field parameters through FEM.

REFERENCES

Adams, M. P., B. Gray, J. H. Ideker, J. E. Tanner, A. Jones, and B. Fournier (2012). Applicability of Standard Alkali-Silica Reactivity Testing Methods for Recycled Concrete Aggregate. The 14th International Conference on Alkali-Aggregate Reaction in Concrete, Austin, Texas.

Alexander, G. B., W. M. Heston, and R. K. Iler (1954). The Solubility of Amorphous Silica in Water. Journal of Physical Chemistry, 58 (6), 453-455.

Amro, M. M. and M. S. Benzagouta (2009). Effect of Pressure and Temperature on Petrophysical Characteristics in the case of Carbonate Reservoirs. Oil Gas European Magazine, 35 (2), 74-78.

ASTM C 1260-07 (2008): Standard Test Method for Potential Alkali Reactivity of Aggregates (Mortar-Bar Method). American Society for Testing Materials, West Conshohocken, Annual Book of ASTM Standards (04.02): Concrete and Aggregates, 677-681.

ASTM C 1293-08a (2008): Standard Test Method for Determination of Length Change of Concrete Due to Alkali-Silica Reaction. American Society for Testing Materials, West Conshohocken, Annual Book of ASTM Standards (04.02): Concrete and Aggregates, 682-688.

ASTM C 1567-07 (2008): Standard Test Method for Determining the Potential Alkali-Silica Reactivity of Combinations of Cementitious Materials and Aggregate (Accelerated Mortar-Bar Method). ASTM International, American Society for Testing Materials, West Conshohocken, Annual Book of ASTM Standards (04.02): Concrete and Aggregates, 776-781.

ASTM C 227-03 (2008): Standard Test Method for Potential Alkali Reactivity of Cement-Aggregate Combinations (Mortar-Bar Method). American Society for Testing Materials, West Conshohocken, Annual Book of ASTM Standards (04.02): Concrete and Aggregates, 152-156.

ASTM C 289-07 (2008): Standard Test Method for Potential Alkali Reactivity of Aggregate (Chemical Method). American Society for Testing Materials, West Conshohocken, Annual Book of ASTM Standards (04.02): Concrete and Aggregates, 179-185.

ASTM C 295-03 (2008): Standard Guide for Petrographic Examination of Aggregate for Concrete. American Society for Testing Materials, West Conshohocken, Annual Book of ASTM Standards (04.02): Concrete and Aggregates, 199-206.

ASTM C 33-07 (2008): Standard Specification for Concrete Aggregates. American Society for Testing Materials, West Conshohocken, Annual Book of ASTM Standards (04.02): Concrete and Aggregates, 12-22.

ASTM C 441-05 (2008): Standard Test Method for Effectiveness of Mineral Admixture or Ground Blast-Furnace Slag in Preventing Excessive Expansion of Concrete Due to the Alkali-Silica Reaction. American Society for Testing Materials, West Conshohocken, Annual Book of ASTM Standards (04.02): Concrete and Aggregates, 250-252.

ASTM C 856-04 (2008): Standard Practice for Petrographic Examination of Hardened Concrete. American Society for Testing Materials, West Conshohocken, Annual Book of ASTM Standards (04.02): Concrete and Aggregates, 438-454.

ASTM C 150-12 (2012): Standard Specification for Portland Cement. ASTM International, Annual Book of ASTM Standards, American Society for Testing Materials, West Conshohocken, Annual Book of ASTM Standards (04.01): Concrete and Aggregates, 157-165.

ASTM C 1608-07 (2012): Standard Test Method for Chemical Shrinkage of Hydraulic Cement Paste. ASTM International, American Society for Testing Materials, West Conshohocken, Annual Book of ASTM Standards (04.01): Concrete and Aggregates, 692-695.

Barneyback, R. S. and D. Sidney (1981). Expression and Analysis of Pore Fluids from Hardened Cement Pastes and Mortars. Cement and Concrete Research, 11, 279-285.

Barringer, W. L. (2000). Application of Accelerated Mortar Bar Tests to New Mexico Aggregates. 11th International Conference on Alkali-Aggregate Reactions in Concrete, Quebec City, Quebec, Canada, 563-572.

Bauer, S., B. Cornel, D. Figurski, T. Ley, J. Miralles, and K. Folliard (2006). Alkali-Silica Reaction and Delayed Ettringite Formation in Concrete: A Literature Review, Report, 0-4085-1, Center for Transportation Research, Texas Department of Transportation.

Bektas, F., L. Turanli, T. Topal, and M. C. Goncuoglu (2004). Alkali Reactivity of Mortars Containing Chert and Incorporating Moderate-Calcium Fly Ash. Cement and Concrete Research, 34, 2209-2214.

Bérubé, M. A., B. Durand, D. Vezina, and B. Fournier (2000). Alkali-Aggregate Reactivity in Quebec. Canada, Journal of Civil Engineering, 27 (2), 226-45.

Bérubé, M. A., J. Duchesne, J. F. Dorion, and M. Rivest (2002). Laboratory Assessment of Alkali Contribution by Aggregates to Concrete and Application to Concrete Structures Affected by Alkali-Silica Reactivity. Cement and Concrete Research, 32, 1215-1227.

Bérubé, M. A., C. Tremblay, B. Fournier, M. D. Thomas, and D. B. Stokes (2004). Influence of Lithium-Based Products Proposed for Counteracting ASR on the Chemistry of Pore Solution and Cement Hydrates. Cement and Concrete Research, 34, 1645-1660.

Bleszynski, R. F. and M. D. A. Thomas (1998). Microstructural Studies of Alkali-Silica Reaction in Fly Ash Concrete Immersed in Alkaline Solutions. Advanced Cement Based Materials, 7, 66-78.

Bolotte, B. (1992). Development of an Accelerated Performance Test on Concrete for Evaluating its Resistance to AAR. 9th International Conference on AAR in Concrete, London, UK, The Concrete Society, 110-116.

Broekmans, M. A. T. M. (2002). The Alkali-Silica Reaction: Mineralogical and Geochemical Aspects of Some Dutch Concretes and Norwegian Mylonites. Ph.D. Thesis, University of Utrecht, 144.

Brouwers, H. J. H. and R. J. van Eijk (2003). Alkali Concentrations of Pore Solution in Hydrating OPC. Cement and Concrete Research, 33, 191-196.

Buck, A. D. and K. Mather (1987). Methods for Controlling Effects of Alkali-Silica Reaction in Concrete. Army Engineer Waterways Experiment Station Vicksburg MS Structures Lab, Accession No. ADA178479, 69.

Callister (Jr.), W. D. (2007). Materials Science and Engineering: An Introduction. John Wiley & Sons, Inc., New York.

Carrasquillo, R. L. and J. Farbiaz (1988). Alkali-Aggregate Reaction in Concrete Containing Fly Ash: Final Report. Center of Transportation Research, Research Report No. 450-3F.

Chatterji, S. (1989). Mechanisms of Alkali-Silica Reaction and Expansion. 8th International Conference on Alkali-Aggregate Reaction in Concrete, Kyoto, 101-105.

Chatterji, S., A. D. Jensen, N. Thaulow, and P. Christemsens (1986). Studies of Alkali Silica Reaction. Part 3. Mechanisms by which NaCl and $Ca(OH)_2$ Affect the Reaction. Cement and Concrete Research, 16 (2), 246-254.

Christensen, R. M. (1979). Mechanics of Composite Materials. Lawrence Livermore Laboratory, University of California, Livermore.

Constantiner, D. and S. Diamond (2003). Alkali Release from Feldspars into Pore Solutions. Cement and Concrete Research, 33, 549-554.

De Grosbois, M. (2000). Evaluation of the Potential Alkali-Reactivity of Concrete Aggregates: Performance of Testing Methods and A Producers Point of View. 11th International Conference of Alkali-Aggregate Reactivity in Concrete, Quebec City, QC, Canada, 267-276.

Deng, Y. (2012). Permeability and Porosity of Tight Rock Materials under Conditions of High Temperature and High Pressure. Applied Mechanics and Materials, 170-173, 719-722.

Diamond, S. (1976). A Review of Alkali-Silica and Expansion Mechanisms: 2. Reactive Aggregate. Cement and Concrete Research, 6 (4), 549-560.

Diamond, S. (1981). Effect of Two Danish Fly Ashes on Alkali Contents of Pore Solutions of Cement-Fly Ash Pastes. Cement and Concrete Research, 11 (3), 383-394.

Diamond, S. (1983). Alkali-Reactions in Concrete-Pore Solution Effects. 6th International Conference on Alkali-Aggregate Reactivity in Concrete, 155-166.

Diamond, S. (1997). Alkali Silica Reactions-Some Paradoxes. Cement and Concrete Composites, 19, 391-401.

Diamond, S. (2000). Chemistry and Other Characteristics of ASR Gels, in: M.-A. Bérubé, B. Fournier, B. Durand (Eds.), 11th International Conference on Alkali Aggregate Reactions in Concrete, Québec, Canada, 31-40.

Diamond, S. and M. Penko (1992). G.M. Idorn International. Symposium. Durability of Concrete, ACI SP-131, 153.

Diamond, S. and N. Thaulow (1974). A Study of Expansion due Alkali-Silica Reaction as Conditioned by the Grain Size of the Reactive Aggregate. Cement and Concrete Research, 4, 591-607.

Fernandes, I., F. Noronha, and M. Teles (2004). Microscopic Analysis of Alkali-Aggregate Reaction Products in a 50-year-old Concrete. Materials Characterization, 53, 295-306.

Fischer-Cripps, A. C. (2002). Nanoindentation. Springer-Verlag, New York.

Folliard, K. J., J. H. Ideker, M. D. A. Thomas, and B. Fournier (2004). Assessing Aggregate Reactivity using the Accelerated Concrete Prism Test. 7th CANMET/ACI International Conference on Recent Advances in Concrete Technology, Supplementary Papers, Las Vegas, Nevada, 269-283.

Folliard K. J., M. D. A. Thomas, B. Fournier, K. E. Kurtis, and J. H. Ideker (2007). The Use of Lithium to Prevent or Mitigate Alkali-Silica Reaction in Concrete Pavements and Structures. Publication No. FHWA-HRT-06-133, Office of Infrastructure Research and Development, Federal Highway Administration, 47.

Folliard, K. J., R. Barborak, T. Drimalas, L. Du, S. Garber, J. Ideker, T. Ley, S. Williams, M. Juenger, B. Fournier, and M. D. A. Thomas (2006). Preventing ASR/DEF in New Concrete. Report No. 0-4085-5, Center for Transportation Research, University of Texas at Austin, Austin, TX.

French, W. J. (1980). Reactions between Aggregates and Cement Paste: An Interpretation of the Pessimum. Quarterly Journal of Engineering Geology, 13 (4), 231-247.

Fournier, B., P. C. Nkinamubanzi, and R. Chevrier (2004). Comparative Field and Laboratory Investigations on the use of Supplementary Cementing Materials to Control Alkali-Silica Reaction in Concrete. 12th International Conference on Alkali-Aggregate Reaction in Concrete, Beijing, China, 1, 528-537.

Fournier, B., R. Chevrier, M. De Grosbois, R. Lisella, K. Folliard, J. Ideker, M. Shehata, M. Thomas, and S. Baxter (2004). The Accelerated Concrete Prism Test (60°C): Variability of the Test Method and Proposed Expansion Limits, in: M. Tang, M. Deng (Eds.), 12th International Conference on Alkali-Aggregate Reaction in Concrete, International Academic Publishers, World Publishing Corporation, Beijing, China, 314-323.

Fournier, B. and V. M. Malhorta (1999). Evaluation of Laboratory Test Methods for Alkali-Silica Reactivity. Cement, Concrete, and Aggregates, 21 (2), 173-184.

Gaboriaud, F., D. Chaumont, A. Nonat, and A. Craievich (2000). Fractal Structure of Basic Silica Gels with Low Ca Content. Journal of Applied Crystallography, 33, 597.

Garcia-Diaz, E., D. Bulteel, Y. Monnin, P. Degrugilliers, and P. Fasseu (2010). ASR Pessimum Behavior of Siliceous Limestone Aggregates. Cement and Concrete Research, 40 (4), 546-549.

Garcia-Diaz, E., J. Riche, D. Bulteel, and C. Vernet (2006). Mechanism of Damage for the Alkali Silica Reaction. Cement and Concrete Research, 36, 395-400.

Gao, X. X., S. Multon, M. Cyr, and A. Sellier (2013). Alkali-Silica Reaction (ASR) Expansion: Pessimum Effect Versus Scale Effect. Cement and Concrete Research, 44, 25-33.

Ghanem, H., D. Zollinger, and R. Lytton (2010). Predicting ASR Aggregate Reactivity in terms of its Activation Energy. Construction and Building Materials, 24, 1101-1108.

Gillott, J. E. (1975). Alkali-Aggregate Reactions in Concrete. Engineering Geology, 9, 303-326.

Gillott, J. E., M. A. G. Duncan, and E. G. Swenson (1973). Alkali-Aggregate Reaction in Nova Scotia. IV. Character of the Reaction. Cement and Concrete Research, 3, 521-535.

Glasser, L. S. D. and N. Kataoka (1981). The Chemistry of Alkali-Aggregate Reaction. Cement and Concrete Research, 21, 647-654.

Gogte, B. S. (1973). An Evaluation of Some Common Indian Rocks with Special Reference to Alkali-Aggregate Reactions, Engineering Geology, 7, 135-153.

Grattan-Bellew, P. E. (1989). Test Methods and Criteria for Evaluating the Potential Reactivity of Aggregates. 8th International Conference on Alkali-Aggregate Reaction in Concrete, Kyoto, Japan, 279-294.

Grattan-Bellew, P. E. (1994). Alkali Contribution from Limestone Aggregate to Pore Solution of Old Concrete. ACI Materials Journal, 91, 173-177.

Grattan-Bellew, P. E. (1997). A Critical Review of Ultra-Accelerated Tests for Alkali-Silica Reactivity. Cement and Concrete Composites, 19, 403-414.

Grattan-Bellew, P. E. (2001). Petrographic and Technological Methods for Evaluation of Concrete Aggregates, in: V. S. Ramachandran, J. J. Beaudoin (Eds.), Handbook of analytical techniques in concrete science and technology Principles, Techniques, and Applications, Noyes Publications, 63-98.

Hansen, W. C. (1944). Studies Relating to the Mechanism by which the Alkali-Aggregate Reaction Proceeds in Concrete. Journal of the American Concrete Institute, 15 (3), 213-227.

Hasson, G., D. Zollinger, and R. Lytton (2010). Determination of the Main Parameters of Alkali Silica Reaction Using System Identification Method. Journal of Materials in Civil Engineering, 22 (9), 865-873.

Hazim, A. and A. Kawaz (2010). Dissolution Rate Constant of Carbonates under Natural Environments. Tikrit Journal of Pure Science, 15 (3).

Hobbs, D. W. in: T. Taylor (Ed.) (1988). Alkali-Silica Reaction in Concrete. London, 22-27.

Hobbs, D. W. and W. A. Gutteridge (1979). Particle Size of Aggregate and Its Influence upon the Expansion Caused by the Alkali-Silica Reaction. Magazine of Concrete Research, 31 (109), 235-242.

Hooton, R. D. (1986). Effect of Containers on ASTM C 441: Pyrex Mortar Bar Expansions. 7th International Conference on Alkali-Aggregate Reaction in Concrete, 351-357.

Ichikawa, T. (2009). Alkali-Silica Reaction, Pessimum Effects and Pozzolanic Effect. Cement and Concrete Research, 39 (8), 716-726

Ichikawa, T. and M. Miura (2007). Modified Model of Alkali-Silica Reaction, Cement and Concrete Research, 37 (9), 1291-1297.

Ideker, J. H., B. L. East, K. J. Folliard, M. D. A. Thomas, and B. Fournier (2010). The Current State of the Accelerated Concrete Prism Test. Cement and Concrete Research, 40, 550-555.

Ideker, J. H., K. J. Folliard, B. Fournier, and M. D. A. Thomas (2006). The Role of "Non-Reactive" Aggregates in the Accelerated (60°C) Concrete Prism Test, in: B. Fournier (Ed.), The Marc-André Bérubé Symposium on Alkali-Aggregate Reactivity in Concrete, 8th CANMET/ACI International Conference on Recent Advances in Concrete Technology, CANMET, Montreal, Canada, 45-70.

Ideker, J. H., T. Drimalas, A. F. Bentivegna, K. J. Folliard, B. Fournier, M. D. A. Thomas, R. D. Hooton, and A. C. Rogers (2012). The Importance of Outdoor Exposure Site Testing. 4th International Conference on Alkali-Aggregate Reaction in Concrete, Austin, TX (Paper 051412-IDEK).

John, D. A., A. B. Poole, and I. Sims (1998). Concrete Petrography: A Handbook of Investigative Techniques. Arnold, U.K, 474.

Johnston, D. P, D. Stokes, and R. Surdahl (2000). A Kinetic-Based Method for Interpreting ASTM C 1260. Cement Concrete Aggregate, 22 (2), 142-149.

Kagimoto, H., I. Inoshita, and M. Kawamura (2004). Threshold OH^- Concentration in Pore Solution of Mortar using Alkali Reactive Aggregates, in: M. Tang, M. Deng (Eds.),

12th International Conference on Alkali-Aggregate Reaction in Concrete, Beijing, China, 728-735.

Kawamura M. and K. Iwahori (2004). ASR Gel Composition and Expansive Pressure in Mortars Under Restraint. Cement and Concrete Research, 26, 47-56.

Kawamura, M., K. Takemoto, and S. Hasaba (1983). Application of Quantitative EDXA Analyses and Microhardness Measurements to the Study of Alkali-Silica Reaction Mechanisms. The 6th International Conference on Alkalis in Concrete, 167-174.

Kawamura, M., N. Arano, and T. Terashima (1998). Composition of ASR Gels and Expansion of Mortars, in: M. Cohen, S. Mindess, J. Skalny (Eds.), Materials Science of Concrete: Special Volume, The Sidney Diamond Symposium, American Ceramic Society, Westerville, OH, 261-276.

Kollek, J. J., S. P. Varma, and C. Zaris (1986). Measurement of OH^- Concentrations of Pore Fluids and Expansion due to Alkali-Silica Reaction in Composite Cement Mortars. 8th International Congress on the Chemistry of Cement, Rio de Janeiro, 183-189.

Kuroda, T., S. Inoue, A. Yoshino, and S. Nishibayashi (2004). Effects of Particle Size, Grading and Content of Reactive Aggregate on ASR Expansion of Mortars Subjected to Autoclave Method, in: M. Tang, M. Deng (Eds.), 12th International Conference on Alkali-Aggregate Reaction in Concrete, International Academic Publishers, Beijing, China, 736-743.

Kuroda T., S. Nishibayashi, S. Inoue, and A. Toshino (2000). Effects of the Particle Size of Reactive Fine Aggregate and Accelerated Test Conditions on ASR Expansion of Mortar Bar. Transactions of the Japan Concrete Institute, 22, 113-118.

Lane, D. S. (1999). Comparison of Results from C 441 and C 1293 with Implications for Establishing Criteria for ASR-Resistant Concrete. Cement, Concrete, and Aggregates, 21 (2), 149-56.

Leemann, A. and P. Lura (2013). E-modulus of the Alkali-silica-reaction Product Determined by Micro-indentation. Construction and Building Materials, 44, 221-227.

Li, G., Y. Zhao, and S. S. Pang (1999). Four-phase Sphere Modeling of Effective Bulk Modulus of Concrete. Cement and Concreete Research, 29, 839-845.

Lindgård, J., Ö. Andiç-Çakır, I. Fernandes, T. F. Rønning, M. D. A. Thomas (2012). Alkali-Silica Reactions (ASR): Literature Review on Parameters Influencing Laboratory Performance Testing, Cement and Concrete Research, 42, 223-243.

Liu, K. W. and A. Mukhopadhyay (2014). A kinetic-Based ASR Aggregate Classification. Construction and Building Materials, 68, 525-534.

Liu, K. W. and A. Mukhopadhyay (2014). Alkali-Silica Reaction in a Form of Chemical Shrinkage. Civil Engineering and Architecture, 2, 235-244.

Lorenzo, P., S. Goni, S. Hernandez, and A. Guerrero (1996). Effect of Fly Ashes with High Total Alkali Content in the Alkalinity of the Pore Solution of Hydrated Portland Cement Paste, Journal of American Ceramics Society, 97 (2), 470-474.

Lothenbach, B. and F. Winnefeld (2006). Thermodynamic Modelling of the Hydration of Portland Cement. Cement and Concrete Research, 36, 209-226.

Marks, V. J. (1996). Characteristics of Iowa Fine Aggregate. Report No. MLR-92-6, Iowa Department of Transportation, 57.

McGowan, J. K. and H. E. Vivian (1952). Studies in Cement-Aggregate Reaction: Correlation between Crack Development and Expansion of Mortars. Australian Journal of Applied Science, 3, 228-232.

Mehta, P. K. and P. J. M. Monteiro, (1992). Concrete: Structure, Properties, and Materials (2nd Edition.). Prentice Hall, Upper Saddle River, New Jersey.

Mindess, S., J. F. Young, and D. Darwin, (2003). Concrete, Prentice Hall, Upper Saddle River, New Jersey.

Moisson, M., M. Cyr, E. Ringot, and A. Carles-Gibergues (2004). Efficiency of Reactive Aggregate Powder in Controlling the Expansion of Concrete Affected by Alkali-Silica Reaction (ASR), in: M. Tang, M. Deng (Eds.), 12th International Conference on Alkali-Aggregate Reaction in Concrete, International Academic Publishers, Beijing, China, 617-624.

Morey, G. W., R. O. Fournier, and J. J. Rowe (1964). The Solubility of Amorphous Silica at 25°C. Journal of Geophysical Research, 69 (10), 1995-2002.

Mukhopadhyay, A. K. and D. G. Zollinger (2009). Development of Dilatometer Test Method to Measure Coefficient of Thermal Expansion (CoTE) of Aggregates. Journal of Materials in Civil Engineering, 21 (12).

Mukhopadhyay, A. K., C. Shon, and D. Zollinger (2006). Activation Energy of Alkali-Silica Reaction and Dilatometer Method. In Transportation Research Record: Journal of Transportation Research Board, No. 1979, Transportation Research Board of the National Academies, Washington D.C., 1-11.

Mukhopadhyay, A. K., G. Hassan, K. W. Liu, and D. Zollinger (2012). A New Kinetic Type Rapid Aggregate ASR Test Method. 14th International Conference on Alkali-Aggregate Reaction in Concrete, Austin, Texas.

Mukhopadhyay, A. K., H. Ghanem, C. S. Shon, D. Zollinger, D. Gress, and D. Hooton (2009). Mitigation of ASR in Concrete-Combined Materials Test Procedure. IPRF Report, DOT/FAA-01-G-003-2.

Mukhopadhyay, A. K., K. W. Liu (2014). ASR Testing: A New Approach to Aggregate Classification and Mix Design Verification. Report No. 0-6656-1, Texas A&M Transportation Institute, Texas A&M University, College Station, TX.

Mukhopadhyay A. K., S. Neekhra and D. G. Zollinger (2004). New Mineralogical Approach to Predict Aggregate and Concrete Coefficient of Thermal Expansion (CoTE). Presented (04-4167, Compendium of papers CD-ROM) in Transportation Research Board, Washington D.C.

Multon, S., M. Cyr, A. Sellier, N. Leklou, and L. Petit (2008). Coupled effects of aggregate size and alkali content on ASR expansion. Cement and Concrete Research, 38, 350-359.

Mura, T. (1987). Micromechanics of defects in soilds. Martinus Nijhoff, Dordrecht, the Netherlands.

Nilsson, L. O. (2006). Modelling Moisture Conditions in Cementitious Materials: Some Present Challenges. 2nd International Symposium on Advances in Concrete through Science and Engineering, Quebec City, Canada.

Nixon, P. J. and I. Sims (1992). RILEM TC106 Alkali Aggregate Reaction-Accelerated Tests Interim Report and Summary of Survey of National Specifications. 9th International Conference on Alkali-Aggregate Reaction in Concrete, Concrete Society, Slough, England, 2, 731-738.

Oliver, W.C. and G. M. Pharr (1992). An Improved Technique for Determining Hardness and Elastic Modulus using Load and Displacement Sensing Indentation Experiments. Journal of Materials Research, 7, 1564-1583.

Ostertag, C. P., C. Yi, and P. Monteiro (2007). Effect of Confinement on Properties and Characteristics of Alkali-Silica Reaction Gel. ACI Materials Journal, 104-M30, 276-282.

Pedneault, A. (1996). Development of Testing and Analytical Procedures for the Evaluation of the Residual Potential of Reaction, Expansion, and Deterioration of Concrete Affected by ASR. M.Sc. Memoir, Laval University, Québec City, Canada, 133.

Phair, J. W., S. N. Tkachev, M. H. Manghnani, and R. A. Livingston (2005). Elastic and Structural Properties of Alkaline-calcium Silica Hydrogels. Journal of Materials Research, 20 (2), 344-349.

Ponce, J. M. and O. R. Batic (2006). Different Manifestations of the Alkali-Silica Reaction in Concrete According to the Reaction Kinetics of the Reactive Aggregate. Cement and Concrete Research, 36, 1148-1156.

Poole, A. B. (1992) Alkali-Silica Reactivity Mechanisms of Gel Formation and Expansion. 9th International Conference in Alkali-Aggregate Reaction in Concrete, London, England, 782-789.

Powers, T. C., and H. H. Steinour (1955). An Investigation of Some Published Researches on Alkali-Aggregate Reaction: I. the Chemical Reactions and Mechanism of Expansion. Journal of the American Concrete Institute, 26 (6), 497-516.

Prezzi, M., P. J. M. Monteiro, and G. Sposito (1997). Alkali-Silica Reaction-Part 1: Use of the Double-Layer Theory to Explain the Behavior of the Reaction Product Gels. ACI Journal, 94 (1), 10-17.

Ramyar, K., A. Topal, and Ö. Andiç-Çakır (2005). Effects of Aggregate Size and Angularity on Alkali-Silica Reaction, Cement and Concrete Research, 35, 2165-2169.

Ranc, R. and L. Debray (1992). Reference Test Methods and a Performance Criterion for Concrete Structures. 9th International Conference on Alkali-Aggregate Reaction in Concrete, London, U.K., 824-831.

RILEM TC 191-ARP (2003): Alkali-Reactivity and Prevention. Assessment, Specification and Diagnosis of Alkali-Reactivity. RILEM Recommended Test Method AAR-1: Detection of Potential Alkali-Reactivity of Aggregates: Petrographic Method, Materials Structure, 36, 480-496.

Rivard, P., M. A. Bérubé, J. P. Ollivier, and G. Ballivy (2003). Alkali Mass Balance during the Accelerated Concrete Prism Test for Alkali-Aggregate Reactivity, Cement and Concrete Research, 33, 1147-1153.

Rodrigues, F. A., P. J. M. Monteiro, and G. Sposito (1999). The Alkali-Aggregate Reaction: The Surface Charge Density of Silica and Its Effect on the Expansive Pressure. Cement and Concrete Research, 29 (4), 527-53.

Sarkar, S. L., D. G. Zollinger, A. K. Mukhopadhyay and L. Seungwook (2004). Appendix 1 Handbook for Identification of Alkali-Silica Reactivity, Airfield Pavement, Advisory Circular No. 150/5380-8, U.S. Department of Transportation Federal Aviation Administration.

Shao, Y., T. Lefort, S. Moras, and D. Rodriguez (2000). Studies on Concrete Containing Ground Waste Glass. Cement and Concrete Research, 30 (1), 91-100.

Shayan, A., A. Xu, H. Morris (2008). Comparative Study of the Concrete Prism Test (CPT 60°C, 100% RH) and Other Accelerated Tests, in: M. A. T. M. Broekmans, B. J. Wigum (Eds.), 13th International Conference on Alkali-Aggregate Reactions in Concrete, Trondheim, Norway, 391-400.

Shayan, A. (1992). The Pessimum Effect in an Accelerated Mortar Bar Test using 1M NaOH Solution at 80°C. Cement and Concrete Composite, 14, 249-255.

Shayan, A. (2002). Value-Added Utilisation of Waste Glass in Concrete, in: IABSE Symposium Melbourne.

Shehata, M. H. and M. D. A. Thomas (2000). The Effect of Fly Ash Composition on the Expansion of Concrete Due to Alkali Silica Reaction. Cement and Concrete Research, 60 (7), 1063-1072

Shehata, M. H. and M. D. A. Thomas (2006). Alkali Release Characteristics of Blended Cements. Cement and Concrete Research, 36, 1166-1175.

Shon, C. S., A. K. Mukhopadhyay, and D. G. Zollinger (2007). Alkali-Silica Reactivity of Aggregate and Concrete Evaluated by Dilatometer Method: Performance-Based Approach. Journal of the Transportation Research Board, No. 2020, 10-19.

Shon, C. S., D. G. Zollinger, and S. L. Sarkar (2003). Application of Modified ASTM C 1260 Test for Fly Ash-Cement Mixtures, Journal of the Transportation Research Board 1834, 93-106.

Shon, C. S., S. Lim, A .K. Mukhopadhyay, D. G. Zollinger, and S. L. Sarkar (2002). New Aggregate Characterization Tests for Thermal and ASR Reactivity Properties. 10th International Conference for Aggregates Research (ICAR) Annual Symposium.

Shon, C. S., S. L. Sarkar, and D. G. Zollinger (2004). Testing the Effectiveness of Class C and Class F Fly Ash in Controlling Expansion due to Alkali-Silica Reaction Using Modified ASTM C 1260 Test Method, Journal of Materials in Civil Engineering, 16 (1), 20-27.

Sibbick, R. G. and C. L. Page (1992). Threshold Alkali Contents for Expansion of Concretes Containing British Aggregates. Cement and Concrete Research, 22, 990-994.

Sorrentino, D., J. Y. Clement, and J. M. Golberg (1992). A New Approach to Characterize the Chemical Reactivity of the Aggregates. 9th International Conference on Alkali-Aggregate Reaction in Concrete, Slough, England, 1009-1016.

Stark, D., B. Morgan, and P. Okamoto (1993). Eliminating or Minimizing Alkali-Silica Reactivity. SHRP-C-343, Construction Technology Laboratories, Purdue University, West Lafayette, Indiana.

Stanton, D. E. (1940). Expansion of Concrete through Reaction between Cement and Aggregate. American Society of Civil Engineers, 66, 1781-1811.

Struble, L. and S. Diamond (1981). Unstable Swelling Behaviour of Alkali Silica Gels. Cement and Concrete Research, 11, 611.

Swamy, R. N. (1992). Testing for Alkali-Silica Reaction. The Alkali Silica Reaction in Concrete, Blackie and Sons, Glasgow, 54-95.

Tang, M. S. and H. Su-Fen, (1980). Effect of $Ca(OH)_2$ on Alkali-Silica Reaction, 8th International Congress of Cement Chemistry. Paris, France, 2, 94-99.

Tatematsu, H. and T. Sasaki, (1989). Proposal of a New Index for a Modified Chemical Method. 8th International Conference on Alkali-Aggregate Reaction in Concrete, Kyoto, Japan, 333-338.

Thaulow, N., U. H. Jakobsen, and B. Clark (1996). Composition of Alkali Silica Gel and Ettringite in Concrete Railroad Ties: SEM-EDX and X-ray Diffraction Analyses. Cement and Concrete Research, 26, 309-318.

Thomas, M. D. A. and F. A. Innis (1998). Effect of Slag on Expansion Due to Alkali-Aggregate Reaction in Concrete. ACI Materials Journal, 95, 716-724.

Thomas, M. D. A. and F. A. Innis (1999). Use of the Accelerated Mortar Bar Test for Evaluating the Efficacy of Mineral Admixtures. Cement, Concrete, and Aggregates, 21 (2), 157-164.

Thomas, M., B. Fournier, K. Folliard, J. Ideker, and M. Shehata (2006). Test Methods for Evaluating Preventive Measures for Controlling Expansion due to Alkali-Silica Reaction in Concrete. Cement and Concrete Research, 36, 1842-1856.

Touma, W., D. Fowler, R. Carrasquillo, K. J. Folliard, and N. R. Nelson (2001). Characterizing the Alkali-Silica Reactivity of Aggregates Using ASTM C 1293, ASTM C 1260, and Their Modifications. Journal of the Transportation Research Board, Transportation Research Board, No. 1757, 157-165.

TxDOT Item 421-024 (2004). Standard Specifications for Hydraulic Cement Concrete. Austin (TX), Texas Department of Transportation.

TxDOT Item 421-031 (2004). Standard Specifications for Hydraulic Cement Concrete. Austin (TX), Texas Department of Transportation.

TxDOT Item 421-034 (2004). Standard Specifications for Hydraulic Cement Concrete. Austin (TX), Texas Department of Transportation.

TxDOT Item 424-001 (2004). Standard Specifications for Precast Concrete Structures (Fabrication). Austin (TX), Texas Department of Transportation.

Uomoto, T, Y. Furusawa, and H. Ohga (1992). A Simple Kinetics Based Model for Predicting Alkali Silica Reaction. 9th International Conference on Alkali-Aggregate Reaction in Concrete, London, England, 2, 1077-1084.

Vivian, H. E. (1947). The Effects on Mortar Expansion of Reactive Component in the Aggregate: Studies in Cement-Aggregate Reactions. Part 10, CSIRO Bull, 256, 13-20.

Vivian, H. E., (1981). A Working Appraisal of Alkali-Aggregate Reaction in Concrete. 5th International Conference on Alkali-Aggregate Reaction in Concrete, Cape Town, South Africa, Paper S252/14.

Wang, H. and J. E. Gillott (1991). Mechanisms of Alkali-Silica Reaction and Significance of Calcium Hydroxide. Cement and Concrete Research, 21, 647-654.

Wenk, H. R., P. J. Monteiro, and K. Shomglin (2008). Relationship between Aggregate Microstructure and Mortar Expansion: A Case Study of Deformed Granitic Rocks from the Santa Rosa Mylonite Zone, Journal of Materials Science, 43, 1278-1285.

Woods, H. (1968). Durability of Concrete Construction. Monograph, American Concrete Institute, Detroit, Michigan, 4.

Zhang, C., A. Wang, M. Tang, B. Wu, and N. Zhang (1999). Influence of Aggregate Size and Aggregate Size Grading on ASR Expansion. Concrete and Cement Research, 29, 1393-1396.

Zhang, X. and G. W. Groves (1990). The Alkali-Silica Reaction in OPC-Silica Glass Mortar with Particular Reference to Pessimum Effects. Advanced Cement Research, 3 (9), 9-13.

Zharikov, V., E. B. Lebedev, A. M. Dorfman, and V. M. Vitovtova (2000). Effect of Saturating Fluid Composition on the Rock Microstructure, Porosity, Permeability and

Vp under High Pressure and Temperature. Physics and Chemistry of the Earth, 25 (2), 215-218.

Zheng, J. and X. Zhou (2008). Three-phase Composite Sphere Model for the Prediction of Chloride Diffusivity of Concrete. Journal of Materials in Civil Engineering, 20 (3), 205-211.

APPENDIX A

STANDARD TEST METHOD FOR DETERMINATION OF COMPOUND ACTIVATION ENERGY OF AGGREGATE DUE TO ALKALI-SILICA REACTION (CHEMICAL METHOD)

1. SCOPE

1.1 This test method covers chemical determination of the reactivity of an as-received aggregate in terms of measuring composite activation energy (CAE) of alkali silica reaction where aggregate reacts with alkaline solution of chemistry similar to pore solution chemistry of Portland-cement concrete.

1.2 This test is intended to offer a rapid and reliable ASR standard test method. A test method where as-received aggregates are immersed in alkaline solution and allowed to react at different temperatures. The test measures solution volume change (i.e., volume contraction) in a closed system over time (till 4-5 days) as the reaction between aggregates and solution proceeds.

1.3 The test method is developed to determine aggregate CAE of ASR. CAE is a measure of aggregate alkali-silica reactivity and is a potential screening parameter to develop CAE based aggregate classification system. The lower the CAE the higher is the reactivity.

1.4 The test method reliably predicts aggregate alkali reactivity in a short period of time and can be effectively used as an alternative to the current test method (e.g., ASTM C 1260).

2. DEFINITION

2.1 Dry Unit Weight-as defined in ASTM Test Method C 138 for fine and coarse aggregates.

2.2 For definitions of other terms relating to concrete or aggregates, see ASTM Terminology C 125.

3. APPARATUS

3.1 Scales

The scales and weights used for weighing materials shall conform to the requirements prescribed in ASTM Specification C 1005.

3.2 Crushing Equipment

A small jaw crusher or other suitable equipment capable of crushing aggregate to pass a 1 ½" sieve.

3.3 Sieves

A 25.4-mm (1"), 12.5-mm (1/2"), 4.75-mm (No. 4), 2.36-mm (No. 8), 1.18-mm (No. 16), 600-µm (No. 30), 300-µm (No. 50), 150-µm (No. 100) sieve.

3.4 De-Airator / Vacuum Pump

A small vacuum pump or other suitable equipment to apply a vacuum pressure of 30 inch-Hg.

3.5 Vibrating Table

A vibrating table with variable-speed control keeps sample material loose.

3.6 Glassware

All glass apparatus and vessels should be carefully selected to meet the particular requirements for each operation. Standard volumetric flasks, burets, and pipets should be of precision grade.

3.7 The VCMD device (Figure A1, Note 1) consists of a stainless steel container (Figure A1a), a brass lid (Figure A1a), a stainless steel hollow tower (Figure A1b), a brass housing to hold linear variable differential transducer (LVDT) with perfect vertical alignment (Figure A1c and A1d), and a stainless steel float (Figure 2A). A detailed drawing of the individual parts (Figures A1a, b, c, and d) and assembled view with all these parts together (Figure A1) are presented below. One end of Tower (Figure A1b) is screwed into the lid (Figure A1a) and the other end screwed into the LVDT housing (Figure A1c) with O-rings in all three junctions (i.e., (i) between the container and lid, (ii) between the lid and tower and (iii) between the tower and LVDT housing). The LVDT (Note 2) is placed into the center hole of the LVDT housing and pushed into a O-ring (2-112 buna-n) placed at the bottom of the LVDT. With the proper tightening of the six set screws (come though the side of the housing), a perfect vertical alignment of the LVT is ensured.

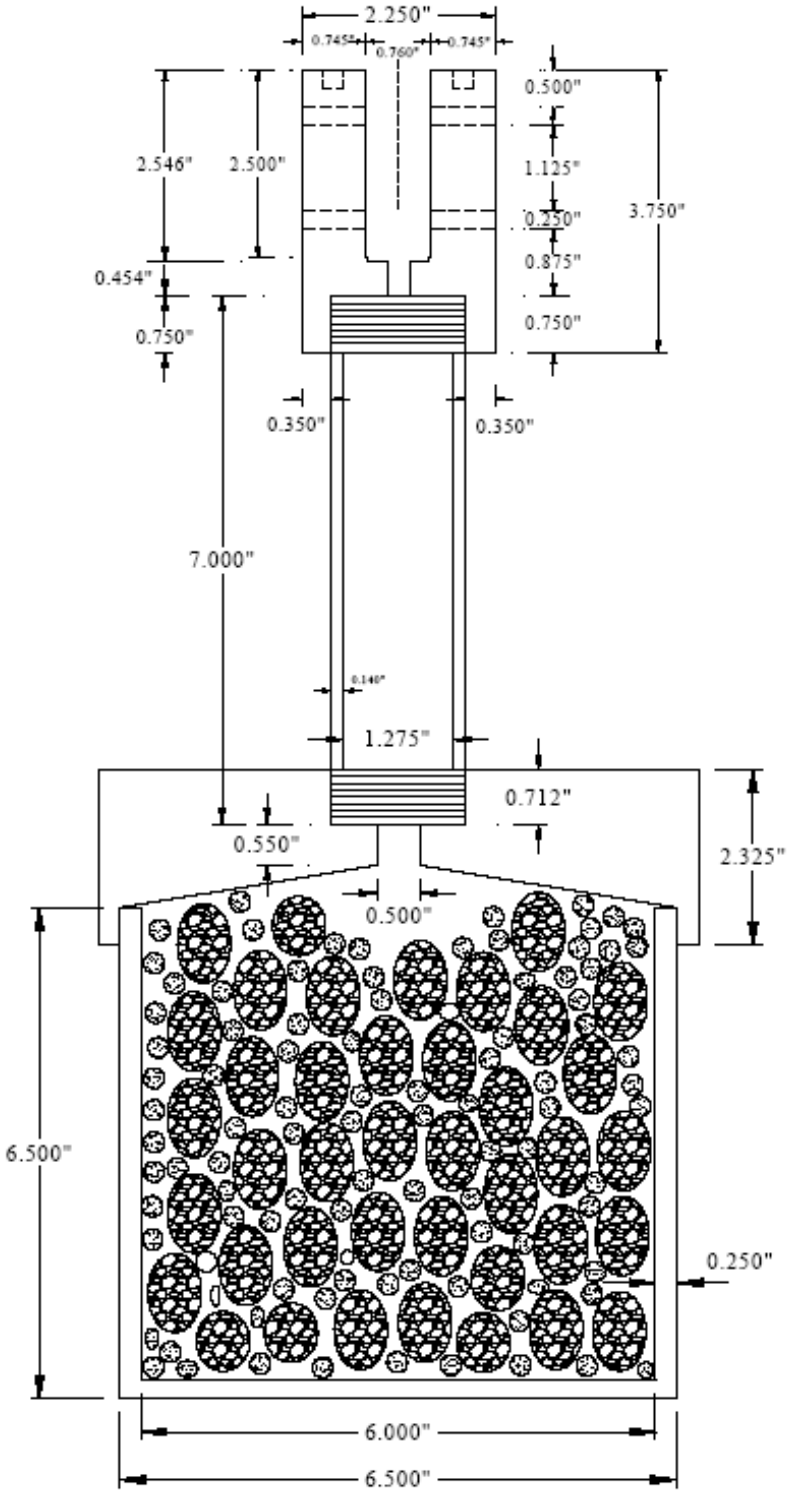

Figure A1 Cross-Sectional View of the Device.

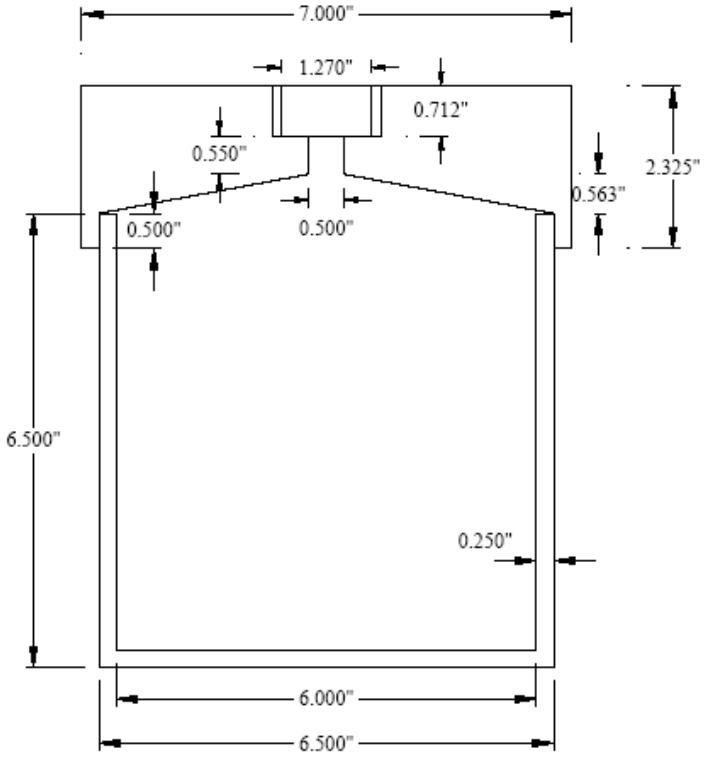

Figure A1a Stainless Steel Continer + Brass Lid.

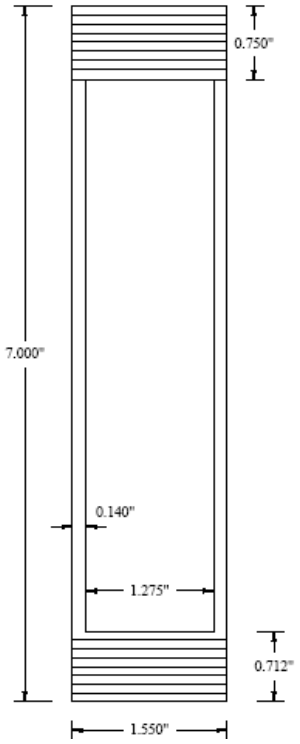

Figure A1b Stainless Tower.

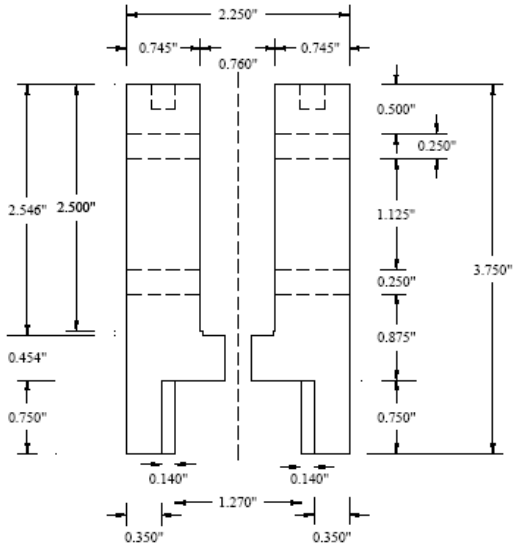

Figure A1c LVDT Housing.

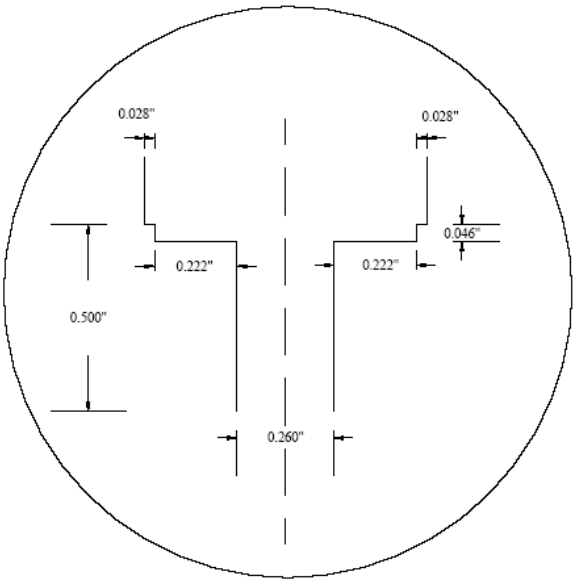

Figure A1d Detailed Drawings of the Central Part of the Housing in Figure A1c.

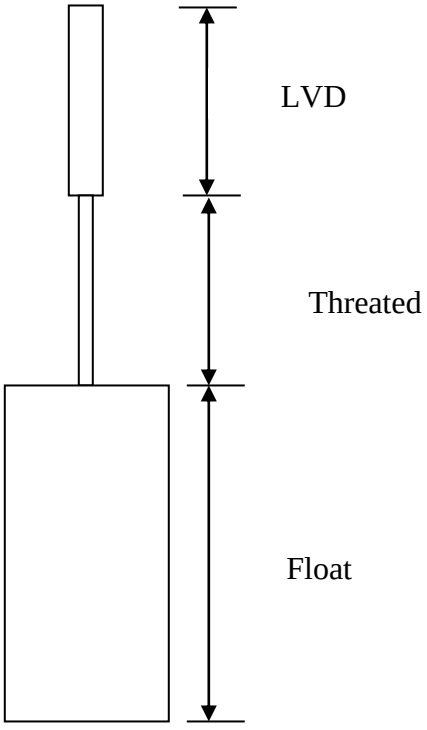

Figure A2 A Schematic Diagram of the Float System.

3.8 Oven

A convection oven with temperature control in the range of 40.0 to 100.0±1.0°C.

3.9 The combinations of number of oven and VCMD to measure CAE at one level of alkalinity are summarized in Table A1.

Note 1: The pot is made of Stainless steel: "1.4401 X5CrNiMo17-12-2 316 S31600" (ASTM C 182). The type of brass used for the lid is the Naval brass (ASTM B 21); similar to admiralty brass; is a 40% zinc brass and 1% tin. The tower is made from Stainless steel S31600 (ASTM C 182).

Note 2: The LVDT should have a nominal linear range of ±1 inch and operating temperature range up to 150°C.

Table A1 Combinations of Oven and VCMD.

Option	60°C	70°C	80°C	No. of VCMDs	No. of Oven	No. of Days	CAE
1	3	3	3	9	3	5	3 replicas
2	2	2	2	6	3	5	2 replicas
3	1	1	1	3	3	5	without replicas
4	1	1	1	3	1	15	3 replicas for a single aggregate E_a without replicas for 3 aggregates
5	3	3	3	8	2	15	1^{st} aggr. -E_a with 3 replicas 2^{nd} aggr. - E_a with 3 replicas 3^{rd} aggr. - E_a with 2 replicas
						10	1^{st} aggr. - E_a with 3 replicas 2^{nd} aggr. - E_a W/O replicas

Options 1 and 2 are the ideal combinations; 3 and 4 are minimum requirements for determination of activation energy; 5 is the current combination for this test.

4. REAGENTS AND MATERIALS

4.1 Sodium Hydroxide (NaOH)

UPS or technical grade may be used, provided the Na^+ and OH^- concentrations are shown by chemical analysis to lie between 0.49N and 0.51N.

4.2 Calcium Hydroxide ($Ca(OH)_2$)

UPS or technical grade may be used.

4.3 Purity of water

De-ionized or distilled water is recommended (ASTM D 1193).

4.4 Soak Solution

Each liter of solution shall contain 20.0 g of NaOH dissolved in 900 ml of water, and shall be diluted with additional deionized or distilled water to obtain 1.0 L of solution. Additional 1 g of $Ca(OH)_2$ per liter need to be added in order to saturate the solution.

Warning-Before using NaOH, review (1) the safety precautions for using NaOH; (2) first aid for burns; and (3) the emergency response to spills, as described in the manufacturer's Material Safety Data Sheet or other reliable safety literature. NaOH can cause very severe burns and injury to unprotected skin and eyes. These should include full-face shields, rubber aprons, and gloves impervious to NaOH. Gloves should be checked periodically for pin holes.

5. SAMPLE PREPARATION

5.1 Obtain as-received bulk aggregate sample and wash in accordance with ASTM D 75. Dry the aggregate samples to essentially constant mass, preferably in an oven at 110 ± 5°C (230 ± 9°F) in accordance with ASTM Test Method C 29. A fixed representative gradation is selected for both coarse and fine aggregates (Tables A2 and A3) in order to compare the results between different aggregates. As a result, the oven dried aggregates need to be sieved out in order to separate the different size fractions (Tables A2 and A3).

To prepare a test sample, recombine these size fractions according to the gradation requirement in Tables A2 and A3 for fine and coarse aggregates, respectively.

Table A2 Grading Requirements for Fine Aggregates.

Sieve Size		Mass, %
Passing	Retained on	
9.5 mm (3/8")	4.75 mm (No. 4)	4
4.75 mm (No. 4)	2.36 mm (No. 8)	13
2.36 mm (No. 8)	1.18 mm (No. 16)	17
1.18 mm (No. 16)	600 μm (No. 30)	38
600 μm (No. 30)	300 μm (No. 50)	23
300 μm (No. 50)	150 μm (No. 100)	5

Table A3 Grading Requirements for Coarse Aggregates.

Sieve Size		Mass, %
Passing	Retained on	
9.5 mm (1 1/2")	25.4 mm (1")	2
25.4 mm (1")	12.5 mm (1/2")	43
12.5 mm (1/2")	4.75 mm (No. 4)	54
4.75 mm (No. 4)	4.1 m (No. 8)	1

5.2 Dry unit weight

as defined in ASTM Test Method C 138 for fine and coarse aggregates.

5.3 Number of Samples

Test three samples (at least two) for each temperature to verify repeatability. Each test sample is around 8 to 9 lb depending on the dry unit weight of aggregate (ASTM C 29).

6. PROCEDURE

6.1 Determine the weight of the test sample based on the unit weight (sub-section 7.2) to fill 80% of the container volume (~ 8-9 lb)

6.1.1 Add alkaline solution (0.5N NaOH + saturated $Ca(OH)_2$) to the container till the aggregate sample is immersed. For fine aggregates, poking the aggregate with a metal rod will accelerate penetration of the solution to the bottom of the pot. Gently tap the side of the pot to remove any large air bubbles.

6.2 Screw the lid onto the container with proper placement of the O-ring. Make sure the lid is properly seated and tightened. Add some more solution through the tower to the container to ensure that the aggregate sample is fully immersed. Screw the tower with the lid.

6.3 Connect vacuum system to the tower. Turn on the vacuum pump and wait until vacuum of at least 25-inch Hg is achieved within 5 minutes. An attainment of the above vacuum is an indication of the leak-proof situation of the container-lid-tower assembled system. If the expected vacuum is not achieved, it possibly indicates some leaking though the container-lid junction and the following actions, i.e., (i) tightening the lid and/or (ii) remove the lid followed by rechecking/replacing the O-ring followed by reassemble and vacuum test again should be performed in order to ensure leak-proof situation. Turn off the vacuum pump when proper vacuum is achieved.

6.4 Keep the container to stand overnight under room temperature to allow aggregate saturation. Rubber stopper or cork can be placed at the top of the tower to reduce solution loss due to evaporation.

6.5 Place the container on vibro-deairator and connect to vacuum system to the tower. Vacuum under low vibration for 2 hours to remove air bubbles and ensures further saturation. The vacuum of at least 25-inch Hg is required. Repeat the same procedure (sub-section 6.3) if the expected vacuum is not achieved.

6.6 Place the container in the oven and heat it to a temperature of 60°C with rubber stopper or cork at the top of the tower. It takes around 5 hours to reach 60°C from the room temperature (25°C).

6.7 Remove the container from the oven and place it on vibro-deairator and connect to the vacuum system again in order to apply a second stage of vacuuming at high temperature under light vibration for 45 minutes. This facilitates further removal of air bubbles that may generate during heating and ensures an almost fully saturation stage. The vacuum of at least 25-inch Hg is required (as in sub-section 6.5).

6.8 Remove the container from vibro-vacuum system and place inside the oven.

6.9 The stainless steel float with threaded and LVDT rod (Figure A2) is weighted and then inserted through the tower. The LVDT housing is then placed at the top of the tower. Insert the LVDT into the housing and ensure perfect vertical alignment (Note 3).

6.10 View float level (i.e., measure of solution level) from the LVDT displacement reading on the computer and adjust alkaline solution level (remove LVDT and pour or remove solution through the tower) in order to achieve appropriate initial level (Note 4).

6.11 Finally, the LVDT is securely placed in the LVDT housing using set of screws and ensure a perfect vertical alignment.

6.12 Set up the oven temperature to the selected target temperature (60 or 70 or 80°C) and let the computer record the solution volume change in a form of float movement through LVDT-data acquisition system over time (4 days).

Note 3: The free movement of the float is assured by rotating the LVDT. This removes any sticking issues due to improper placement of the float system.

Note 4: An initial float level of -0.9 to -0.8 is the best to accommodate high net solution volume expansion (thermal expansion) due to temperature change from the starting temperature (temperature after second stage vacuum) to the target temperatures (60, 70, and 80°C) with a LVDT of -1 to 1 inch measurement range.

6.13 Terminate the test and remove the device from the oven. Allow the device to cool down before removing the LVDT. Unscrew the set screws from the side of the LVDT housing and remove the LVDT housing (Note 5).

6.14 Unscrew the lid from the container (Note 6). Remove the sample from the container and thoroughly clean the container, lid, and tower (Note 7).

6.15 Repeat the procedures (6.1 to 6.14) for the remaining two temperatures.

Note 5: When remove the housing from the tower, use care to avoid bending the thread and/or LVDT rod connecting the float to the LVDT. Dry and weigh the float and compare the mass to the initial mass. If the mass has increased by more than a few tenths of a gram, the float most likely has a leak. Check that the O-ring between the pot and lid is not cracked or otherwise damaged, discolored or dirty. Make sure that the groove on which the O-ring sits is clean.

Note 6: It may be necessary to tap on the handles with a rubber mallet to break the lid loose.

Note 7: Scrub the inside of the container with steel wool and water. DO NOT use soap or detergent. Rinse all parts thoroughly with de-ionized or distilled water after cleaning.

7. CALCULATION

7.1 Reference Reading

Average of 1 hour LVDT reading at the thermally stabilized period (It takes around 5 to 8 hrs for the alkaline solution to reach the target temperature and be stabilized at that temperature) represents the reference level (Figure A3) or initial level for ASR. Subtract the subsequent LVDT displacement values from the reference level to obtain the displacement (Δh) due to ASR.

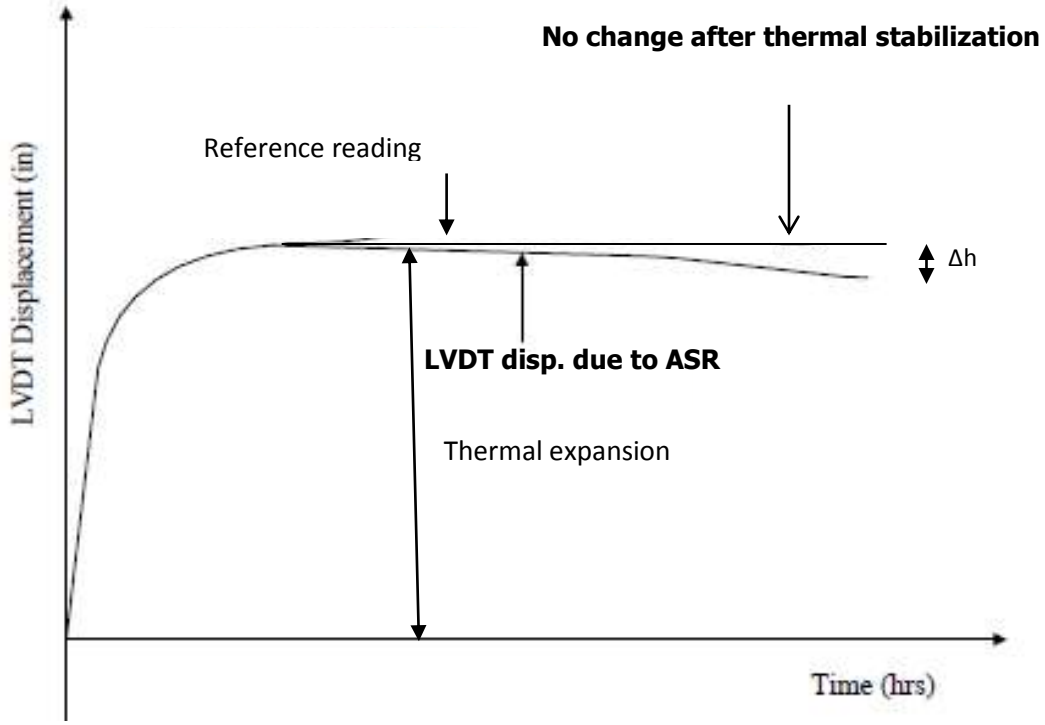

Figure A3 A Schematic Draw of Reference Reading.

7.2 Calculate the displacement due to ASR (Δh) (Figure A3).

7.3 Multiply the calibrated displacement by the area of the tower and divide by the volume of the sample to obtain the change in solution volume due to ASR. Calculate the volume change at percentage as follows:

$$V(\%) = \frac{\Delta V_{ASR}}{V_{Aggregate}} \times 100$$

$$\Delta V_{ASR} = r^2 \pi \Delta h$$

where:

V(%)= Percent volume change of solution due to ASR.

ΔV_{ASR}= Measured volume change of solution due to ASR.

$V_{Aggregate}$= Initial volume of aggregate (80% of the container).

r= Radius of the tower

7.4 Compound Activation Energy (CAE)

A kinetic-type model (Note 9) below is used to model measured non-linear type volume change data over time. By fitting the model to measured volume change data over time, the reaction rate (β) is calculated.

$$\varepsilon = \varepsilon_0 e^{-(\frac{\rho}{t-t_0})^{\beta}}$$

where:

ε_0 = ASR ultimate volume change.

β = Rate constant.

t_0 = Theoretical Initial time of ASR (hr).

ρ = Time corresponding to a volume change ($\varepsilon_0/\varepsilon$).

7.5 The rate constant (β) values at multiple temperatures (minimum 3 temperatures) are then determined and CAE is calculated by plotting ln(β) versus (1/T).

7.6 The slope of the linear regression is equal to (-CAE/R) based on Arrhenius equation, where R is the universal gas constant and CAE is the compound activation energy (KJ/mol).

7.7 Data from at least three temperatures must be generated at the recommended testing period of 4 days to determine aggregate CAE (Note 10).

Note 8- Plot the LVDT displacement of each float versus time. Check for sticking of the LVDT which will appear as a flat line in the plot often followed by a large change in displacement

Note 9: A computer program shown in Figure A4 is developed for CAE calculation and ASR aggregate classification. The program can be downloaded via Texas A&M Transportation Institute. The computer system requires MATLAB 7.11.0.584 (R2010b) and Microsoft Office Excel 2007.

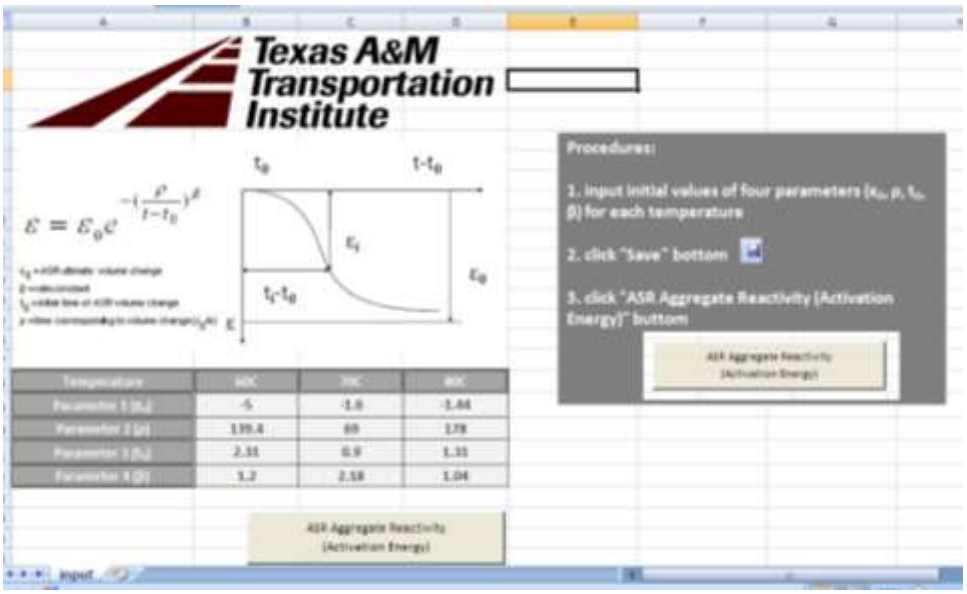

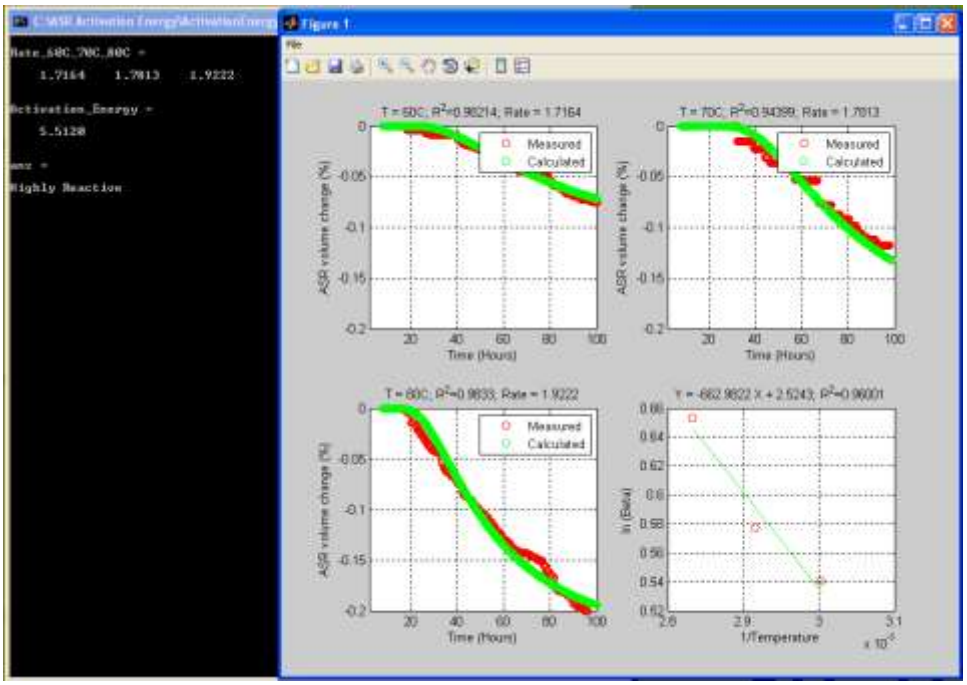

Figure A4 A Computer Program for CAE Calculation and Aggregate Classification.

Note 10: The activation energy (E_a) is the energy barrier that has to overcome to initiate ASR taking into account the combined effect of alkalinity, temperature, and time. The concept of ASR Ea can be considered as a composite single parameter of alkali silica reactivity of different reactive component(s) in aggregate. The use of term "compound activation energy" will be more appropriate than "activation energy" for heterogeneous and multi-phase aggregate materials.

8. PRECISION

It has been found that the average within-laboratory coefficient of variation for materials with reaction rate at the same test conditions is within 10%. The reaction rate within the same laboratory under the same condition should not differ by more than 15%.

APPENDIX B

ALL SOLUTION VOLUME CHANGE OVER TIME DATA AT DIFFERENT TEMPERATURES AND ALKALINITIES FOR THE TESTED AGGREGATES AND REPEATABILITY CALCULATION

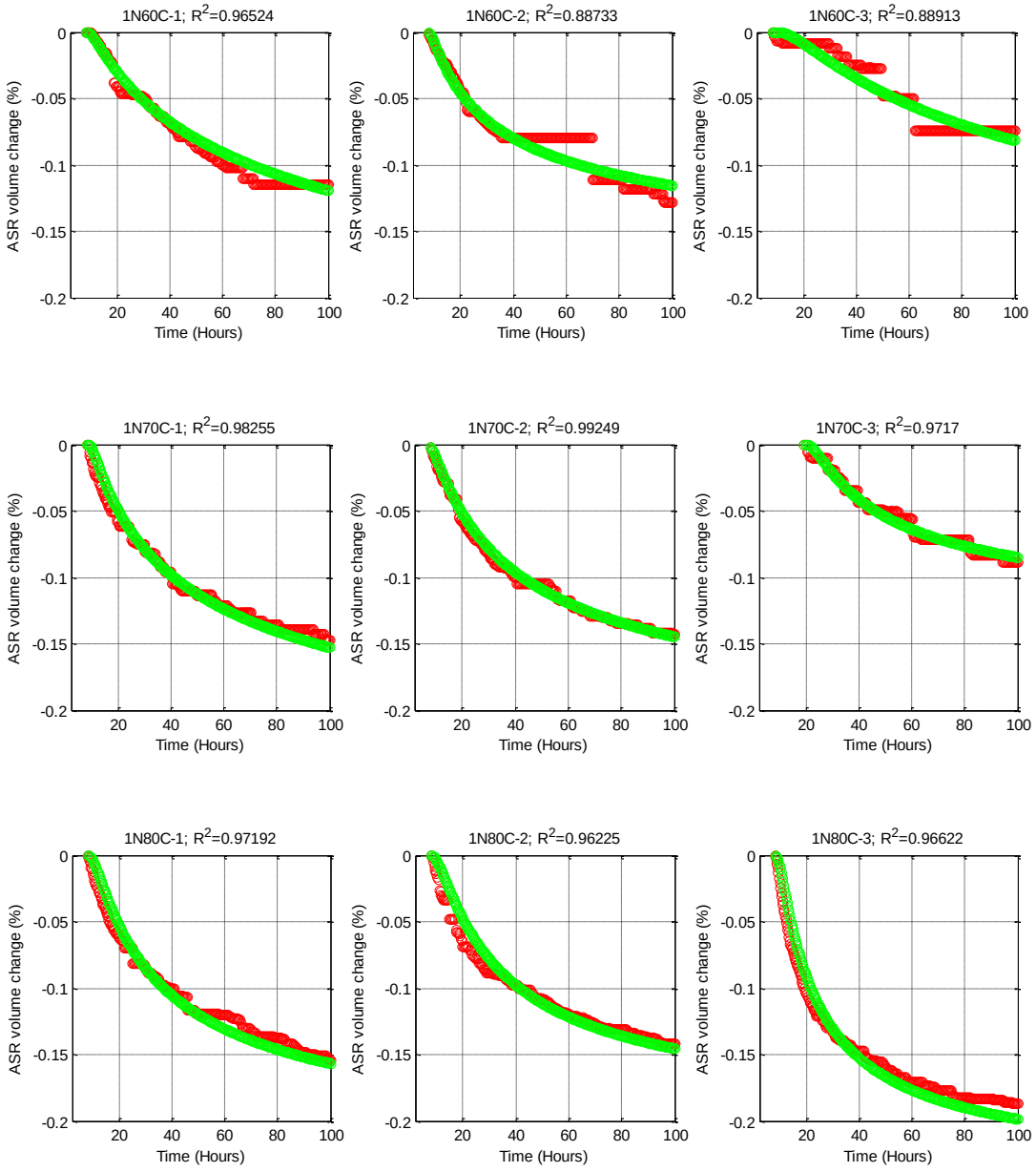

Figure B1-1 Repetition of Measured (Red) and Modeled (Green) Solution Volume Change over Time for FA1 with 1N NH + CH at Each Temperature (60, 70, and 80°C).

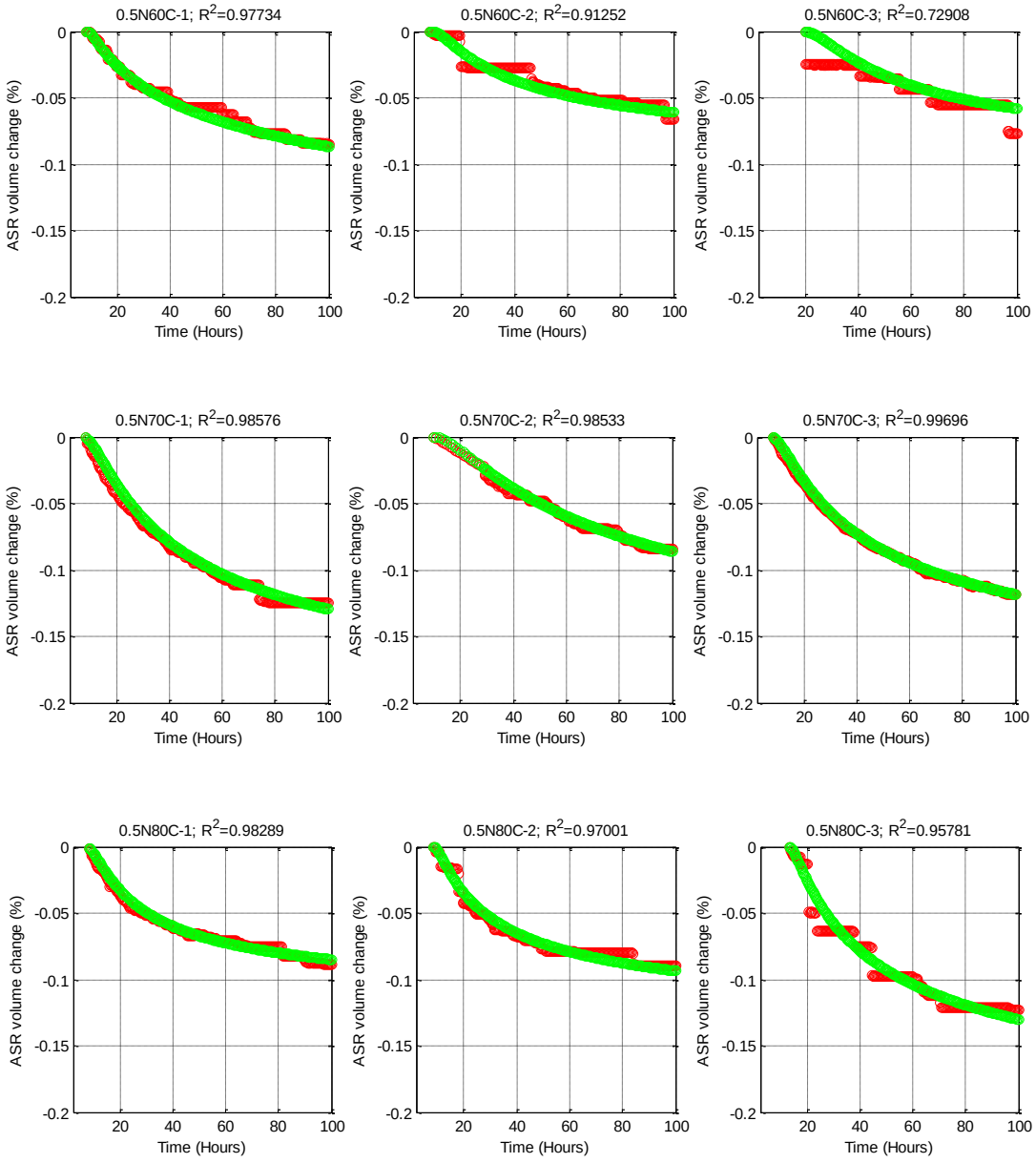

Figure B1-2 Repetition of Measured (Red) and Modeled (Green) Solution Volume Change over Time for FA1 with 0.5N NH + CH at Each Temperature (60, 70, and 80ºC).

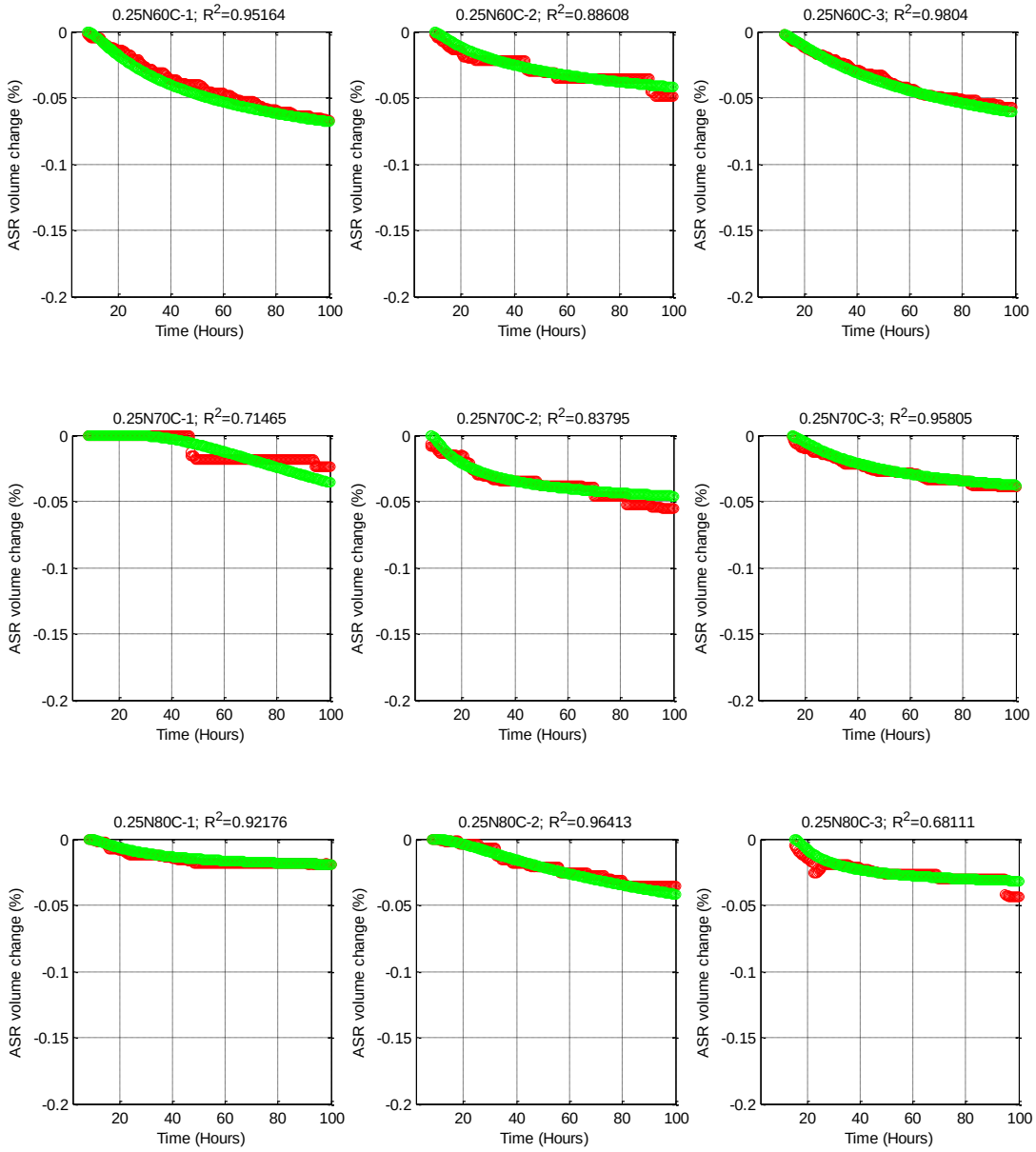

Figure B1-3 Repetition of Measured (Red) and Modeled (Green) Solution Volume Change over Time for FA1 with 0.25N NH + CH at Each Temperature (60, 70, and 80°C).

Table B1 Calculated Rate Constant Based on the Modeled Curve (Green) in Figures B1-1 to B1-3 for FA1.

Normality	Temperature °C	β			Average	COV %
		Test 1	Test 2	Test 3		
1	60	0.3968	0.4237	0.4468	0.4224	5.92
	70	0.4954	0.5069	0.5345	0.5123	3.92
	80	0.5842	0.6195	0.6134	0.6057	3.12
0.5	60	0.3776	0.3645	0.3872	0.3764	3.03
	70	0.4842	0.4835	0.5107	0.4928	3.15
	80	0.5964	0.6062	0.6014	0.6013	0.81
0.25	60	0.3143	0.3322	0.3253	0.3239	2.79
	70	0.4108	0.4309	0.4067	0.4161	3.11
	80	0.5792	0.6009	0.6038	0.5946	2.26

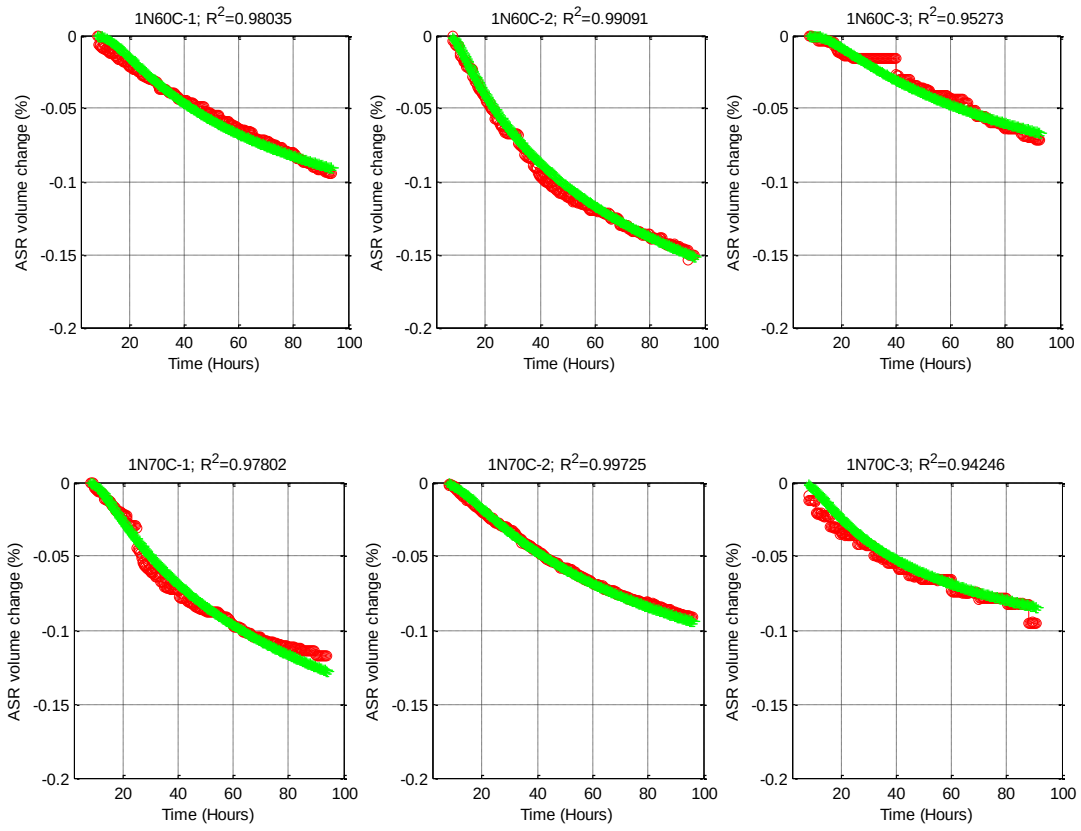

Figure B2-1 Repetition of Measured (Red) and Modeled (Green) Solution Volume Change over Time for FA2 with 1N NH + CH at Each Temperature (60, 70, and 80°C).

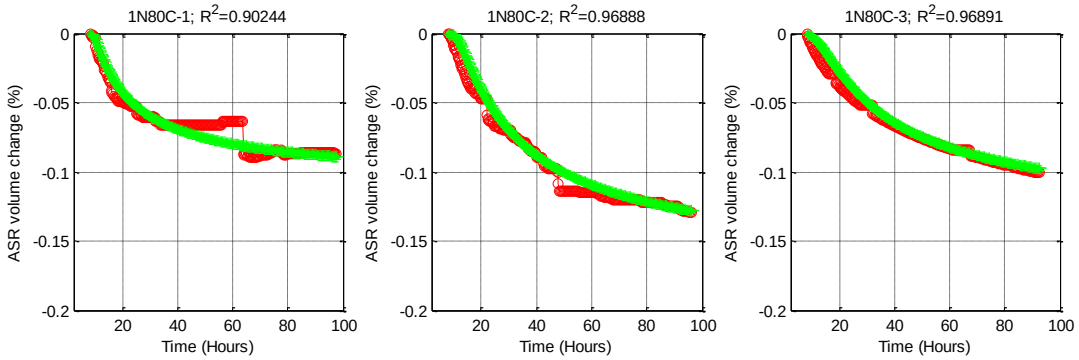

Figure B2-1 Continued.

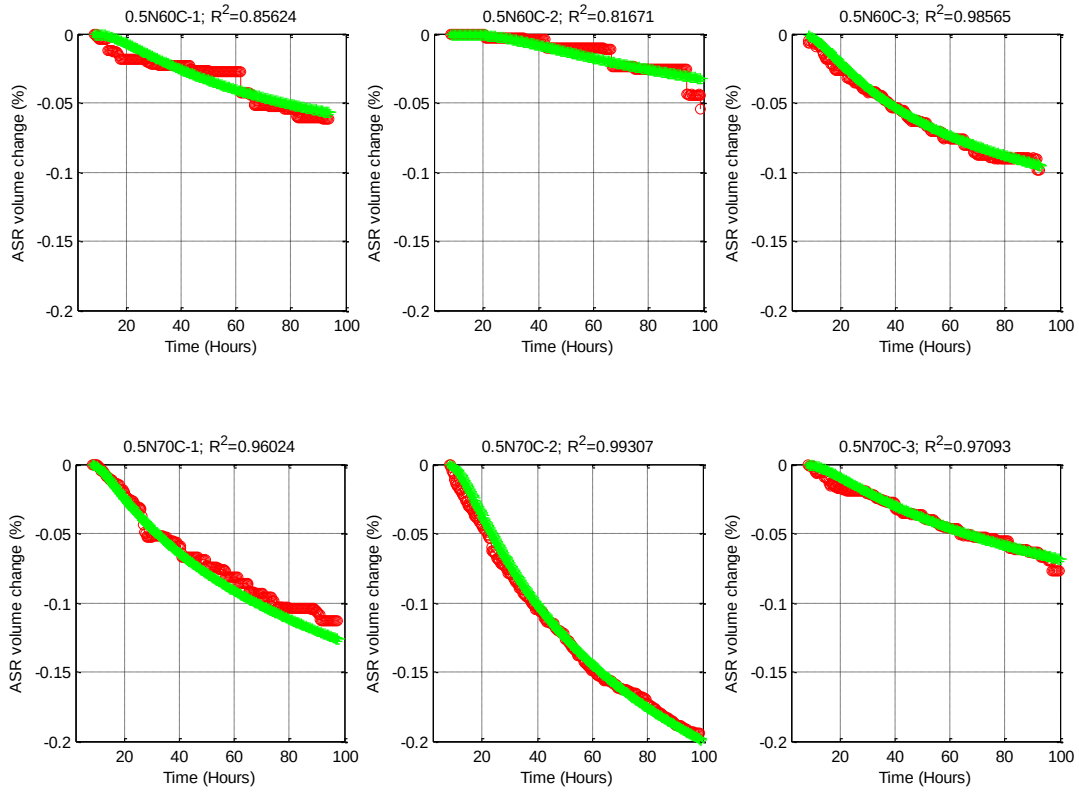

Figure B2-2 Repetition of Measured (Red) and Modeled (Green) Solution Volume Change over Time for FA2 with 0.5N NH + CH at Each Temperature (60, 70, and 80°C).

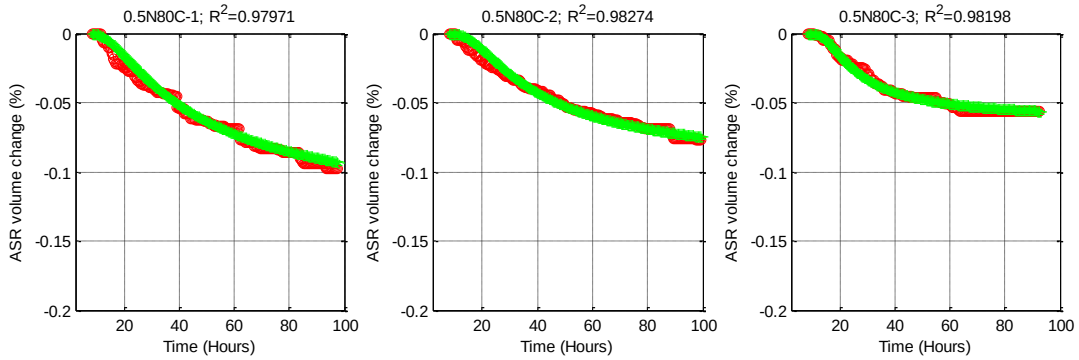

Figure B2-2 Continued.

Table B2 Calculated Rate Constant Based on the Modeled Curve (Green) in Figures B2-1 and B2-2 for FA2.

Normality	Temperature °C	β			Average	COV %
		Test 1	Test 2	Test 3		
1	60	0.3967	0.3703	0.4453	0.4041	9.41
	70	0.4331	0.4343	0.3975	0.4216	4.96
	80	0.7058	0.7888	0.6497	0.7148	9.79
0.5	60	0.4827	0.5525	0.5287	0.5213	6.81
	70	0.4067	0.3742	0.3418	0.3742	8.67
	80	1.0449	0.9979	1.1317	1.0582	6.41

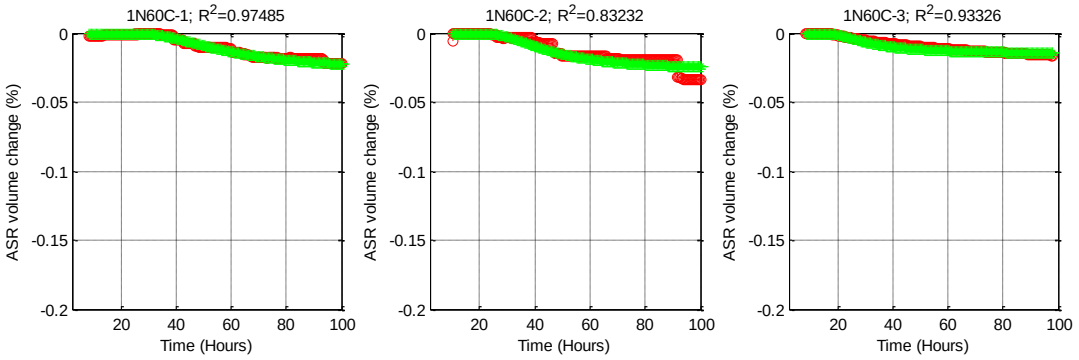

Figure B3-1 Repetition of Measured (Red) and Modeled (Green) Solution Volume Change over Time for FA3 with 1N NH + CH at Each Temperature (60, 70, and 80°C).

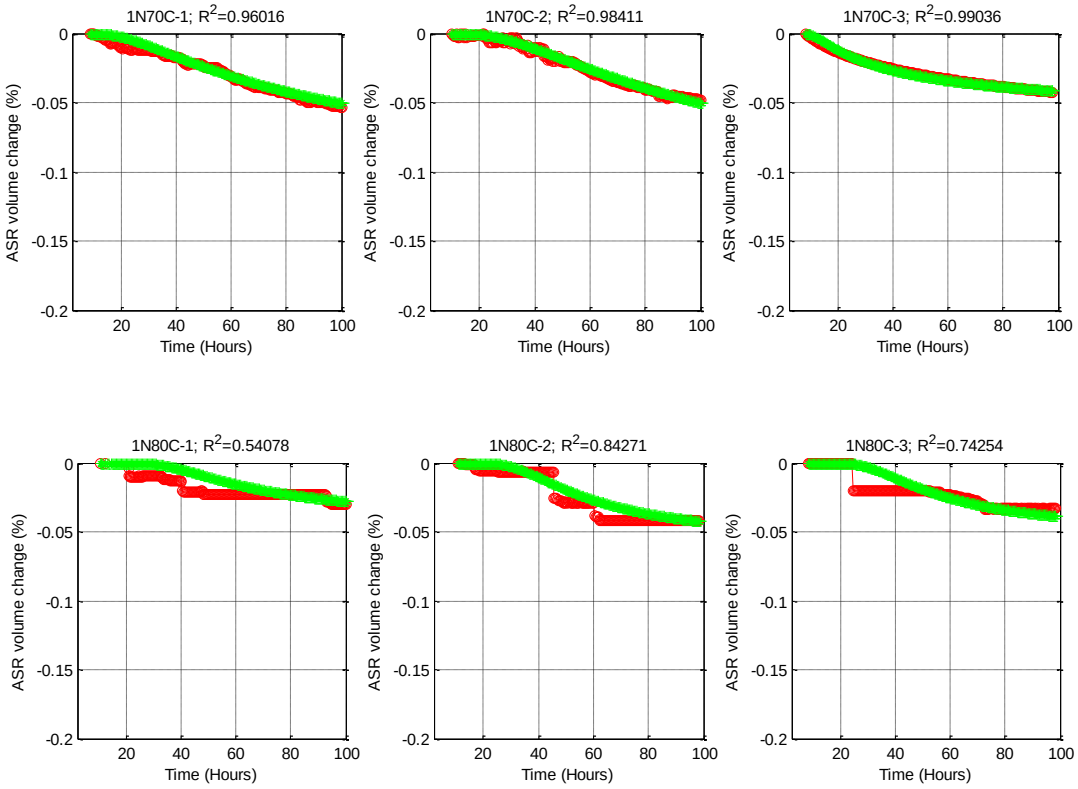

Figure B3-1 Continued.

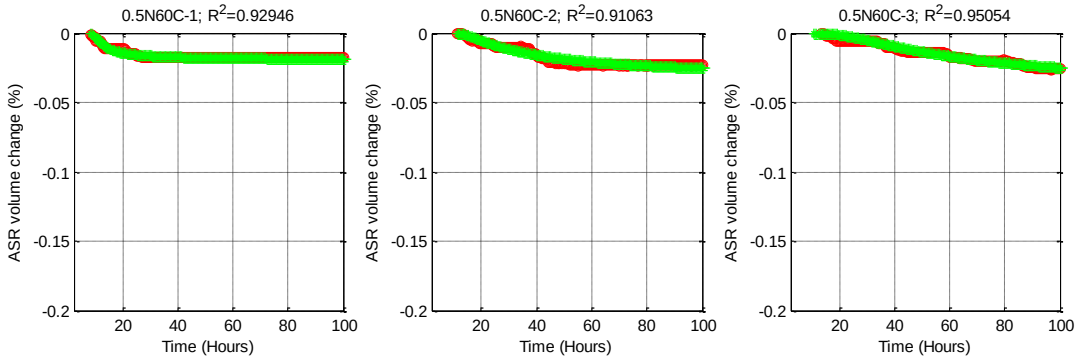

Figure B3-2 Repetition of Measured (Red) and Modeled (Green) Solution Volume Change over Time for FA3 with 0.5N NH + CH at Each Temperature (60, 70, and 80ºC).

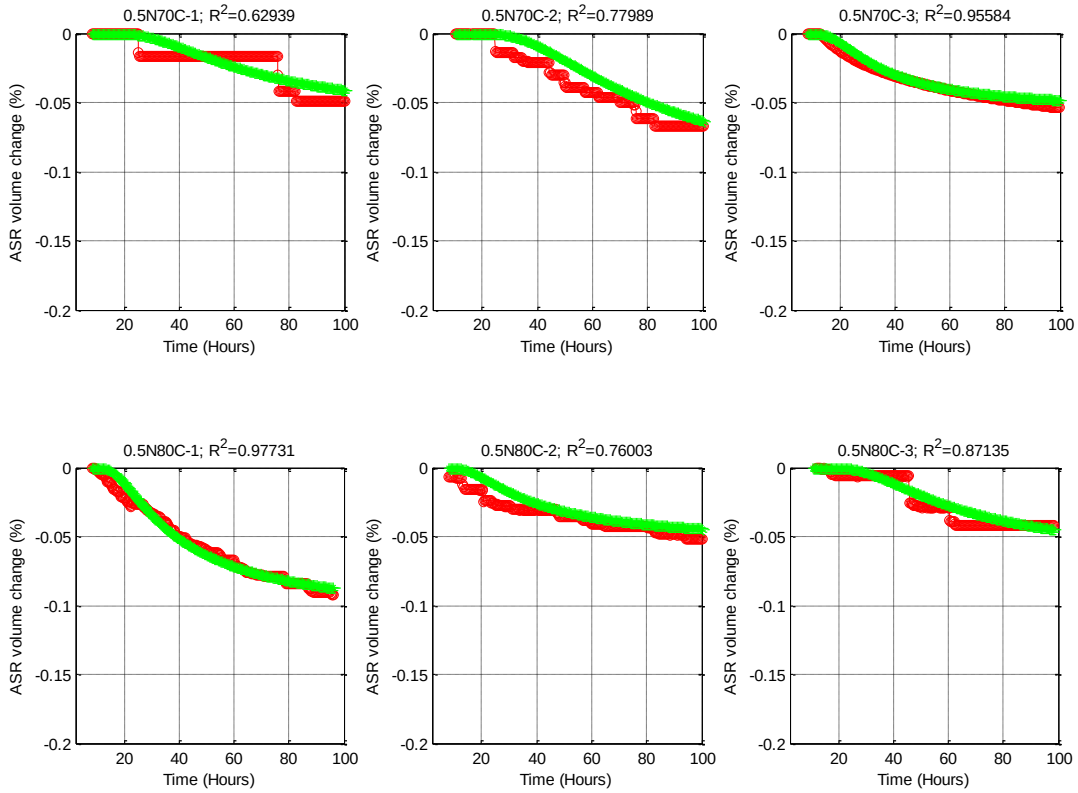

Figure B3-2 Continued.

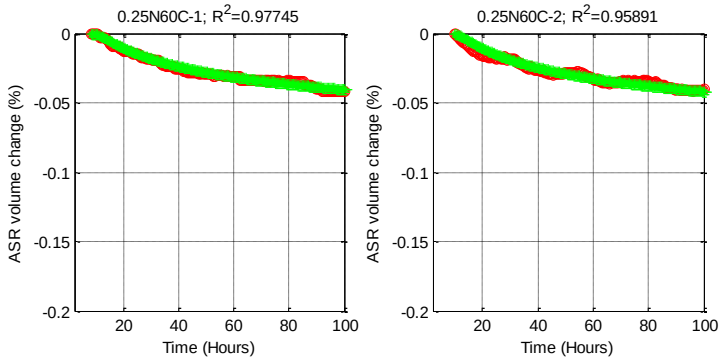

Figure B3-3 Repetition of Measured (Red) and Modeled (Green) Solution Volume Change over Time for FA3 with 0.25N NH + CH at 60°C.

Table B3 Calculated Rate Constant Based on the Modeled Curve (Green) in Figures B3-1 to B3-3 for FA3.

Normality	Temperature °C	β			Average	COV %
		Test 1	Test 2	Test 3		
1	60	2.3667	2.3405	2.2128	2.3067	3.57
	70	0.6553	0.6243	0.5530	0.6109	8.59
	80	2.0763	1.8154	1.8116	1.9011	7.98
0.5	60	0.9568	0.8001	0.8658	0.8742	9.00
	70	1.6858	1.5363	1.5995	1.6072	4.67
	80	1.2058	1.2911	1.3948	1.2972	7.30
0.25	60	0.4695	0.4703	-	0.4699	0.12

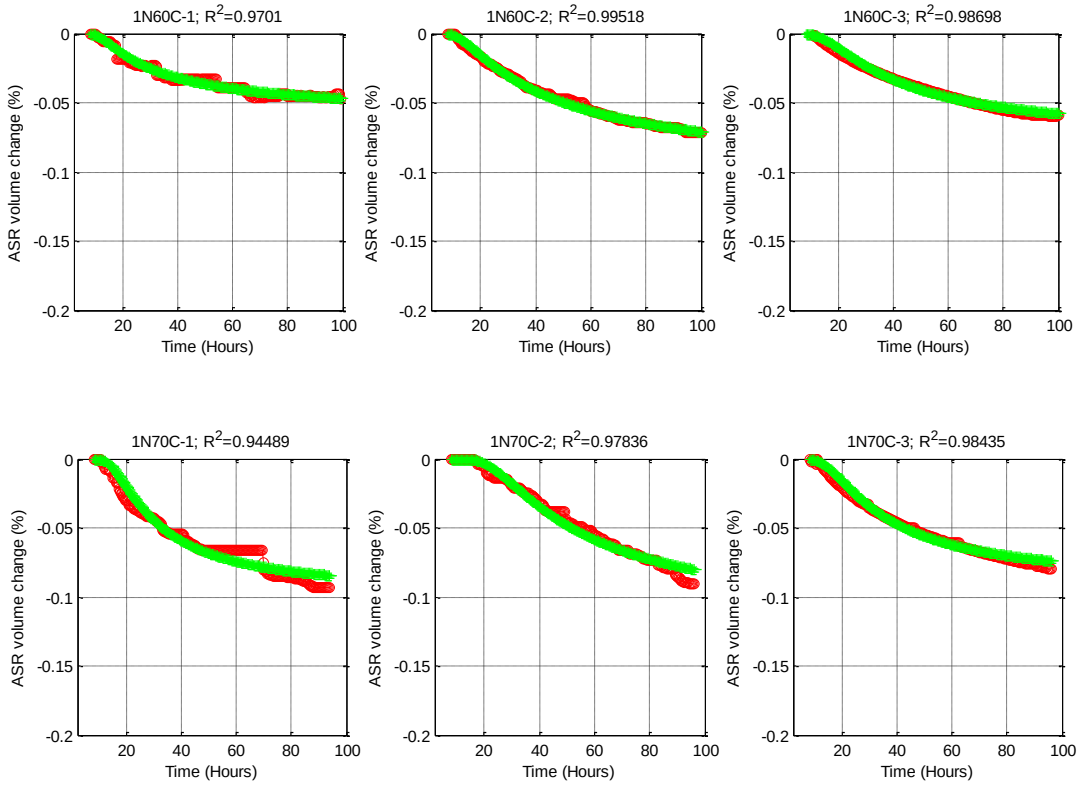

Figure B4-1 Repetition of Measured (Red) and Modeled (Green) Solution Volume Change over Time for FA4 with 1N NH + CH at Each Temperature (60, 70, and 80°C).

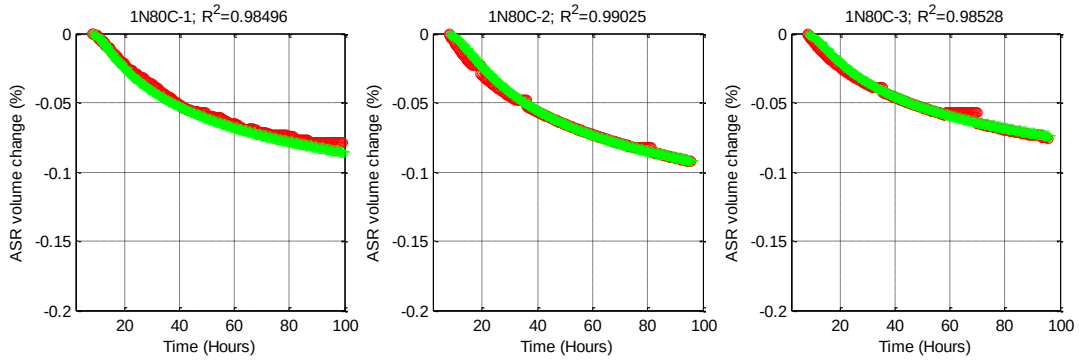

Figure B4-1 Continued.

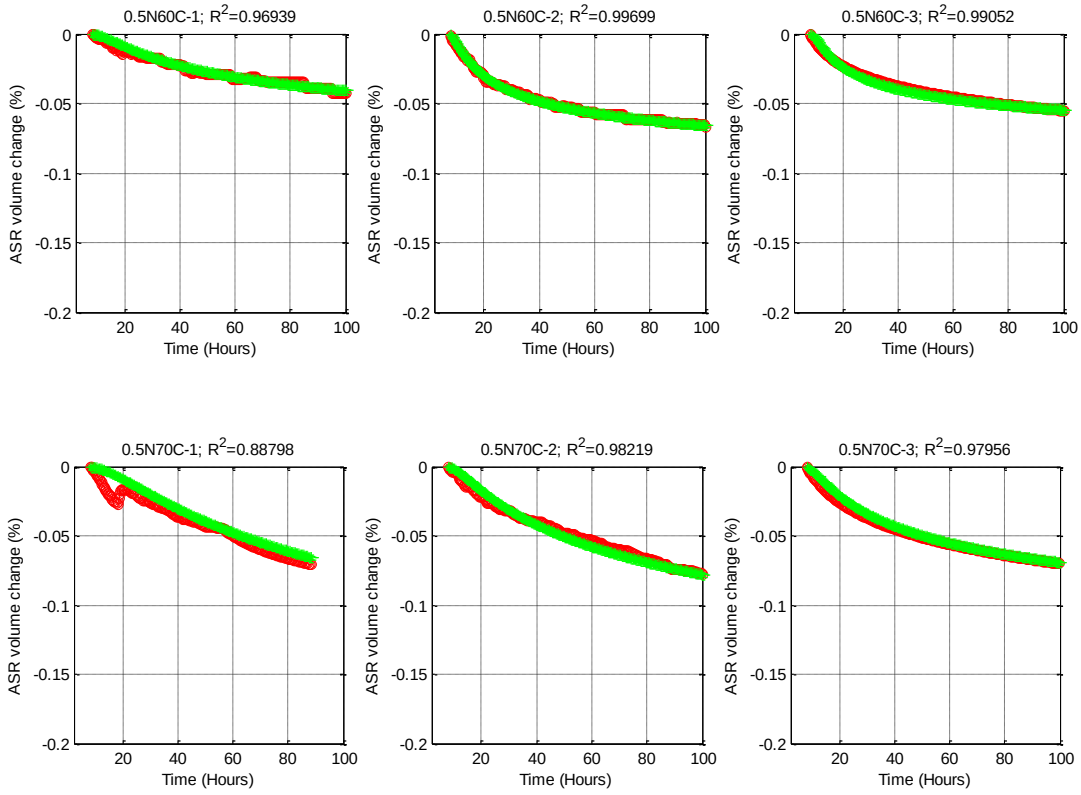

Figure B4-2 Repetition of Measured (Red) and Modeled (Green) Solution Volume Change over Time for FA4 with 0.5N NH + CH at Each Temperature (60, 70, and 80ºC).

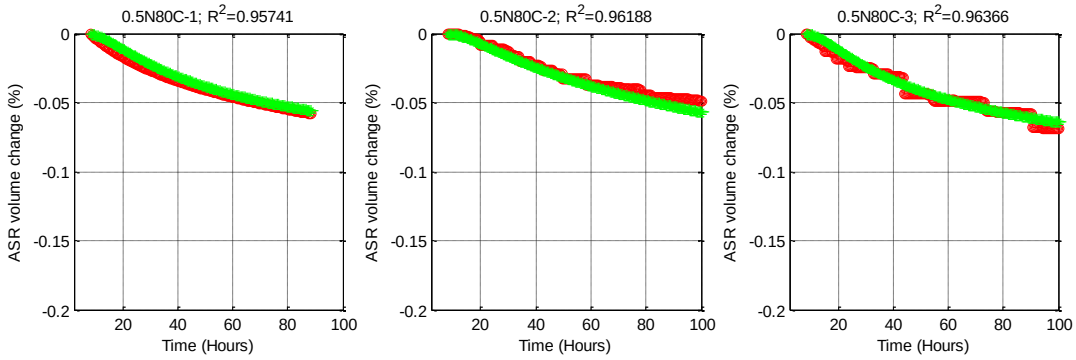

Figure B4-2 Continued.

Table B4 Calculated Rate Constant Based on the Modeled Curve (Green) in Figures B4-1 and B4-2 for FA4.

Normality	Temperature °C	β			Average	COV %
		Test 1	Test 2	Test 3		
1	60	1.0373	0.9809	1.1602	1.0595	8.65
	70	1.4079	1.2426	1.4394	1.3633	7.75
	80	0.4127	0.4131	0.4001	0.4086	1.81
0.5	60	0.4378	0.4961	0.4840	0.4726	6.51
	70	0.3211	0.3507	0..3971	0.3563	10.75
	80	0.5183	0.5628	0.4991	0.5267	6.20

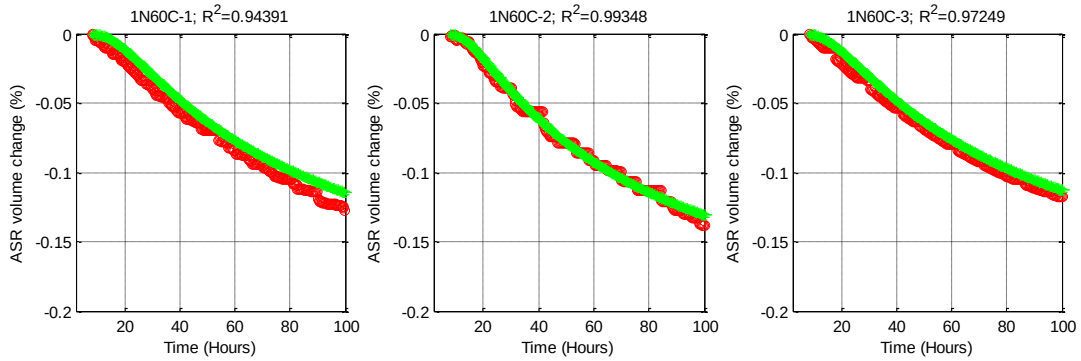

Figure B5-1 Repetition of Measured (Red) and Modeled (Green) Solution Volume Change over Time for FA5 with 1N NH + CH at Each Temperature (60, 70, and 80°C).

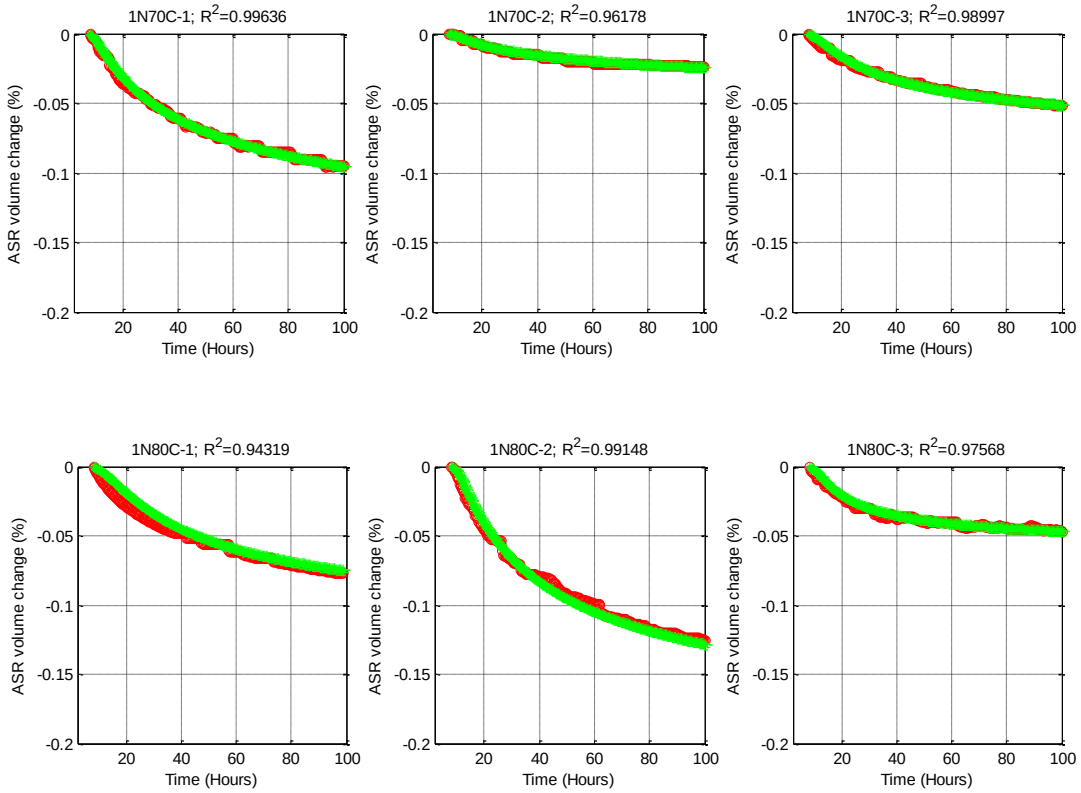

Figure B5-1 Continued.

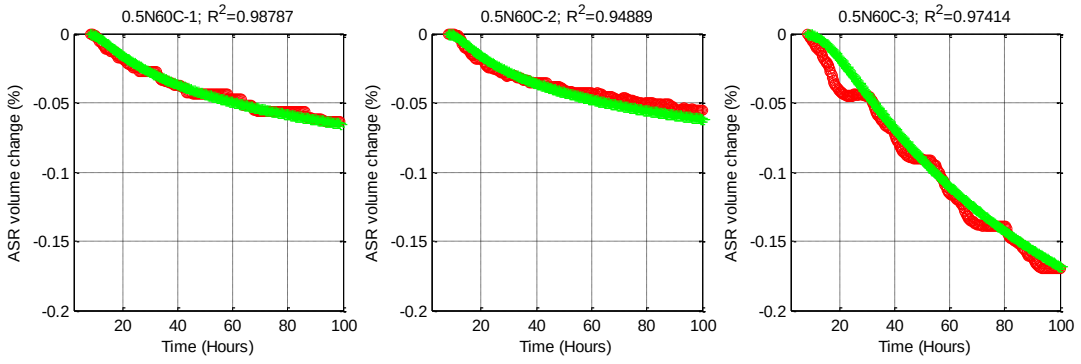

Figure B5-2 Repetition of Measured (Red) and Modeled (Green) Solution Volume Change over Time for FA5 with 0.5N NH + CH at Each Temperature (60, 70, and 80°C).

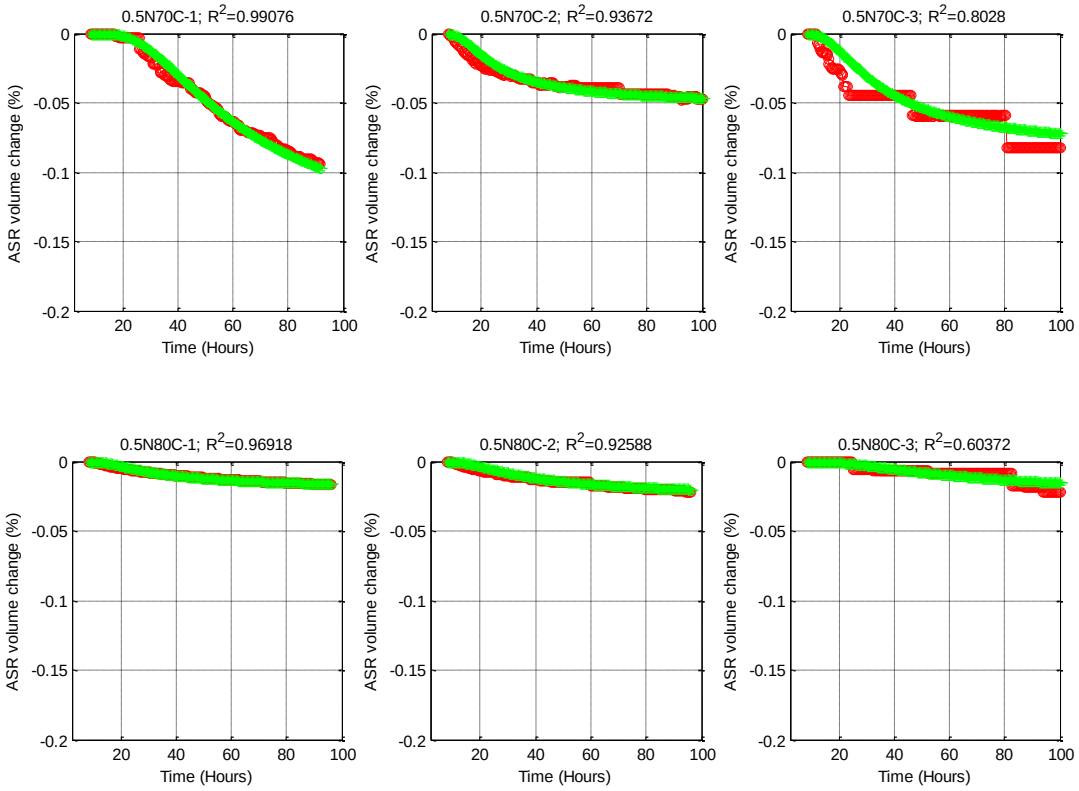

Figure B5-2 Continued.

Table B5 Calculated Rate Constant Based on the Modeled Curve (Green) in Figures B5-1 and B5-2 for FA5.

Normality	Temperature °C	β			Average	COV %
		Test 1	Test 2	Test 3		
1	60	0.5897	0.6514	0.5557	0.5989	8.10
	70	0.4869	0.4287	0.4829	0.4662	6.97
	80	0.5458	0.5448	0.6434	0.5780	9.80
0.5	60	0.4388	0.4589	0.3911	0.4296	8.11
	70	1.4461	1.2625	1.5160	1.4082	9.30
	80	1.0655	1.0419	1.1912	1.0995	7.30

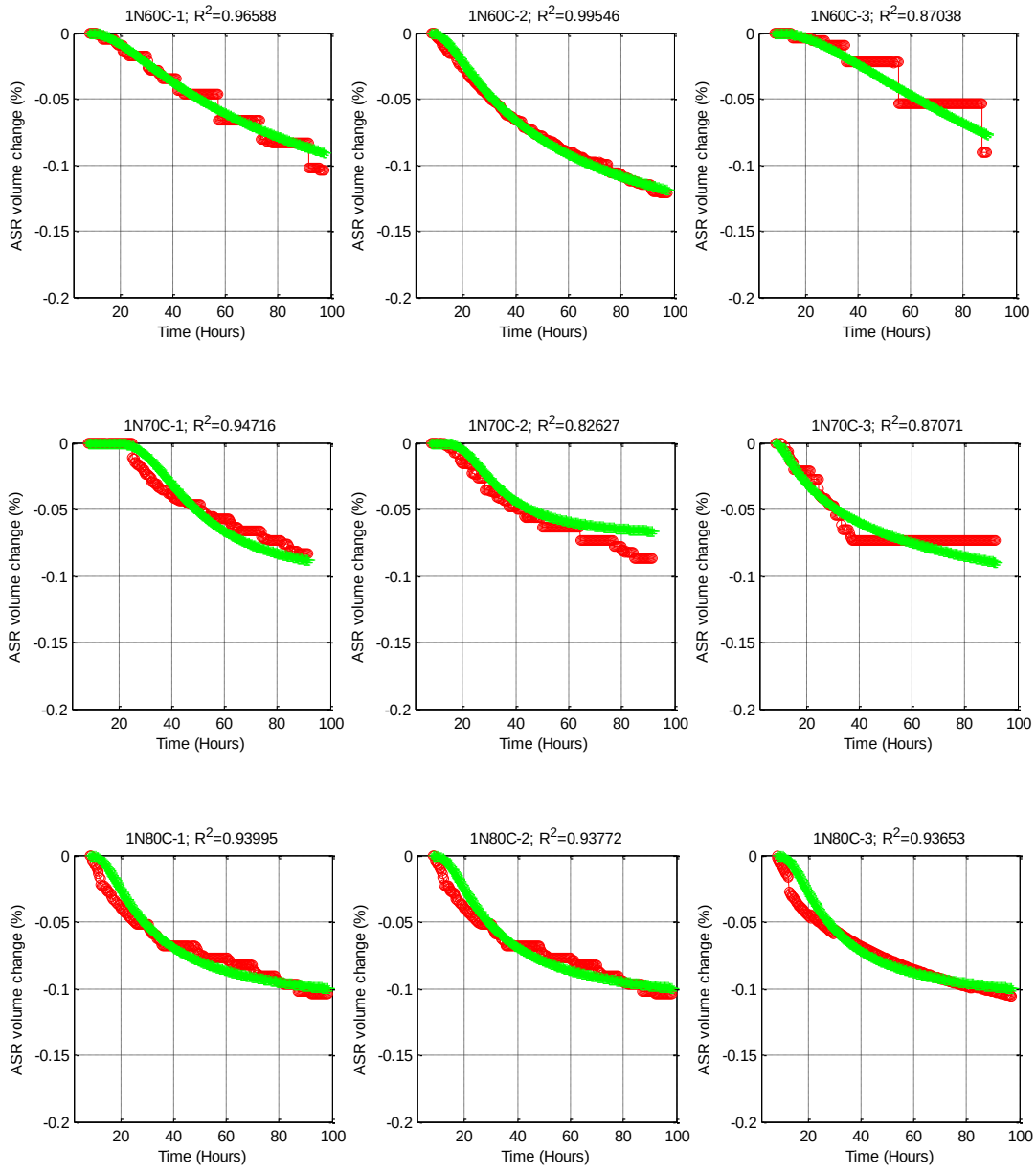

Figure B6-1 Repetition of Measured (Red) and Modeled (Green) Solution Volume Change over Time for CA1 with 1N NH + CH at Each Temperature (60, 70, and 80°C).

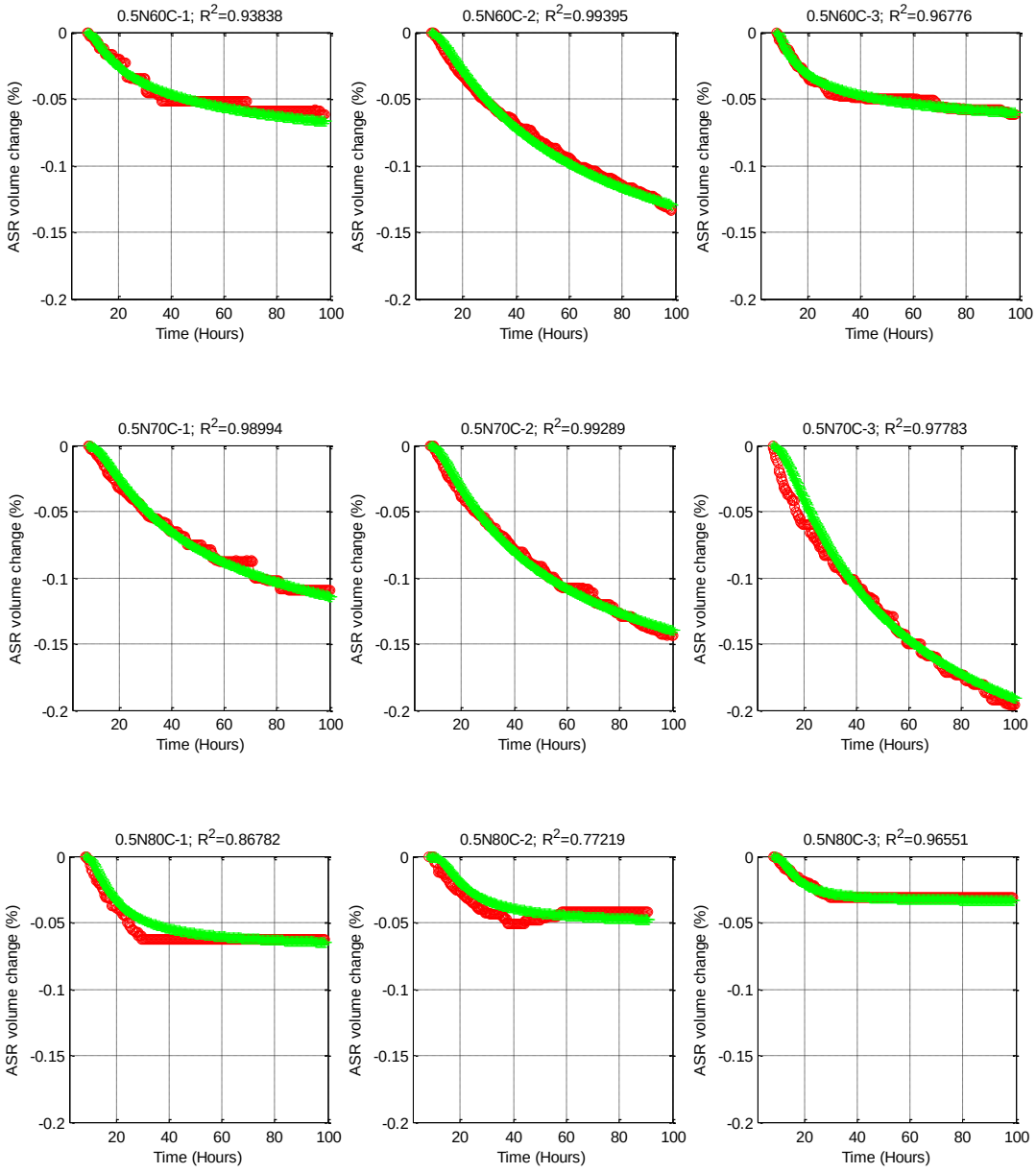

Figure B6-2 Repetition of Measured (Red) and Modeled (Green) Solution Volume Change over Time for CA1 with 0.5N NH + CH at Each Temperature (60, 70, and 80^{o}C).

Table B6 Calculated Rate Constant Based on the Modeled Curve (Green) in Figures B6-1 and B6-2 for CA1.

Normality	Temperature °C	β			Average	COV %
		Test 1	Test 2	Test 3		
1	60	0.6944	0.7421	0.7189	0.7185	3.32
	70	2.2579	2.4291	1.8542	2.1804	13.54
	80	1.0957	1.1256	1.1239	1.1151	1.51
0.5	60	0.5092	0.4898	0.4963	0.4984	1.98
	70	0.5640	0.6029	0.5015	0.5561	9.20
	80	1.3119	1.6959	1.5701	1.5260	12.83

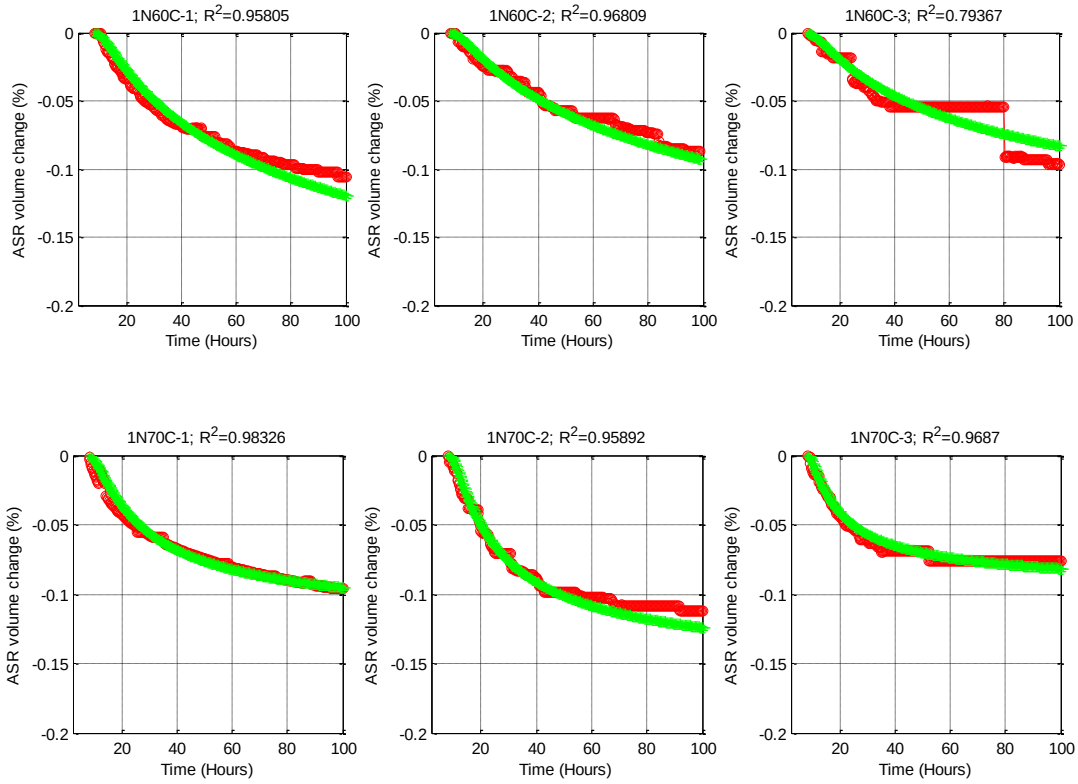

Figure B7-1 Repetition of Measured (Red) and Modeled (Green) Solution Volume Change over Time for CA2 with 1N NH + CH at Each Temperature (60, 70, and 80°C).

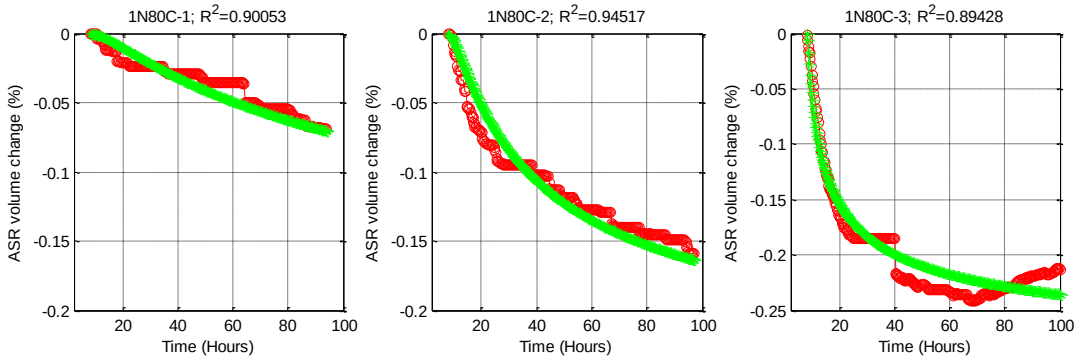

Figure B7-1 Continued.

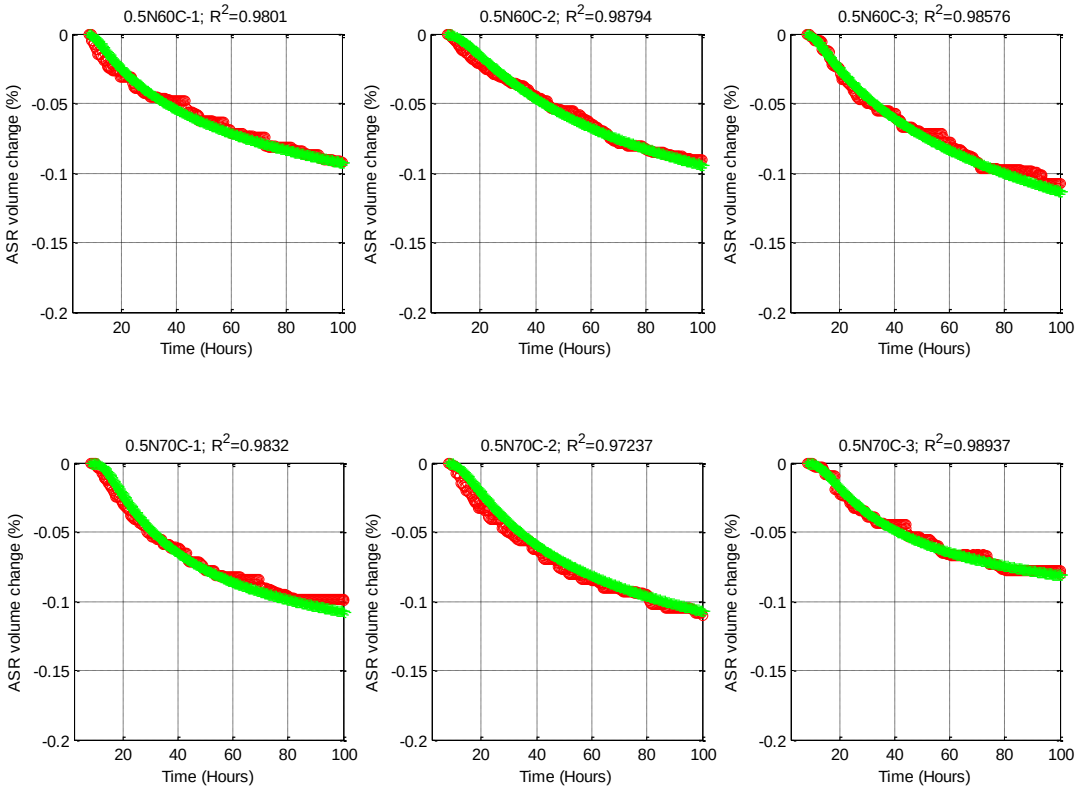

Figure B7-2 Repetition of Measured (Red) and Modeled (Green) Solution Volume Change over Time for CA2 with 0.5N NH + CH at Each Temperature (60, 70, and 80ºC).

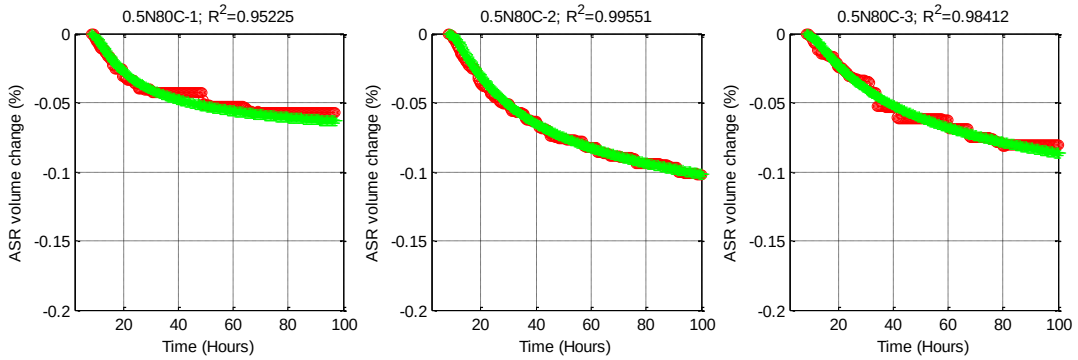

Figure B7-2 Continued.

Table B7 Calculated Rate Constant Based on the Modeled Curve (Green) in Figures B7-1 and B7-2 for CA2.

Normality	Temperature °C	β			Average	COV %
		Test 1	Test 2	Test 3		
1	60	0.4320	0.4047	0.3883	0.4083	5.41
	70	0.6528	0.7064	0.7712	0.7101	8.35
	80	0.4414	0.4457	0.4496	0.4456	0.92
0.5	60	0.4263	0.4097	0.3738	0.4033	6.65
	70	0.7733	0.6349	0.7348	0.7143	10.00
	80	0.5728	0.5457	0.5683	0.5623	2.58

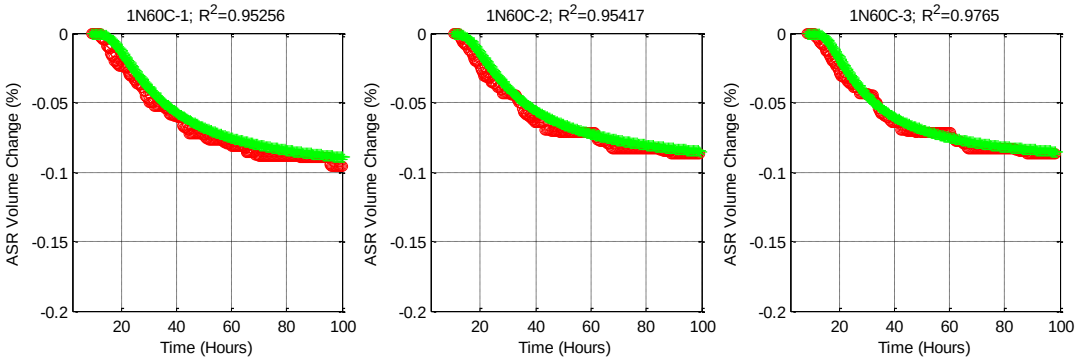

Figure B8-1 Repetition of Measured (Red) and Modeled (Green) Solution Volume Change over Time for CA3 with 1N NH + CH at Each Temperature (60, 70, and 80°C).

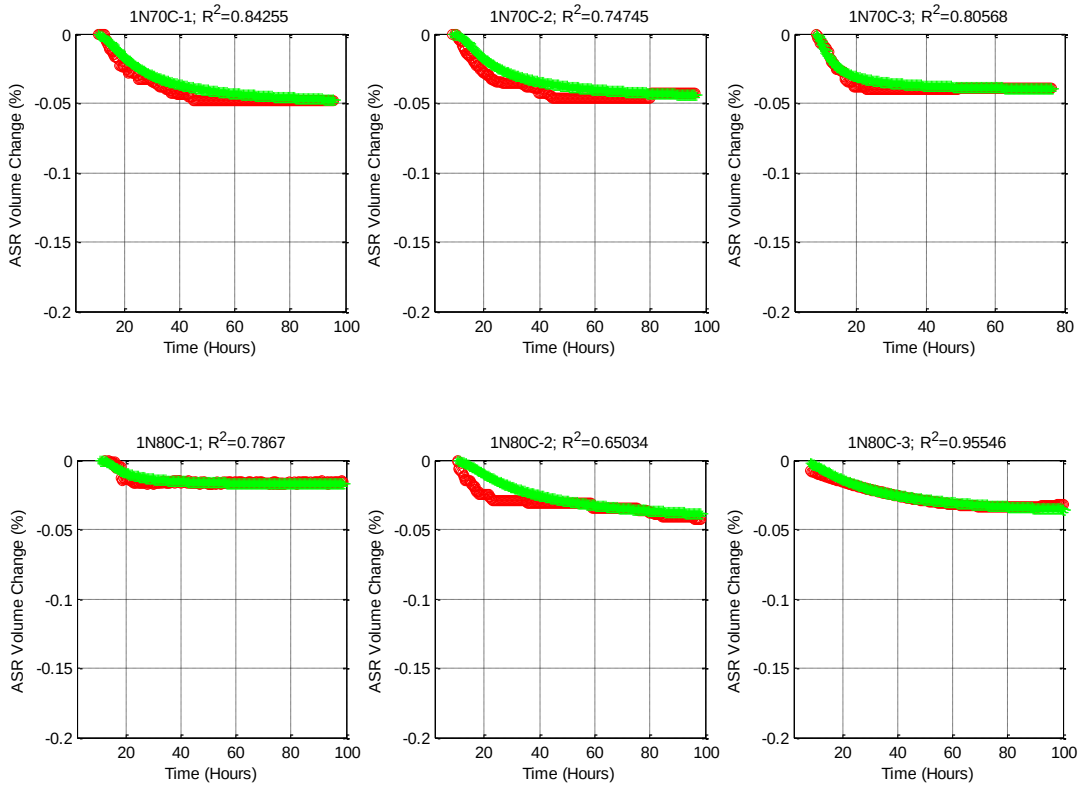

Figure B8-1 Continued.

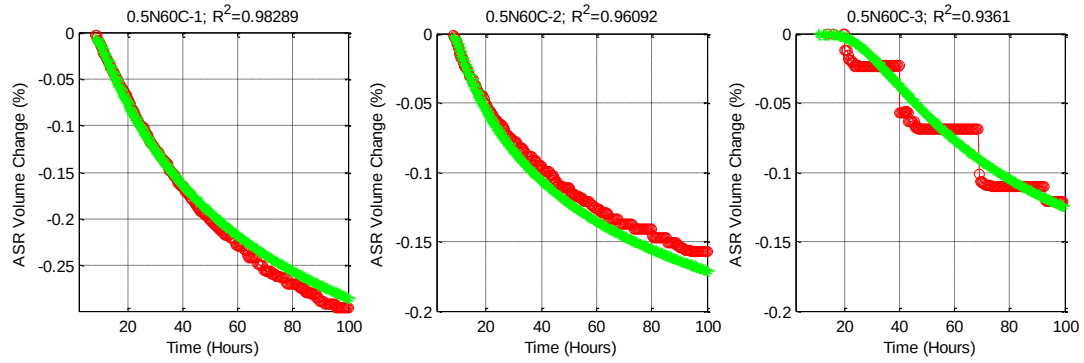

Figure B8-2 Repetition of Measured (Red) and Modeled (Green) Solution Volume Change over Time for CA3 with 0.5N NH + CH at Each Temperature (60, 70, and 80°C).

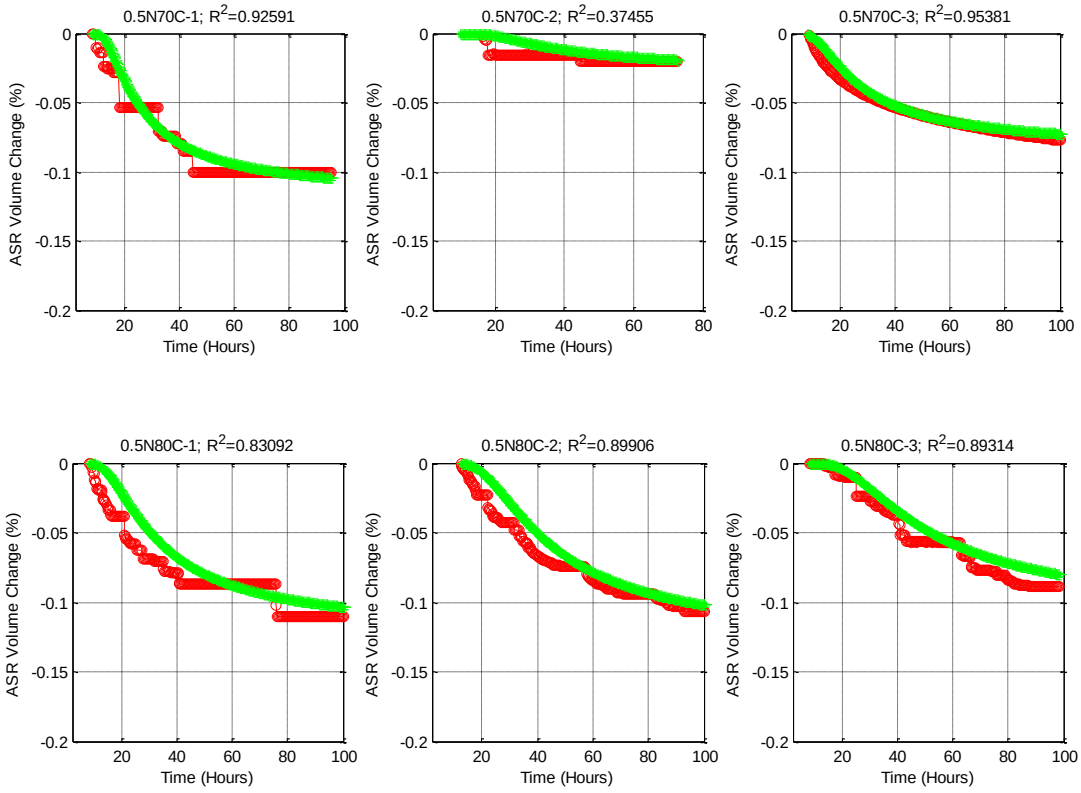

Figure B8-2 Continued.

Table B8 Calculated Rate Constant Based on the Modeled Curve (Green) in Figures B8-1 and B8-2 for CA3.

Normality	Temperature °C	β			Average	COV %
		Test 1	Test 2	Test 3		
1	60	1.3907	1.2561	1.4342	1.3603	6.83
	70	1.5180	1.3416	1.3226	1.3941	7.73
	80	0.9583	0.8650	1.0517	0.9583	9.74
0.5	60	0.2020	0.2540	0.2437	0.2332	11.81
	70	1.2116	1.1167	1.3263	1.2182	8.62
	80	1.3043	1.2332	1.4871	1.3415	9.76

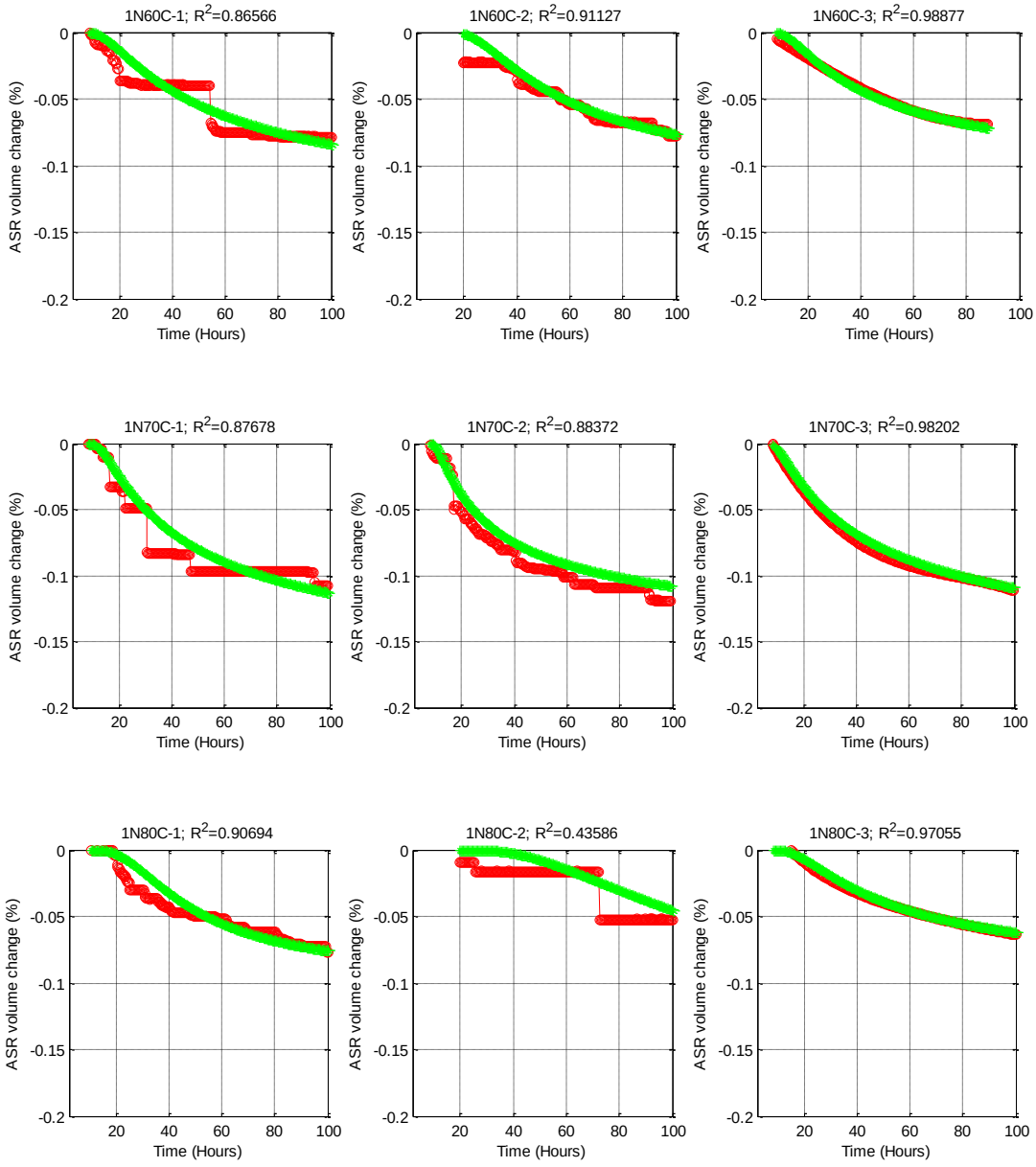

Figure B9-1 Repetition of Measured (Red) and Modeled (Green) Solution Volume Change over Time for CA4 with 1N NH + CH at Each Temperature (60, 70, and 80°C).

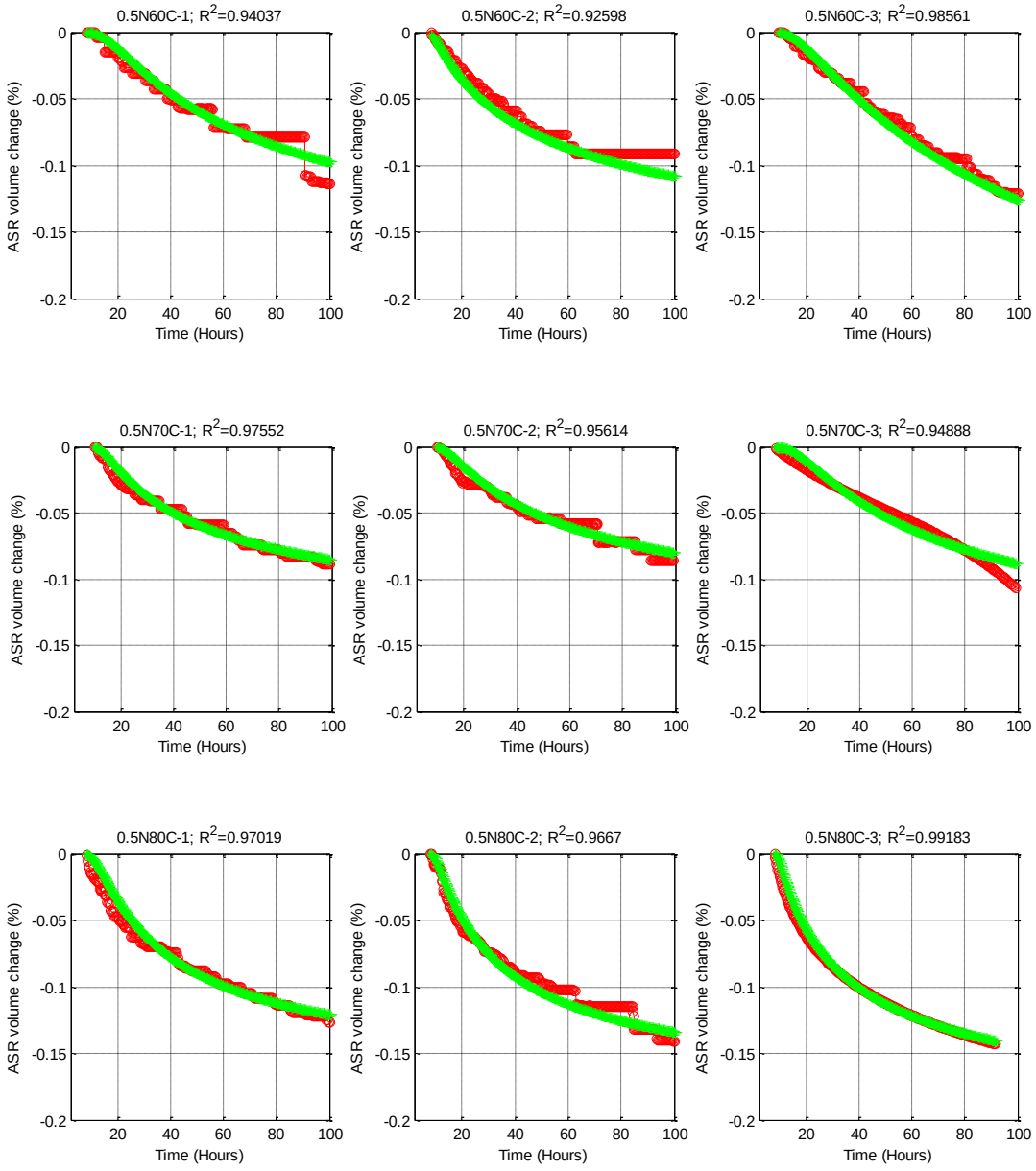

Figure B9-2 Repetition of Measured (Red) and Modeled (Green) Solution Volume Change over Time for CA4 with 0.5N NH + CH at Each Temperature (60, 70, and 80°C).

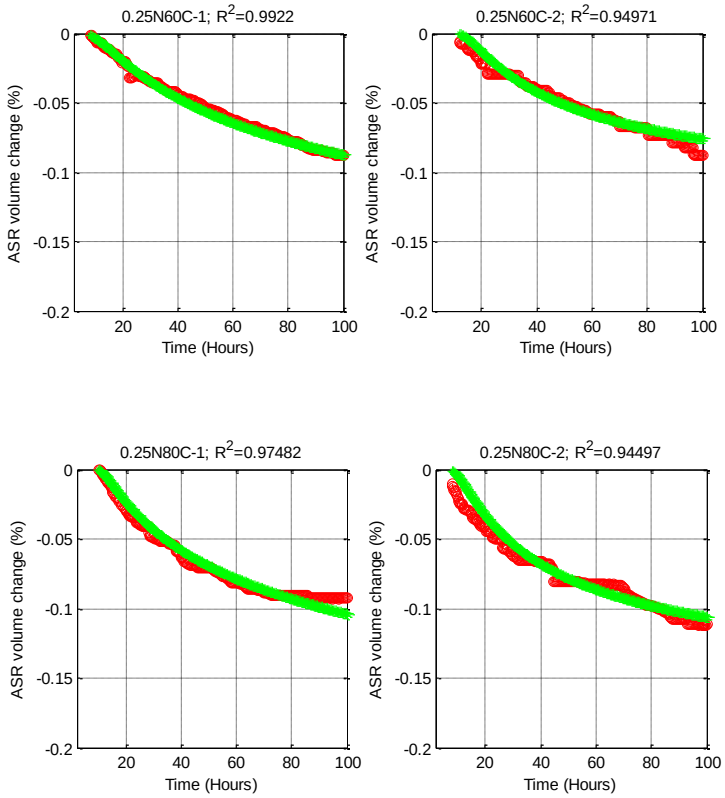

Figure B9-3 Repetition of Measured (Red) and Modeled (Green) Solution Volume Change over Time for CA4 with 0.25N NH + CH at 60 and 80ºC.

Table B9 Calculated Rate Constant Based on the Modeled Curve (Green) in Figures B9-1 to B9-3 for CA4.

Normality	Temperature ºC	β			Average	COV %
		Test 1	Test 2	Test 3		
1	60	0.5758	0.5712	0.4889	0.5453	8.97
	70	0.6668	0.5908	0.5489	0.6022	9.93
	80	0.9143	0.9145	0.8938	0.9075	1.31
0.5	60	0.3613	0.4297	0.4019	0.3976	8.65
	70	0.5806	0.5111	0.5299	0.5405	6.65
	80	0.5533	0.5601	0.4670	0.5268	9.85
0.25	60	0.3419	0.3217	-	0.3318	4.30
	80	0.4717	0.4500	-	0.4609	3.33

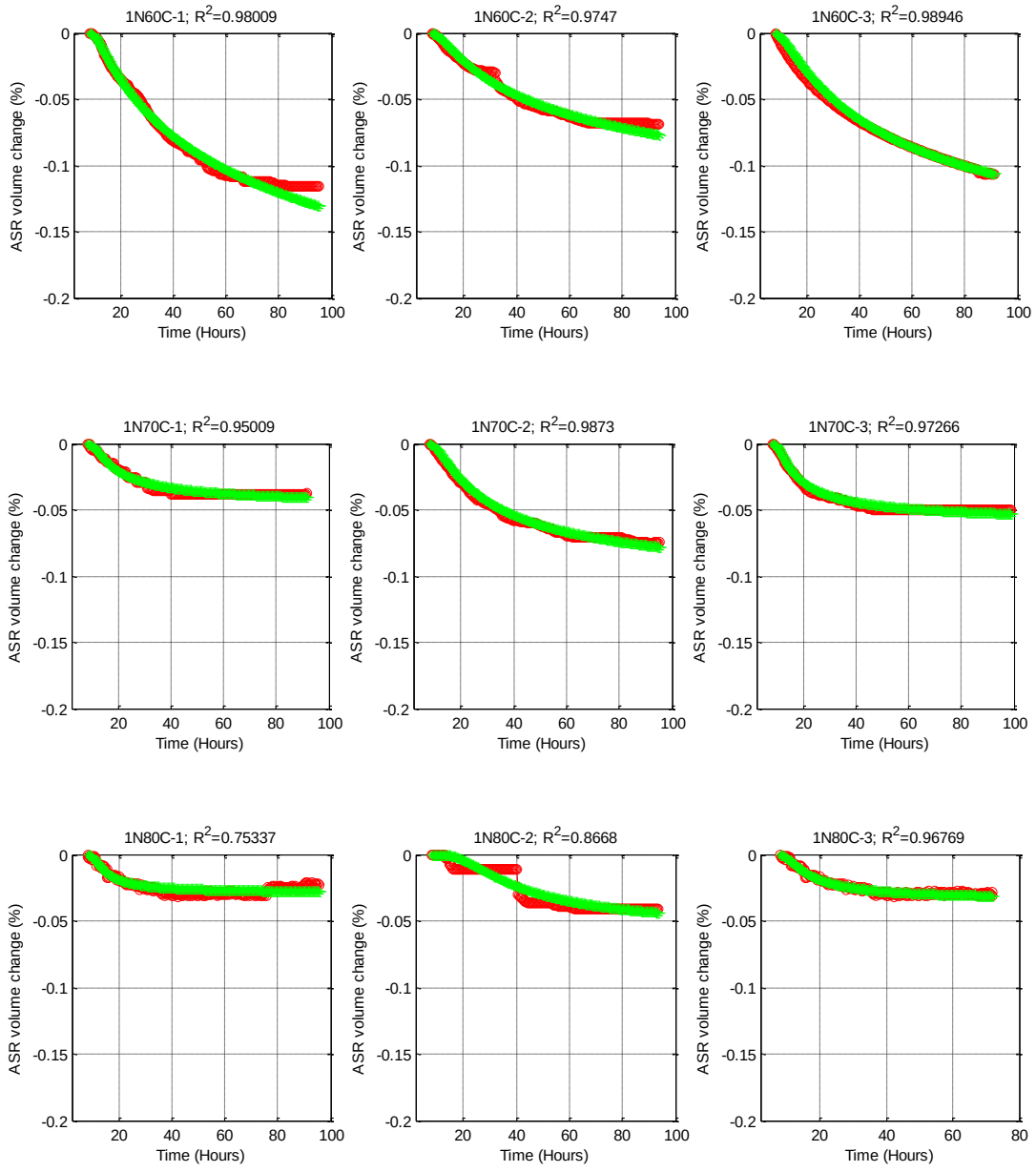

Figure B10-1 Repetition of Measured (Red) and Modeled (Green) Solution Volume Change over Time for CA5 with 1N NH + CH at Each Temperature (60, 70, and 80°C).

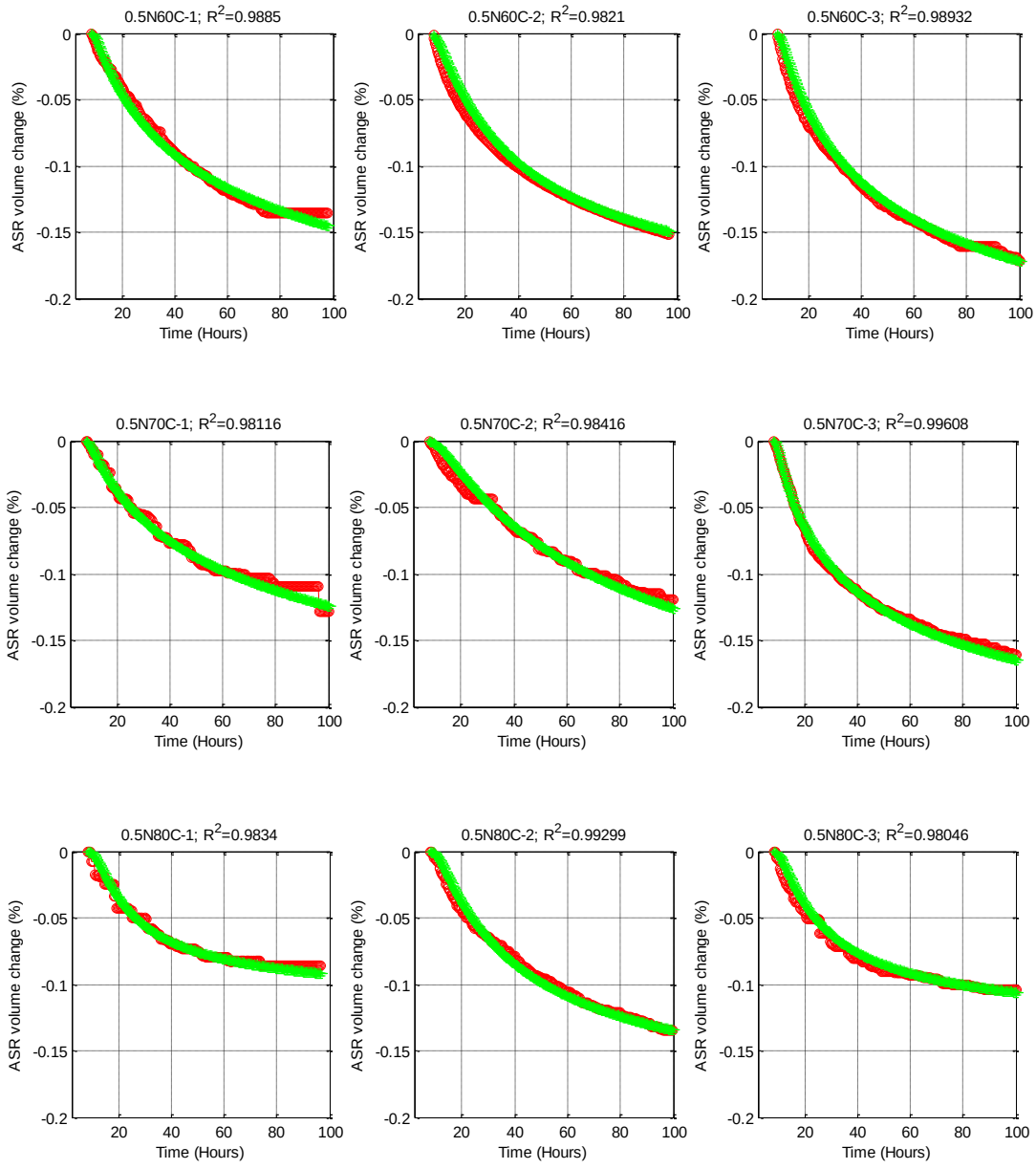

Figure B10-2 Repetition of Measured (Red) and Modeled (Green) Solution Volume Change over Time for CA5 with 0.5N NH + CH at Each Temperature (60, 70, and 80°C).

Table B10 Calculated Rate Constant Based on the Modeled Curve (Green) in Figures B10-1 and B10-2 for CA5.

Normality	Temperature °C	β			Average	COV %
		Test 1	Test 2	Test 3		
1	60	0.4100	0.4437	0.3827	0.4121	7.41
	70	0.8098	0.7052	0.8182	0.7777	8.09
	80	1.3975	1.2784	1.4792	1.3850	7.29
0.5	60	0.3739	0.4481	0.4009	0.4076	9.21
	70	0.3843	0.3372	0.4099	0.3771	9.78
	80	0.8449	0.7014	0.7346	0.7603	9.88

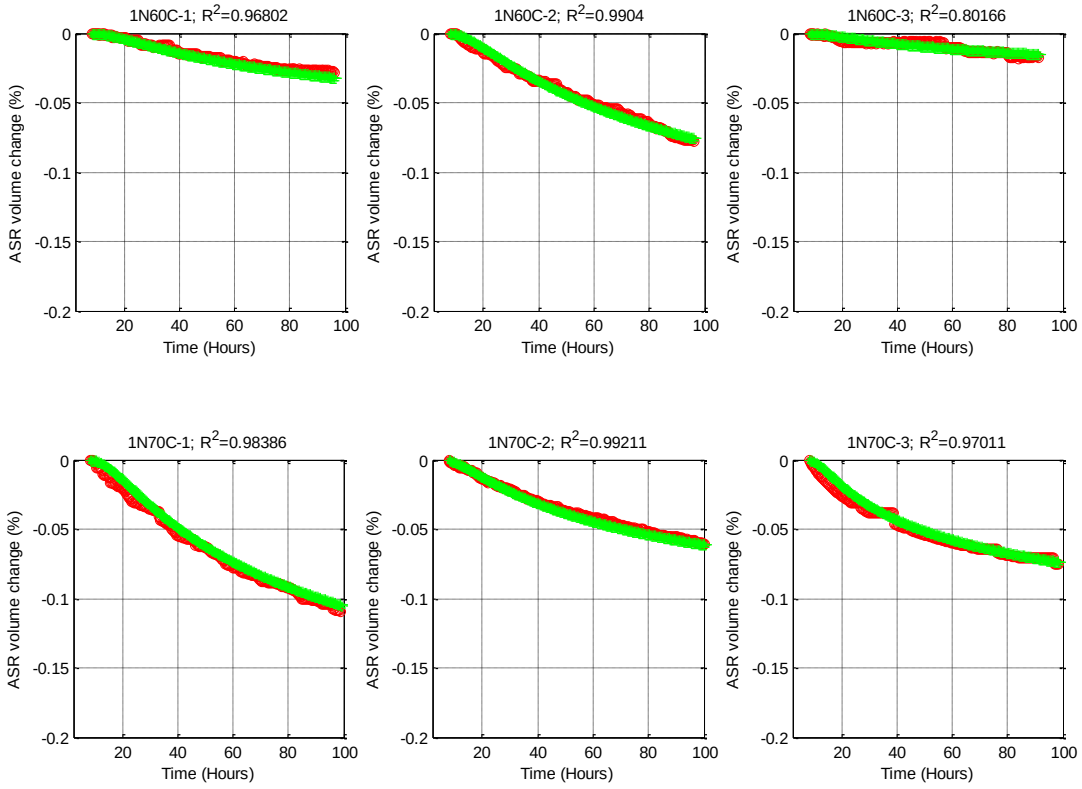

Figure B11-1 Repetition of Measured (Red) and Modeled (Green) Solution Volume Change over Time for CA6 with 1N NH + CH at Each Temperature (60, 70, and 80°C).

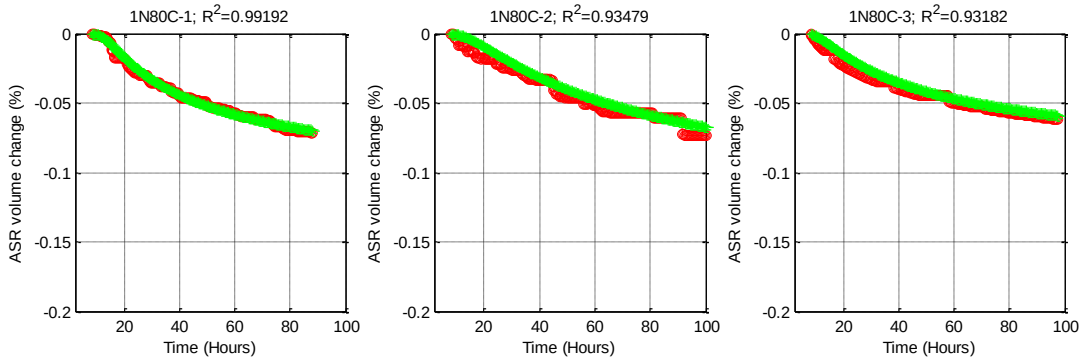

Figure B11-1 Continued.

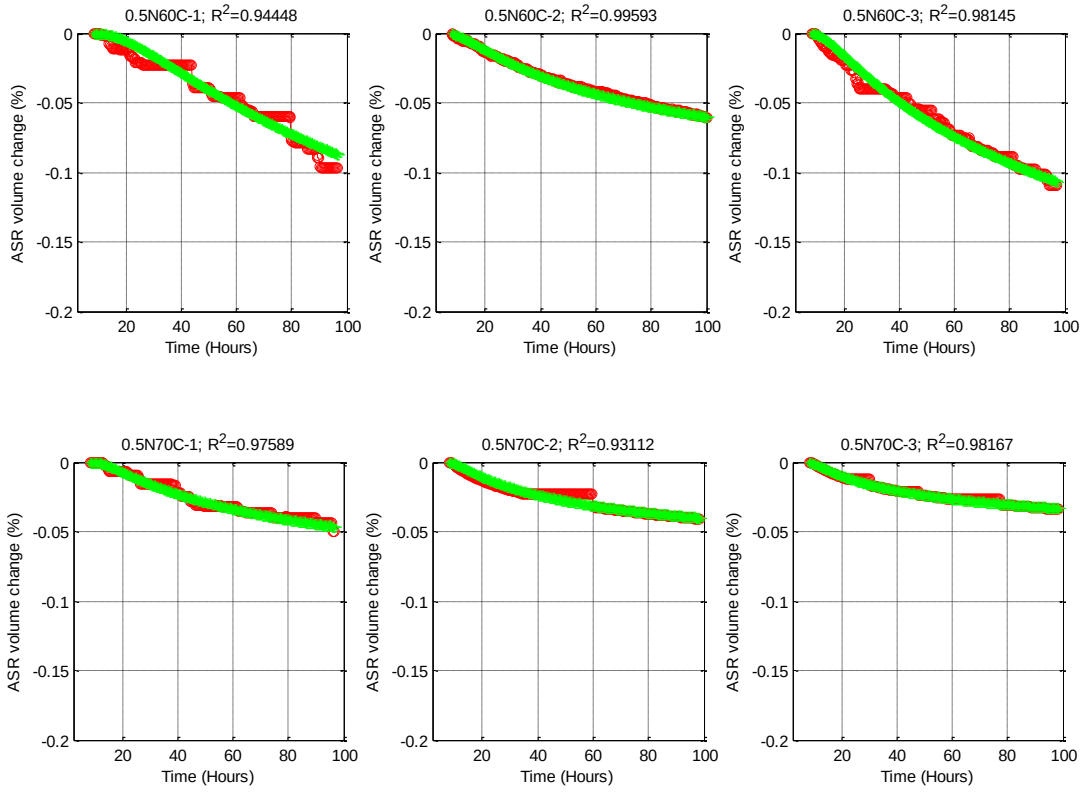

Figure B11-2 Repetition of Measured (Red) and Modeled (Green) Solution Volume Change over Time for CA6 with 0.5N NH + CH at Each Temperature (60, 70, and 80°C).

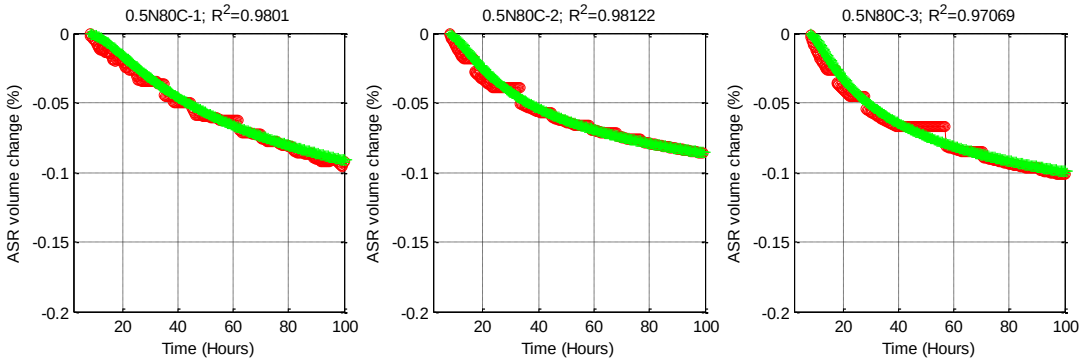

Figure B11-2 Continued.

Table B11 Calculated Rate Constant Based on the Modeled Curve (Green) in Figures B11-1 and B11-2 for CA6.

Normality	Temperature °C	β			Average	COV %
		Test 1	Test 2	Test 3		
1	60	0.5177	0.4456	0.4432	0.4688	9.03
	70	0.4384	0.4055	0.4434	0.4291	4.80
	80	0.6197	0.5263	0.5289	0.5583	9.53
0.5	60	0.3877	0.4122	0.4333	0.4111	5.55
	70	0.5034	0.4554	0.5092	0.4893	6.03
	80	0.3915	0.4302	0.4192	0.4136	4.82

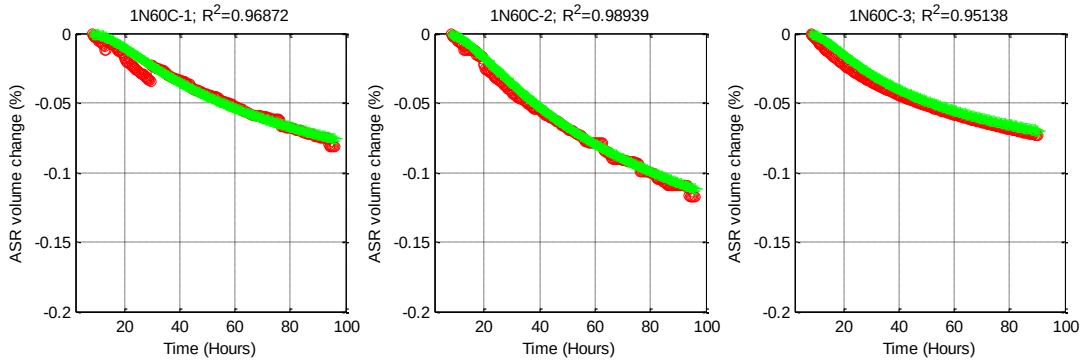

Figure B12-1 Repetition of Measured (Red) and Modeled (Green) Solution Volume Change over Time for CA7 with 1N NH + CH at Each Temperature (60, 70, and 80°C).

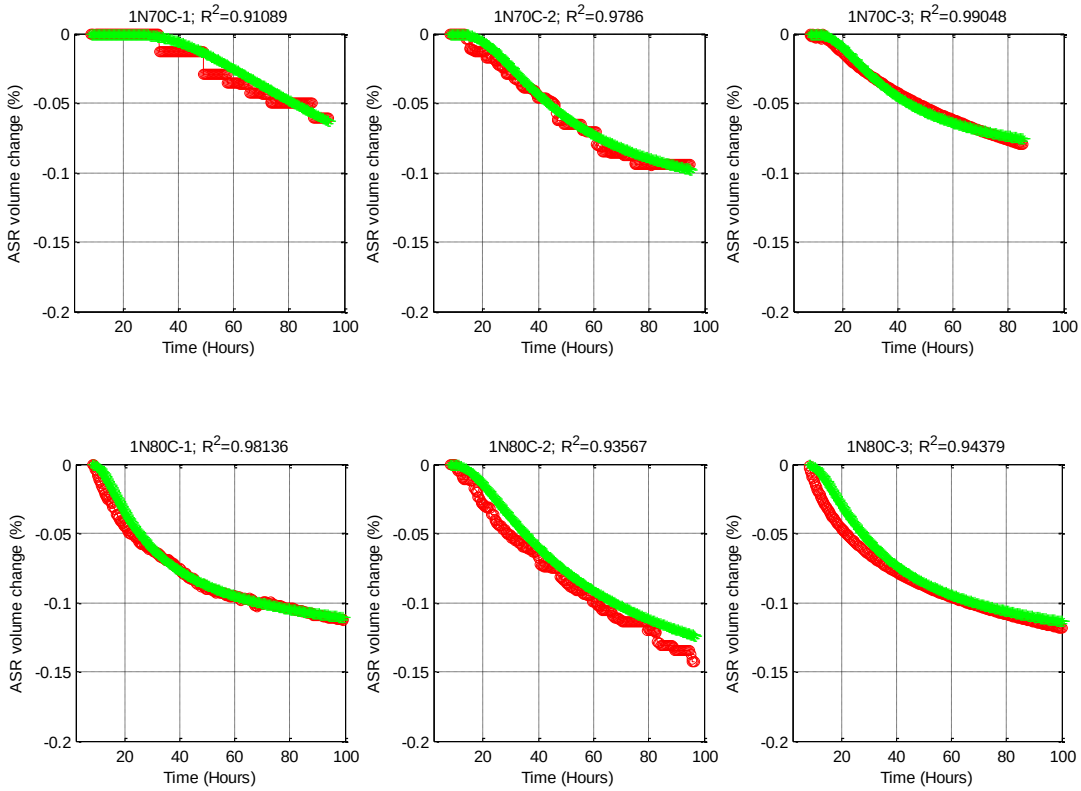

Figure B12-1 Continued.

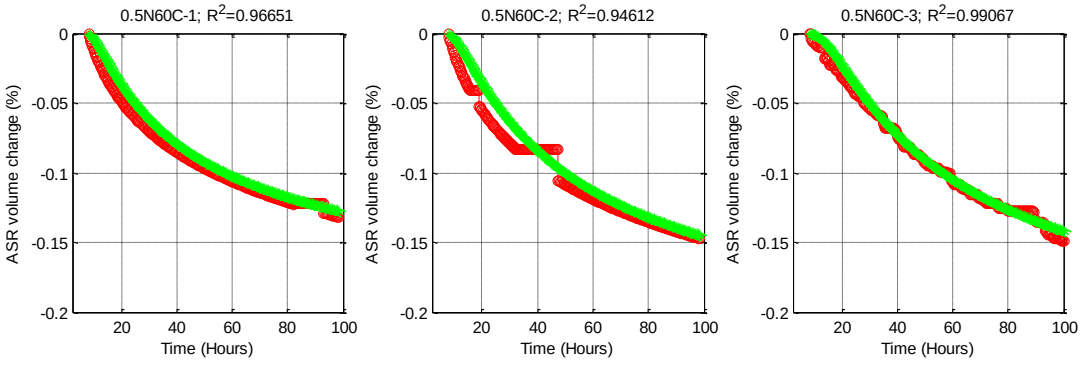

Figure B12-2 Repetition of Measured (Red) and Modeled (Green) Solution Volume Change over Time for CA7 with 0.5N NH + CH at Each Temperature (60, 70, and 80ºC).

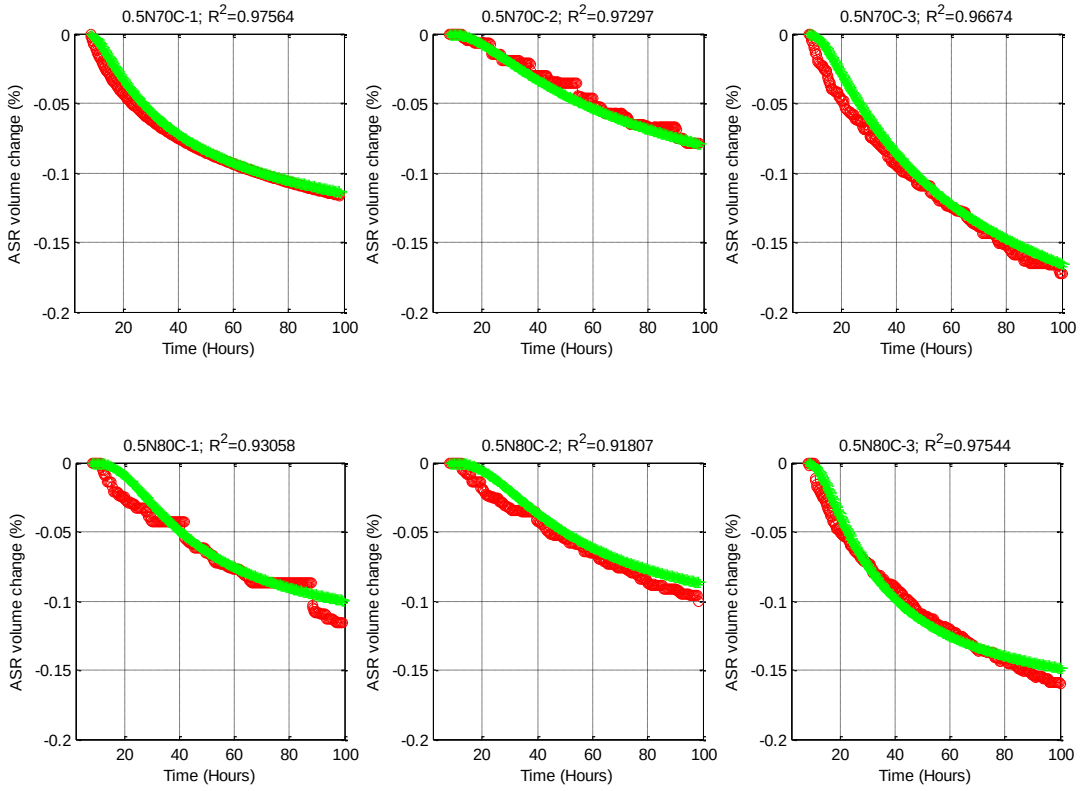

Figure B12-2 Continued.

Table B12 Calculated Rate Constant Based on the Modeled Curve (Green) in Figures B12-1 and B12-2 for CA7.

Normality	Temperature °C	β			Average	COV %
		Test 1	Test 2	Test 3		
1	60	0.4780	0.4678	0.5055	0.4838	4.03
	70	1.1526	1.4464	1.1802	1.2597	12.88
	80	0.8318	1.0191	0.8221	0.8910	12.46
0.5	60	0.4651	0.4542	0.5337	0.4843	8.90
	70	0.5327	0.6363	0.5518	0.5736	9.61
	80	1.5932	1.4526	1.3634	0.8910	12.46

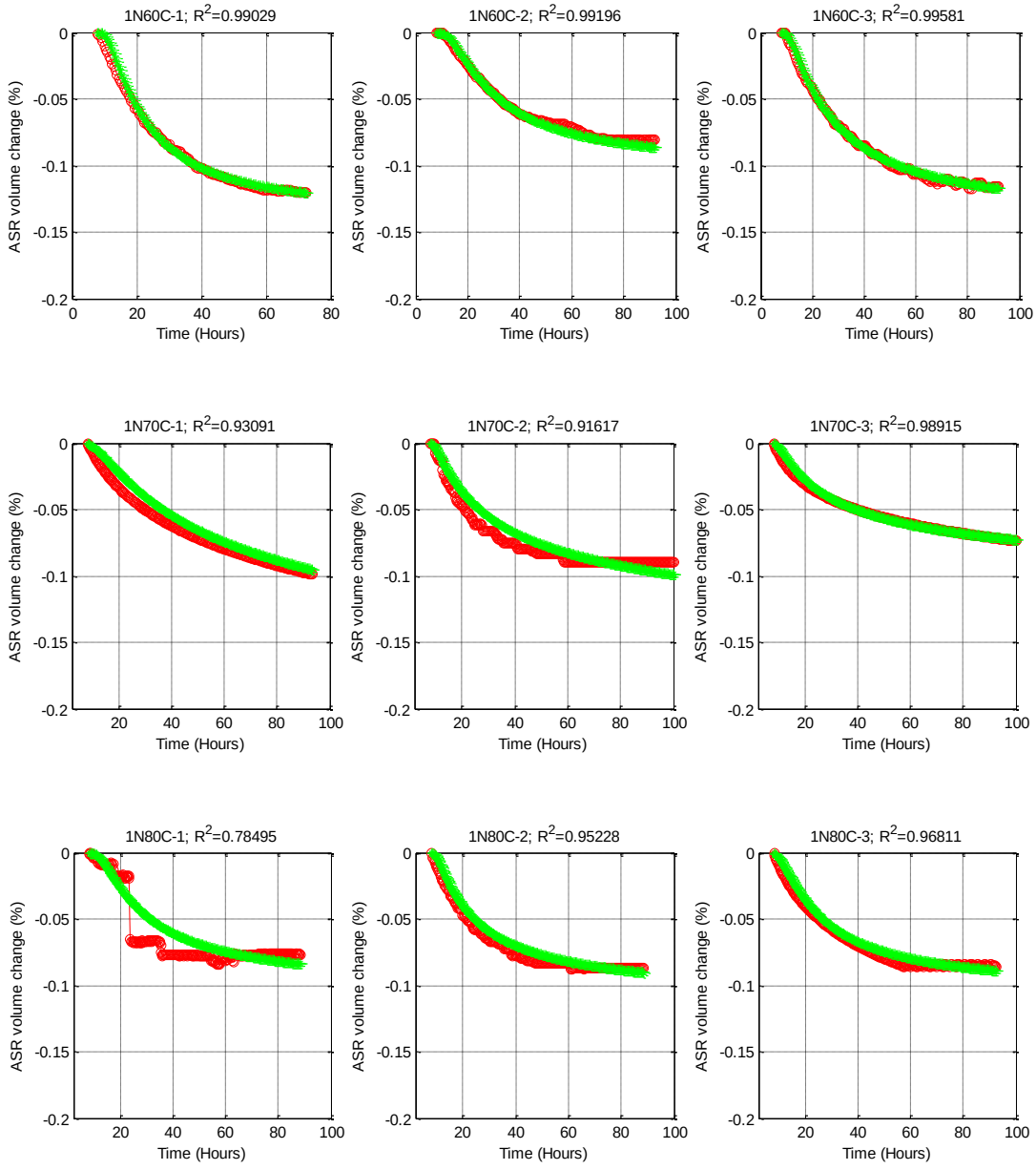

Figure B13-1 Repetition of Measured (Red) and Modeled (Green) Solution Volume Change over Time for CA8 with 1N NH + CH at Each Temperature (60, 70, and 80°C).

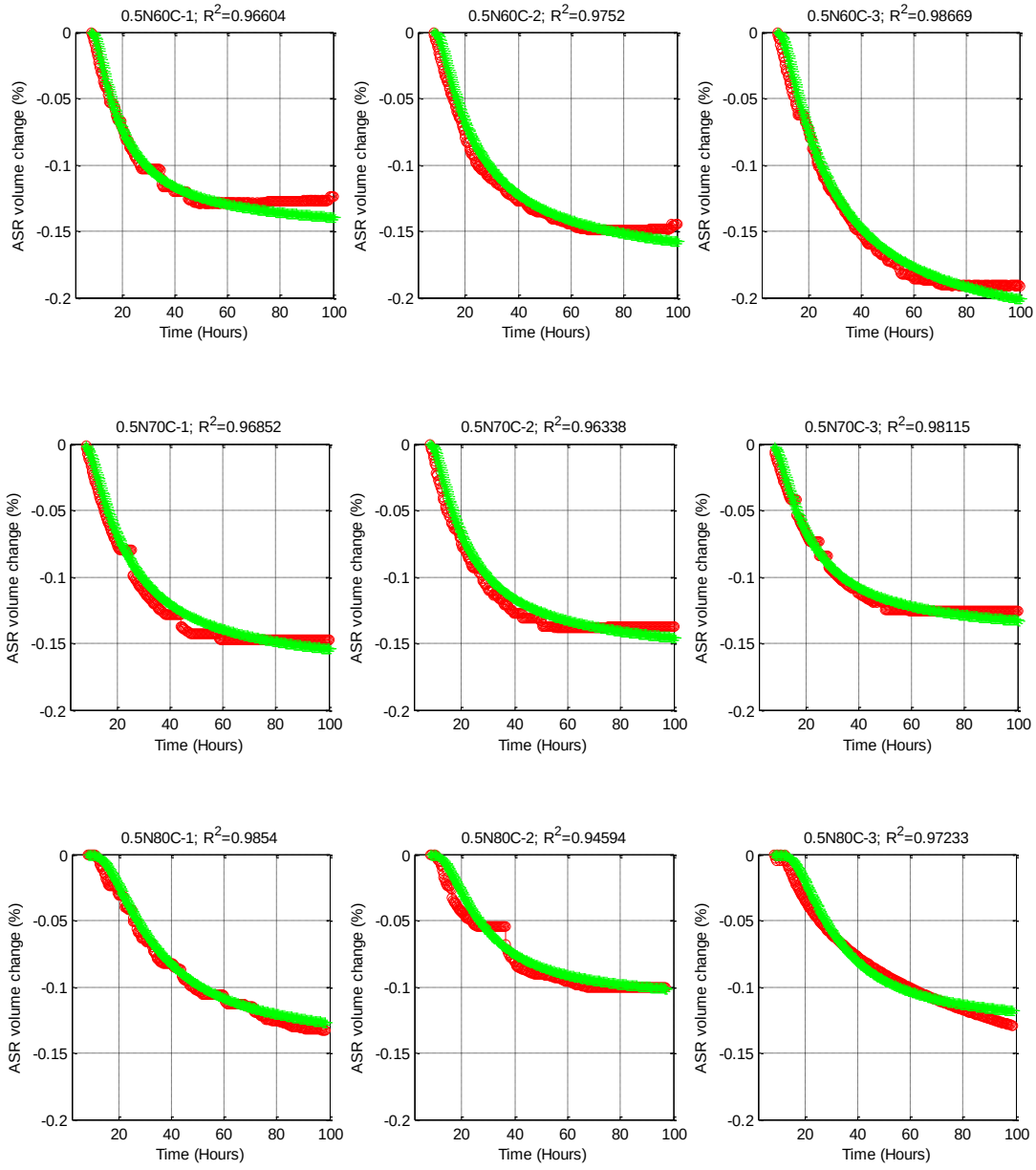

Figure B13-2 Repetition of Measured (Red) and Modeled (Green) Solution Volume Change over Time for CA8 with 0.5N NH + CH at Each Temperature (60, 70, and 80°C).

Table B13 Calculated Rate Constant Based on the Modeled Curve (Green) in Figures B13-1 and B13-2 for CA8.

Normality	Temperature °C	β			Average	COV %
		Test 1	Test 2	Test 3		
1	60	1.0647	1.2581	1.0332	1.1457	10.89
	70	0.4430	0.5449	0.4724	0.4868	10.77
	80	0.7670	0.7529	0.7686	0.7628	1.13
0.5	60	0.9865	0.8676	0.8131	0.8891	9.97
	70	0.9658	0.9695	1.1250	1.0201	8.91
	80	1.8588	1.8607	1.6755	1.7983	5.92

APPENDIX C

MEASURED AND CALCULATED SOLUTION VOLUME CHANGE OVER TIME DUE TO ASR AND CAE CALCULATION AT DIFFERENT LEVELS OF ALKALINITIES FOR THE TESTED AGGREGATES

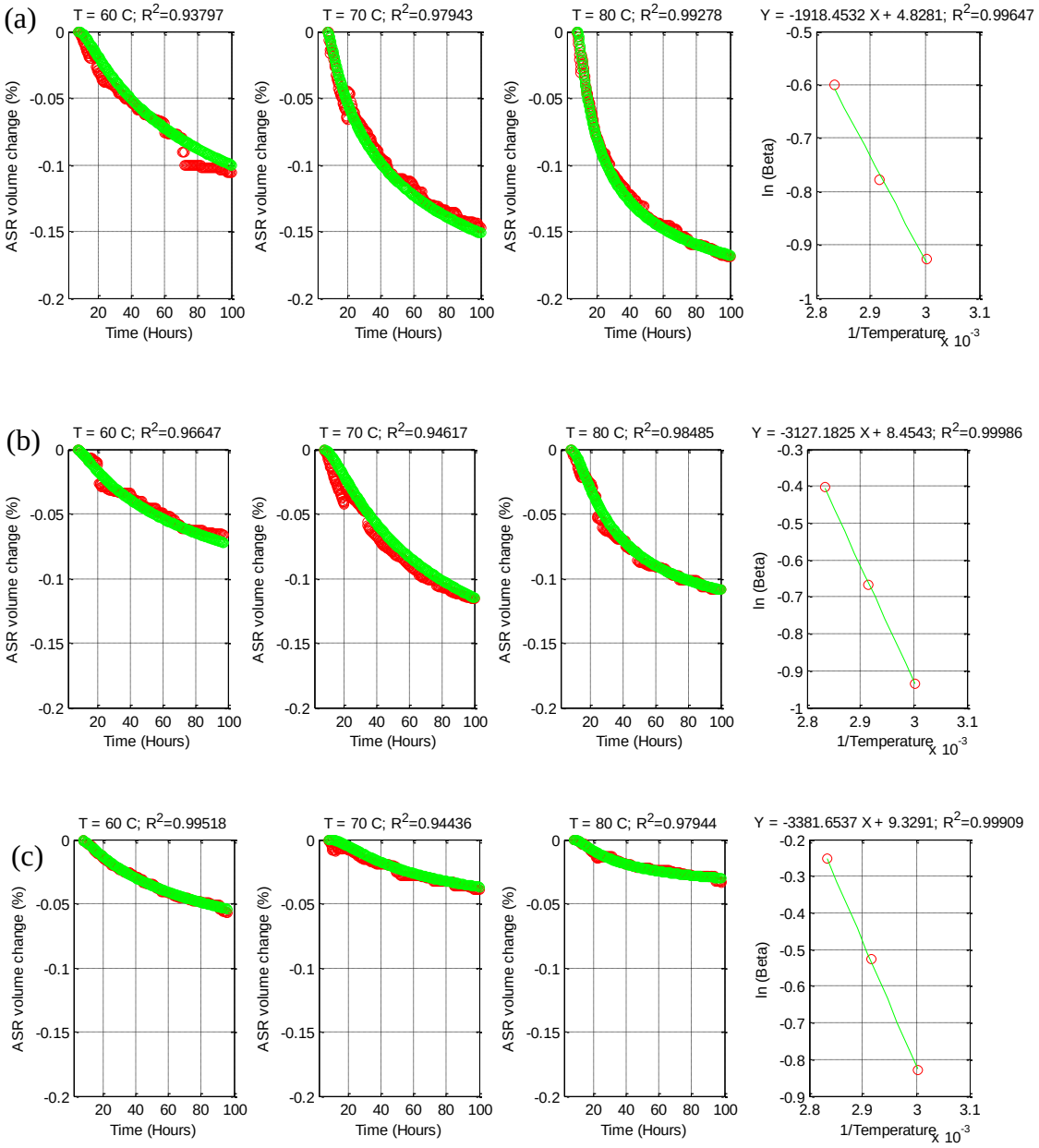

Figure C1 Measured (Red) and Modeled (Green) Solution Volume Change over Time for FA1 with (a) 1N NH + CH, (b) 0.5N NH + CH, and (c) 0.25N NH + CH Solutions at Three Temperatures.

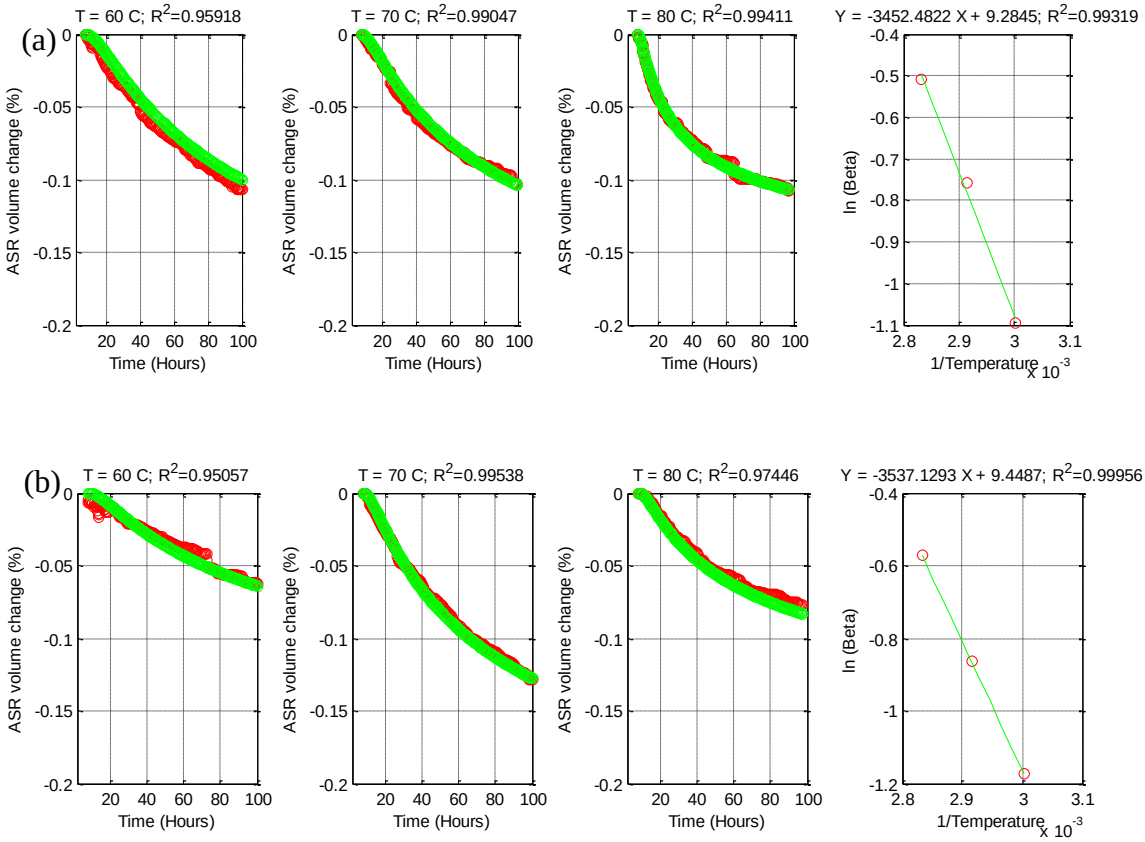

Figure C2 Measured (Red) and Modeled (Green) Solution Volume Change over Time for FA2 with (a) 1N NH + CH and (b) 0.5N NH + CH Solutions at Three Temperatures.

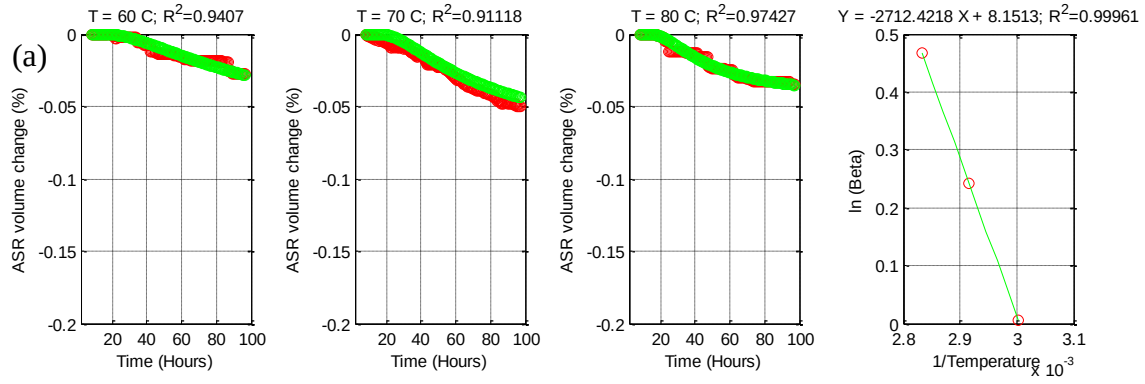

Figure C3 Measured (Red) and Modeled (Green) Solution Volume Change over Time for FA3 with (a) 1N NH + CH and (b) 0.5N NH + CH Solutions at Three Temperatures.

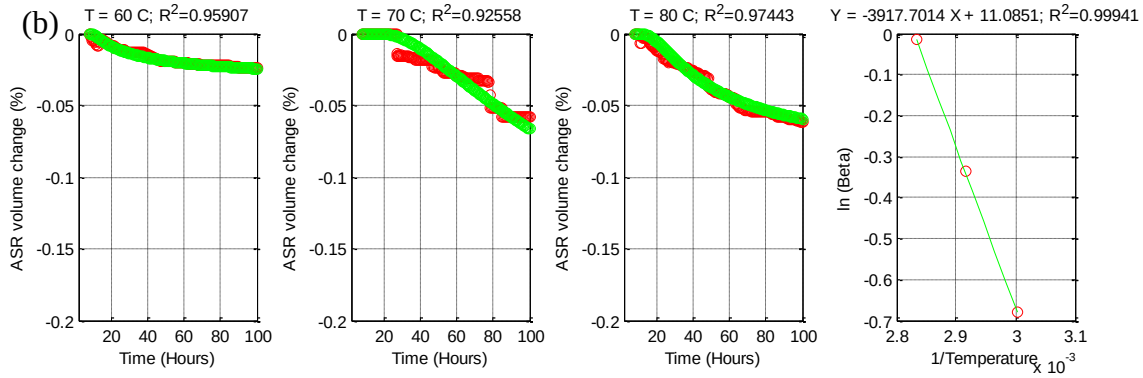

Figure C3 Continued.

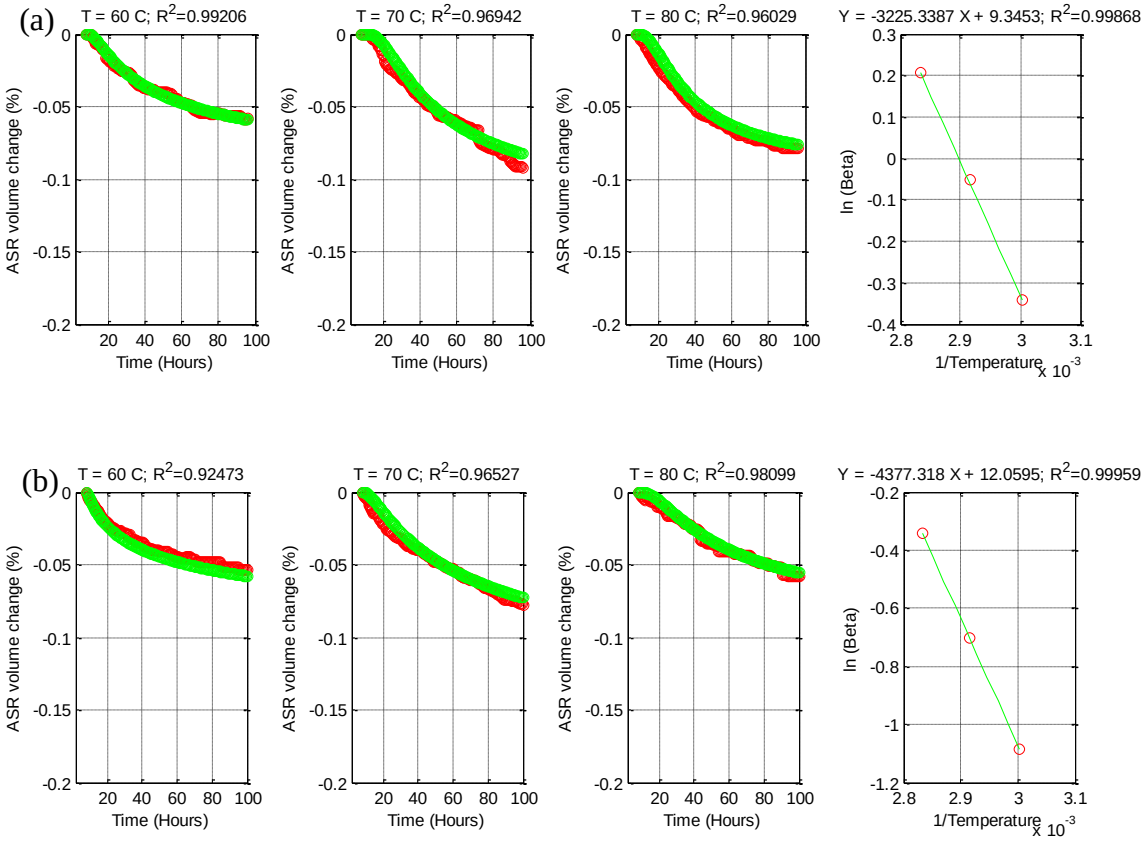

Figure C4 Measured (Red) and Modeled (Green) Solution Volume Change over Time for FA4 with (a) 1N NH + CH and (b) 0.5N NH + CH Solutions at Three Temperatures.

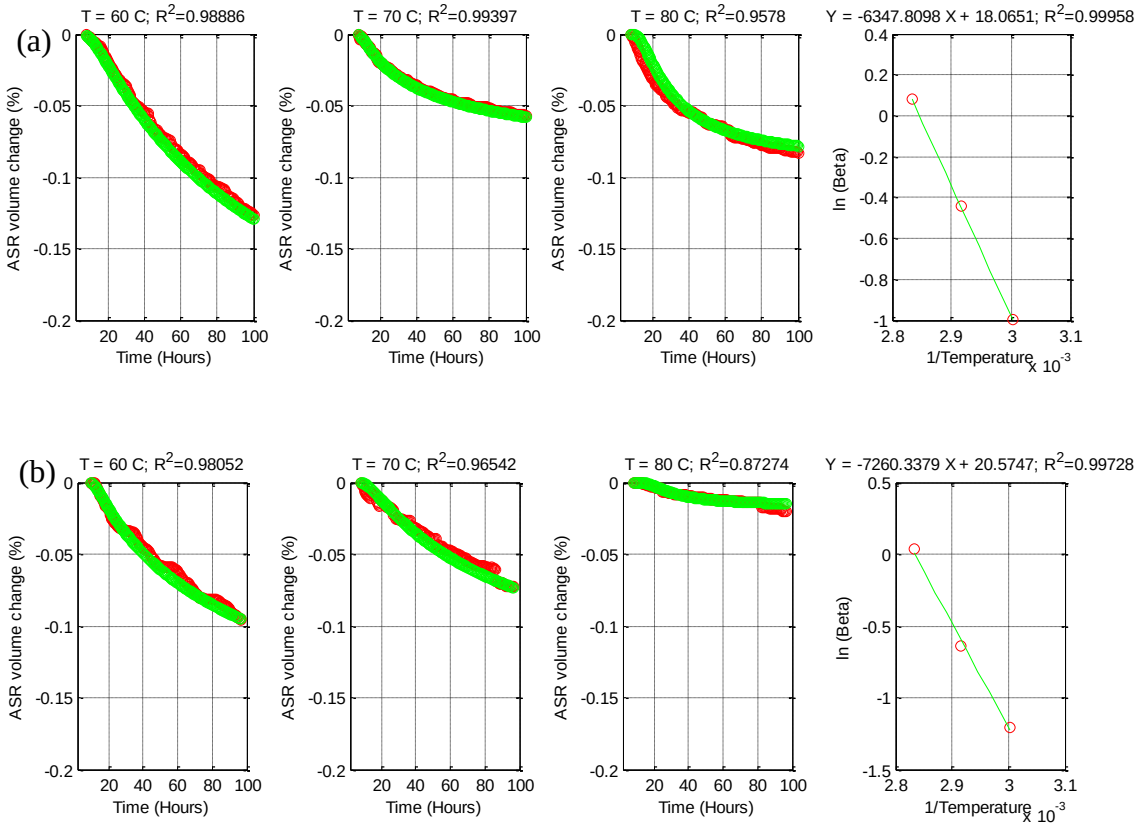

Figure C5 Measured (Red) and Modeled (Green) Solution Volume Change over Time for FA5 with (a) 1N NH + CH and (b) 0.5N NH + CH Solutions at Three Temperatures.

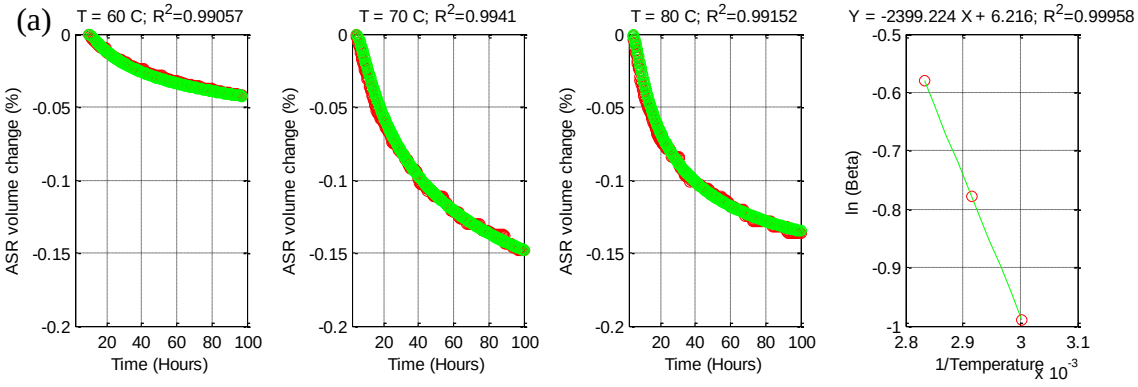

Figure C6 Measured (Red) and Modeled (Green) Solution Volume Change over Time for FA6 with (a) 1N NH + CH and (b) 0.5N NH + CH Solutions at Three Temperatures.

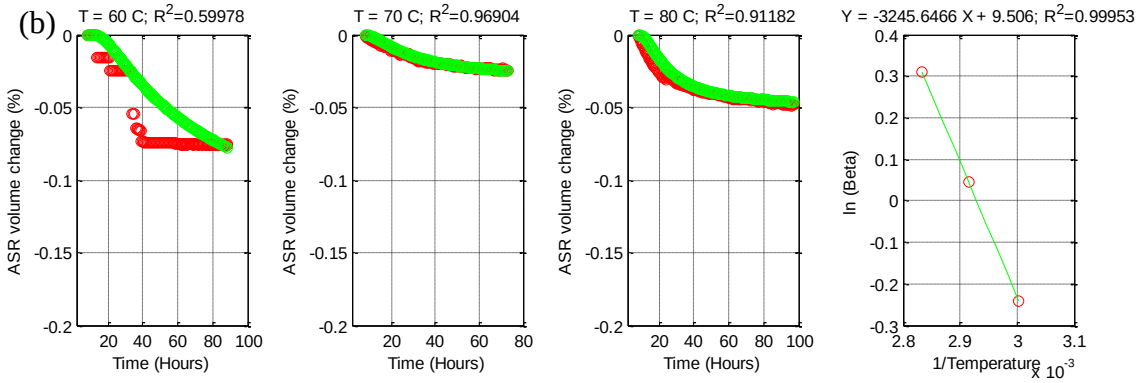

Figure C6 Continued.

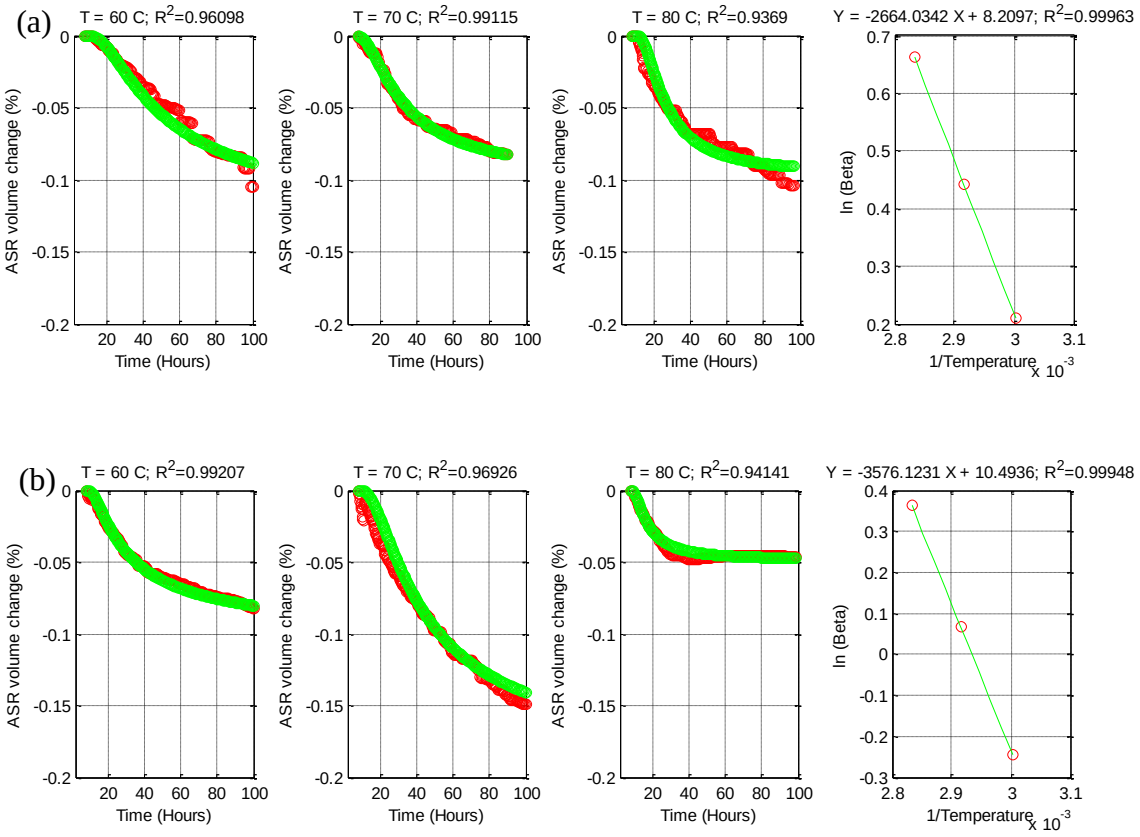

Figure C7 Measured (Red) and Modeled (Green) Solution Volume Change over Time for CA1 with (a) 1N NH + CH and (b) 0.5N NH + CH Solutions at Three Temperatures.

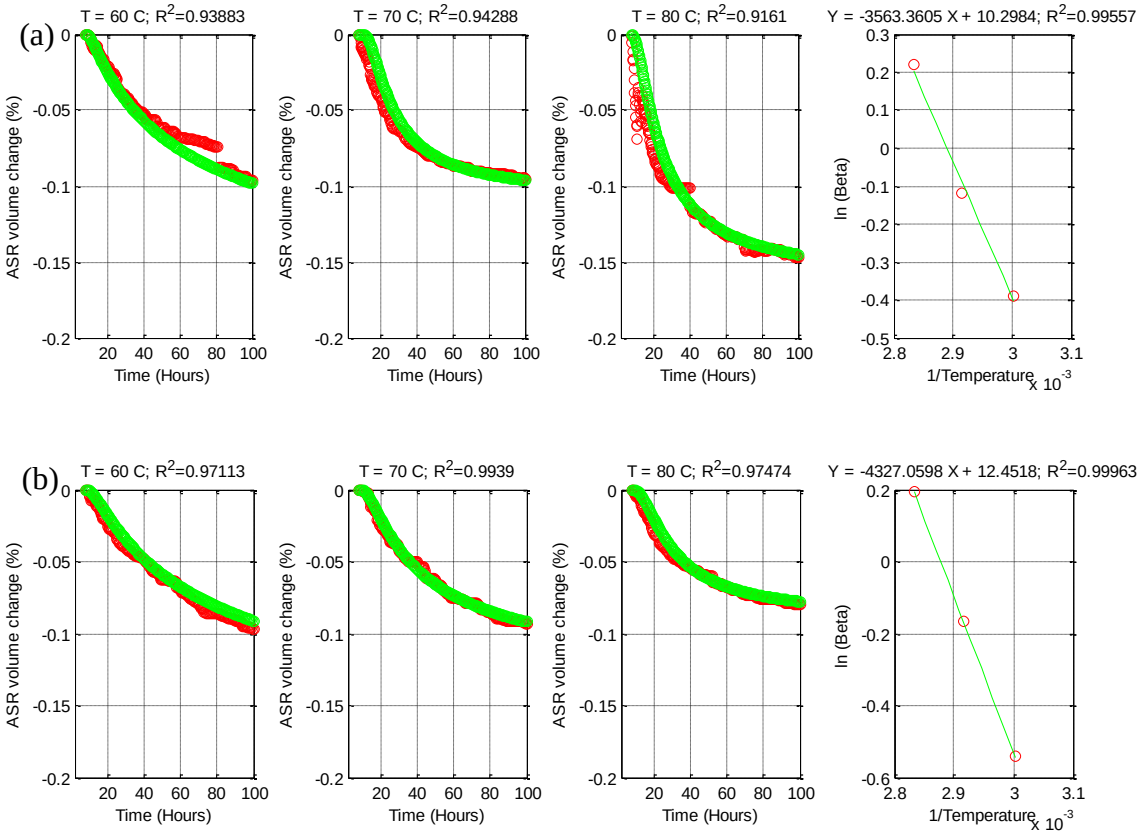

Figure C8 Measured (Red) and Modeled (Green) Solution Volume Change over Time for CA2 with (a) 1N NH + CH and (b) 0.5N NH + CH Solutions at Three Temperatures.

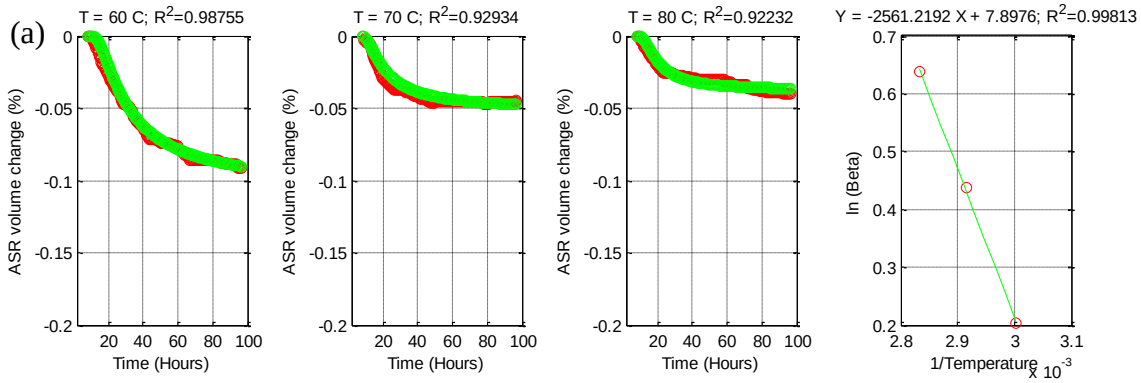

Figure C9 Measured (Red) and Modeled (Green) Solution Volume Change over Time for CA3 with (a) 1N NH + CH and (b) 0.5N NH + CH Solutions at Three Temperatures.

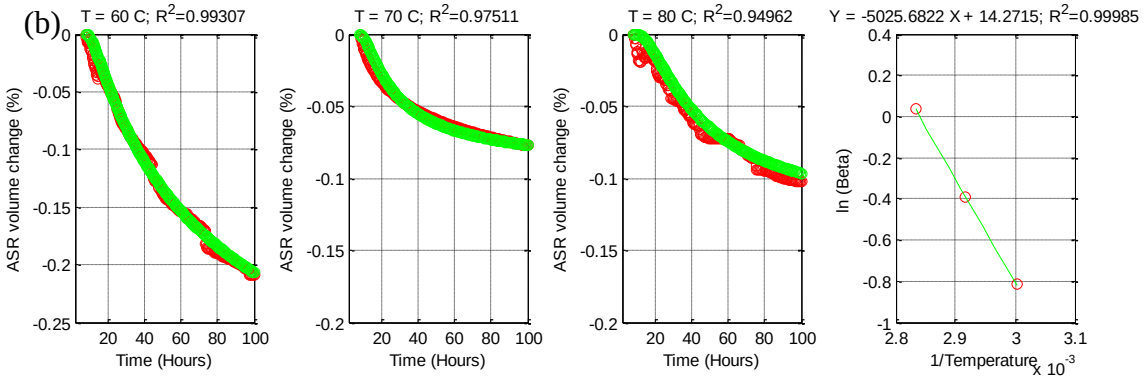

Figure C9 Continued.

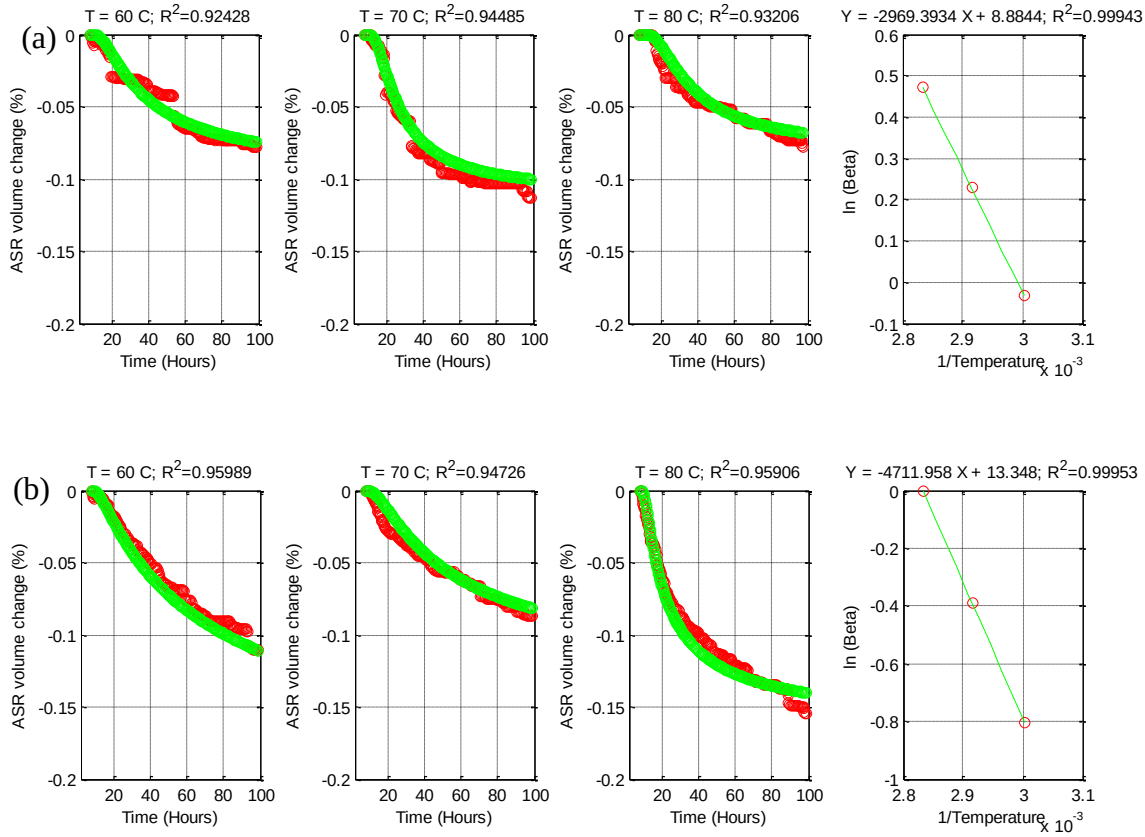

Figure C10 Measured (Red) and Modeled (Green) Solution Volume Change over Time for CA4 with (a) 1N NH + CH, (b) 0.5N NH + CH, and (c) 0.25N NH + CH Solutions at Three Temperatures.

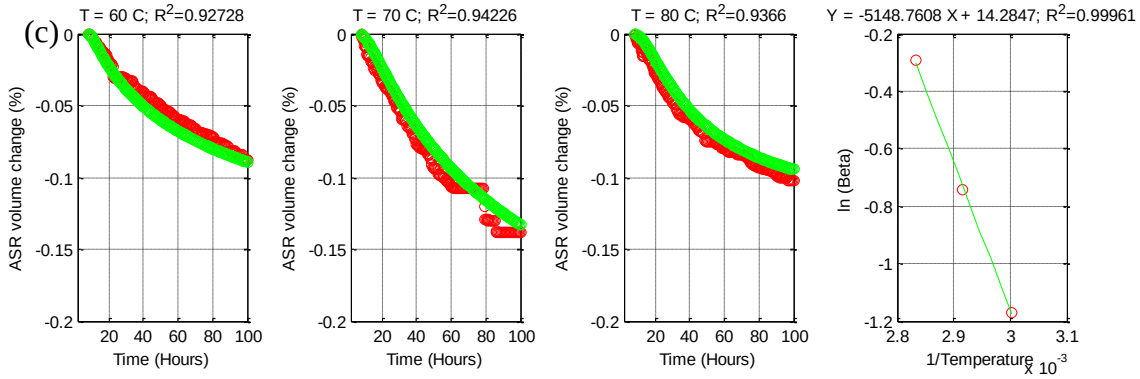

Figure C10 Continued.

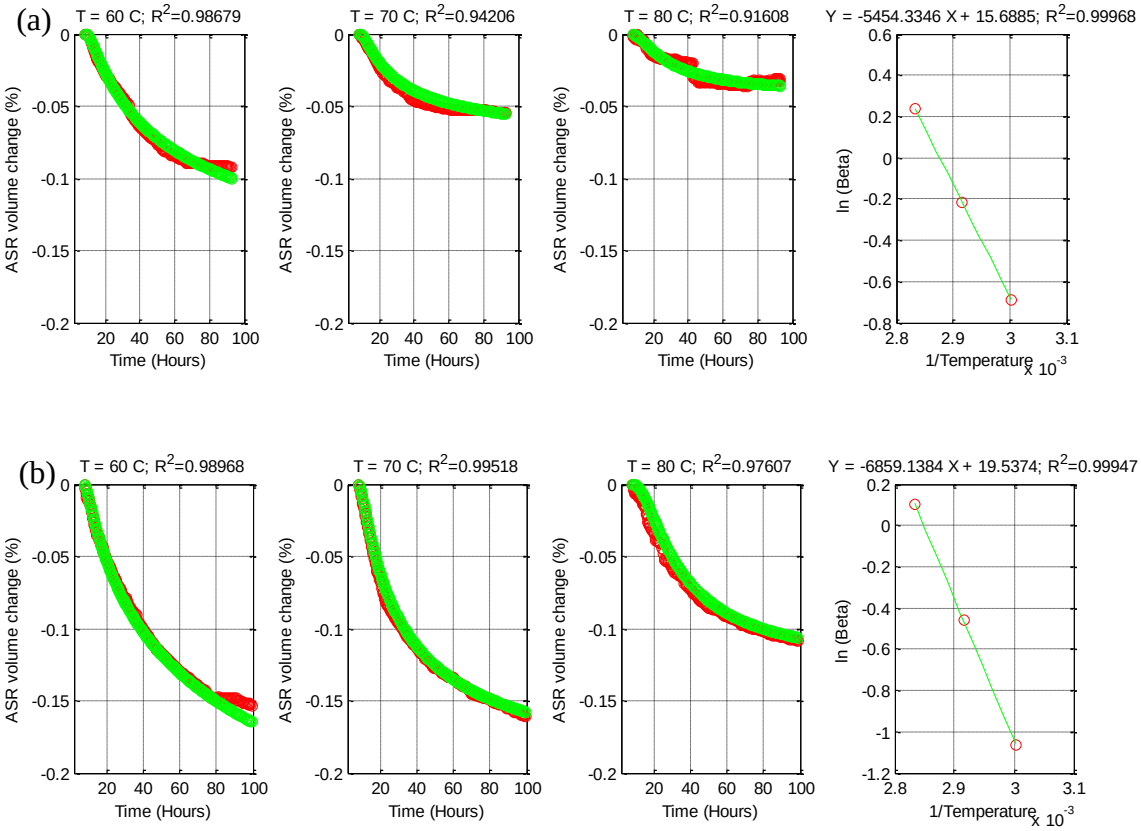

Figure C11 Measured (Red) and Modeled (Green) Solution Volume Change over Time for CA5 with (a) 1N NH + CH and (b) 0.5N NH + CH Solutions at Three Temperatures.

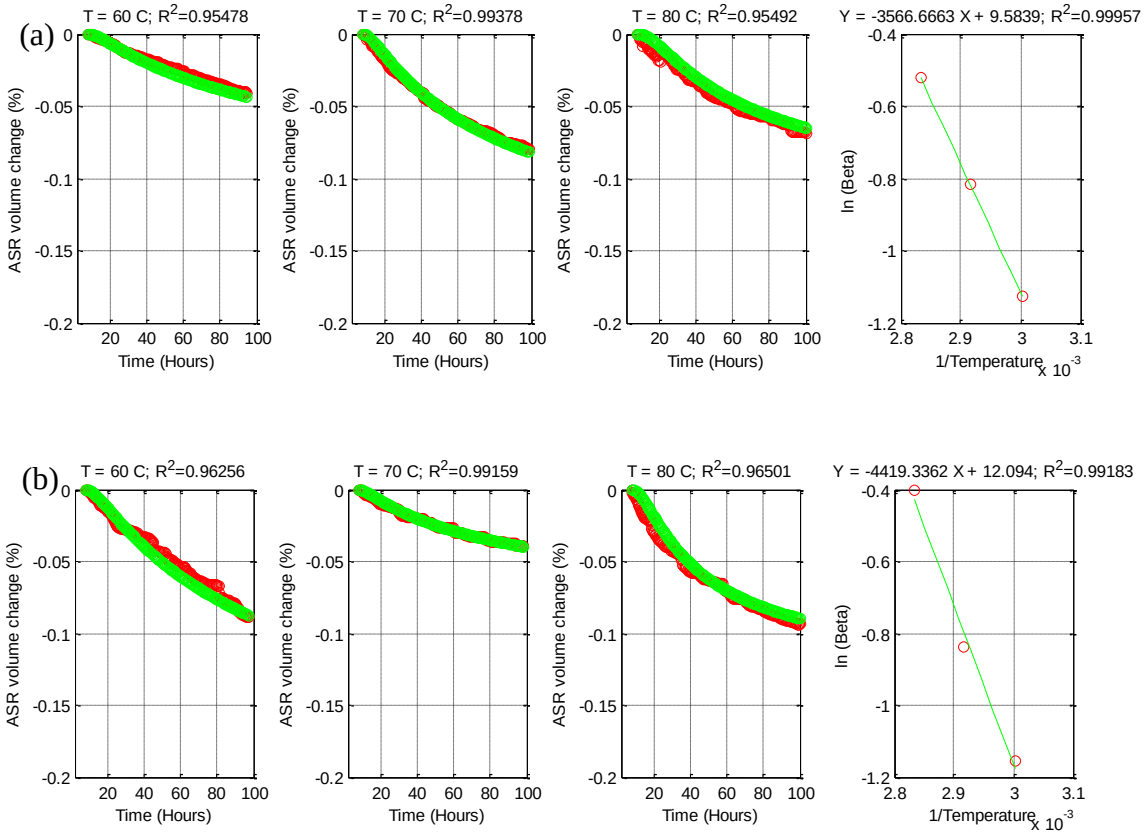

Figure C12 Measured (Red) and Modeled (Green) Solution Volume Change over Time for CA6 with (a) 1N NH + CH and (b) 0.5N NH + CH Solutions at Three Temperatures.

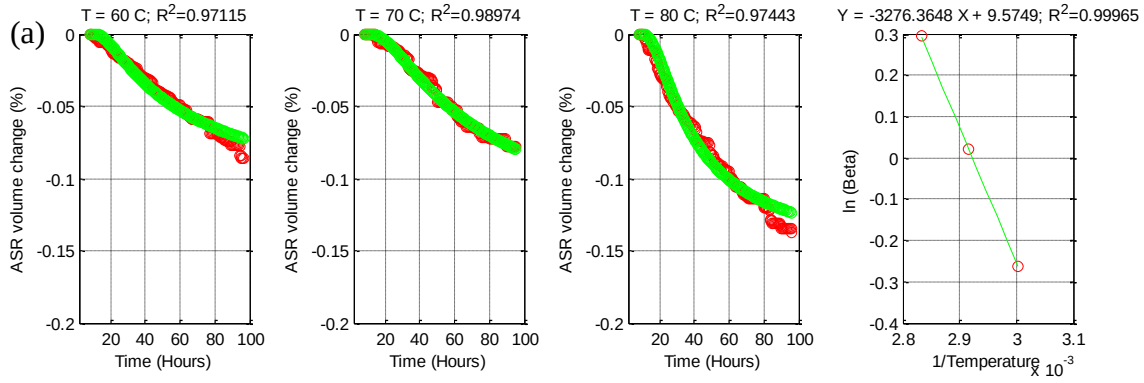

Figure C13 Measured (Red) and Modeled (Green) Solution Volume Change over Time for CA7 with (a) 1N NH + CH and (b) 0.5N NH + CH Solutions at Three Temperatures.

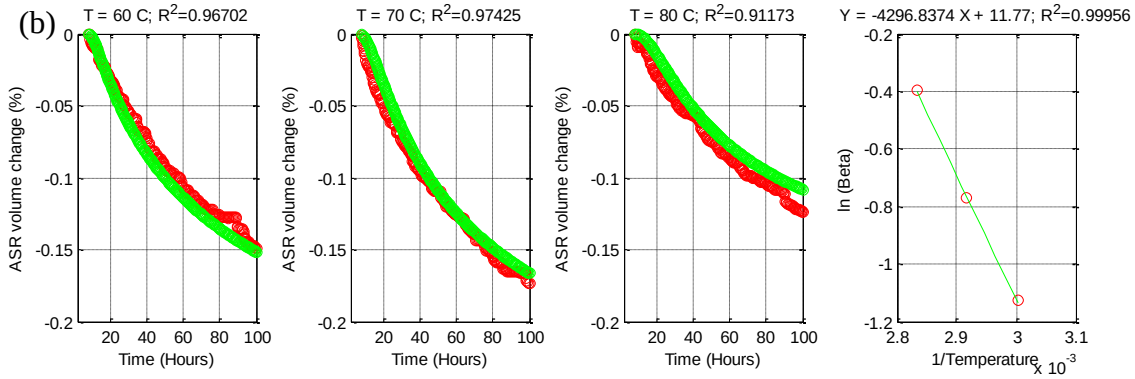

Figure C13 Continued.

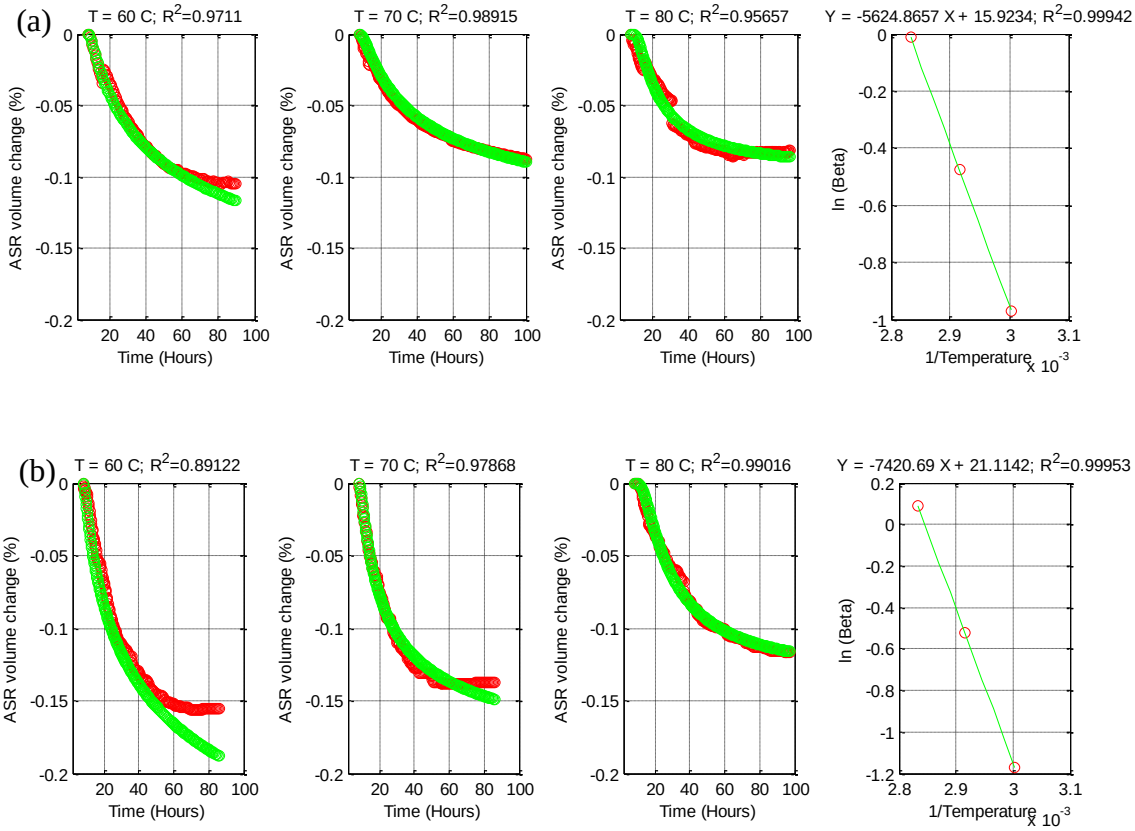

Figure C14 Measured (Red) and Modeled (Green) Solution Volume Change over Time for CA8 with (a) 1N NH + CH and (b) 0.5N NH + CH Solutions at Three Temperatures.

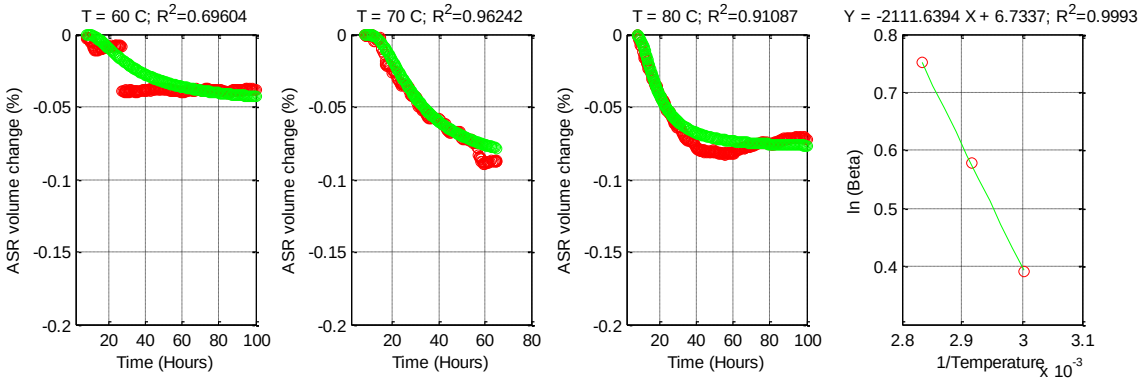

Figure C15 Measured (Red) and Modeled (Green) Solution Volume Change over Time for NMR with 0.5N NH + CH Solution at Three Temperatures.